NON-ADAPTIVE PROTECTION COORDINATION FOR RADIAL DISTRIBUTION FEEDER WITH DISTRIBUTED GENERATION

PETER KIRUI KEMEI

MASTER OF SCIENCE

(Electrical Engineering)

JOMO KENYATTA UNIVERSITY

OF

AGRICULTURE AND TECHNOLOGY

2024

Non-Adaptive Protection Coordination for Radial Distribution Feeder with Distributed Generation

Peter Kirui Kemei

A Thesis Submitted in Partial Fulfilment of the Requirements for the Degree of Master of Science in Electrical and Electronics Engineering of the Jomo Kenyatta University of Agriculture and Technology

2024

DECLARATION

This thesis is my original work and has not been presented for a degree in any other University

Signature……..…… Date……

Peter Kirui Kemei

This thesis has been submitted for examination with our approval as the University Supervisors

Signature……DECEASED …… Date……DECEASED…

Prof David K Murage, PhD
JKUAT, Kenya

Signature……..……Date……

Dr Peter K Kihato, PhD
JKUAT, Kenya

DEDICATION

I would like to take this opportunity to thank my late parents for everything they did to me and their precious advice through my life. Finally I would like to thank my lovely wife Maryline Kemei and my children Ryan Kiprono and Krystol Chepkoech for their encouragement throughout my research period.

ACKNOWLEDGEMENT

I would like to express my deep gratitude to my supervisors, the late Professor David K Murage and Dr. Peter K Kihato for their great support throughout my research. I sincerely appreciate their continuous encouragement. Finally I would like to thank my colleagues for their encouragement throughout my research period.

TABLE OF CONTENTS

LIST OF TABLES

LIST OF FIGURES

LIST OF NOMENCLATURE

Roman Symbols	Quantity
R_s	Stator resistance
X_s	Stator leakage reactance
X_m	Magnetizing reactance
R_2	Rotor resistance
X_2	Rotor leakage reactance
s	Slip

LIST OF APPENDICES

ACRONYMS AND ABBREVIATIONS

CLR	Current Limiting Reactor
DFIG	Doubly Fed Induction Generator
DG	Distributed Generation
ETAP	Electrical Transients Analysis Program
FCL	Fault Current Limiter
IEEE	Institute of Electrical and Electronics Engineers
MMT	Minimum Melting Time
NEC	National Electric Code
OCPD	Over-Current Protective Device
OCR	Over-Current Relay
SFCL	Superconducting Fault Current Limiter
SSFCL	Solid State Fault Current Limiter
TCC	Time-Current Characteristic
TCT	Total Clearing Time
WTG	Wind Turbine Generator

ABSTRACT

The connection of Distributed Generations (DGs) into a power systems distribution network improves the network's voltage profile, power quality and enhances voltage stability hence the distribution networks can withstand higher loading conditions reducing the network's overdependence on the main grid in improving its security and reliability. However, DG connection into a radial distribution network causes an increase on the network's short circuit current levels with the increase in the short circuit current levels creating a miss-coordination amongst the Over-Current Protective Devices (OCPDs) during a fault hence affecting the reliability of the over-current protection schemes implemented to protect the distribution network. In this research a conventional Fuse-Fuse over-current protection scheme was modelled to protect a radial test feeder from faults and the fuses coordinated while clearing the single line to ground (SLG) faults occurring at the feeder nodes without DGs connected. While clearing faults occurring in the test feeder, coordination is achieved if the upstream fuse minimum melting time (MMT) characteristics and the downstream fuse total clearing time (TCT) characteristics have a time coordination margin not less than 0.025 seconds between them. When Wind Turbine Generators (WTGs) were connected into the radial test feeder, the short circuit current levels increased; the network sequence reactance reduced; and the fuse-fuse time coordination margins reduced to levels less than the 0.025 seconds minimum threshold. Diminishing Fuse-Fuse time coordination margins to levels less than 0.025 seconds due to the increase in the networks' short circuit current levels upon WTG connection rendered the Fuse-Fuse over-current protection scheme inadequate and insufficient in protecting the radial test feeder from short circuit faults.This research considered the use of Fault Current Limiters (FCLs) to improve on the problem of diminishing fuse-fuse time coordination margins introduced by the WTGs by reducing the prospective fault currents in the test feeder to lower manageable levels not to cause further Fuse-Fuse miss-coordination. Series Current Limiting Reactors (CLRs) were introduced as additional impedances into the feeder to increase the feeder sequence reactance which had reduced due to WTGs connection. Once the WTGs were coupled into the radial test feeder using the CLRs, the feeder short circuit current levels reduced, the network sequence reactance increased and the diminishing time coordination margins between the fuses increased to levels above 0.025 seconds which is the minimum threshold for Fuse-Fuse coordination. CLRs reduced the prospective fault currents contribution from the WTGs to lower manageable levels not to cause further diminishing fuse-fuse time coordination margins thus restoring Fuse-Fuse coordination hence improving on the Fuse-Fuse over-current protection scheme reliability and efficiency in protecting the feeder.

CHAPTER ONE

INTRODUCTION

1.1 Background

As the global electrical energy demand grows there is a significant need to diversify both the conventional and the renewable electrical energy generation technologies to fulfil the increase in demand. Power systems security, electrical energy distribution efficiency and growing environmental concerns are the main reasons that have resulted in the significant use of renewable energy technologies for Distributed Generations (DGs) (Lopes et al., 2007). Integration of the DGs into a distribution network provides various benefits: they improve the voltage and the power quality of the electrical distribution network; they improve on the transmission and distribution network congestion; and they provide a more affordable capacity for utilizing renewable energy sources to the electrical energy generating companies (Kamel et al. 2013). However, DG connection into a distribution network has associated several technical, economic and regulatory implications with power systems protection and over-current protective devices (OCPDs) coordination being one of the major issues (Antonova et al., 2012).

Selective coordination in distribution network's over-current protection schemes involves the process of selecting OCPDs and there appropriate arrangement in the circuit to clear faults occurring in the network according to a pre-set sequence of operation (Muljadi et al., 2010). When an upstream and a downstream OCPD operate in a manner that only one appropriate device responds during a fault the two devices are said to be selectively coordinated (Aderibigbe et al., 2022).

Fuse-Fuse protection is an example of the over-current protection schemes implemented to protect distribution networks from faults. Fuse-Fuse coordination is an essential feature critical for a reliable operation of the Fuse-Fuse over-current protection scheme and when the fuses miss-coordinate the reliability of the distribution network is highly affected (Soria et al., 2014).

There are two broad approaches for undertaking over-current protection and coordination studies in distribution networks once DGs have been integrated into the network; the adaptive and the non-adaptive protection approaches. These two methodologies are best distinguished based on the OCPDs used in each particular protection scheme. If programmable OCPDs having electronic storage capabilities are used to implement the protection scheme, then that scheme falls under the adaptive protection approach while if the OCPDs used do not have both an electronic memory and programmable abilities then that scheme falls under the non-adaptive protection approach (Tambun et al., 2021).

Wind turbine generators (WTGs) are the most widely used form of renewable energy generation technologies as distributed generations and an important aspect of the WTGs is their short circuit current contribution into an electric power distribution network during a fault since the magnitudes of the short circuit currents are needed for sizing the OCPDs used to develop the over-current protection schemes to protect the distribution networks (Aderibigbe et al., 2022). The task of evaluating the short circuit currents from the WTGs can be a very challenging exercise due to the topological and operational differences between the different types of WTG's short circuit models available but the electrical generators design industry have classified the WTG's short circuit models into four broad categories labeled as the Type I, Type II, Type III and Type IV WTGs (ELG4126, nd). The short circuit behaviour for Type I, Type II, and Type III WTG models are similar hence they are all represented as Type III WTG with only the Type IV WTG model having a different short circuit behaviour. Type III WTG is the most studied among the four WTG models and is referred to as the Doubly-Fed Induction Generator (DFIG) (ELG4126, nd).

1.2 Problem Statement

Conventional power system distribution networks are passive and are designed to have a radial power flow from the main grid supply through the downstream feeders to the loads but once a DG is connected at the feeder lateral nodes, the network becomes an active network and it experiences a sharp increase in its short circuit current levels. One of the over-current protection schemes which is highly affected

by the sharp increase in the short circuit current levels brought about by the DGs is the fuse-fuse over-current protection scheme and once the DGs have been connected into a distribution network, the fuse-fuse over-current protection scheme experiences fuse-fuse miss-coordination during a fault due to the increase in the short circuit current levels. Fuse-Fuse miss-coordination impacts a lot on the reliability of the distribution networks' over-current protection scheme rendering it inadequate and insufficient in protecting the distribution networks from faults.

A selectively coordinated fuse-fuse over-current protection scheme requires that the fuses coordinating while clearing faults have a time coordination margin not less than 0.025 seconds which is the minimum time margin for fuse-fuse coordination as stipulated by National Electric Code (NEC) 240.101. The high short circuit currents introduced into the distribution networks by the DGs causes diminishing/reduction on the fuse-fuse coordination time margins to levels below the 0.025 seconds minimum threshold causing the fuses to miss coordinate while clearing faults occurring in the distribution networks thus affecting the distribution network reliability in clearing faults.

1.3 Justification

New solutions to minimize on the fuse-fuse miss coordination upon DG connection have to be developed with the subject on how to reduce the short circuit currents levels being given a considerable attention while designing the Fuse-Fuse over-current protection scheme. Apart from replacing the old low current rated fuses with new high current rated fuses to withstand the increased fault current levels from the DGs, the fault currents can be reduced to levels which the existing old lower rated fuses can easily handle by use of Fault Current Limiters (FCLs).

These research investigated the impacts of integrating two WTG models, the DFIGs and the Type IV WTGs on a conventional Fuse-Fuse over-current protection scheme modelled to protect a radial test feeder. A Fuse-Fuse protection scheme was modelled in the Electrical Transient Analysis Program (ETAP) software for IEEE 13 nodes radial test feeder and the impacts the DFIGs and the Type IV WTGs have on the diminishing time coordination margins between the coordinating fuses during a

fault event were analysed. The research presented an analysis on how the use of current limiting reactors (CLRs) to interface the DFIGs and the Type IV WTGs into the radial test feeder reduced the short circuit contribution from the WTGs hence restoring fuse-fuse coordination by increasing the diminishing fuse-fuse time coordination margins to time margins above 0.025 seconds.

1.4 Objectives

1.4.1 The Main Objective

To develop a non-adaptive over-current protection coordination scheme to mitigate the impacts DFIGs and Type IV WTGs connection have on a radial feeder conventional Fuse-Fuse over-current protection scheme.

1.4.2 The Specific Objectives

1. To develop a conventional Fuse-Fuse over-current protection scheme on a radial feeder.
2. To investigate the impacts the DFIGs and the Type IV WTGs have on the radial feeder short circuit currents and sequence reactance.
3. To investigate the impacts the DFIGs and the Type IV WTGs have on the conventional Fuse-Fuse over-current protection scheme time coordination margins.
4. To develop a non-adaptive over-current protection scheme utilizing series current limiting reactors to mitigate on the impacts the DFIGs and Type IV WTGs connection have on the conventional Fuse-Fuse over-current protection scheme.

1.5 Scope

The IEEE 13 node radial test feeder was chosen for the purposes of testing and validating this research (Kersting, 2001). To achieve the objectives, firstly a conventional Fuse-Fuse over-current protection scheme was modelled to protect the radial test feeder. Secondly DFIGs and Type IV WTGs were integrated into the test feeder to investigate the impacts the DFIGs and the Type IV WTGs have on the

conventional Fuse-Fuse protection scheme. Finally, 2 Ohms series CLRs were used to interface the DFIGs and the Type IV WTGs into the radial test feeder to mitigate on the impacts the short circuit current increase and the reduction on the sequence reactance have on the diminishing fuse-fuse time coordination margins brought about by the WTG connection. The radial feeder was modelled based on the IEEE 13 node radial test feeder descriptions in the ETAP electrical software with the following assumptions.

1. The DGs used are the DFIGs and the Type IV WTGs Models.
2. Focus is on Fuse-Fuse coordination for SLG faults occurring in the radial test feeder.
3. The analysis does not include islanding operation of the radial test feeder.

1.6 Contribution of Thesis

Most studies done have concentrated on the short circuit currents contribution by the WTGs during faults and little have been done on the impacts the DFIGs and Type IV WTGs have on the distribution network's over-current protection and coordination schemes. This research has gone a step ahead and studied how an increase in the DFIGs and Type IV WTGs capacities from 1MW to 3MW, and how the change in the location of their placement on the distribution networks' affects the: SLG fault levels; the positive, negative and zero sequence reactance levels; the fuse-fuse time coordination margins; and the location of the coordinating fuses' minimum melting time (MMT) and total clearing time (TCT) characteristics on the time current characteristic (TCC) curves. This research also presented a detailed study on how CLRs can be used to mitigate on the impacts caused by the DFIGs and Type IV WTGs on: the increase on the SLG fault levels; the reduction on the positive, negative and zero sequence reactance levels; the diminishing fuse-fuse time coordination margins; and the shifting of the fuses MMT and TCT on the TCC curves.

1.7 List of Publications

1. Impacts of Placement of Wind Turbine Generators with Different Interfacing Technologies on Radial Distribution Feeder Short Circuit Currents. Proceedings of sustainable research and innovation conference. JKUAT, ISSN: 2079-6226, pp. 206-212, May 2019.
2. Impacts of Short Circuit on Wind Turbine Generator Interfaced Radial Distribution Feeder Sequence Impedances. Proceedings of sustainable research and innovation conference. JKUAT, ISSN: 2079-6226, pp. 250-255. May 2019.
3. Fuse-Fuse Protection Coordination Scheme ETAP Model for IEEE 13 Node Radial Test Distribution Feeder. European Journal of Engineering and Technology Research. EJENG ISSN: 2736-576X Volume 4 Issue 9, pp. 224-234, September 2019.
4. Impacts of Wind Turbine Generator Interfacing Technology, Capacity and the Location of Placement on IEEE 13 Node Radial Test Feeder Short Circuit Currents. International Research Journal of Innovations in Engineering and Technology-IRJIET.ISSN: 2581-3048Volume 7, Issue 1. pp. 65-76. January 2023.
5. Impacts of DFIG and Type IV WTG' Capacity and the Location of Placement on IEEE 13 Node Radial Test Feeder Positive, Negative and Zero Sequence Reactance in Short Circuits. International Research Journal of Innovations in Engineering and Technology-IRJIET.ISSN: 2581-3048 Volume 7, Issue 2. pp. 1-15. February 2023.

1.8 Organization of Thesis

This thesis is organized into five chapters: Chapter one entails the introduction to: how the conventional radial distribution networks are protected from faults ; why the conventional distribution networks over-current protection schemes are designed for OCPD's coordination without the consideration of DGs; the available remedies, the adaptive and the non-adaptive protection approaches which can be used to minimize

the impacts the DGs have on the distribution network's over-current protection schemes in order to achieve OCPD's coordination.

Chapter two is the literature review section. It gives a description of what entails: DGs in terms of their sizes and the available technologies for interfacing them into the main grids; The WTGs classifications with their short circuit models and how they respond during short circuit faults; The OCPD's TCC curves and how they coordinate while clearing faults occurring in the electrical networks; The various types of fault current limiting techniques with their applications; The sequence components theory and applications in power systems faults analysis; The power systems equipment protection requirements, landmarks, damage curves and how the OCPDs are placed in order to protect the equipment from faults; The impacts of DGs on the distribution networks' short circuit current levels and on the conventional feeder protection schemes; and finally the suitable application areas for the adaptive and the non-adaptive over-current protection and coordination approaches.

Chapter three of the thesis is the methodology. It entailed the development of the IEEE 13 nodes radial test feeder fuse-fuse over-current protection scheme in the ETAP electrical software and how connection of DFIGs and Type IV WTGs on the feeder impacts on the feeder: short circuit current levels; sequence reactance levels; fuse-fuse coordination time margins; and the location of the fuses' MMT and TCT curves on the TCC curve. Data on how a 2 ohms CLR was used to mitigate on the DFIGs and the Type IV WTGs impacts on the fuse-fuse over-current protection scheme were also found in chapter three.

Chapter four is the results, discussion and data analysis section. It gives a detailed discussion on how integration of DFIGs and Type IV WTGs impacted on the test feeder: short circuit current levels; sequence reactance levels; fuse-fuse time coordination margins; and the location of the fuses' MMT and TCT curves on the TCC curves. It presents a detailed analysis on how CLRs can be used to: reduce the short circuit levels; increase the feeder sequence reactance; increase fuse-fuse time coordination margins; and the location of the coordinating fuses curves on the TCC curves. A detailed summary on how the DFIGs and the Type IV WTGs impacts on

the conventional fuse-fuse over-current protection schemes developed for protecting the radial test feeder was presented here.

Chapter five section one is a conclusion on how the CLRs can be used to enhance the distribution networks overcurrent protection and coordination schemes reliability and efficacy once DGs have been connected into the feeder. Section two gives the recommendations which can be investigated in further researches to ascertain how best the CLRs can be sized and placed in the distribution network to improve on the over-current protection schemes efficiency and reliability.

CHAPTER TWO

LITERATURE REVIEW

2.1 Distributed Generations

2.1.1. Classification of Distributed Generations

The term Distributed Generation (DG) can be loosely defined as a small-scale electrical generator working as a local generation plant for assisting the main utility grid (Rini et al., 2017). To clarify on the DG concepts some categories have been used to define the sizes of the DG units and are presented in Table 2.1 (Rini et al., 2017).

Table 2.1: Distributed Generation Sizes

TYPE	SIZE
Micro Distributed Generation	$1W < 5kW$
Small Distributed Generation	$5kW < 5MW$
Medium Distributed Generation	$5MW < 50MW$
Large Distributed Generation	$50MW < 300MW$

There are several types of distributed electrical energy generation technologies utilizing either the conventional electrical energy generation technologies or the renewable energy generation technologies with the most commonly utilized technologies by DGs being: the fuel cells; the micro turbines; the photovoltaic cells; the small hydro power plants; the diesel generators and the wind turbine generators (Elmarkabi, 2004). The type of the generation technology used to generate the electrical power dictates the type of the electrical generator to be used and how the DG will be interfaced into the main grid (Seema, 2015). The three major classes for the electrical energy generation technologies are; the synchronous generator technology; the induction generator technology; or the power electronic device technologies and based on the form of technology used in generating the electrical energy, the DGs can be interfaced with the main grid either directly into the grid or either through the use of power electronic converters.

2.1.2 Distributed Generation Technologies

i. **Synchronous Generators**

Figure 2.1 shows a block diagram of a synchronous generator interfaced DG System (Seema, 2015). Synchronous generators are conventional electrical generators which convert mechanical power from its rotating turbines to generate both active and reactive power. Synchronous generators used in the main grid generation plants are large enough to regulate the voltages of the main grid and are thus operated at varied power factors (Seema, 2015). In contrast, the size and the capacity of most of the synchronous generators employed in DGs are relatively small in size as compared to the larger main grid synchronous generators. The synchronous generators used in DGs are not larger and sufficient enough to regulate the voltage of the main grid hence they are generally operated at unity power factor to supply only the active power (Seema, 2015).

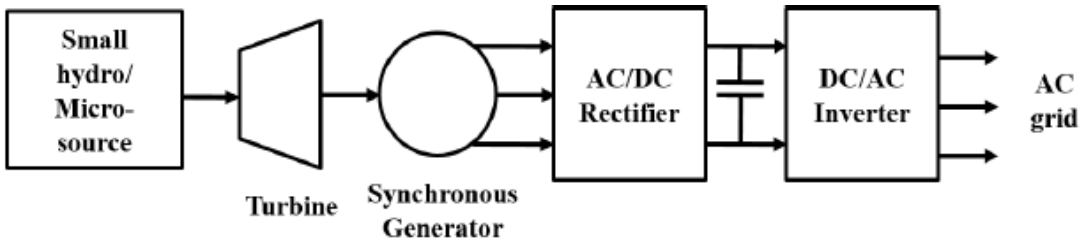

Figure 2.1: Block Diagram of Synchronous Generator Interfaced DG System

ii. **Induction Generators**

Figure 2.2 shows a block diagram of an induction generator interfaced DG System. Induction generators convert mechanical power into electrical power when they are rotated at speeds greater than the synchronous speed. They are mainly used with wind turbines and with some low head hydro applications. The major advantage of the use of induction generator is that they are relatively less expensive, they require less maintenance and are robust compared to synchronous generators however, induction generators cannot be operated in islanded mode since they require other sources of power to provide excitation in their rotor windings (Seema, 2015). They require reactive power which is supplied either from the electric power system

network itself or from independent sources like the capacitor banks to provide the necessary excitation (Seema, 2015).

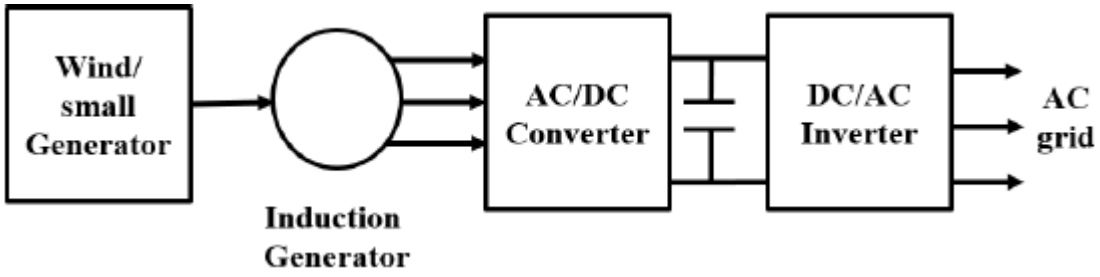

Figure 2.2: Block Diagram of Induction Generator Interfaced DG System

iii. Power Electronic Devices

DGs utilizing renewable energy sources like the fuel cells, the photovoltaic cells and battery storage systems generate DC power. This power is first converted to AC power of the desired voltage and frequency using electronic power converters and inverters before being fed into the main grid as shown in Figure 2.3 (Seema, 2015).

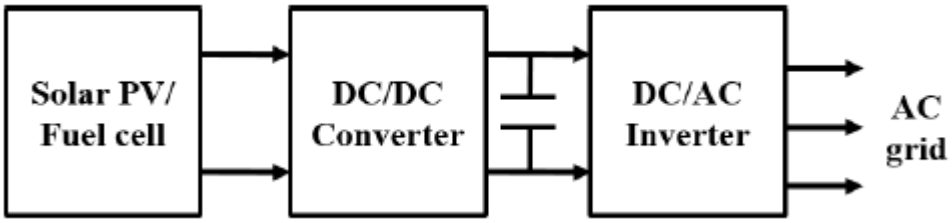

Figure 2.3: Block Diagram of a Power Electronics Converter Interfaced DG System

2.2 Wind Turbine Generator Technologies

2.2.1. Classification of Wind Turbine Generators

A. Type I Wind Turbine Generator

Generic models have been developed for four major WTG topologies the first topology being referred to as a Type I WTG. This machine drives a pitch-regulated squirrel cage induction generator which is directly coupled to the grid as shown in Figure. 2.4 (Muljadi et al., 2010). Type I WTG experiences large torque swings which occur due to high wind speeds during turbulence creating a poor power factor

hence compensating capacitor banks are used/needed to couple the Type I WTG into the main grid (Jadhar, & Harchandani, 2015).

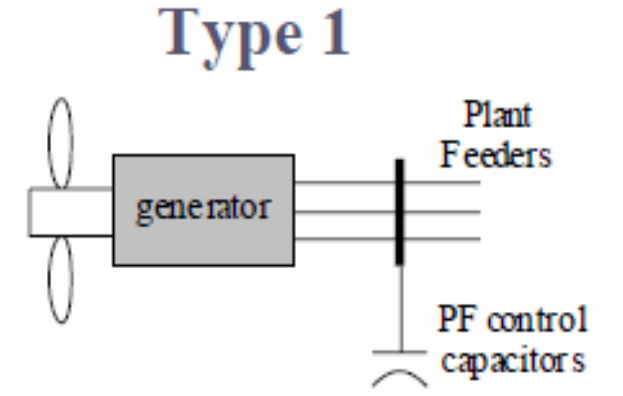

Figure 2.4: Type I Wind Turbine Generator

B. Type II Wind Turbine Generator.

It is an induction generator operating at variable slip utilizing a wound rotor whose rotor windings are brought out via slip rings and brushes and then coupled to a resistive bank as shown in Figure. 2.5 (Muljadi et al., 2010). A disadvantage of using the Type I WTG is the large torque swings that occur with turbulence in the wind speed hence by varying the resistance of the rotor windings of the Type II WTG, a more dynamic response to wind turbulence can be achieved by allowing a change in speed in the rotor reducing the large torque swings hence prolonging the life of the mechanical components of Type II WTG. Type II WTG still requires compensating capacitor banks to achieve its operations within the required typical power factor limits (Jadhar, & Harchandani, 2015)..

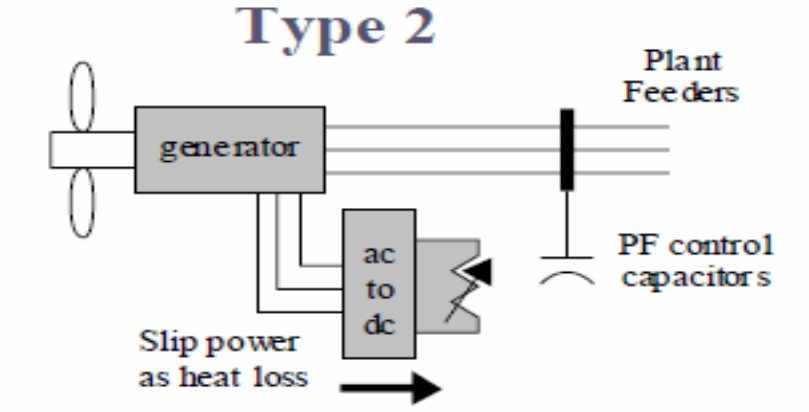

Figure 2.5: Type II Wind Turbine Generator

C. Type III Wind Turbine Generator.

Type III WTG is a pitch-regulated wound rotor induction generator and instead of the dynamically controlled resistors connected between its rotor terminals as the Type II WTG, it has a power converter connected between its rotor terminals and the main grid (Muljadi et al., 2010). The stator windings are also directly coupled to the grid hence it is commonly referred to as the Doubly-Fed Induction Generator (DFIG) as shown in Figure. 2.6.

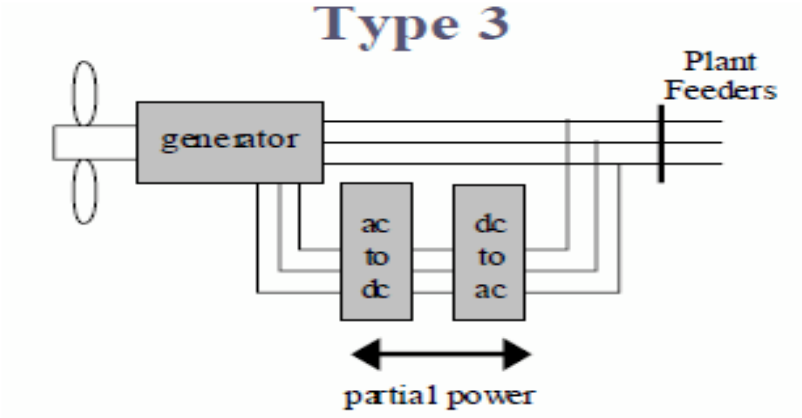

Figure 2.6: Type III Wind Turbine Generator

The addition of the power converter between the rotor windings and the grid allows the same benefits of the Type II design without the resistive losses and the ability to provide reactive power support without external capacitor banks hence a variable speed operation that allows for a more efficient energy capture below rated wind

speeds (Jadhar, & Harchandani, 2015). Its power converter is protected from the high short-circuit currents by either a crowbar or a chopper circuit. The type of protective device used to protect the rotor converter has a significant impact on the short-circuit behaviour of the Type III WTG (Jadhar, & Harchandani, 2015).

D. Type IV Wind Turbine Generator.

Type IV WTG is pitch-regulated and features a power converter through which the entire power of the generator is processed. The generator may be either an induction or a synchronous machine as shown in Figure. 2.7 (Jadhar, & Harchandani, 2015). In the Type IV design the wind turbine generator is decoupled from the grid through a power converter which is rated to the full output of the turbine having the same advantages of the Type III design with variable speed operation and reactive power support (Muljadi et al., 2010).. Since the generator is decoupled from the grid the stator windings can operate at variable frequencies hence expanding the types of the machines that can be used. The main disadvantage of the Type IV WTG is that they require sophisticated collector protection for the fault current (Jadhar, & Harchandani, 2015).

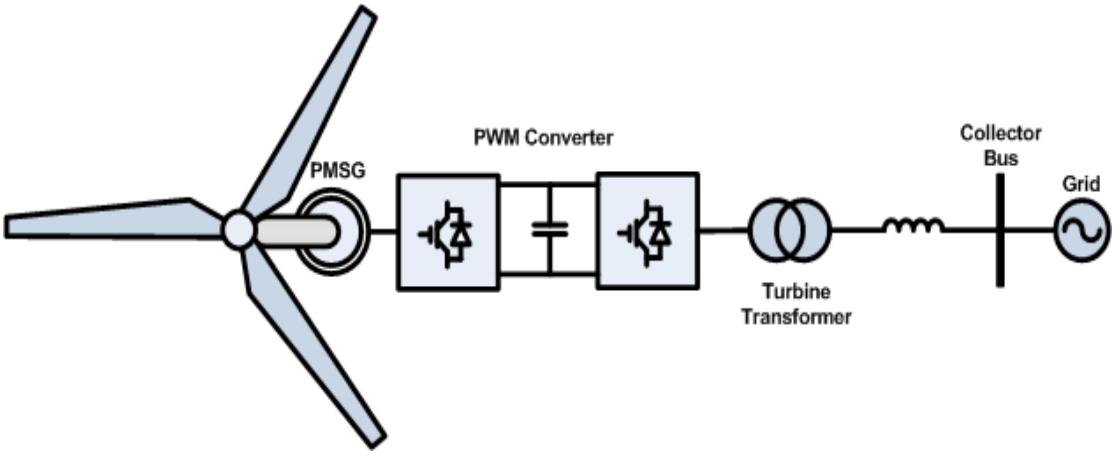

Figure 2.7: Type IV Wind Turbine Generator

2.2.2. Synchronous and Induction Machines Short Circuit Models

Wind turbine generators are designed for a maximum wind speed, called the survival speed, above which they do not survive however, they produce maximum power at a

wide spectrum of wind speeds. The survival speed of commercial wind turbines ranges from 25 m/s to 30 m/s (Muljadi, & Gevorgian, 2011). Wind turbines have three modes of operation: Below rated wind speed operation; around rated wind speed operation; and above the rated wind speed operation.

The major difference between an induction machine and a synchronous machine in regards to their behaviour during a fault is their method/mode of excitation. For a synchronous machine the excitation is provided from an independent DC source that is unaffected by a fault on the power system. Due to this separate excitation, synchronous machines continues to supply high transient currents throughout the duration of a fault event hence a drop in the line voltages caused by a fault will not affect its operations (Muljadi, & Gevorgian, 2011). Wind power plants on the other hand do not employ the synchronous machines for energy production. Wind power plants either employ an induction machine with a direct connection to the main electrical grid, or they decouple the induction machine from the main grid through power electronic devices (Muljadi, & Gevorgian, 2011). The drop in the line voltages during a fault makes an induction machine lose its excitation hence the machine would only supply transient currents to the fault for one or two cycles (Muljadi, & Gevorgian, 2011).

A. Synchronous Machines Short Circuit Model

A synchronous machine for short circuit modelling can be represented with a Thevenin equivalent circuit where the voltage and impedance represent the worst case condition which is the highest short circuit current contribution immediately following a fault as shown in Figure. 2.8.

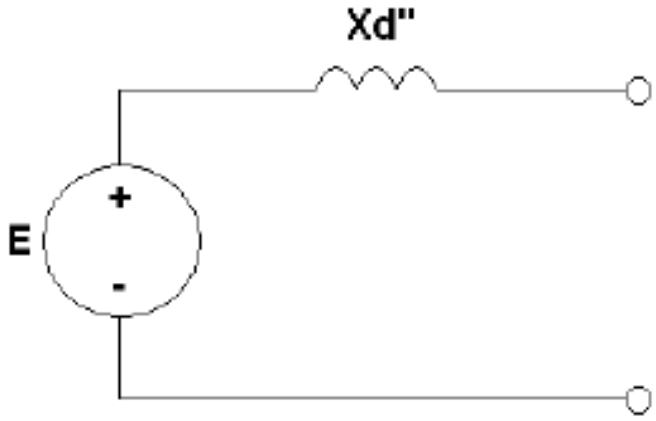

Figure 2.8: Synchronous Machine Short Circuit Equivalent

B. Induction Machines Short Circuit Models

I. Type I WTG Short Circuit Model

Most induction machines on the electric power grid are small enough such that their contribution to the fault current can be neglected, however the induction machines used in Type I WTG are large enough that they are taken into account for determining the total fault current (Muljadi, & Gevorgian, 2011). The equivalent machine impedance for fault calculations for a Type I WTG is the sum of the stator and rotor reactance as shown in Figure. 2.9 (Muljadi, & Gevorgian, 2011).

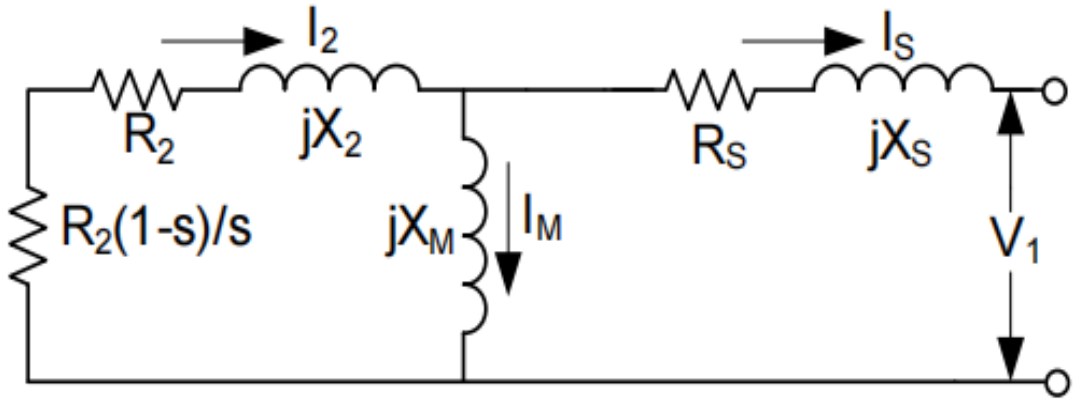

Figure 2.9: Sub-Transient Induction Machine Equivalent Circuit

II. Type II WTG Short-Circuit Model

The addition of the external rotor resistance to a Type II WTG acts as an impedance in the short circuit equivalent, thus lowering the maximum available fault currents of the induction machine. However, the Type II WTG is operated such that the external rotor resistance is applied only when necessary since the losses in the resistor bank equate to lost energy production from the generator (Muljadi, & Gevorgian, 2011). This makes the short circuit behaviour for a Type II WTG machine similar to that of a Type I WTG machine hence the same equivalent circuit for a Type I WTG machine shown in Figure. 2.9 is also used for a Type II WTG machine (Muljadi, & Gevorgian, 2011).

III. Type III WTG Short-Circuit Model

The short circuit behaviour of Type III WTG is modelled differently depending on the method used in protecting its rotor power converter. Figure. 2.10 and Figure. 2.11 shows the two methods used to protect the power converter on the rotor circuit for the Type III WTG.

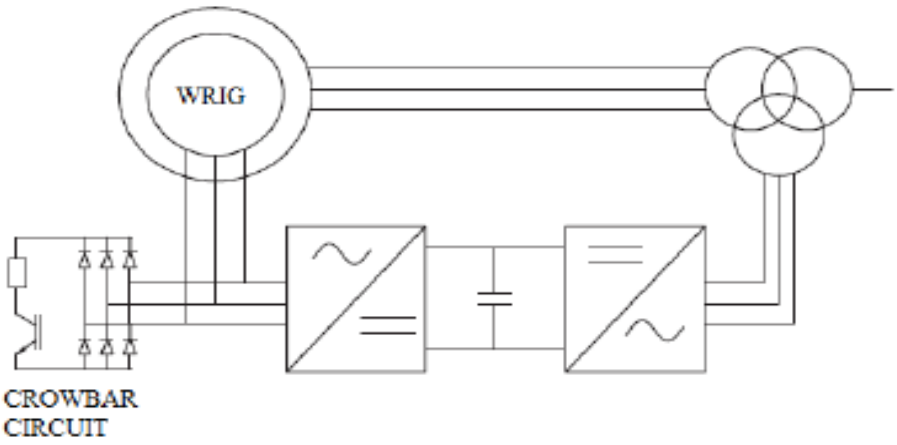

Figure 2.10: Type III WTG Crowbar Protection of the Power Converter

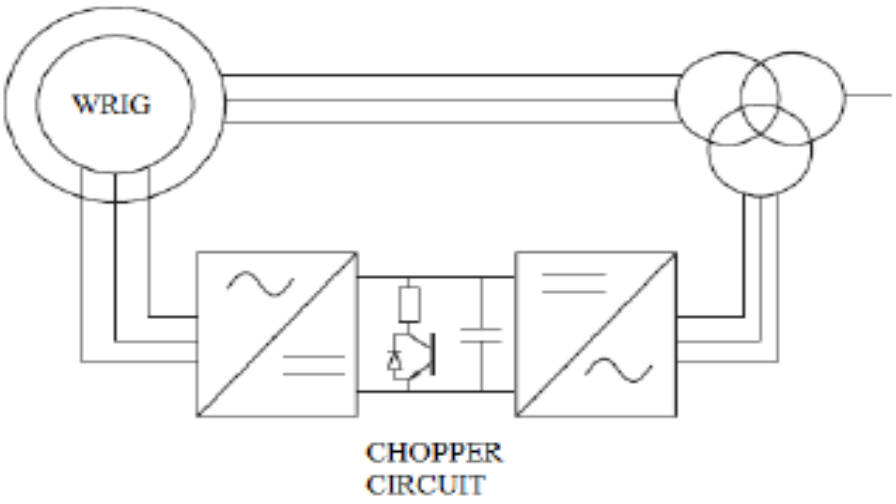

Figure 2.11: Type III WTG Chopper Protection of the Power Converter

The crowbar circuit diverts the short-circuit currents away from the power converter, essentially shorting out the rotor windings (Muljadi, & Gevorgian, 2011). The removal of the power converter during a fault makes the Type III WTG behave similar to the Type I WTG and the Type II WTG designs, where the worst case short circuit current is based on the internal impedance of the induction machine as shown in Figure 2-10. With a chopper circuit, better grid support such as low voltage ride through, is achieved during a fault by keeping the rotor converter active, but still limiting the currents to protect the sensitive electronic components within the power converters (Muljadi, & Gevorgian, 2011). When this method is used the short circuit contribution from a Type III WTG is similar to that of a Type IV WTG and the equivalent circuit is shown in Figure. 2-11.

IV. Type IV WTG Short-Circuit Model

Unlike the Type I, Type II and Type III designs where the short circuit behaviour is dominated by the generator characteristics, it is the design of the power converter that drives the electrical behaviour of the Type IV WTG (Muljadi, & Gevorgian, 2011). The power converter in the Type III design with the chopper circuit protection is sensitive to excessive currents, so too is the converter in a Type IV WTG design. In order to protect the power electronic devices a current limit of 1.1pu is designed

into the power converter (Muljadi, & Gevorgian, 2011). Rather than the common voltage source behind an impedance short circuit equivalent used to model other generators, the Type IV WTG is a current source designed for maximum short circuit contribution as shown in Figure. 2.12.

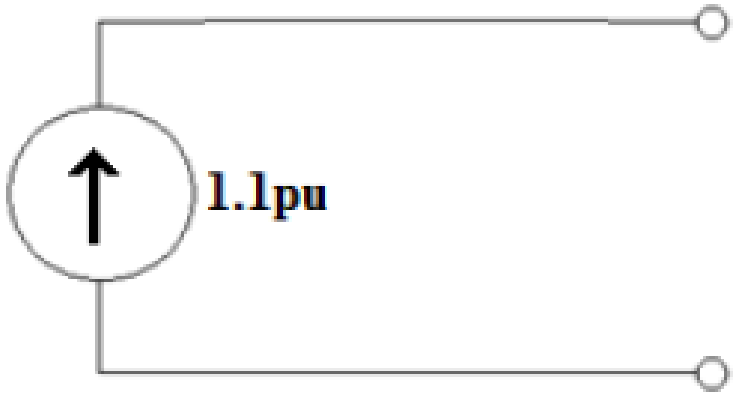

Figure 2.12: Type IV WTG Short-Circuit Equivalent

2.3 Over-Current Protective and Current Limiting Devices

An electrical power system is composed of several sections generally categorized into: the generating stations; the transmission and the distribution infrastructures; and the loads. While these are the basic elements of an electrical power systems network, there are other important components over-current protective devices (OCPDs) being some of them. Protection relaying and OCPD's coordination are some of the features of a power system network design concerned with minimizing damage to equipment and interruptions to service when electrical failures occur (Square, 2006). The function of the OCPDs is to cause the prompt removal from service of any element of a power system which has been affected by a short circuit or when the element operates in an abnormal manner that might cause damage and interfere with the effective operation of the rest of the system.

2.3.1 The Fuses

i. Classification of Fuses

A fuse is a thermal tripping device in an electric circuit, the operation of which depends on the thermal capacity of the fusing element, its melting temperature and the current flow previous to the fault condition. Fuses offer the least amount of adjustments amongst the OCPDs and a fuse improperly applied might fail to operate resulting in considerable damage to the power system equipment and also can lead to a miss-coordination amongst the other OCPDs in the circuit (Square, 2006). Fuses are classified into two broad classes: the low voltage fuses and the power fuses. Low voltage fuses are designed for applications of 600V or lower and are categorized into two general types, the plug type and the cartridge type. Power fuses are rated over 600V and they provide consistent and fast protection for equipment short circuit faults where it is not economically viable to use circuit breakers (Square, 2006).

ii. Fuse Timing Response

Fuse timing response for a given level of over-current is separated into the melting time which is the time required to melt the current responsive element and the arcing time which is the time elapsed from the melting of the current responsive element to the final interruption of the circuit as shown in Figure 2.13 (Square, 2006). The arcing time is dependent upon the circuit characteristics such as the operating voltage and the network impedance.

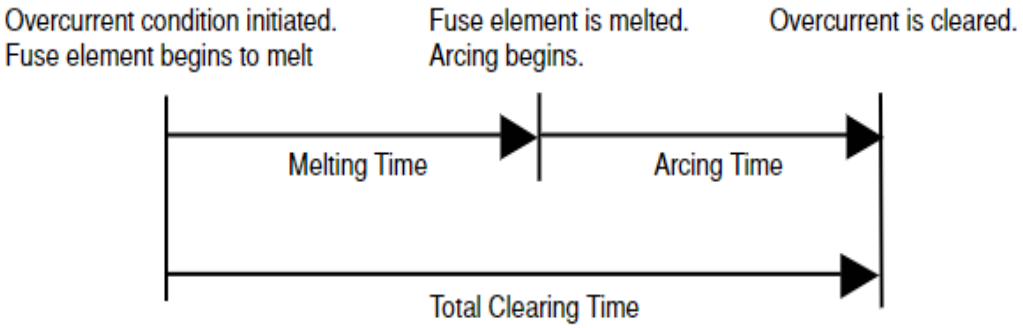

Figure 2.13: Fuse Timing Response

Fuses are typically assigned a Minimum Melting Time (MMT) characteristic and a Total Clearing Time (TCT) characteristic by their manufactures and these two time characteristics are used to define the boundaries for the fuses' coordination through their TCC curve as shown in Figure 2.14 (Square, 2006). For short circuit currents with time durations below and to the left of the fuse TCC curve, the fuse will not blow or be damaged. Short circuit currents with time duration above and to the right of the fuse TCC curve, the fuse will start melting within a minimum time given by the MMT characteristic and it would finally disconnect the circuit at a maximum time given by the TCT characteristic. The voltage ratings of a fuse is selected to be equal to or greater than the nominal system voltage on which it is being applied (Square, 2006). This rating is not a measure of its ability to withstand a specified voltage while carrying current, but rather it is the ability of the fuse to prevent the open circuit voltage of the system from restraining and establishing an arc once the fuse link has parted (Square, 2006). The continuous current rating of a fuse should be equal to or less than the current carrying capacity of the circuit it is protecting (Square, 2006). Figure 2-14 Square (2006) shows the typical behaviour of a fuse MMT curve and TCT curve. Both the MMT and the TCT curves are used to define the fuse operating points for fuse-fuse coordination purposes

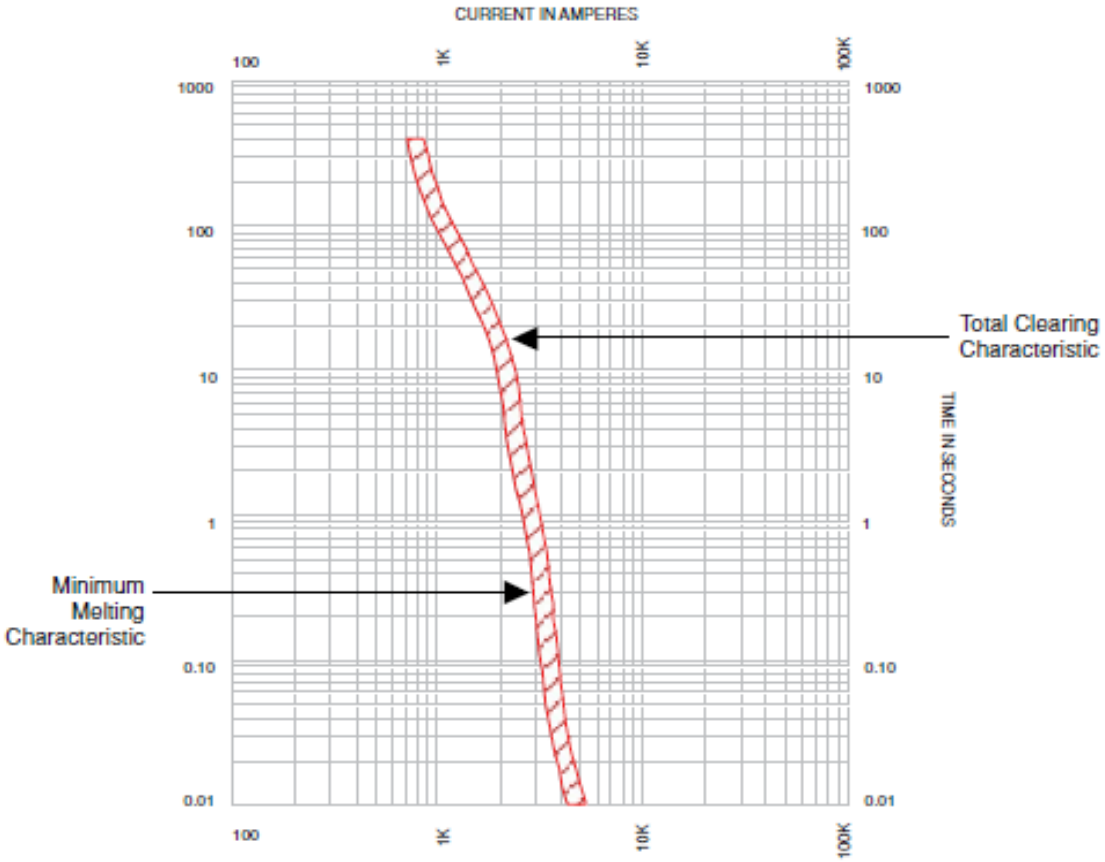

Figure 2.14: Fuse MMT and TCT Time Current Characteristic Curves

Source: (Square, 2006)

2.3.2 The Circuit Breakers

A circuit breaker has two regions which are usually used for coordination, the overload region, and the instantaneous region, and these regions indicate the different interrupting features of the circuit breaker. Within the overload region, the curve describes how the circuit breaker will operate during an overload. Within the instantaneous region, the curve is usually much steeper and completely vertical, until it meets the “foot” and the operation of the circuit breaker within this region is due to a short circuit event. A circuit breaker has two operating curves the minimum unlatching curve and the maximum interrupting curve as shown in Figure 2.15 (Square, 2006).

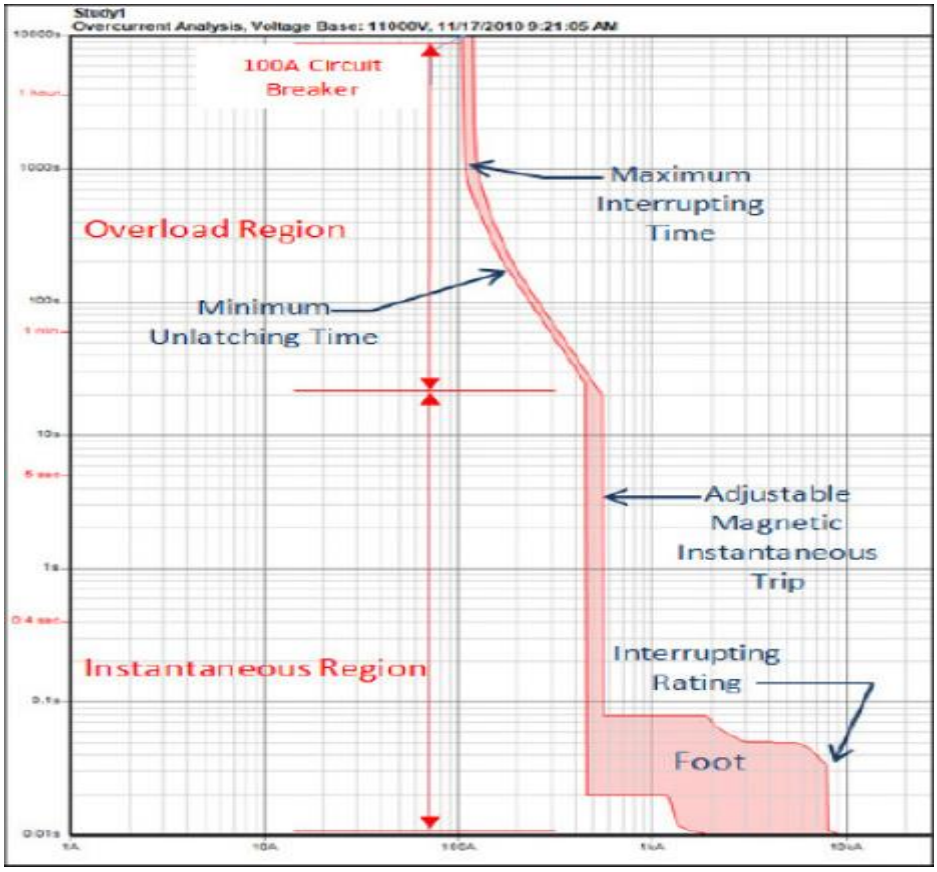

Figure 2.15: Circuit Breaker Time Current Characteristic Curves

Source: (Square, 2006)

The most critical characteristic for a circuit breaker is the interrupting rating which is the absolute maximum current for which the device has been designed to operate at and this interrupting rating is represented on the TCC curve with the vertical cut-off at the right hand side of the foot as shown in Figure 2.15 (Square, 2006). The requirement that the TCC curves should not overlap is a tall order for some circuit breakers due to their instantaneous regions overlapping particularly at the foot.

2.3.3 The Re-Closer

A re-closer is a device designed to initiate isolation of a part of the electric power system in case of a fault or other abnormal conditions. A Re-closer detects a fault and then opens for a pre-programmed number of times before closing automatically. This automatic close is referred to as an auto-reclose and the multiple open and close

operations are utilized to clear transient/temporary faults occurring in the power system. If the fault is permanent the re-closer will eventually open and not attempt to close until instructed by the operator. This state is referred to as the re-closer lockout and manufacturers have standardized on a maximum of three or four protection trip operations before lockout occurs (Javadian, & Massaeli, 2011). A re-closer has two types of curves, the fast reclose curve and the slow reclose curve and the operating sequence of a re-closer is between the two curves. The two curves are used to coordinate a re-closer with other OCPDs in a power system network during a fault and there is always a time interval between the two set of curves when the re-closer remains open with a sequence of fast-fast operation and slow-slow operation (Javadian, & Massaeli, 2011). Figure 2.16 shows the re-closer slow and fast reclose curves.

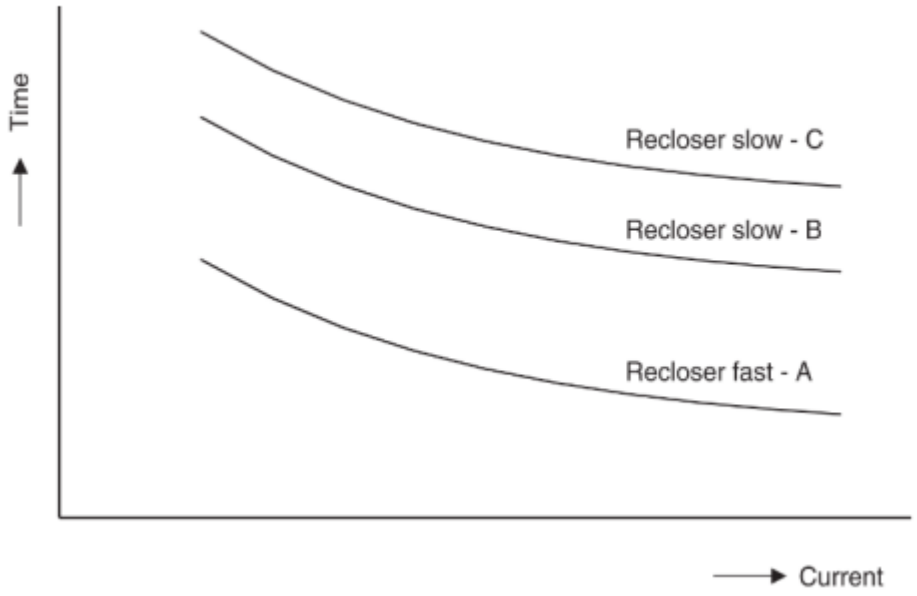

Figure 2.16: Re-closer Fast and Slow Reclose Curves

2.3.4 The Over-Current Relay

An over-current relay (OCR) is an inverse definite minimum time dependant OCPD in which its operating time is approximately inversely proportional to the fault current near its pick-up value and becomes substantially constant slightly above it.

Relays have a long working time at low products of setting currents and generally short working time at high multiples of the setting currents (Hewiston et al., 2004). OCRs are classified based on their characteristic curves which define their speed of operation as normal inverse, very inverse or extremely inverse with the relays' defining curves shown in Figure. 2.17 (Hewiston et al., 2004).

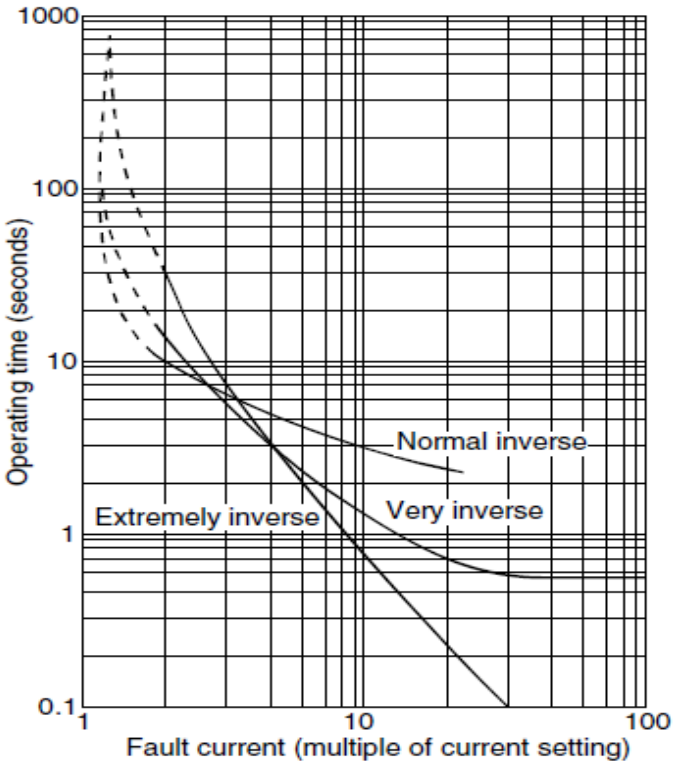

Figure 2.17: Over-Current Relay Time Current Characteristic Curves

2.3.5 Fault Current Limiting Reactor

A FCL reactor is a coil used to limit currents during a fault condition. It is widely used for fault current limitation in medium and low voltage distribution systems and is the simplest type among the fault current limiters. A FCL reactor has a large value of the inductive reactance and a low value of the ohmic resistances and its current limiting strategy is achieved by inserting an additional impedance in series with the transmission and distribution lines as shown in Figure 2.18 (Soria et al., 2014; Akpeh et al., 2015; Akpeh et al., 2015b).

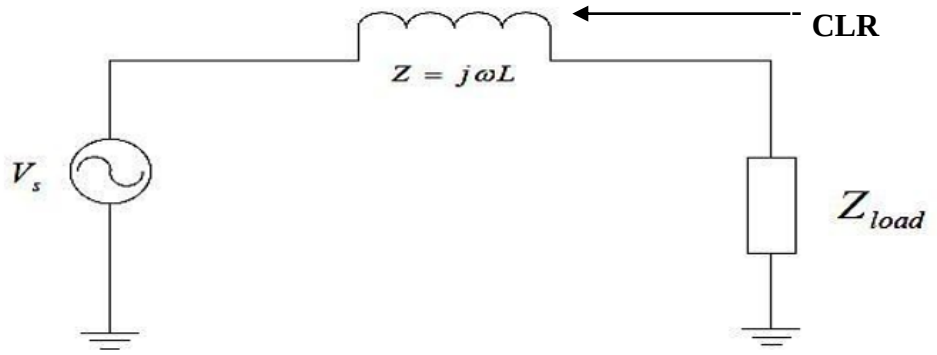

Figure 2.18: Fault Current Limiting Reactor

2.3.6 Pyrotechnic Fault Current Limiters

The pyrotechnic FCLs consists of an extremely fast switch which is capable of carrying a high rated current but is incapable of limiting fault currents. In the pyrotechnic FCL, the rated current flows through the main bus where explosive material is connected to act as an opening switch when the short circuit is detected. After the explosion, the short circuit current flows through a fuse capable of interrupting the high magnitudes of the short circuit fault currents (Soria et al., 2014; EL-Ela et al., 2022). The advantages of pyrotechnic FCL is their fast actuation, low losses under regular operation, and a high current reduction rate. However, some drawbacks are reported as spurious trips, non-automatic recovery and the need to replace the explosives after the FCL actuation (EL-Ela et al., 2022; Majeed et al., 2023). Figure 2.19 shows the pyrotechnic FCL.

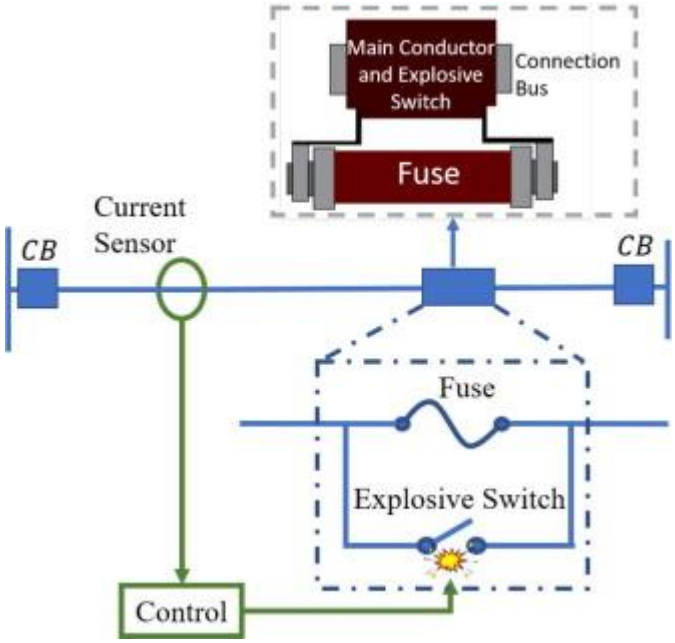

Figure 2.19: Pyrotechnic Fault Current Limiter

2.3.7. Superconducting Fault Current Limiters

The superconducting fault current limiter (SFCL) is a novel electrical equipment which has the capability to reduce the fault current level within the first cycle of fault current occurrence. It uses the properties of superconductors to reduce the value of the fault currents since superconductor materials lose their electrical resistance below certain critical values of temperature, magnetic field, and current density (Majeed et al., 2023; Alam et al., 2018). SFCLs utilizes variable impedance which is connected in series with the electrical system that varies depending on the power systems operating conditions (Majeed et al., 2023; Alam et al., 2018). When a fault occur, the SFCL limits the fault current by an increased inductive or resistive impedance of conducting layer due to the large fault current. The impedance rises to a value where the fault current is correspondingly reduced to a lower level where the OCPDs are capable of handling. SFCLs are basically of two types, the resistive and the inductive types as shown in Figure 2.20 and Figure 2.11 respectively (Alam et al., 2018).

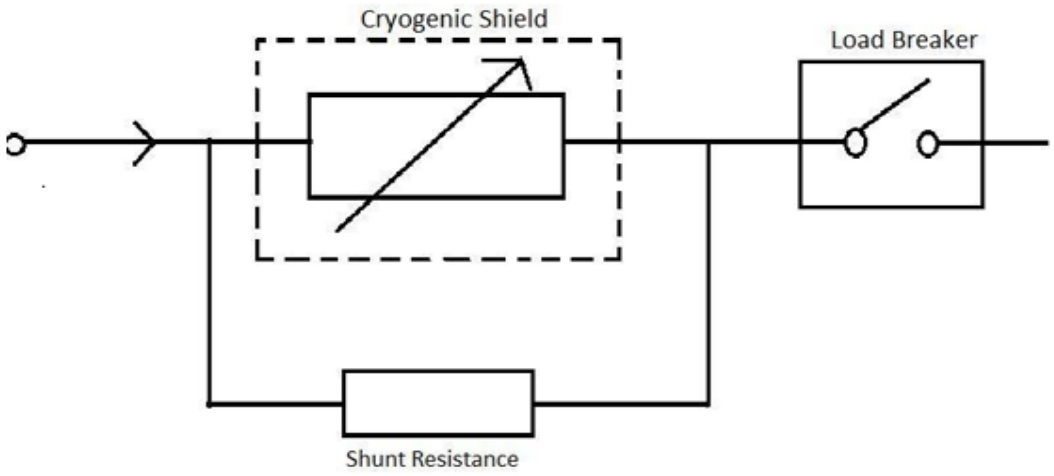

Figure 2.20: Resistive Type SFCL

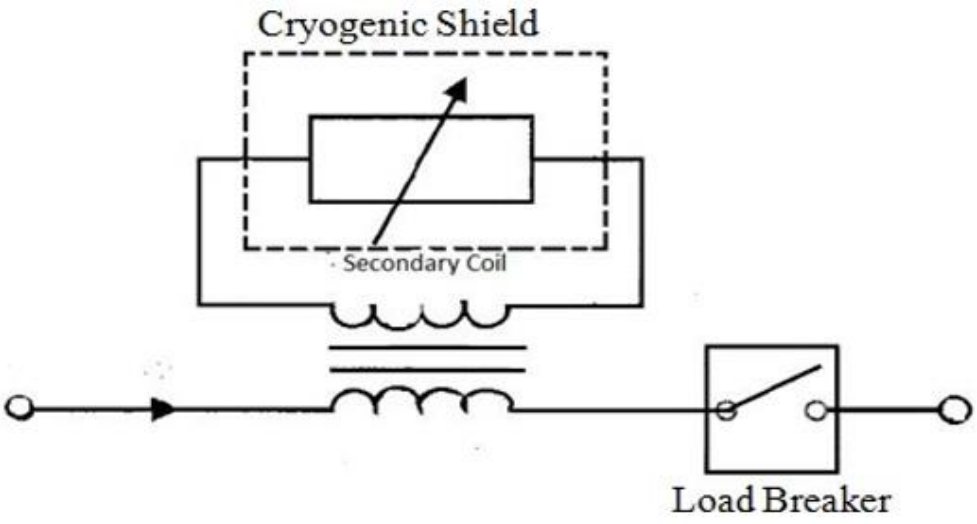

Figure 2.21: Inductive Shielded Type SFCL

2.3.8. Solid State Fault Current Limiters

The solid-state fault current limiters (SSFCL) consist of semiconductor devices which are able to interrupt a fault current during its rise before the peak value is reached (Majeed et al., 2023; Alam et al., 2018). SSFCLs use a combination of inductors, capacitors and thyristors to achieve fault limiting functionality with the current limiting behaviour of SSFCLs based on on/off status change of semiconductor switching devices (Majeed et al., 2023; Alam et al., 2018). A current limiting impedance is connected in parallel with the solid state switch so that the

current continue to flow but at a limited level after the solid state switch interrupts the fault current. SSFCL can be classified into, the series, the bridge and the resonant types as shown in Figure 2.22, Figure 2.23 and Figure 2.24 respectively (Majeed et al., 2023; Alam et al. 2018)

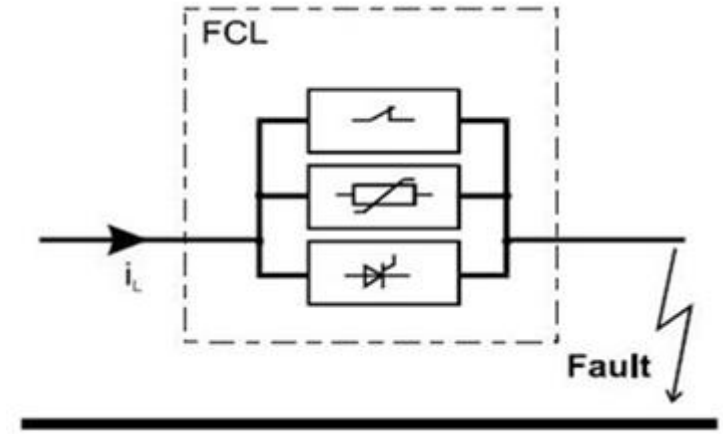

Figure 2.22: Series Switch-Type FCL

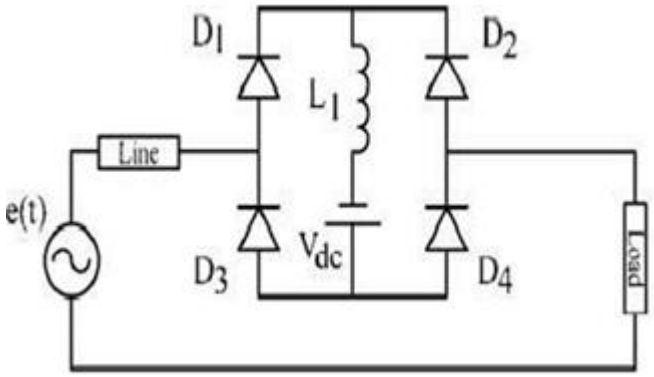

Figure 2.23: Bridge Type SSFCL

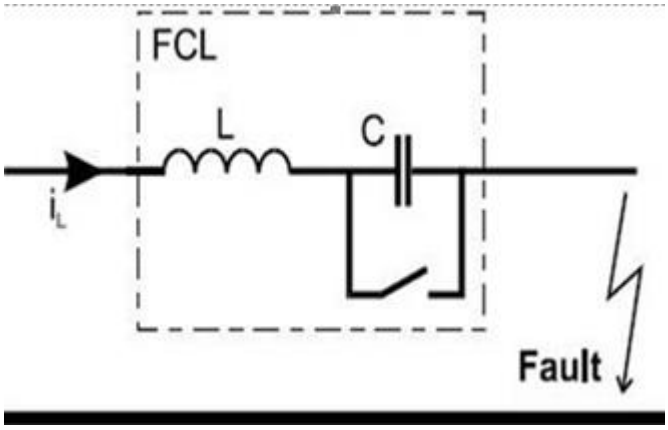

Figure 2.24: Resonance Type SSFCL

2.4 Symmetrical Components

2.4.1 Symmetrical Components Theory

The basic theory of symmetrical components stipulates that the phase currents and voltages in three phase electrical systems can be represented by a set of three symmetrical components. During the normal and balanced operations of a power system network the system phase currents are equal in magnitudes and are displaced by exactly 120° from each other hence only the positive sequence currents flows through the network. During a fault, the phase currents become unbalanced and of unequal magnitudes with their phase displacement being more or less than 120º (Dupuis et al., 2017; Gonen, 2009; Schweitzer, & Zocholl, 2004). The imbalances in the magnitudes and the phase angles on the network phase currents gives rise to the negative and the zero sequence components of currents and voltages. The presence of the negative and the zero sequence currents in a power system network describes the presences of an unbalanced condition commonly caused by short circuit faults (Dupuis et al., 2017; Gonen, 2009; Schweitzer, & Zocholl, 2004).

The impedance offered by an equipment or circuit to flow of positive sequence currents is called the positive sequence impedance while the negative sequence impedance is the impedance offered by the network to the flow of negative sequence currents. The negative sequence currents have a rotation opposite that of the positive sequence currents (Dupuis et al., 2017; Gonen, 2009; Schweitzer, & Zocholl, 2004).

The impedances offered by any circuit or equipment to zero sequence currents is called the zero sequence impedance.

2.4.2 Synchronous Machines Sequence Impedances

The positive, negative and zero sequence impedances of rotating machines are generally different. The positive sequence impedance of a synchronous generator is equal to the synchronous impedance of the machine with the negative sequence impedance being much less than the positive sequence impedance (Schweitzer, & Zocholl, 2004).

The sub-transient reactance for a synchronous generator is used to determine the current during the first cycle after a fault as occurred and it represents the positive sequence impedance. Negative sequence impedance is 70-95% of the sub transient reactance hence the impedance can be approximated by the sub transient reactance (Gonen, 2009; Schweitzer, & Zocholl, 2004). With sinusoidally distributed three phase windings, the net flux at any point in the air gap is zero hence, zero sequence impedance is only a small percentage of the positive sequence impedances (Dupuis et al., 2017; Gonen, 2009; Schweitzer, & Zocholl, 2004).

2.4.3 Induction Machines Sequence Impedances

In induction machines, the transient state of the fault current is damped quickly within the first two cycles and during the fault, the rotor is driven by inertia of the load and the rotor itself. There is no DC field excitation on the rotors for induction machines during a fault hence the rotor winding is short circuited with the rotor excitation only due to the induced fields in the rotor from the rotating stator magneto motive force. As stator excitation is lost and rotor slows down, the excitation force is lost quickly (Dupuis et al., 2017; Gonen, 2009; Schweitzer, & Zocholl, 2004).

The positive sequence currents circulating in the stator windings of a three phase induction motor generates a rotating magnetic field that crosses the air gap. During normal operation, the rotor of the induction motor rotates at a slightly lower speed than the speed of the magnetic flux generated by the stator. The difference in speed

causes low frequency currents to flow in the rotor bars hence the current contribution of an induction motor rotor to a terminal fault reduces and disappears completely after a few cycles and as a consequence, only the sub transient value of reactance is assigned for the positive and the negative sequence impedance the impedance value being equal to the locked rotor reactance (Dupuis et al., 2017; Gonen, 2009; Schweitzer, & Zocholl, 2004). Zero sequence impedance can be treated in similar ways as synchronous machines since the rotor plays no significant role with only the machine grounding having a significant role in determining the path taken by the zero sequence currents.

2.4.4 Power Transformers Sequence Impedances

Since transformers have the same impedance with reversed phase rotation, their positive and negative sequence impedances are equal this value being equal to the impedance of the transformer. However, the zero sequence impedance depends upon the grounding/earth connection. If there is a through circuit for the neutral currents, zero sequence impedance will be equal to the positive sequence impedance otherwise it will be infinite (Dupuis et al., 2017; Gonen, 2009; Schweitzer, & Zocholl, 2004). The impedance to the flow of zero sequence currents in three phase transformers is generally lower than the positive sequence impedance because there is no return for the zero sequence exciting flux, hence the flux linkages with the zero-sequence exciting currents are low (Dupuis et al., 2017; Gonen, 2009; Schweitzer, & Zocholl, 2004).

2.4.5 Transmission Lines Sequence Impedances

The positive sequence and the negative sequence impedances of a transmission line are the same this value being equal to the impedance of the line. This is because the phase rotation of currents does not make any difference in the constants of the line. However, the zero sequence impedance is usually much greater than the positive or negative sequence impedance of lines (Dupuis et al., 2017; Gonen, 2009; Schweitzer, & Zocholl, 2004).

2.5 Equipment Protection Requirements, Landmarks and Damage Curves

Equipment protection is an important part of the protection coordination process. Every equipment has its own protective requirements and limitations which are described and identified by use of their various protection landmarks and damage curves (Smith, 2006). Protection coordination is performed by comparing the protection landmark points for each of the equipment to be protected with the OCPD's curves on a TCC curve. A TCC curve is a log-log type of graph having a time plot on its vertical axis and current plot on the horizontal axis. The procedure involved in applying the characteristic curves in a coordination study is to select or set the various protective devices such that their characteristic curves from the load to the source are located from left to right of the TCC with no overlapping of the curves. This results in a set of coordinated curves on one composite TCC graph (Smith, 2006).

2.5.1 The Power Transformer Protection Requirements

Appropriate transformer protection should be used with the objectives of protecting the electrical power system in case of a transformer failure and to protect the transformer itself from the power system disturbances. OCPDs such as fuses, circuit breakers, re-closers and relays have well defined operating characteristics (Smith, 2006). The TCC curves for these OCPDs should be coordinated with the transformer capability curves and protection landmark points namely, the transformer full load ampere mark, the transformer magnetizing inrush current points and both the thermal and the mechanical transformer damage curves for a coordinated power transformer protection to be achieved (Smith, 2006).

i. The Transformer Full Load Ampere Mark

The Full Load Ampere (FLA) is the rated continuous current carrying capacity of a transformer at a referenced ambient temperature and allowable temperature rise. The FLA mark is located at the top of the transformer TCC at the 1000 seconds mark as shown in Figure 2.25 (Smith, 2006).

ii. The Transformer Through-Fault Damage Curves

The power transformer through-fault damage curves, both the thermal and mechanical curves, are plotted at the top three decades of the transformer TCC curve from the 2 seconds mark to the 1000 seconds mark as shown in Figure 2.25 (Smith, 2006).

iii. The Transformer Magnetizing Inrush Current Points

As shown in Figure.2.25, one or more magnetizing inrush current points may be plotted on a TCC curve for a power transformer. The magnetizing inrush currents are expressed in peak amperes with the most common points being at 8 or 12 times the rated FLA at 0.1 seconds mark and/or at 25 times of the rated FLA at 0.01 seconds mark (Smith, 2006).

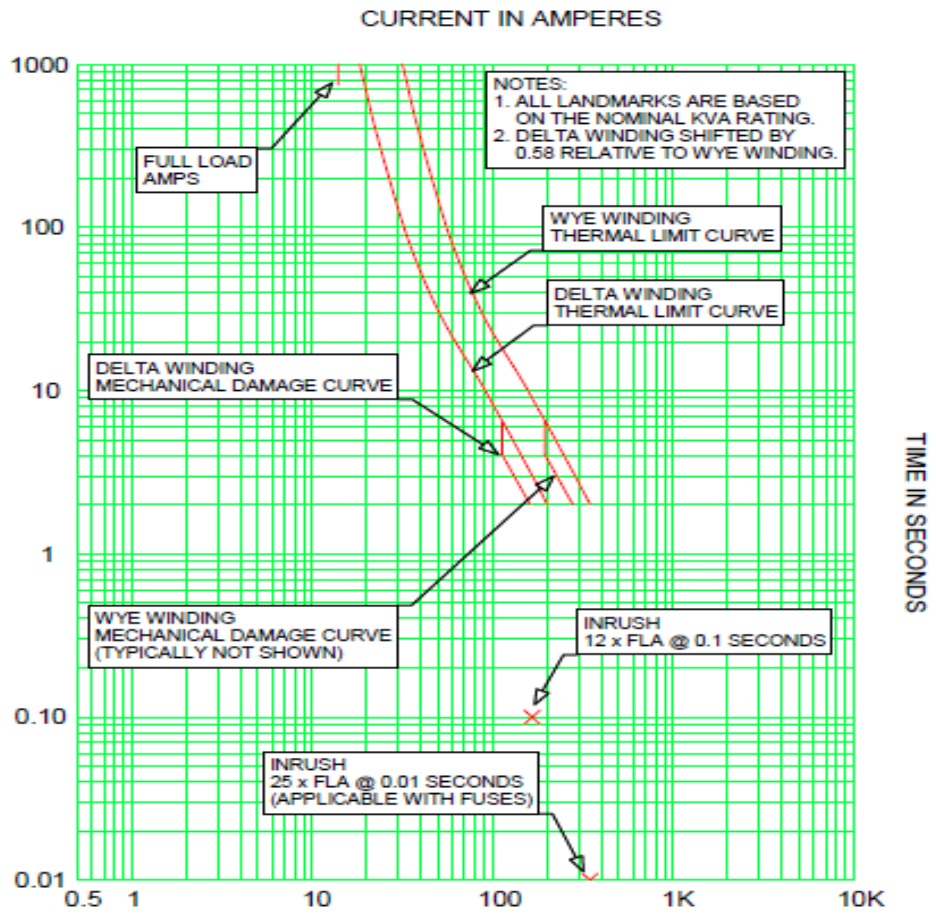

Figure 2.25: Transformer TCC Curves, Full load Ampere Mark, Magnetizing Inrush Points, Mechanical and Thermal Damage Curves

iv. The Power Transformer Protection Settings

After identifying the transformer FLA mark, the magnetizing inrush points and the thermal and mechanical damage curves, the transformer operation and damage area are now identified (Smith, 2006). The transformer operating area is located to the left and below the FLA mark and to the left and below the transformer magnetizing inrush points while the transformer damage area is located to the right and above the through-fault damage curves. The OCPD's TCC curves used to protect the power transformer are set: above the transformer FLA mark; above the transformer magnetizing inrush points; and below the transformer through-fault damage curves as shown in Figure 2.26 (Smith, 2006).

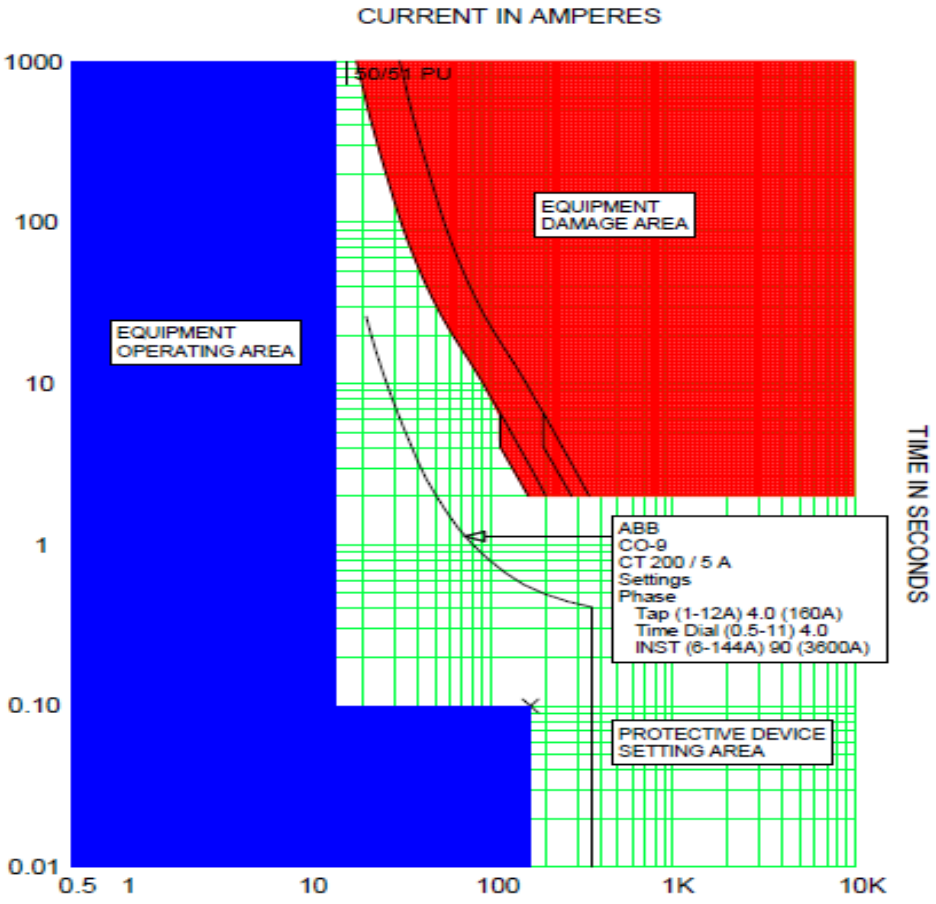

Figure 2.26: Transformer Over-Current Protective Devices TCC Setting Curves

2.5.2 The Overhead Lines, Underground Cable Conductors and Nodes Protection Requirements.

i. The Overhead Lines, Underground Cable Conductors and Nodes Ampacity Mark

The ampacity is the rated continuous current carrying capacity of a conductor at a referenced ambient temperature and allowable temperature rise. If a conductor is loaded continuously above its rated ampacity the insulation temperature design limits will be exceeded (Smith, 2006). This will lead to loss of conductor life and not instantaneous failure. If a bare aerial conductor is loaded continuously above its rated ampacity the mechanical strength of the conductor is reduced. This will lead to loss of the conductor mechanical life and may result in instantaneous conductor failure. The electrical conductor's ampacity landmark is located at the top decade of the conductor's TCC curve at the 1000 seconds mark as shown in Figure 2.27 (Smith, 2006).

ii. Overhead Lines, Underground Cable Conductors and Nodes Intermediate Thermal Overload Limit Curve

The intermediate thermal overload limit curve of an electrical conductor is the over-current operating limit that if exceeded will damage the insulation of an insulated power conductor. This will lead to loss of conductor life and not an instantaneous conductor failure. Intermediate thermal overload limit curves are based on the thermal inertia of the conductor the insulation and the surrounding material. The electrical conductor intermediate overload limit curve is located at the upper 2 decades starting from the 10 seconds mark to the 1000 seconds mark as shown in Figure. 2.27 (Smith, 2006).

i. **Overhead Lines, Underground Cable Conductors and Nodes Short Circuit Damage Curve.**

As shown in Figure. 2.27, this is the ampere limit that if exceeded will damage the conductor or the insulation of a power conductor. Short circuit damage curves are plotted in the lower three decades of the conductor TCC curve starting at the 10 seconds mark downwards to the 0.01 seconds mark (Smith, 2006).

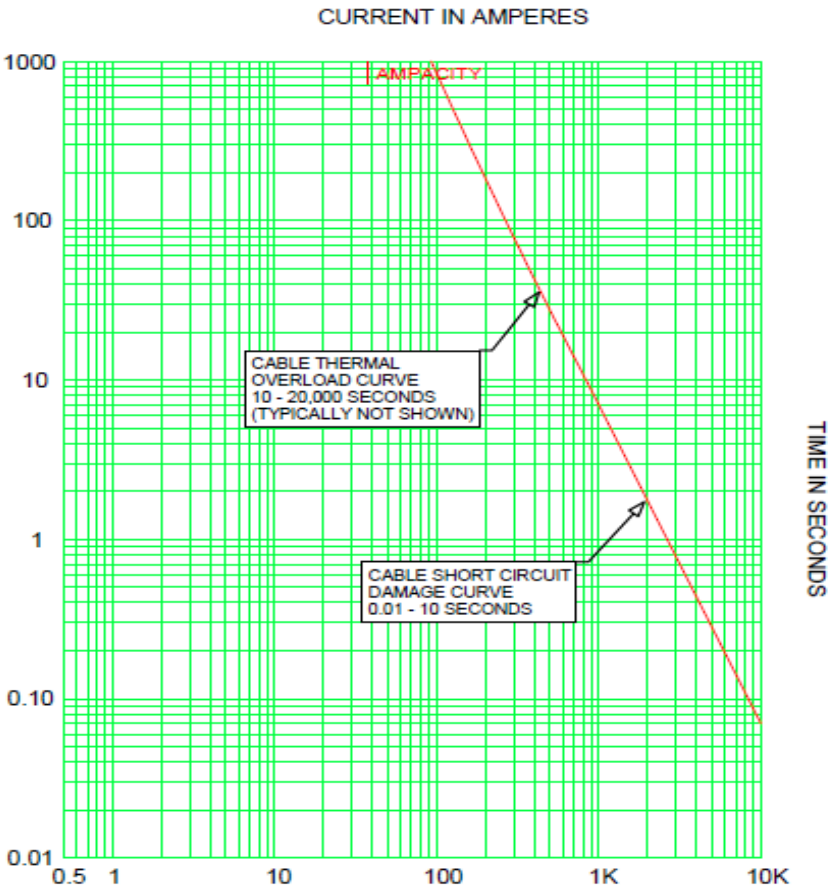

Figure 2.27: Overhead Lines, Underground Cables Conductor and Nodes TCC Curves, Ampacity Mark and Short Circuit Damage Curves

ii. **Overhead Lines, Underground Cable Conductors and Nodes Protection Settings**

The conductors and the nodes operating area is located to the left and below the ampacity mark while the damage area is located to the right and above the intermediate thermal overload limit curve and above the short circuit damage curve. The OCPD's TCC curves used to protect the conductors and the nodes are set: below the ampacity mark; below the intermediate thermal overload limit curve; and below the short circuit damage curve s as shown in Figure 2.28 (Smith, 2006).

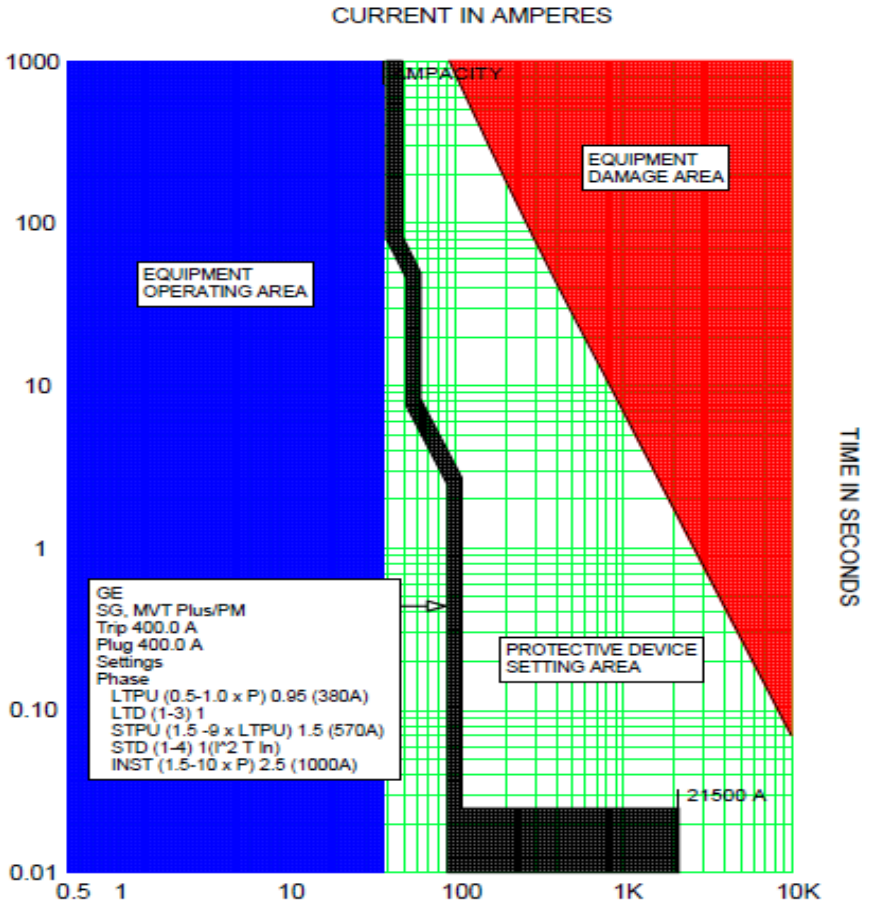

Figure 2.28: Overhead Lines, Underground Cables Conductor and Nodes Over-Current Protective Device TCC Setting Curves

2.5.3 Equipment Over-Current Protection Constraints.

i. Feeder Protection Constraints

While protecting feeders, selectivity between the upstream and the downstream OCPDs is achieved by establishing suitable time margins between their operating points. NEC article 240-101 states that “Feeders rated over 1000 V must have over current protection provided either by a fuse rated not more than 300% of the feeder ampacity or by a circuit breaker with a long time trip element set not more than 600% of the feeder ampacity” (ELG4126, nd). The OCPDs must clear the faults prior to reaching the withstand capability of the equipment to be protected hence the

OCPDs must be set to provide over-current protection as per the NEC 240.101 requirements (ELG4126, nd). Selective coordination is achieved by using the following minimum recommended time margins between protective devices.

i. Re-closer — Fuse coordination: The recommended coordination minimum time margins of 0.12 seconds is required between the Re-closer and the fuse TCC curves (ELG4126, nd).
ii. Fuse — Fuse coordination: The total clearing time (TCT) of the downstream fuse must be less than 75% of the minimum melting time (MMT) of the upstream fuse to account for pre-loading. This translates to a minimum of 0.025 seconds time margin between the downstream fuse TCT curve and the upstream fuse MMT curve (ELG4126, nd).
iii. Fuse — Re-closer coordination: The recommended coordination minimum time margins of 0.12 seconds between the fuse and the Re-closer TCC curves (ELG4126, nd).

ii. Power Transformer Protection Constraints

A power transformer primary winding and secondary winding protective devices must be set within the NEC450.3 requirements for transformer overload protection to allow the normal magnetizing inrush currents to flow (Hewiston et al., 2004). The transformer primary winding protective device must not operate for the normal magnetizing inrush currents that occur when energizing the transformer. The inrush point is established at 8 times the power transformer FLA for a period of 0.1 seconds for transformers under 2500 kVA and for transformers above 2500 kVA the inrush point is 10 or 12 times the transformer full load current for a period of 0.01 seconds (Hewiston et al., 2004). The transformer protection coordination constraints states that the continuous current ratings for the OCPDs used in protecting the power transformers are (Hewiston et al., 2004);

i. Transformers having percentage impedance less than 10% the primary windings protection must have an upstream fuse rated at 300% of the FLA ratings.

ii. Transformers rated over 1000V on the secondary winding and having percentage impedance less than 6% the secondary winding protection must have a downstream fuse rated at 250% of the FLA rating.

iii. Transformers rated over 1000V on the secondary winding and having percentage impedance between 6-10% the secondary winding protection must have a downstream fuse rated at 225% of the FLA rating.

iv. Transformers rated less than 1000V on the secondary winding and having percentage impedance less than 10% the secondary winding protection must have a downstream fuse rated at 125% of the FLA rating (Contreras et al., 2012).

2.6 Radial Distribution Power System Network Protection Coordination

The distribution network is a very important component of a power systems network since it is at this level that much of the power is utilized by the end users (Soria et al., 2014). Conventional electrical distribution systems are radial in nature designed for unidirectional power flow thus requiring simple protection schemes usually implemented by using fuses, circuit breakers, re-closers, over-current relays and sectionalizing switches (Elmarkabi, 2004). The distribution networks extends to remote areas consisting of several feeder lines, which are generally overhead and are exposed making them vulnerable to breakdowns resulting not only in mechanical damages but also electrical faults as well (Zayandehroodi et al., 2011). Distribution network's over-current protection and coordination is influenced heavily by both the equipment to be protected and the OCPD's ratings, settings, location for placement and their operating characteristics. A highly reliable performance of a distribution network can be achieved by installing different types of OCPDs leaving the coordination between them a critical aspect due to the varied operating characteristics of the various OCPDs (Zayandehroodi et al., 2011). Selective operation of the OCPDs used in protecting the feeders can be achieved by applying several methods of discriminating on faults so that we attain coordination for only the appropriate devices to function.

2.6.1. Methods of Faults Discrimination.

The major importance of any protection scheme is the identification of the faulty section of the power system network and its isolation from the rest of the system in minimum time. The common methods used for faults discrimination are those techniques which discriminate according to the location of the fault and those which discriminate as to the type of the fault. Those which discriminate based on the fault location are the most commonly used in distribution feeder over-current protection philosophies (Gonen, 2009). These forms of discrimination are the ones in which the behaviour of the OCPDs are dependent upon where they are located in the network relative to the point of fault occurrence. Fault discrimination can be achieved by grading the OCPDs either by their operating time, the fault current magnitudes, and the distance of fault location and the direction of flow of the fault currents.

i. Time Graded Systems

To ensure selectivity of operation under all circumstances in a radial feeder, the operating time of a protection scheme is increased from the far end of the protected circuit towards the generating point or main grid. This can be conveniently achieved with the help of OCPDs having time lag features added to them to allow closer grading by time between successive protective devices in the network (Gonen, 2009). As the number of OCPDs in series increases, the operating time increases towards the main grid, thus the high magnitude fault currents near the main grid are cleared after a longer interval of time which is a drawback to this scheme (Gonen, 2009).

ii. Current Magnitude Graded Systems.

This form of discrimination monitors the current magnitudes in the network since, during a fault, the magnitude of the fault currents will also vary with the location of the fault (Ravindranath & Chander, 1977).The OCPDs are set to pick-up at progressively higher currents towards the source enabling simple radial feeders to be protected based on their fault current magnitudes. The short-circuit currents along the length of the protected circuit increases as the distance from the fault location to the main grid decreases (Gonen, 2009).

iii. Current and Time Graded Systems

Schemes where speed of fault clearance is proportional to the magnitude of the fault currents are usually preferred where the higher the fault current the faster the OCPD's operating time (Gonen, 2009). This form of scheme is possible with inverse time over-current characteristics where grading is possible over a wide range of currents hence the OCPDs can be set within the design limits to any value of the IDMT required.

iv. Distance Graded Systems

The other method of detecting faults on transmission and distribution lines is by impedance measurement. This is accomplished by relay units that respond to a ratio of voltage to current hence that makes a component of impedance. Discrimination in a distance graded system is obtained by limiting the distance relay operation to a certain range of impedance with the operating limits of a distance relay usually given in terms of the impedance components, the resistance and the reactance (Gonen, 2009).

v. Direction of Current Flow Graded Systems

When it is important to limit tripping for faults in only one direction in a multiple source circuit, the use of directional relays becomes necessary. This grading is called direction of current flow graded system. The directional relays require two inputs which are the operating current and a reference which does not change with fault location. For phase relays, the polarizing quantity is the system voltage at the relay location. For ground directional reference, the zero sequence voltage is used (Gonen, 2009).

2.6.2 Zones of Protection

i. Primary Protection Zone

A distribution power system network is divided into various primary protection zones namely; generator protection zones, power transformer protection zones, bus/node protection zones, overhead lines protection zones, underground cables protection zones and the load protection zones. The main protection scheme for a given zone of protection is called the primary protection scheme (Gonen, 2009). A primary protection zone is that part of a power system guarded by a certain/specific protective device and usually contains one or at most two elements of the system. The primary protection zones are arranged to overlap each other so that no part of the power systems remains unprotected. Each primary zone has its own OCPDs for disconnecting that zone from the rest of the system during a fault.

ii. Back-Up Protection Zone

Back-Up protection is provided for possible primary OCPD's failures. Back-up OCPDs are slower than the primary OCPDs and they isolate more of the power system elements than is necessary when clearing a fault. The backup protection must not operate until primary protection has had a chance to clear a fault .Because of this, there is a time delay associated with the backup protection with respect to the primary protection. Operation of a protective device in its back-up zone before a primary device operates indicates a lack of coordination among the devices or a primary protective device failure (Gonen, 2009).

2.6.3 Re-closer - Fuse Coordination

A re-closer is a device which has the ability to interrupt the distribution circuit for a predetermined period of time during a fault event then automatically recloses to re-energize the circuit once again. When a re-closer is coordinating with a fuse for a temporary fault, the re-closer fast reclose curve operates first. If the fault persists after the fast reclose curve closes, then the fault is a permanent one and the fuse MMT indicated as fuse MM curve must operate to clear the fault and the fault should

be cleared in a TCT indicated as the fuse TC curve on the Re-closer-Fuse coordination curve of Figure 2-29 (Javadian, & Massaeli, 2011; Funmilayo, 2010).

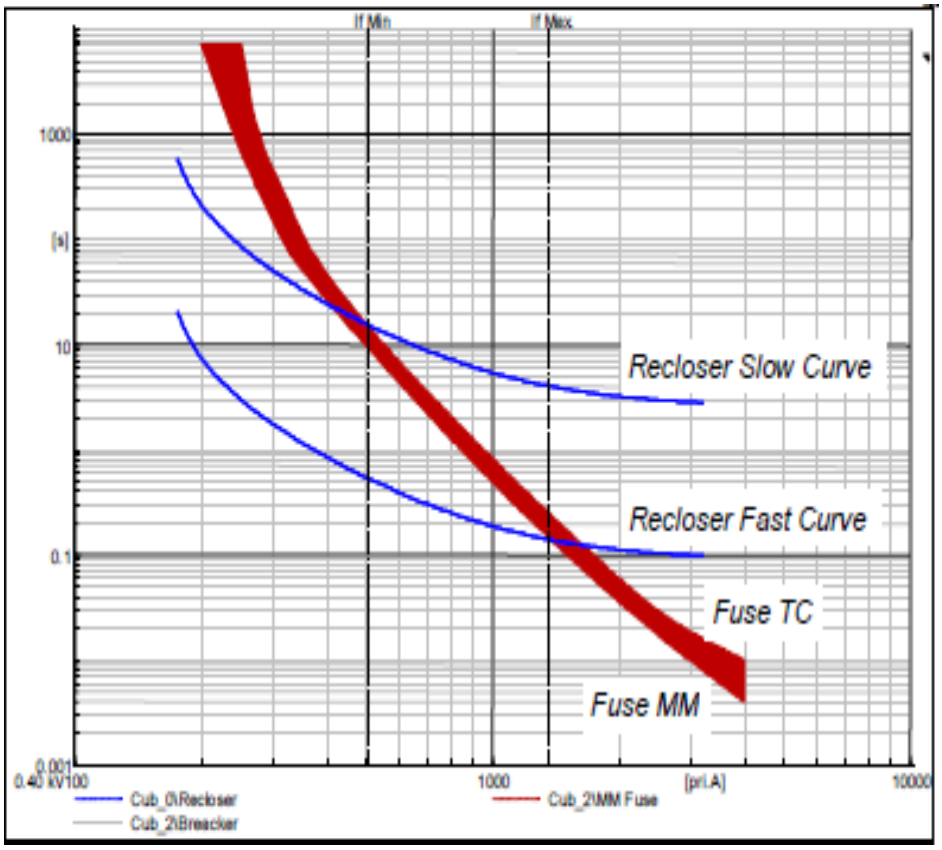

Figure 2.29: Re-Closer-Fuse Coordination TCC Curves

2.6.4 Fuse-Fuse Coordination.

The essential criterion for fuse-fuse coordination is that the TCT for the downstream fuse should not exceed 75 percent of the MMT of the upstream fuse for the same current level as indicated in Figure 2.30 (Bussman Cooper, nd). The factor of 75 percent compensates for effects such as the load current, the ambient temperature, or the fatigue in the fusing element caused by the heating effect of the fault currents passing through the fuse to a downstream fault but were not sufficiently large enough to melt the fuse (Bussman Cooper, nd). The coordination between the upstream fuse and the downstream fuse is achieved by drawing the fuses TCCs as shown in Figure 2.30.

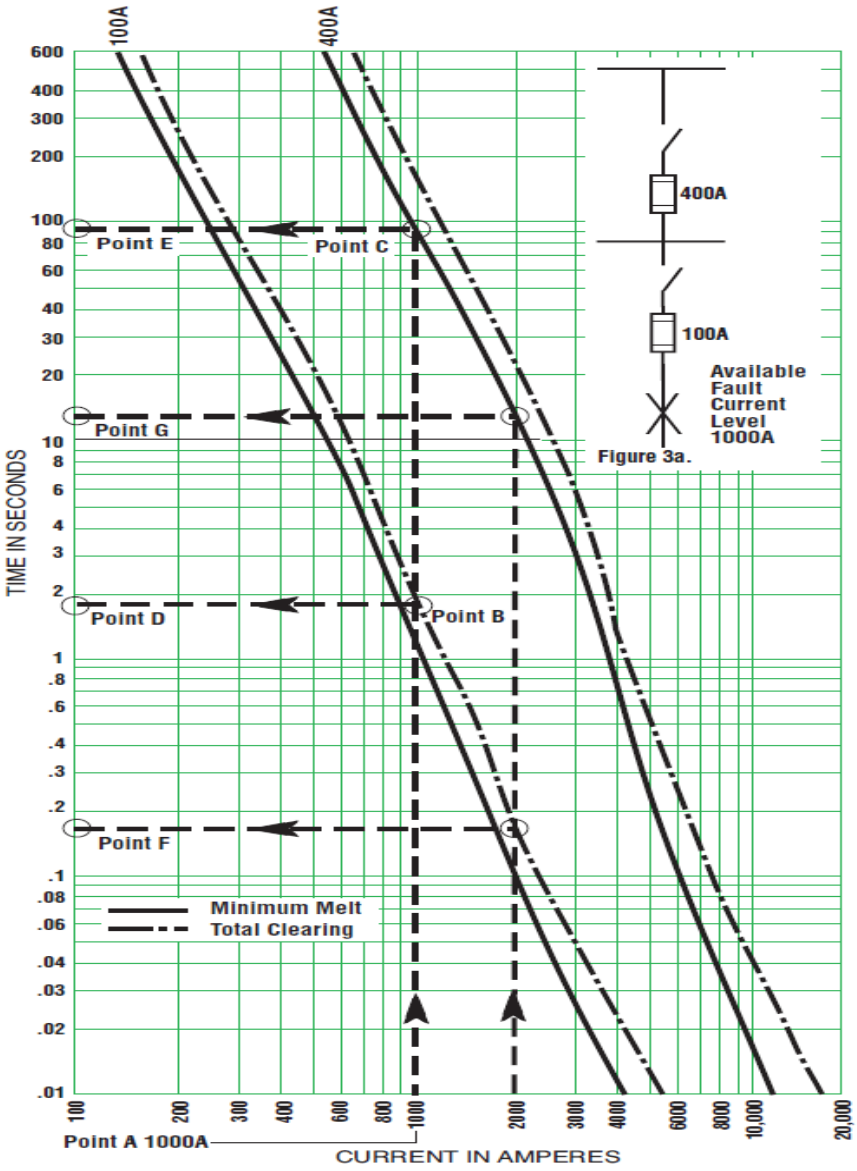

Figure 2.30: Fuse-Fuse Coordination TCC Curves

In the system shown in Figure 2.30, the available short circuit current is 1000 A at the downstream 100A fuse located at point A on the horizontal scale. Following a vertical line up from the 1000 A on the horizontal axis up to the intersection of the TCT for the 100A fuse at point B (from point A to B on the graph), then, from that intersection point B follow a horizontal line left to the vertical axis mark at point D. Point D shows how long the 100A fuse will experience the short circuit fault of 1000 A before opening the circuit. In a selectively coordinated system, only the fuse 100A will operate. If a vertical line from B is continued up to the MMT curve at a point C,

then over to the left to point E, the MMT to operate the upstream 400A fuse is found. The difference between the upstream fuse MMT and the downstream fuse TCT is 88 seconds thus, selective coordination is ensured with a 1000 A short circuit fault between the upstream 400A fuse and the downstream 100A fuse (Bussman Cooper, nd).

2.7 Impacts of Distributed Generation on Distribution Network Protection Coordination

2.7.1. Impacts of DGs on Distribution Network Short Circuit Current Levels

The presence of DGs in a distribution network affects the fault current levels by creating an increase as compared to when there is no DG connection (Ravindranath & Chander, 1977). When DGs are connected to a radial distribution network, in the event of a fault occurrence, all OCPDs downstream of its connection point will experience an increase in the short-circuit currents for all downstream faults with the nature of the DG interfacing technology also affecting the short circuit current levels. With increase in the number and the capacity of the DGs penetrating a given distribution network/feeder, the short circuit current levels are altered enough to cause miss-coordination among the OCPDs during a fault leading to unnecessary OCPD operations hence a reduction on the reliability of the feeder (Elmarkabi, 2004). As the fault current increases, it is apparent that it becomes more difficult to coordinate two or more OCPDs. The higher the current level at which two OCPDs are coordinated, the more difficult the coordination efforts become because their TCC curves are located/placed at the instantaneous region of the composite TCC curves below the 0.1 seconds mark at the foot (Elmarkabi, 2004)

2.7.2 Impacts of DGs on Conventional Feeder Protection Schemes

A feeder is an overhead distribution line or underground cable used for distribution of electrical power. Feeders are usually radial in nature with the loads tapped off along the several sections/segments at the nodes. The main objective on feeder protection strategies is to maintain a high level of service continuity to the maximum number of users with minimum loss of power during intolerable conditions. The presence of a fault can damage the feeder components when not promptly cleared or isolated from it. Owing to the radial nature of the feeders, simple OCPDs are traditionally employed to clear temporary and permanent faults. Injection of DG currents to a distribution network results in the feeder losing its unidirectional power flow configuration and consequently losing the existing coordination sequence amongst its OCPDs during a fault. The conventional radial feeder protection design based on fuse-fuse coordination, re-closer-fuse coordination and relay-relay coordination may fail due to the increase on the short circuit currents and the bi-directional power flow introduced by the DGs (Elmarkabi, 2004).The extent at which protection coordination is affected by DG interconnection in a distribution network depends on: the sizes of the DGs; the number of DG units; the DG interfacing technology; and the location of DGs on the distribution network. Coordination may be lost completely in some cases while in other cases the coordination range diminishes (Elmarkabi, 2004).

i. Impacts of DGs on Over-Current Relay Performance

The OCRs have been most commonly used as an efficient device to protect radial distribution networks. Each OCR in a protection system has a set of parameters that will determine its zone of protection. Conventional OCRs operate with fixed parameters and settings hence it becomes difficult to ensure their proper protection coordination when the operating conditions changes once the DGs are installed (Elmarkabi, 2004). OCRs are set to protect a certain part of the feeder which is referred to as the reach. The reach of the relay is determined by the minimum fault current it is set to pick-up at (Elmarkabi, 2004). Depending on the DG location, the DG interfacing technology, the capacity and the state of the network to which the DG

is connected, DGs may cause relay settings which were previously adequate to under-reach or over-reach (Elmarkabi, 2004).

Presence of a DG on the lateral end of a feeder reduces the reach of the OCR placed at the main grid supply point thus leaving medium impedance faults at the end of the feeder undetected as shown in Figure. 2.31. The reduction in reach is due to the fact that the DG contributes to the fault current thus decreasing the fault current seen by the OCR connected at the main utility grid (Elmarkabi, 2004).

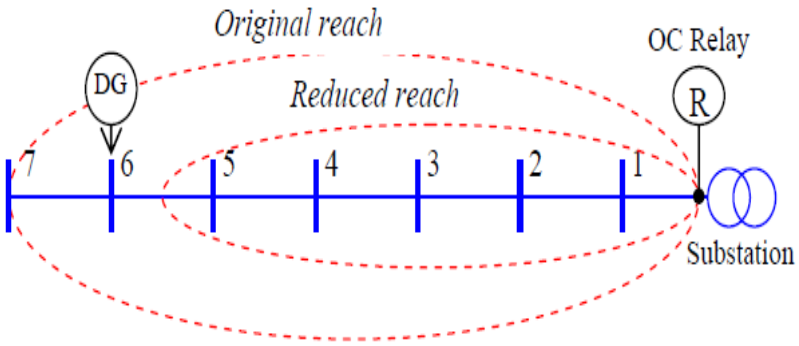

Figure 2.31: Relay Reach with and without DG

ii. **Impacts of DGs on Re-closer Operations**

One of the important parameters of a re-closer is the maximum current the re-closer can withstand called the maximum withstand current. With DGs connected upstream of the re-closer as shown in Figure 2.32 Elmarkabi (2004), the fault current seen by the re-closer will increase. This would not normally create a problem as long as the new re-closer current does not exceed the re-closer maximum withstand capability. However, if the current flowing through the circuit is greater than the maximum re-closer withstand, the re-closer will be exposed to high mechanical and thermal stresses which might cause a re-closer failure (Elmarkabi, 2004).

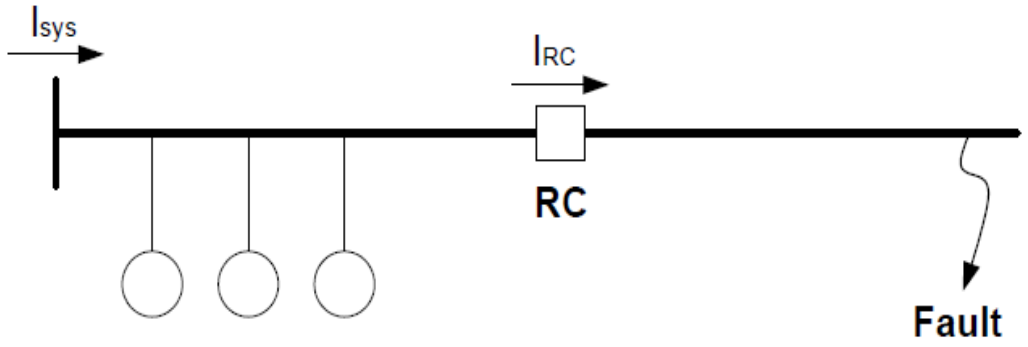

Figure 2.32: Re-closer Operation for DG Located Upstream and Fault Located Downstream

Where there are DGs downstream of a re-closer, the re-closer will see fault currents in the reverse direction if the fault is upstream of the re-closer as seen in Figure. 2.33 (Elmarkabi, 2004). If the Re-closer current exceeds the minimum tripping values of the re-closer, the re-closer will trip for faults upstream which is unacceptable. This can be only solved by upgrading the re-closer by using a directional OCR making the re-closer trip only if the rec-closer current exceeds the minimum tripping value in a certain direction.

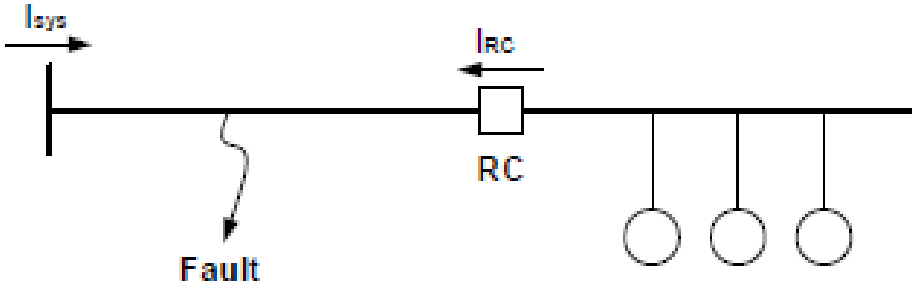

Figure 2.33: Re-closer Operation for DG Located Downstream and Fault Located Upstream

iii. Impacts of DGs on Re-closer-Fuse Coordination

The philosophy of feeder protection is that a fuse should only operate for permanent faults within its reach but for temporary faults, the re-closer should disconnect the

circuit with its fast operation and give the fault a chance to clear. Only if the fault is permanent should the fuse be allowed to blow. This is called fuse saving scheme. For a feeder topology where both the DG and the fault are located downstream of the re-closer, the fault current flowing through the fuse is greater than that flowing through the re-closer as shown in Figure. 2.34 (Elmarkabi, 2004). This might cause the fuse to trip faster than the re-closer for temporary faults hence a miss-coordination between them will impact a lot on the feeder reliability considerably since this will cause both the re-closer and the fuse to operate faster at the high fault current levels. The required margins between the re-closer fast curve and the fuse minimum melting curve could be reduced enough for both the re-closer and the fuse to lose coordination.

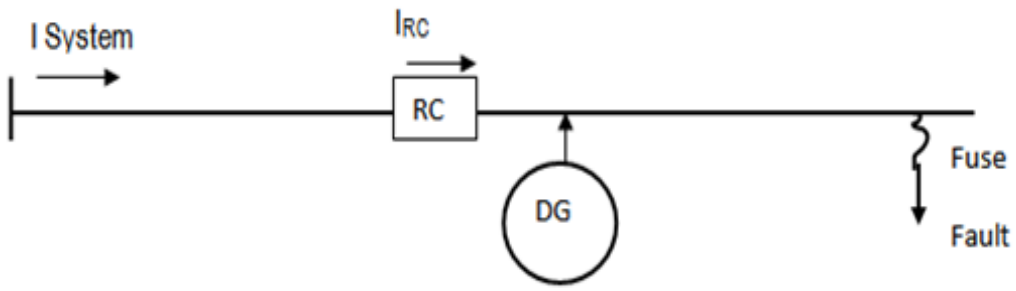

Figure 2.34: Re-closer Operation for DG Located Downstream and Fault Located Downstream

iv. Impacts of DGs on Fuse-Fuse Coordination

In the system shown in Figure 2.35 (Bussman Cooper, nd), when the available short circuit current was 1000 A the downstream fuse and the upstream fuse coordinated with a time coordination margin of 88 seconds measured between points D and E. However, when the short circuit fault currents increased from 1000 A to 2000 A, the location of the fault current shifted from point A to a new location H on the horizontal scale. Following a vertical line up from the 2000 A on the horizontal axis up to the intersection of the TCT for the 100A fuse at point J (from point H to J on the graph), then, from that intersection point J follow a horizontal line left to the vertical axis mark at point F. Point F shows that the downstream 100 A fuse will experience the increased short circuit fault of 2000 A for 0.18 seconds before

opening the circuit. If a vertical line from J is continued up to the MMT curve at a point K, then over to the left to point G, the MMT to operate the upstream 400A fuse is found to be 12.5 seconds. The difference between the 400A fuse MMT and the 100A fuse TCT is 12.32 seconds for 2000 A a reduction from the 88 seconds when the fault current was 1000 A (Bussman Cooper, nd).

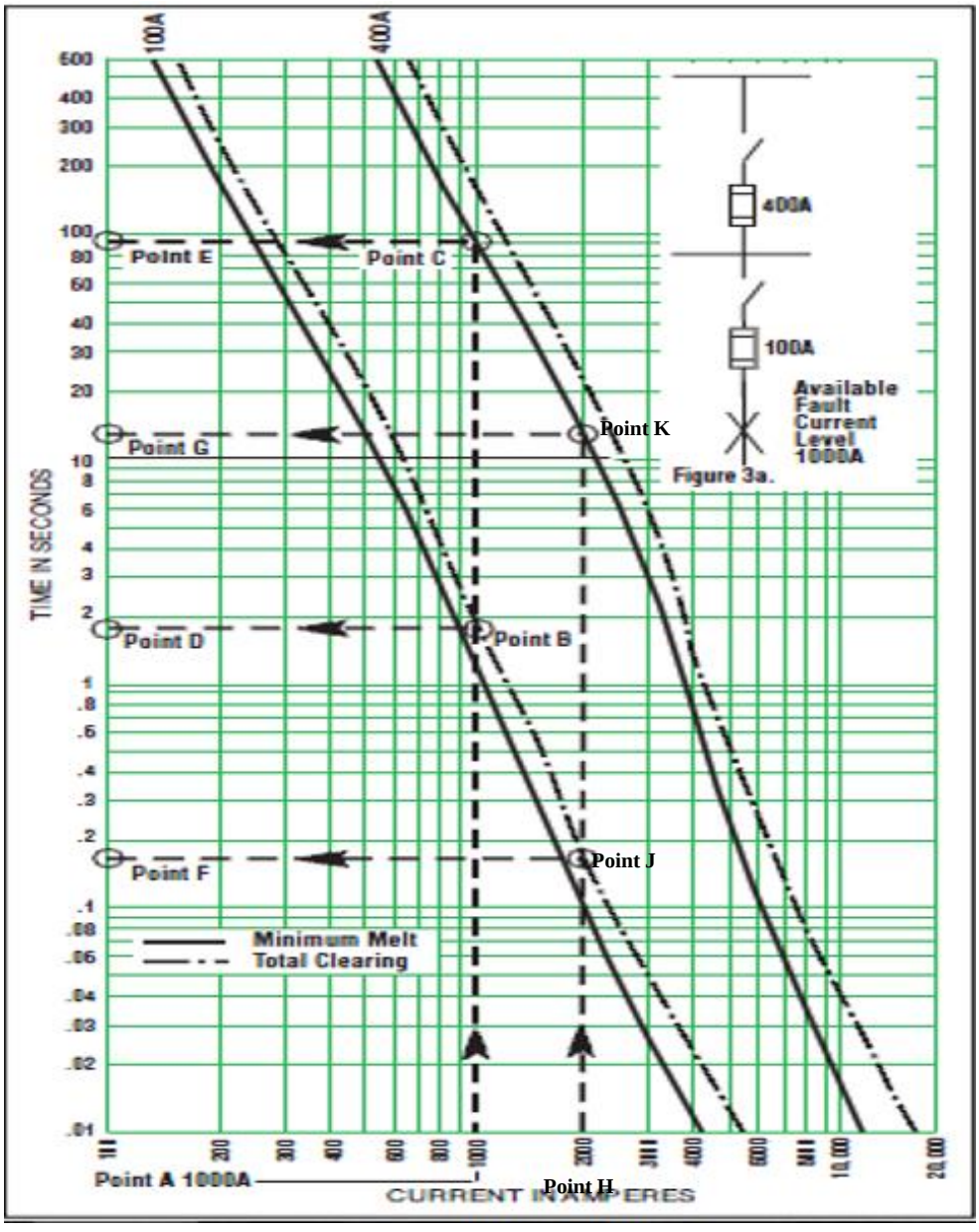

Figure 2.35: Fuse-Fuse Coordination with increased Short Circuit Current

2.7.3. Adaptive and Non-Adaptive Protection Approaches

The need to re-coordinate OCPDs on a distribution network arises once a DG is connected into it. Different methodologies have been presented for implementing the coordination between the various OCPDs to mitigate the impacts of DGs on the distribution network's inherent OCPDs miss-coordination. These methods are generally grouped into two; Adaptive and Non-Adaptive based coordination techniques (AL-Kababjie & M AL-Taee, 2009).

Adaptive protection is an online approach that tends to modify the OCPDs settings as per the corresponding changes in the power systems operating conditions. This approach requires OCPDs whose settings can be easily altered online as the power system operating conditions changes. The adaptive protection approaches utilizes electronic relays, computer architectures and communication channels and they can in-cooperate the use of computer control algorithms which are highly dependent on the fault types, the fault currents levels and the fault location to perform coordination (Paliwal et al., 2012). . On the other hand, Non-Adaptive protection approaches operate by selective replacement or physically changing the OCPDs' settings and ratings following a change in the distribution network's operating condition once a DG is connected into it. Non-Adaptive protection coordination schemes also involves techniques limiting the magnitudes of the short circuit currents flowing in a distribution network once the DGs have been connected. Techniques which involves upgrading of the system components, insertion of current limiting devices and any other technique which does not involve an on-line adjustment of the OCPD's settings is termed as the Non-Adaptive approach of over-current protection coordination.

Researches in papers (AL-Kababjie & AL-Taee, 2009; Bui et al 2021). (Contreras et al., 2012; Shobole et al., 2020; Tian et al., 2019; Valenzuela et al., 2021) have all employed the adaptive protection approaches to mitigate on the impacts the DGs have on over-current protection schemes used to protect the particular networks under the study. In (AL-Kababjie & AL-Taee, 2009) an intelligent distance relay is developed in MATLAB simulink and is used to protect a section of the 400 kV Iragi National Super Grid consisting of 19 buses and 27 transmission lines. An adaptive distance relay was developed using the artificial neural network architecture with the input data being the changes in the lines resistances, reactance, and the angle of the

line impedance once DGs were connected into the super grid. In (Bui et al 2021). an adaptive and scalable protection approach has been developed to coordinate OCRs once DGs were connected into a 22 kV Ho Chi Minh City distribution network developed in ETAP upon the connection of photovoltaic generator system, battery energy storage system and diesel generators in the distribution network. An online algorithm was developed to automatically alter the Time Dial Settings (TDS) for the inverse-time over-current relay functions once the DGs were connected. In (Contreras et al., 2012) intelligent digital relays are utilized to protect a portion of the IEEE 13 nodes radial test feeder from faults occurring in it once the DGs were connected. An algorithm developed in MATLAB was used to automatically modify the OCRs' trip parameters based on the system topological changes detected once the DGs were connected. In (Shobole et al., 2020) an adaptive protection technique which is based on the characteristics of both the fault and the load current variations referred to as the time multiplier setting (TMS) is proposed. Intelligent OCRs monitor the status of the circuit breakers and the DGs. If any status change occurs the relay coordination algorithm is automatically triggered to evaluation new TMS which shall be used to update the new OCRs' characteristic curves once the DGs have been connected. This methodology was developed in DigSILENT electrical software and validated on the Antalya Vicinity solar power plant in Turkey. In (Tian et al., 2019) an adaptive control and coordination strategy is developed for a DFIG generator so that once the DFIG is connected into a ring distribution network, it will be compatible with the networks' protection logics. Firstly, an adaptive control strategy simulating the inertia/damping characteristics and excitation principles of synchronous generators is developed to achieve seamless switching between the DFIG grid-connection and island mode hence making distant synchronization possible. Next, an algorithm coordinating the DFIG islands controlled by the adaptive control strategy and the remote tie switches based on the local inspection of synchronization conditions to achieve the safety grid connection of the DFIG. (Valenzuela et al., 2021) Focuses on the implementation of a topological reconfiguration tool which is oriented to change the structure of primary feeders based on the changing statues of the switchgears. Once the distribution network was reconfigured, an algorithm of protection coordination is executed based on the peer-

to-peer communication between MATLAB and DigSILENT which then develops an adaptive calculation to determine the current settings and the time multiplier settings for the switchgears.

Researches in papers, (Kamel et al., 2013; Funmilayo, 2010; Douglin, 2012; Yousaf et al., 2017) have all employed the non-adaptive protection approaches to mitigate the impacts the DGs have on over current protection schemes. In Kamel etal. (2013), to overcome the impacts of DGs on fuse-fuse miss-coordination, the directional protection features utilized in the re-closers to limit flow of the fault currents from the DGs in only one particular directions was activated so that fuse-fuse coordination was achieved. In Funmilayo (2010), due to fuse fatigue, fuse blowing and fuse miss-operations once DGs were connected into the distribution network, the fuses on the lateral nodes of the distribution network were removed and replaced with multi-function Re-closers/relays to address the three specific issues affecting the fuses. In Douglin (2012) the pick-up setting of the substation relays once DGs were connected were evaluated based on the smart meter data from the previous years. The relay setting were manually adjusted based on electrical energy demand levels available in the smart meter used to determine the seasonal maximum demands for each section of the distribution network. These seasonal maximum demand smart meter data were used to determine the pick-up settings for the substation relays for each season. Yousaf et al., 2017) Shows that coordination amongst the relays, the fuses and the re-closer can be regained by use of the re-closer fast reclose curves to achieve fuse saving for temporary faults once DGs have been connected. The research presented data for a fuse overcurrent relay protection coordination scheme for an 11kV Haripur grid distribution feeder on ETAP.

Those techniques which involves upgrading of the system components, insertion of current limiting devices and any other technique which does not involve an on-line adjustment of the OCPD's settings also fall in the Non-Adaptive approach of over-current protection coordination. Researches in papers, Abdel-Salam et al., (2017), Amon et al. (2009), have all employed the non-adaptive protection approach of utilizing fault current limiters to mitigate the impacts the DGs have on over current protection schemes used to protect the particular networks under study. In Abdel-

Salam et al. (2017) unidirectional fault current limiters having low resistance for downstream faults and high resistance for upstream faults have been presented. A unidirectional fault current limiter has been proposed to restore the coordination among the OCRs in the presence of the DGs which caused an increase in the network fault current levels hence disrupting the existing time intervals of the OCRs. (Amon et al., 2009). Presents a detailed application of a 15 kV CLR installed at Furnas substation and a 362 kV CLR installed at the Eletronorte substation both of the Brazilian power grid. The research gave a detailed application of CLR to achieve fault current limitation at the substations. Most studies done have concentrated on the short circuit currents contribution by the WTGs during faults and little have been done on the impacts the WTGs have on the distribution networks' over current protect schemes' coordination. Papers (Golrang, 2014; Yin, 2021; Yin, 2021b; Aishwarya, 2014). Bhasker et al., 2014).have presented results on the various techniques which can be used to evaluate the fault current contribution by the DFIG (Golrang, 2014; Bhasker et al., 2014; Yadav et al., 2014).

2.7.4. Summary

The most common ways of handling the ever increasing short circuit current levels in the power systems network is by use of the fuses and the circuit breakers. Use of fuses to limit the high short circuit currents is undesirable because fuses cause an entire system to be shut down on the occurrence of faults while the circuit breakers on the other hand allow the first few cycles of the fault currents to pass through before interrupting them (Varetsky & Gajdzica, 2023). Apart from using fuses and circuit breakers, upgrading the power system equipment with their OCPDs to withstand the increased fault current levels, another form of limiting the fault currents is the introduction of devices which reduces the short circuit currents to levels which the existing equipment and OCPDs can easily handle. Fault Current Limiters (FCLs) have the potential to reduce the fault currents and make possible the use of lower rated OCPDs in protecting the power system networks.

Recent trends in deregulation and restructuring of the power grid due to introduction of DGs in the distribution network operations and the stringent regulations the DGs

have to meet before being integrated into the distribution networks (Varetsky & Gajdzica, 2023; Basso, 2014), have invoked a renewed interest in the use of the FCL technologies to limit the high short circuit current contribution by the DGs into the distribution networks. FCL have been employed in power systems for differing purposes such as stability enhancement, protection improvement, fault current reduction and fault ride through capability enhancements with the primary benefit of FCLs being that it saves the utility companies the cost of removing lower rated OCPDs and replacing them with higher rated OCPDs in existing installations once the network's short circuit current capacity increases. FCLs reduces the magnitudes of the fault currents to levels the existing protection device can handle and they are inserted as series impedances into a power systems to limit the fault currents to acceptable limits.

This research investigated the use of series current limiting reactors to improve on the diminishing time coordination margins for a fuse-fuse over-current protection scheme developed in ETAP for protecting the IEEE 13 nodes radial test feeder.

CHAPTER THREE

SIMULATION OF IEEE 13 NODE RADIAL TEST FEEDER WITH DFIGS AND TYPE IV WTGS FOR PROTECTION COORDINATION ANALYSIS

3.1 The IEEE 13 Node Radial Test Feeder Model

3.1.1 The IEEE 13 Node Radial Test Feeder Configuration

The IEEE 13 nodes radial test feeder is a short, unbalanced and relatively highly loaded 4.16 kV feeder considered as a good model to be used to investigate the impacts WTGs have on a fuse-fuse over-current protection scheme modelled to protect the feeder. The feeder features: A 5000 kVA delta/star solidly grounded 115/4.16 kV substation transformer connected at the main grid node; One substation voltage regulator consisting of three single phase units connected in star; Eight overhead distribution lines and two underground cables with variety of lengths and phasing; Unbalanced distributed and spot loads totaling 4054 kVA; Two shunt capacitor banks one having a single phase connection and the other a three phase connection; and a 500 kVA star/star solidly grounded 4.16/0.48 kV in-line transformer. Figure. 3.1 shows the schematic layout of the IEEE 13 node radial test feeder without showing the different connected loads or the nature and configuration of the components of the feeder. Some assumptions taken into consideration while performing the modelling and simulation are:

i. The distributed load between NODE632 and NODE671 was modeled as a spot load and connected at NODE632
ii. The short circuit current contribution by the motoring loads was considered minimal at 1% of their locked-rotor current and the short circuit contribution by the WTGs was set at 600% of their locked-rotor current.
iii. The WTGs considered for analysis were all solidly grounded.

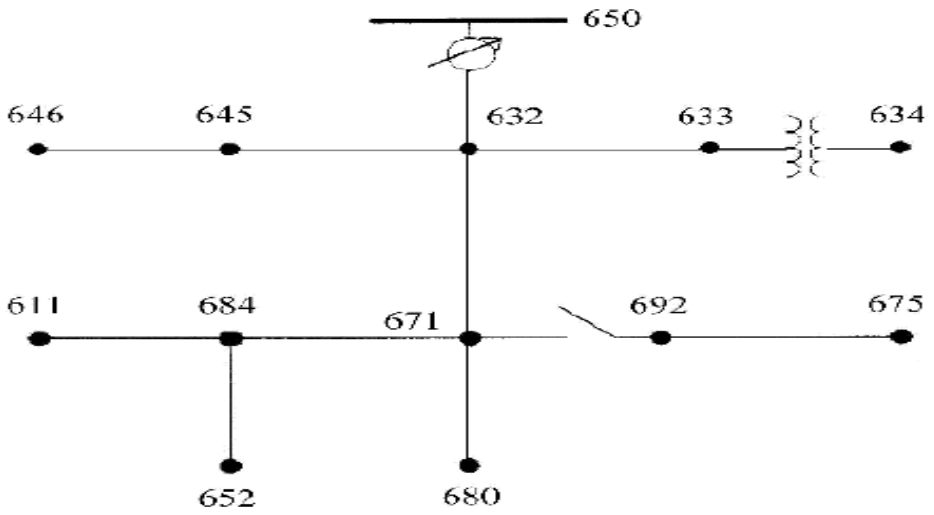

Figure 3.1: The IEEE 13 Node Radial Test Feeder Schematic Diagram

3.1.2 The IEEE 13 Node Radial Test Feeder Fuse-Fuse Over-Current Protection Scheme ETAP Model

IEEE 13 node radial test feeder was modelled using ETAP electrical software as per the NEC240:101 and NEC450.3 regulations. There are four main components of the IEEE 13 node radial test feeder and each was modeled to be protected by fuses. These components are namely the nodes, the underground cables, the overhead distribution lines and the in-line transformer.

Figure 3.2 shows a fuse-fuse over-current protection scheme one line diagram developed in ETAP for the feeder with a total of 23 fuses. The overhead lines and the underground cables segments were given specific identification codes chosen with reference to the node points they have been connected in between. Each fuse was given a unique identification code based on the line or the cable segment it is protecting.

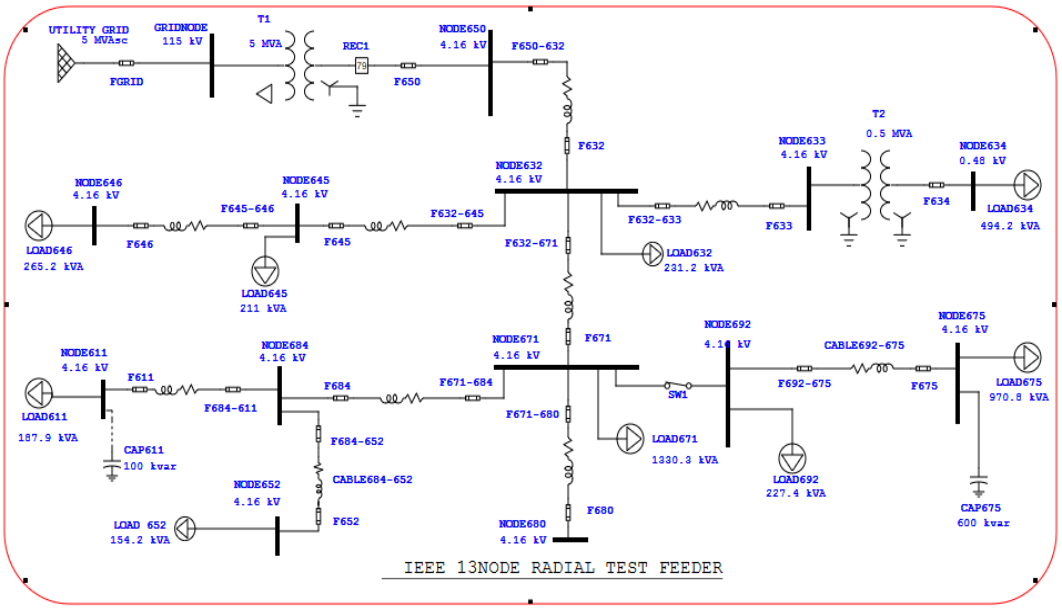

Figure 3.2: IEEE 13 Node Radial Test Feeder ETAP Fuse-Fuse Over-Current Protection Scheme One Line Diagram

The upstream fuse was given a code describing the two node points between which the line or the cable has been connected and the downstream fuse was given a code based on the node the line or the cable has been terminated at. Table 3.1 gives the identification names and codes for all the fuses used to protect the eight overhead lines, the two underground cables and the in-line transformer referenced as T2.

Table 3.1: Overhead Lines, Underground Cables and In-Line Transformer Fuses

Segment	Source Node	Load Node	Upstream Fuse	Downstream Fuse
LINE632-645	632	645	F632-645	F645
LINE632-633	632	633	F632-633	F633
LINE645-646	645	646	F645-646	F646
LINE650-632	650	632	F650-632	F632
LINE632-671	632	671	F632-671	F671
LINE671-684	671	684	F671-684	F684
LINE671-680	671	680	F671-680	F680
LINE684-611	684	611	F684-611	F611
CABLE684-652	684	652	F684-652	F652
CABLE692-675	692	675	F692-675	F675
T2	633	634	F633	F634

3.2 IEEE 13 Node Radial Test Feeder Fuse-Fuse Coordination without WTGs

3.2.1 Short Circuit Currents and Sequence Reactance without WTGs

Table 3.2: SLG Fault Currents and Sequence Reactance without WTGs

Faulted Node	NODE671	NODE684	NODE611
SLG (A)	715	697	679
Positive Sequence (Ω)	4.13252	4.18005	4.26642
Negative Sequence Ω)	4.13252	4.18005	4.26642
Zero Sequence (Ω)	1.6829	1.8121	1.89837

3.2.2 Fuse-Fuse Coordination for SLG Faults without WTGs

A. Fuse-Fuse Time Margins for SLG Faults without WTGs

Table 3.3: Fuse-Fuse Time Margins for SLG Faults without WTGs

Fault Location	Upstream Fuse	Down-Stream Fuse	Fault Current (A)	Time Margin (s)
LINE671-684	F671	F671-684	715	1.093
NODE684	F671-684	F684	697	0.986
LINE684-611	F684	F684-611	697	0.482
NODE611	F684-611	F611	679	0.231

B. Fuse-Fuse TCC Curves for SLG Faults without WTGs

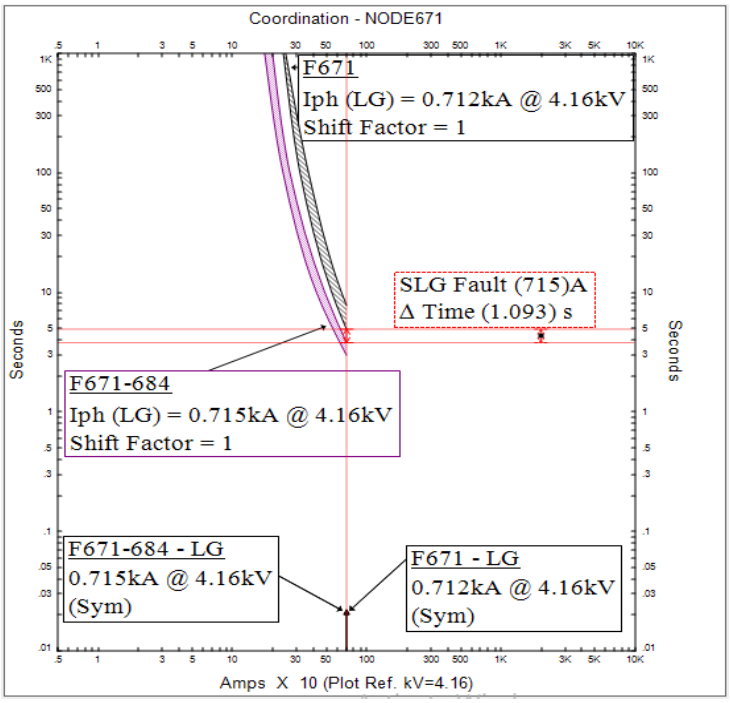

Figure 3.3: Fuses F671 and F671-684 TCC Curves for SLG Fault on LINE671-684 without WTG

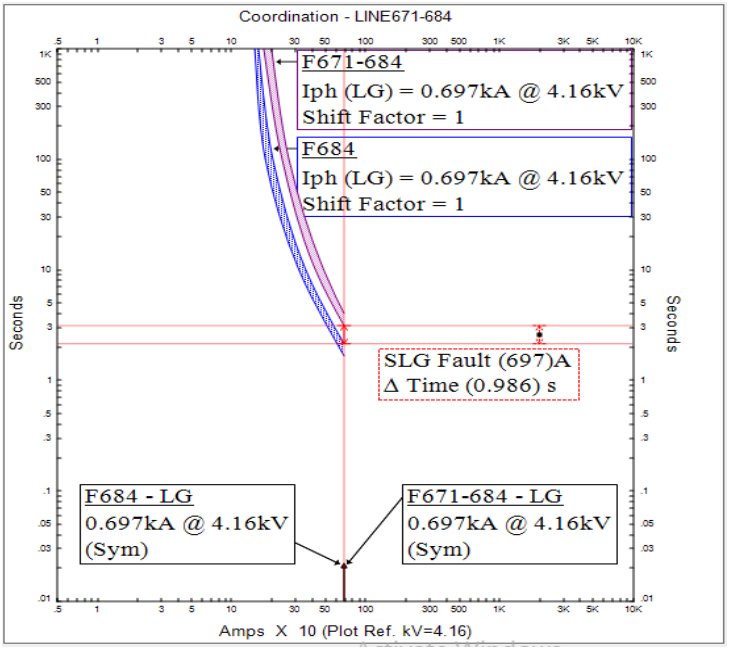

Figure 3.4: Fuses F671-684 and F684 TCC Curves for SLG Fault at NODE684 without WTG

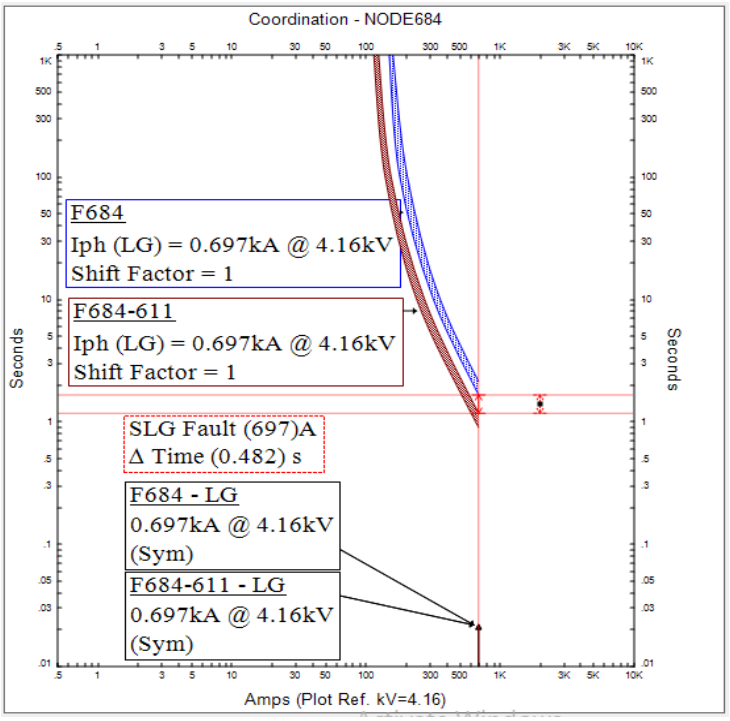

Figure 3.5: Fuses F684 and F684-611 TCC Curves for SLG Fault on LINE684-611 without WTG

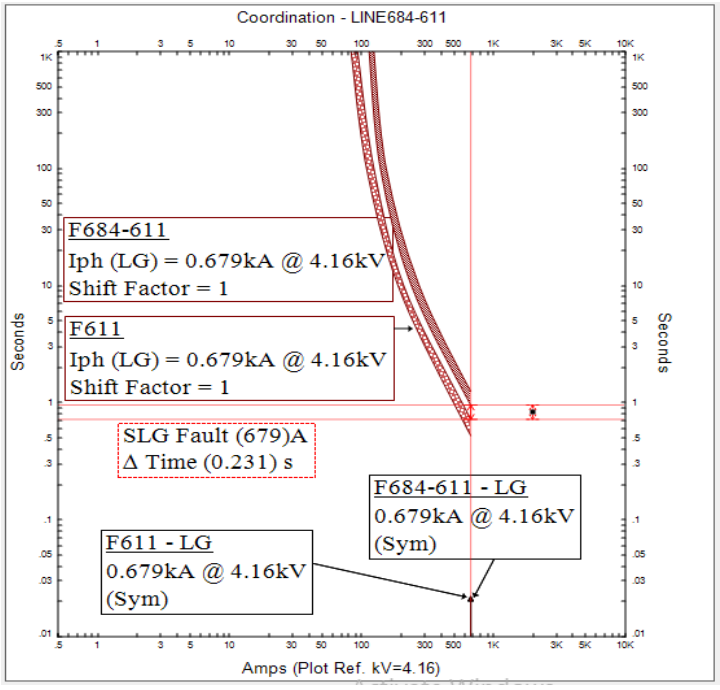

Figure 3.6: Fuses F684-611 and F611 TCC Curves for SLG Fault at NODE611 without WTG

3.3 IEEE 13 Node Radial Test Feeder Fuse-Fuse Coordination with WTGs

3.3.1 Short Circuit Currents and Sequence Reactance with DFIGs and Type IV WTGs

A. NODE671 SLG Fault Currents and Sequence Reactance with 1MW and 3MW DFIGs

Table 3.4: NODE671 SLG Fault Currents and Sequence Reactance with 1MW and 3MW DFIGs

DFIG Location	NODE650		NODE632		NODE671	
	1MW	3MW	1MW	3MW	1MW	3MW
SLG (A)	1308	1857	1489	2459	1799	3889
Positive Sequence (Ω)	1.92472	1.12062	1.73507	0.90253	1.54271	0.6835
Negative Sequence (Ω)	1.85427	1.07782	1.66127	0.8588	1.46572	0.63892
Zero Sequence (Ω)	1.65297	1.60912	1.39319	1.13448	0.97719	0.5269

B. NODE671 SLG Fault Currents and Sequence Reactance with 1MW and 3MW Type IV WTGs

Table 3.5: NODE671 SLG Fault Currents and Sequence Reactance with 1MW and 3MW Type IV WTGs

Type IV WTG Location	NODE650		NODE632		NODE671	
	1MW	3MW	1MW	3MW	1MW	3MW
SLG (A)	774	1034	787	1091	804	1166
Positive Sequence (Ω)	3.42559	1.88175	3.30482	1.63278	3.17605	1.38187
Negative Sequence (Ω)	3.42559	1.88175	3.30482	1.63278	3.17605	1.38187
Zero Sequence (Ω)	1.68075	1.67527	1.62736	1.49085	1.49779	1.07866

C. NODE684 SLG Fault Currents and Sequence Reactance with 1MW and 3MW DFIGs

Table 3.6: NODE684 SLG Fault Currents and Sequence Reactance with 1MW and 3MW DFIGs

DFIG	NODE650		NODE632		NODE671	
Location	1MW	3MW	1MW	3MW	1MW	3MW
SLG (A)	1251	1741	1416	2263	1696	3439
Positive Sequence (Ω)	1.97225	1.16815	1.78260	0.95006	1.59024	0.73103
Negative Sequence (Ω)	1.90181	1.12535	1.70880	0.90633	1.51325	0.68645
Zero Sequence (Ω)	1.78218	1.73832	1.52240	1.26368	1.10640	0.65611

D. NODE684 SLG Fault Currents and Sequence Reactance with 1MW and 3MW Type IV WTGs

Table 3.7: NODE684 SLG Fault Currents and Sequence Reactance with 1MW and 3MW Type IV WTGs

Type IV WTG	NODE650		NODE632		NODE671	
Location	1MW	3MW	1MW	3MW	1MW	3MW
SLG (A)	751	992	764	1045	780	1114
Positive Sequence (Ω)	3.47312	1.92929	3.35235	1.68031	3.22358	1.42940
Negative Sequence (Ω)	3.47312	1.92929	3.35235	1.68031	3.22358	1.42940
Zero Sequence (Ω)	1.80995	1.80447	1.75656	1.62005	1.62699	1.20786

E. NODE611 SLG Fault Currents and Sequence Reactance with 1MW and 3MW DFIGs

Table 3.8: NODE611 SLG Fault Currents and Sequence Reactance with 1MW and 3MW DFIGs

DFIG Location	NODE650		NODE632		NODE671	
	1MW	3MW	1MW	3MW	1MW	3MW
SLG (A)	1191	1626	1341	2074	1590	3028
Positive Sequence (Ω)	2.05862	1.25433	1.86897	1.03643	1.67661	0.81739
Negative Sequence(Ω)	1.98818	1.21172	1.79517	0.9927	1.61457	0.77283
Zero Sequence (Ω)	1.86845	1.82459	1.60866	1.34995	1.19266	0.74238

F. NODE611 SLG Fault Currents and Sequence Reactance with 1MW and 3MW Type IV WTGs

Table 3.9: NODE611 SLG Fault Currents and Sequence Reactance with 1MW and 3MW Type IV WTGs

Type IV WTG Location	NODE650		NODE632		NODE671	
	1MW	3MW	1MW	3MW	1MW	3MW
SLG (A)	728	952	740	1001	754	1065
Positive Sequence (Ω)	3.55949	2.01566	3.43872	1.76668	3.30995	1.51577
Negative Sequence (Ω)	3.55949	2.01566	3.43872	1.76668	3.30995	1.51577
Zero Sequence (Ω)	1.89622	1.89074	1.84283	1.70632	1.71326	1.29413

3.3.2 Fuse-Fuse Coordination for SLG Faults with 1MW Type IV WTGs

A. Fuse-Fuse Time Margins for SLG Faults with 1MW Type IV WTGs

Table 3.10: Fuse-Fuse Time Margins for SLG Faults with 1MW Type IV WTG at NODE650

Fault Location	Upstream Fuse	Down-Stream Fuse	NODE650	
			Fault Current (A)	Time Margin (s)
LINE671-684	F671	F671-684	774	0.842
NODE684	F671-684	F684	751	0.844
LINE684-611	F684	F684-611	751	0.412
NODE611	F684-611	F611	728	0.202

Table 3.11: Fuse-Fuse Time Margins for SLG Faults with 1MW Type IV WTG at NODE632

Fault Location	Upstream Fuse	Down-Stream Fuse	NODE632	
			Fault Current (A)	Time Margin (s)
LINE671-684	F671	F671-684	787	0.795
NODE684	F671-684	F684	764	0.815
LINE684-611	F684	F684-611	764	0.397
NODE611	F684-611	F611	740	0.196

Table 3.12: Fuse-Fuse Time Margins for SLG Faults with 1MW Type IV WTG at NODE671

Fault Location	Upstream Fuse	Down-Stream Fuse	NODE671	
			Fault Current (A)	Time Margin (s)
LINE671-684	F671	F671-684	804	1.915
NODE684	F671-684	F684	780	0.781
LINE684-611	F684	F684-611	780	0.379
NODE611	F684-611	F611	754	0.189

B. Fuse-Fuse TCC Curves for SLG Faults with 1MW Type IV WTGs Connected at NODE671

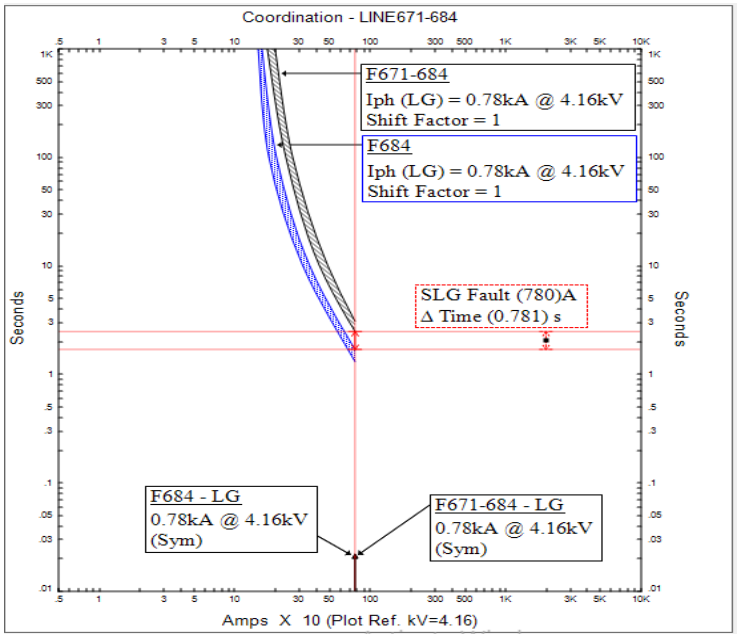

Figure 3.7: Fuses F671-684 and F684 TCC Curves for SLG Fault at NODE684 with 1MW Type IV WTGs Connected at NODE671

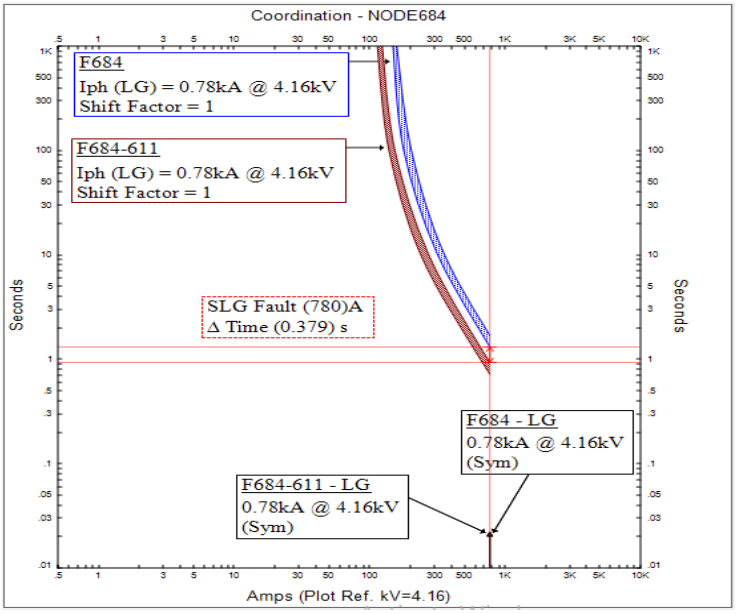

Figure 3.8: Fuses F684 and F684-611 TCC Curves for SLG Fault on LINE684-611 with 1MW Type IV WTGs Connected at NODE671

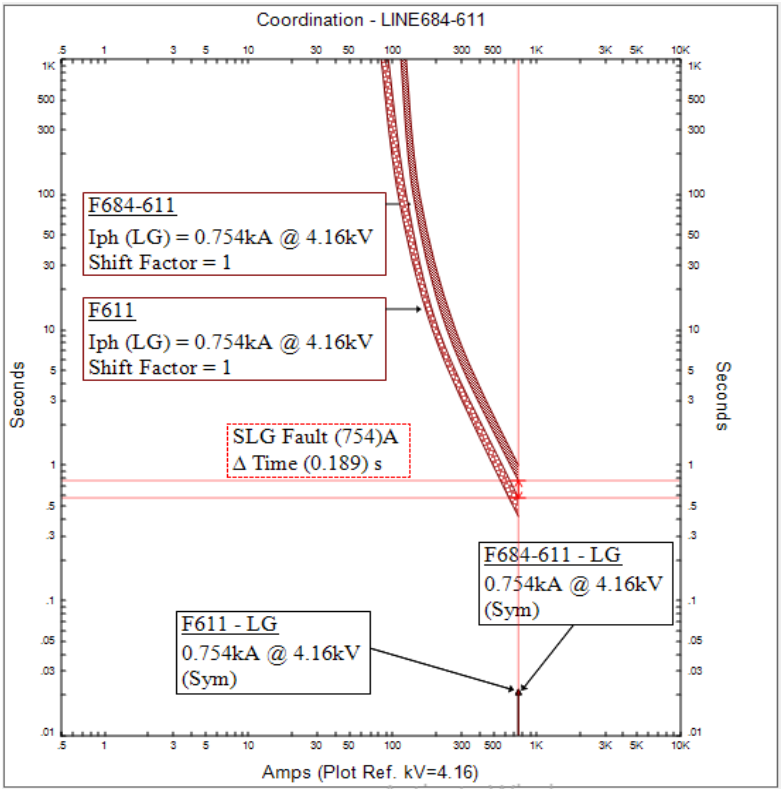

Figure 3.9: Fuses F684-611 and F611 TCC Curves for SLG Fault at NODE611 with 1MW Type IV WTGs Connected at NODE671

3.3.3 Fuse-Fuse Coordination for SLG Faults with 1MW DFIGs

A. Fuse-Fuse Time Margins for SLG Faults with 1MW DFIGs

Table 3.13: Fuse-Fuse Time Margins for SLG Faults with 1MW DFIG at NODE650

Fault Location	Upstream Fuse	Down-Stream Fuse	NODE650	
			Fault Current (A)	Time Margin (s)
LINE671-684	F671	F671-684	1308	0.179
NODE684	F671-684	F684	1251	0.286
LINE684-611	F684	F684-611	1251	0.117
NODE611	F684-611	F611	1191	0.088

Table 3.14: Fuse-Fuse Time Margins for SLG Faults with 1MW DFIG at NODE632

Fault Location	Upstream Fuse	Down-Stream Fuse	NODE632	
			Fault Current (A)	Time Margin (s)
LINE671-684	F671	F671-684	1489	0.122
NODE684	F671-684	F684	1416	0.213
LINE684-611	F684	F684-611	1416	0.084
NODE611	F684-611	F611	1341	0.07

Table 3.15: Fuse-Fuse Time Margins for SLG Faults with 1MW DFIG at NODE671

Fault Location	Upstream Fuse	Down-Stream Fuse	NODE671	
			Fault Current (A)	Time Margin (s)
LINE671-684	F671	F671-684	1799	3.42
NODE684	F671-684	F684	1696	0.139
LINE684-611	F684	F684-611	1696	0.051
NODE611	F684-611	F611	1590	0.049

B. Fuse-Fuse TCC Curves for SLG Faults with 1MW DFIG Connected at NODE671

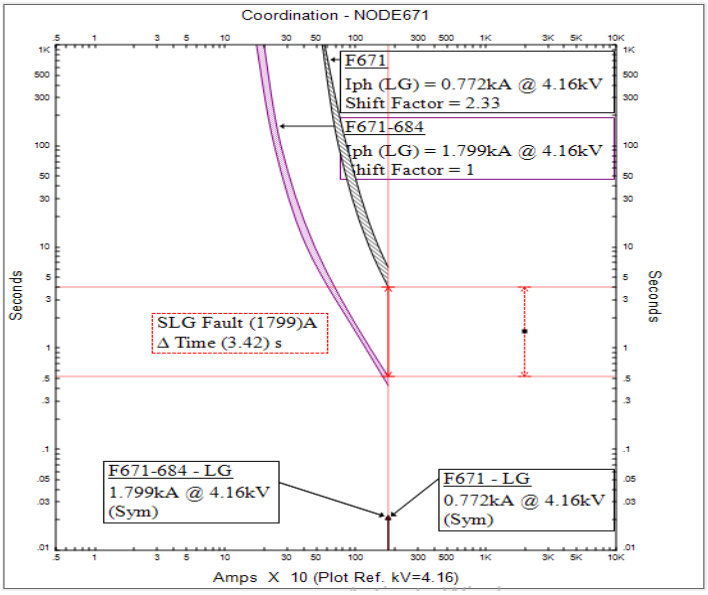

Figure 3.10: Fuses F671 and F671-684 TCC Curves for SLG Fault on LIN671-684 with 1MW DFIGs Connected at NODE671

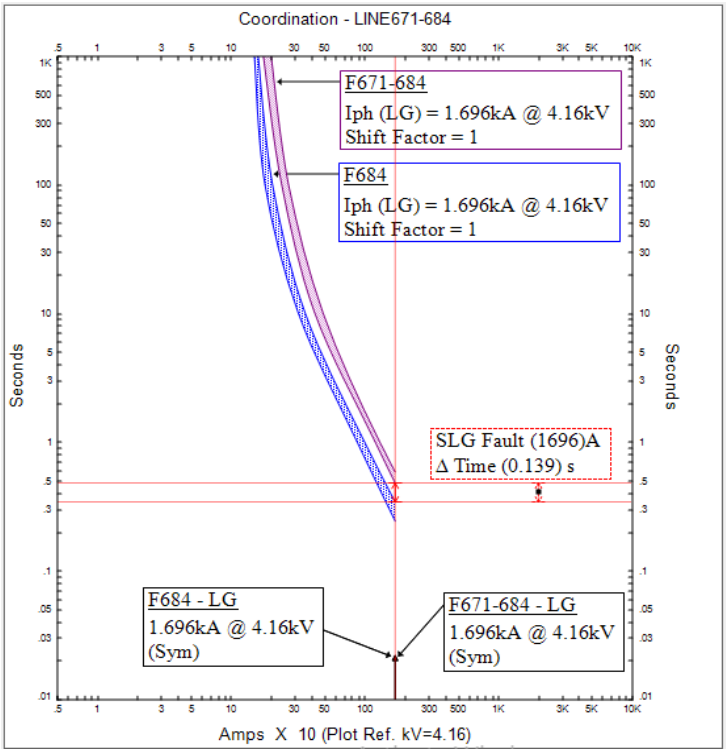

Figure 3.11: Fuses F671-684 and F684 TCC Curves for SLG Fault at NODE684 with 1MW DFIGs Connected at NODE671

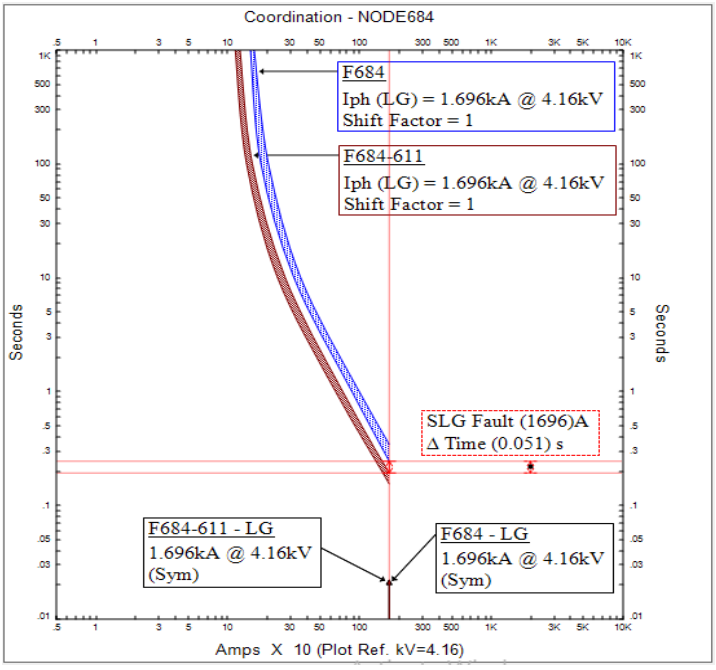

Figure 3.12: Fuses F684 and F684-611 TCC Curves for SLG Fault on LINE684-611 with 1MW DFIGs Connected at NODE671

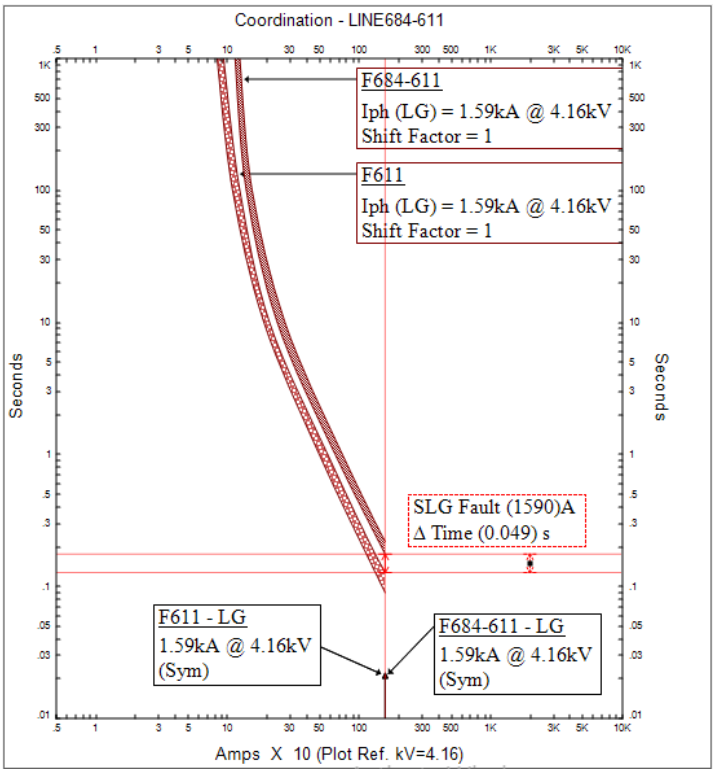

Figure 3.13: Fuses F684-611 and F611 TCC Curves for SLG Fault at NODE611 with 1MW DFIGs Connected at NODE671

3.3.4 Fuse-Fuse Coordination for SLG Faults with 3MW Type IV WTGs

A. Fuse-Fuse Time Margins for SLG Faults with 3MW Type IV WTGs

Table 3.16: Fuse-Fuse Time Margins for SLG Faults with 3MW Type IV WTG at NODE650

Fault Location	Upstream Fuse	Down-Stream Fuse	NODE650	
			Fault Current (A)	Time Margin (s)
LINE671-684	F671	F671-684	1034	0.349
NODE684	F671-684	F684	992	0.476
LINE684-611	F684	F684-611	992	0.212
NODE611	F684-611	F611	952	0.128

Table 3.17: Fuse-Fuse Time Margins for SLG Faults with 3MW Type IV WTG at NODE632

Fault Location	Upstream Fuse	Down-Stream Fuse	NODE632	
			Fault Current (A)	Time Margin (s)
LINE671-684	F671	F671-684	1091	0.298
NODE684	F671-684	F684	1045	0.429
LINE684-611	F684	F684-611	1045	0.186
NODE611	F684-611	F611	1001	0.118

Table 3.18: Fuse-Fuse Time Margins for SLG Faults with 3MW Type IV WTG at NODE671

Fault Location	Upstream Fuse	Down-Stream Fuse	NODE671	
			Fault Current (A)	Time Margin (s)
LINE671-684	F671	F671-684	1166	3.069
NODE684	F671-684	F684	1114	0.373
LINE684-611	F684	F684-611	1114	0.159
NODE611	F684-611	F611	1065	0.106

B. Fuse-Fuse TCC Curves for SLG Faults with 3MW Type IV WTG Connected at NODE671

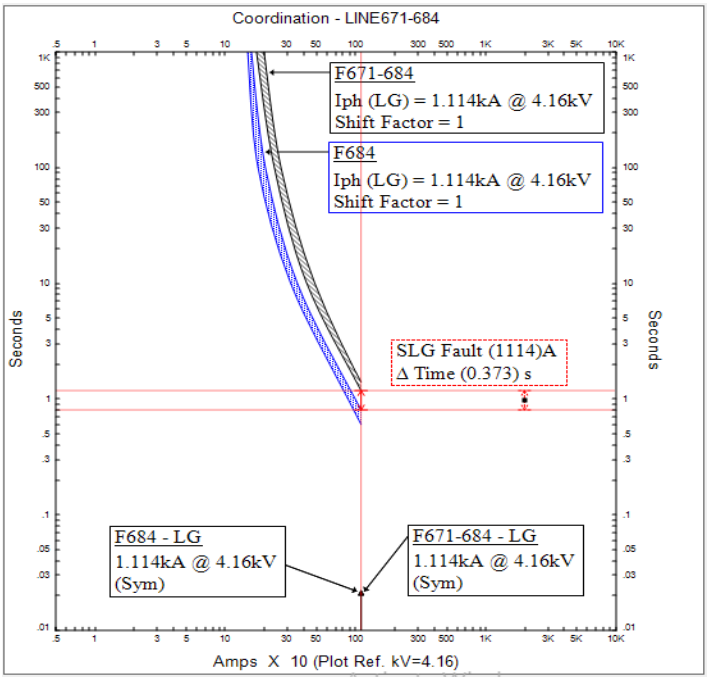

Figure 3.14: Fuses F671-684 and F684 TCC Curves for SLG Fault at NODE684 with 3MW Type IV WTG Connected at NODE671

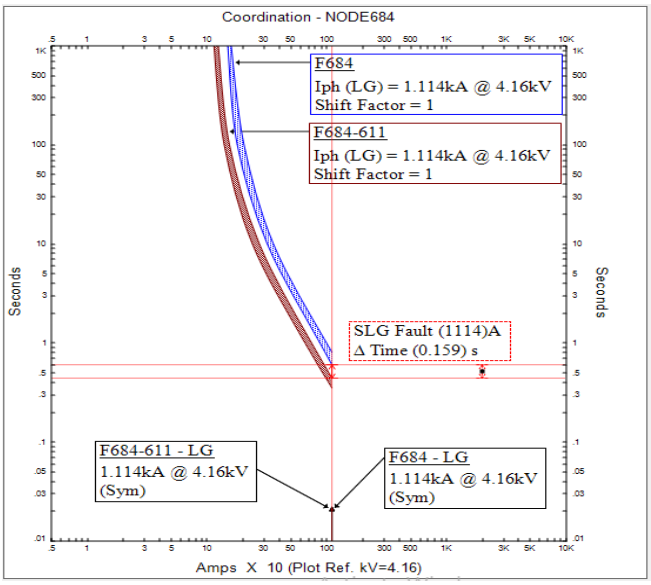

Figure 3.15: Fuses F684 and F684-611 TCC Curves for SLG Fault on LINE684-611 with 3MW Type IV WTG Connected at NODE671

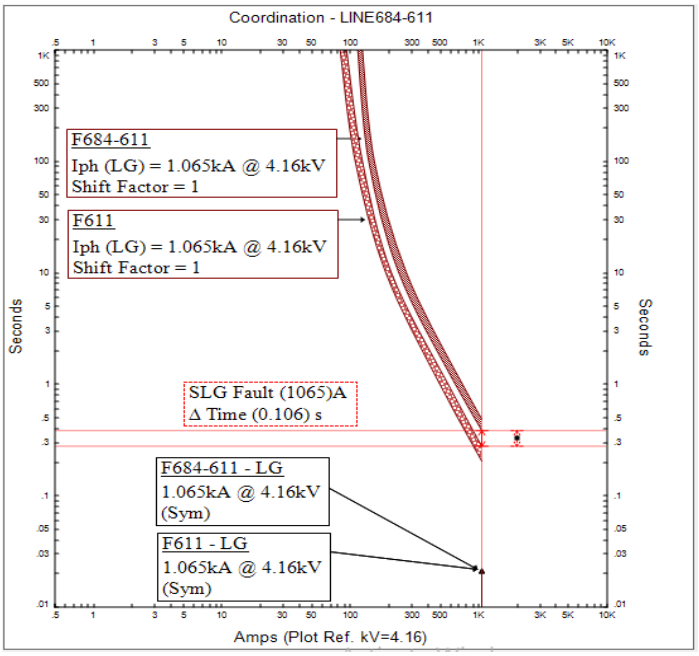

Figure 3.16: Fuses F684-611 and F611 TCC Curves for SLG Fault at NODE611 with 3MW Type IV WTG Connected at NODE671

3.3.5 Fuse-Fuse Coordination for SLG Faults with 3MW DFIG Connected at NODE650

A. Fuse-Fuse Coordination Time Margins for SLG Faults with 3MW DFIG Connected at NODE650

Table 3.19: Fuse-Fuse Time Margins for SLG Faults with 3MW DFIG Connected at NODE650

Fault Location	Upstream Fuse	Down-Stream Fuse	NODE650	
			Fault Current (A)	Time Margin (s)
LINE671-684	F671	F671-684	1857	0.065
NODE684	F671-684	F684	1741	0.13
LINE684-611	F684	F684-611	1741	0.048
NODE611	F684-611	F611	1626	0.047

B. Fuse-Fuse TCC Curves for SLG Faults with 3MW DFIG Connected at NODE650

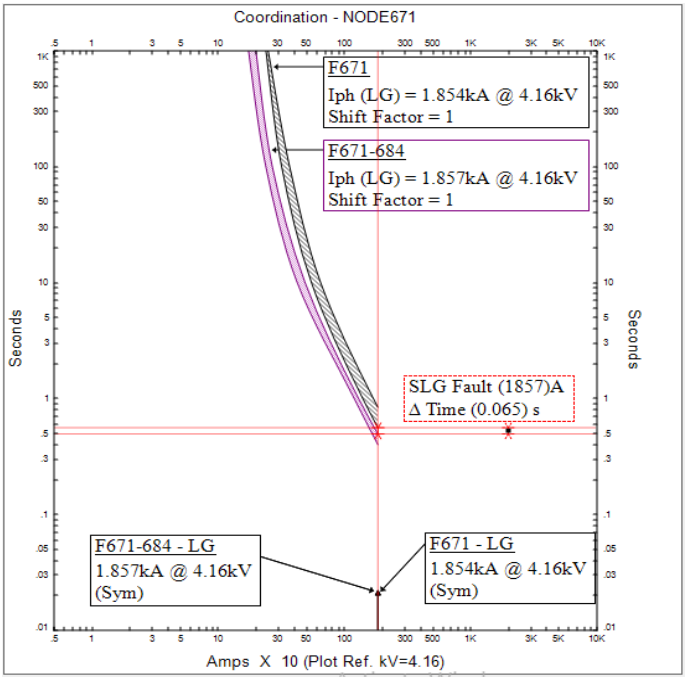

Figure 3.17: Fuses F671 and F671-684 TCC Curves for SLG Fault on LINE671-684 with 3MW DFIG Connected at NODE650

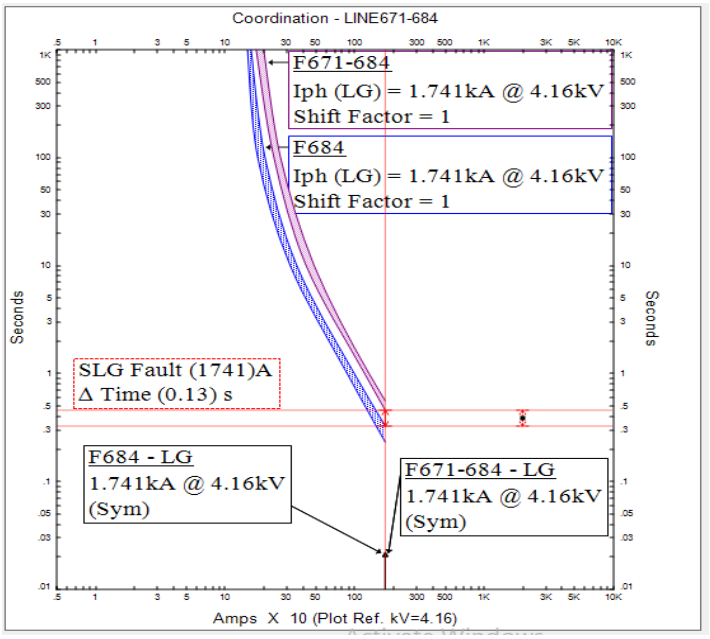

Figure 3.18: Fuses F671-684 and F684 TCC Curves for SLG Fault at NODE684 with 3MW DFIG Connected at NODE650

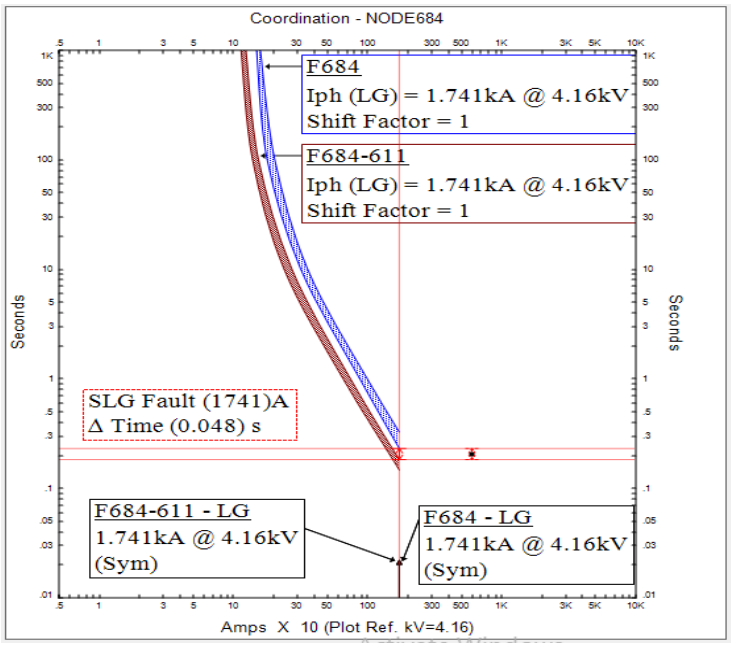

Figure 3.19: Fuses F684 and F684-611 TCC Curves for SLG Fault on LINE684-611 with 3MW DFIG Connected at NODE650

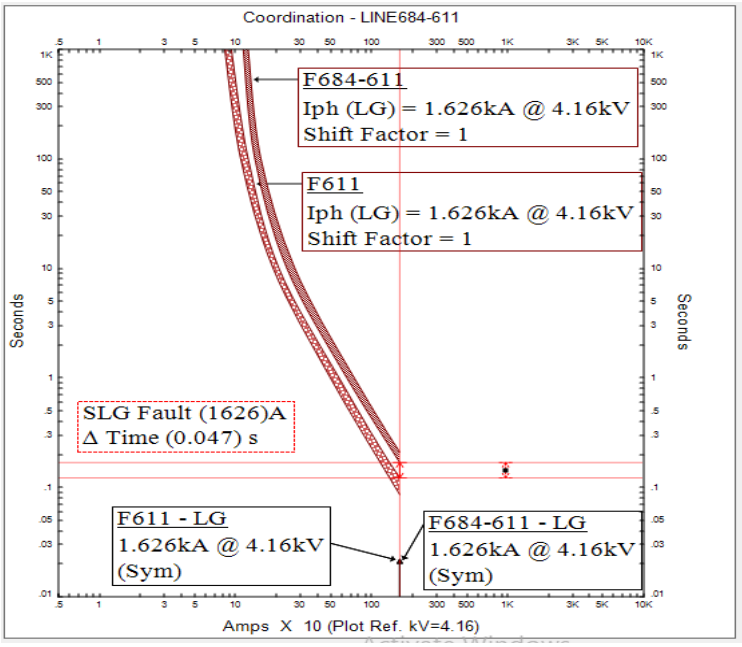

Figure 3.20: Fuses F684-611 and F611 TCC Curves for SLG Fault at NODE611 with 3MW DFIG Connected at NODE650

3.3.6 Fuse-Fuse Coordination for SLG Faults with 3MW DFIG Connected at NODE632

A. Fuse-Fuse Coordination Time Margins for SLG Faults with 3MW DFIG Connected at NODE632

Table 3.20: Fuse-Fuse Time Margins for SLG Faults with 3MW DFIG Connected at NODE632

Fault Location	Upstream Fuse	Down-Stream Fuse	NODE632	
			Fault Current (A)	Time Margin (s)
LINE671-684	F671	F671-684	2459	0.029
NODE684	F671-684	F684	2263	0.067
LINE684-611	F684	F684-611	2263	0.022
NODE611	F684-611	F611	2074	0.0245

B. Fuse-Fuse TCC Coordination Curves for SLG Faults with 3MW DFIG Connected at NODE632

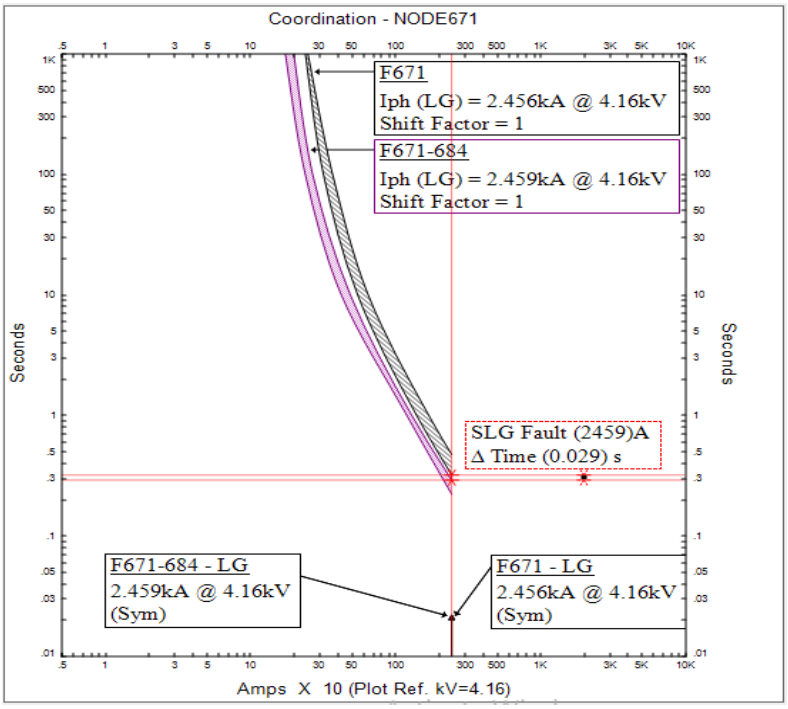

Figure 3.21: Fuses F671 and F671-684 TCC Curves for SLG Fault on LINE671-684 with 3MW DFIG Connected at NODE632.

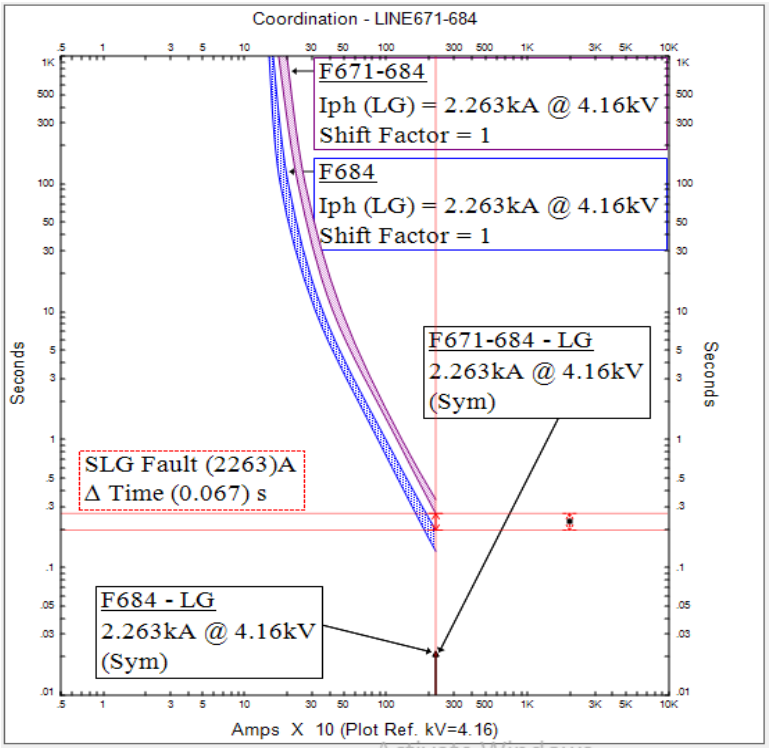

Figure 3.22: Fuses F671-684 and F684 TCC Curves for SLG Fault at NODE684 with 3MW DFIG Connected at NODE632

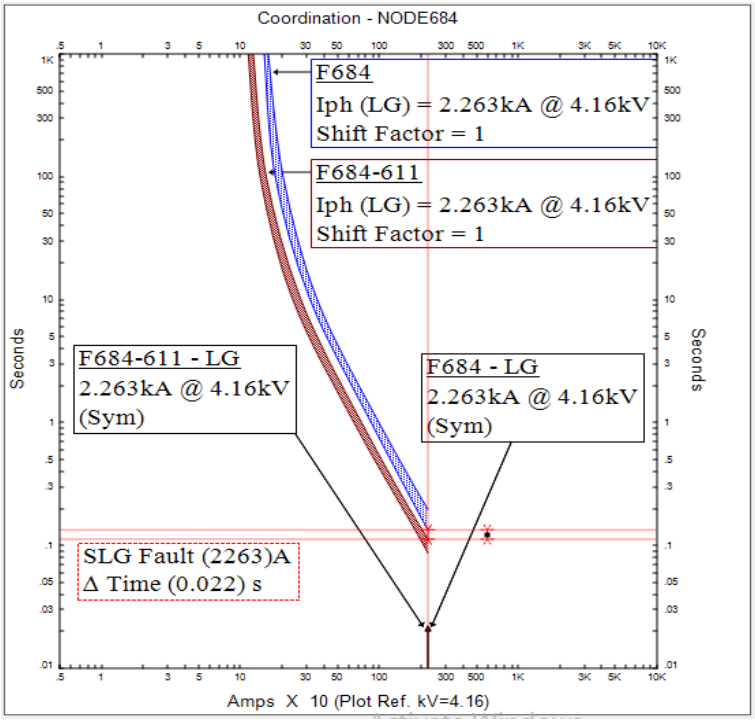

Figure 3.23: Fuses F684 and F684-611 TCC Curves for SLG Fault on LINE684-611 with 3MW DFIG Connected at NODE632

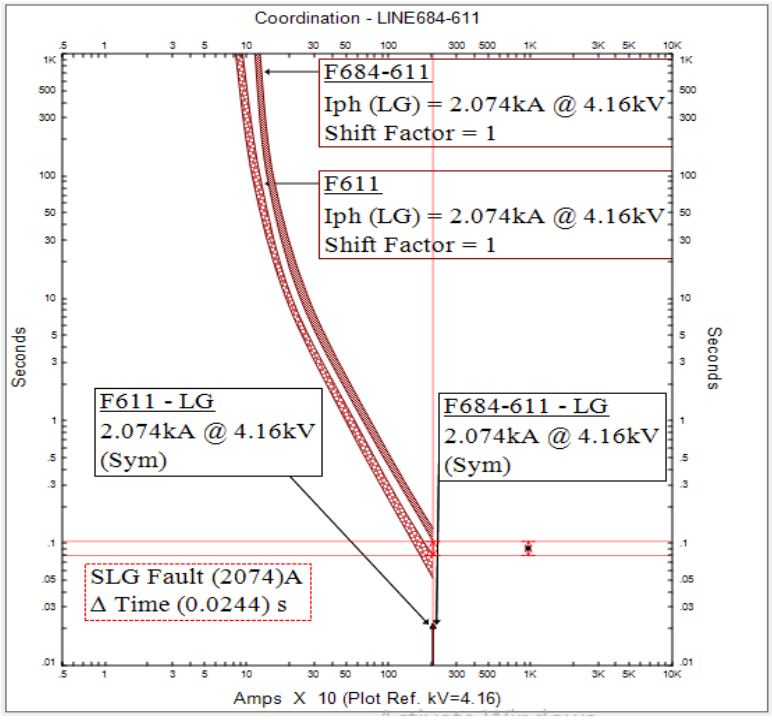

Figure 3.24: Fuses F684-611 and F611 TCC Curves for SLG Fault at NODE611 with 3MW DFIG Connected at NODE632

3.3.7 Fuse-Fuse Coordination for SLG Faults with 3MW DFIG Connected at NODE671

A. Fuse-Fuse Coordination Time Margins for SLG Faults with 3MW DFIG Connected at NODE671

Table 3.21: Fuse-Fuse Time Margins for SLG Faults with 3MW DFIG Connected at NODE671

Fault Location	Upstream Fuse	Down-Stream Fuse	NODE671	
			Fault Current (A)	Time Margin (s)
LINE671-684	F671	F671-684	3889	3.455
NODE684	F671-684	F684	3439	0.0193
LINE684-611	F684	F684-611	3439	0.0038
NODE611	F684-611	F611	3028	0.0032

Fuse-Fuse TCC Coordination Curves for SLG Faults with 3MW DFIG Connected at NODE671

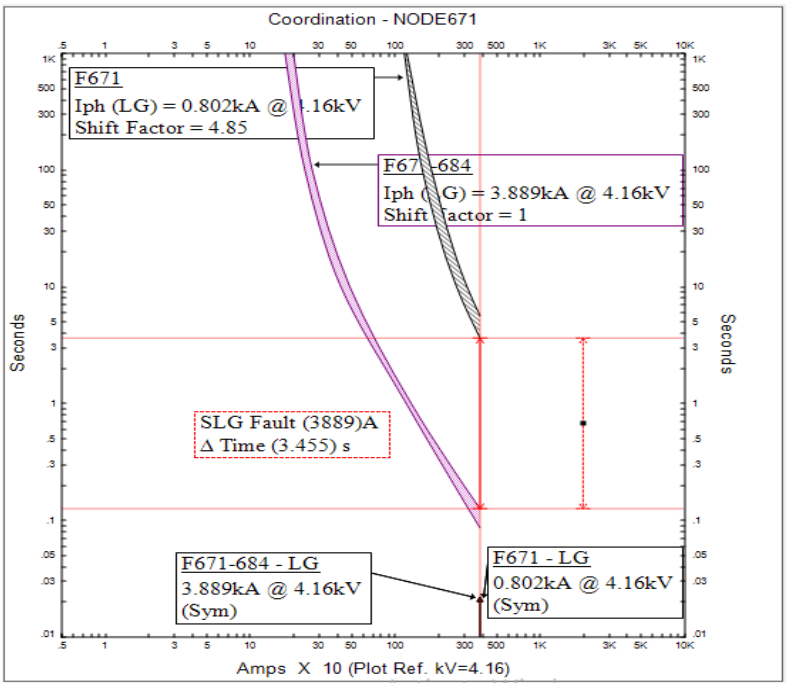

Figure 3.25: Fuses F671 and F671-684 TCC Curves for SLG Fault on LINE671-684 with 3MW DFIG Connected at NODE671

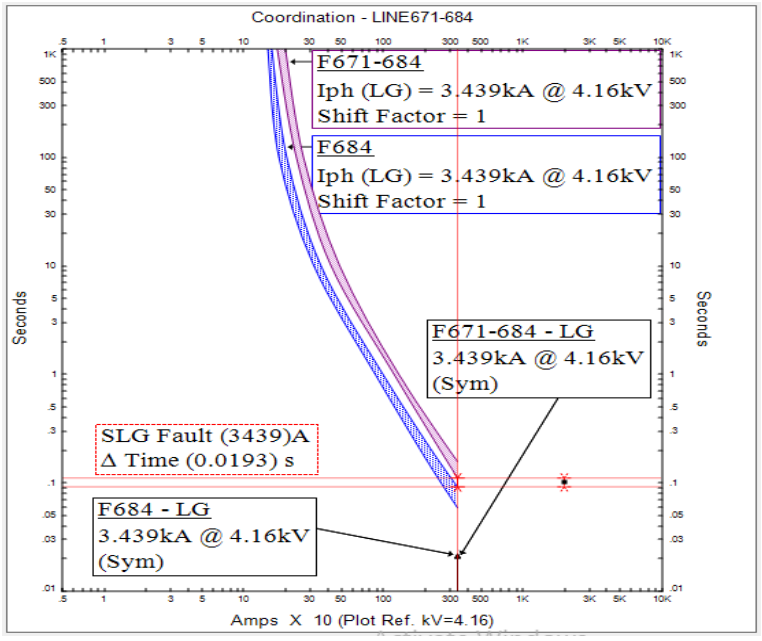

Figure 3.26: Fuses F671-684 and F684 TCC Curves for SLG Fault at NODE684 with 3MW DFIG Connected at NODE671

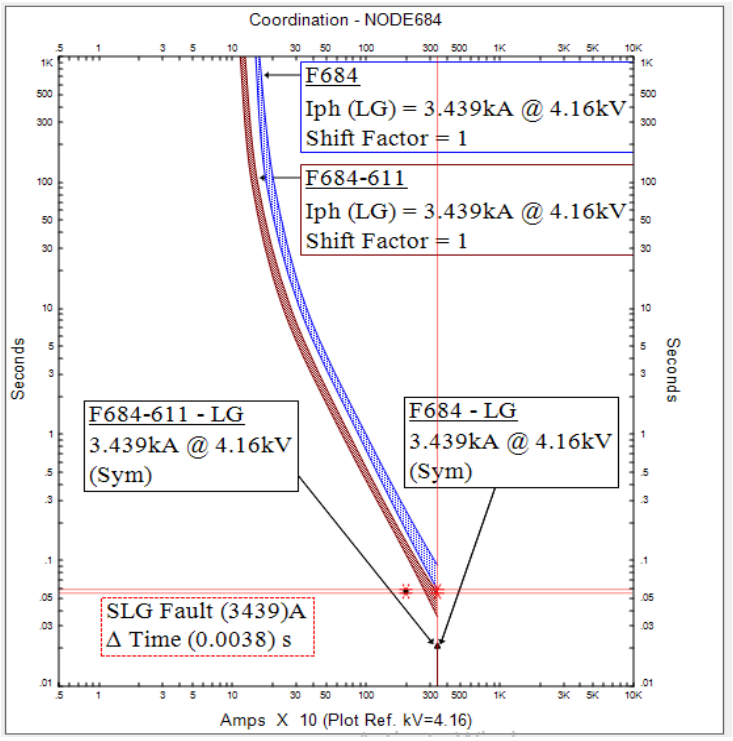

Figure 3.27: Fuses F684 and F684-611 TCC Curves for SLG Fault on LINE684-611 with 3MW DFIG Connected at NODE671

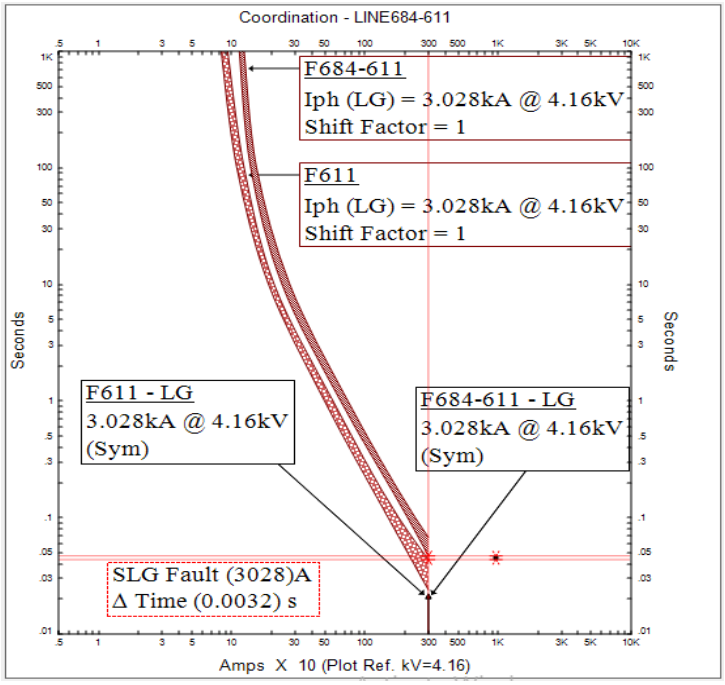

Figure 3.28: Fuses F684-611 and F611 TCC Curves for SLG Fault at NODE611 with 3MW DFIG Connected at NODE671

3.4 IEEE 13 Node Radial Test Feeder Fuse-Fuse Coordination with 2 Ohms CLR Interfaced' DFIGs.

3.4.1 Short Circuit Currents and Sequence Reactance with 2 Ohms CLR Interfaced DFIGs.

A. NODE671 SLG Faults and Sequence Reactance with 2 Ohms CLR Interfaced' 3MW DFIGs

Table 3.22: NODE671 SLG Faults and Sequence Reactance with 2 Ohms CLR Interfaced' 3MW DFIGs

DFIG Location	NODE650	NODE632	NODE671
SLG (A)	1240	1388	1631
Positive Sequence (Ω)	2.05062	1.86745	1.68128
Negative Sequence (Ω)	2.03015	1.84589	1.65869
Zero Sequence (Ω)	1.65791	1.43324	1.05969

B. NODE684 SLG Faults and Sequence Reactance with 2 Ohms CLR Interfaced' 3MW DFIGs

Table 3.23: NODE684 SLG Faults and Sequence Reactance with 2 Ohms CLR Interfaced' 3MW DFIGs

DFIG Location	NODE650	NODE632	NODE671
SLG (A)	1189	1324	1546
Positive Sequence (Ω)	2.09816	1.91498	1.72881
Negative Sequence (Ω)	2.07769	1.89343	1.70622
Zero Sequence (Ω)	1.78712	1.56245	1.18889

C. NODE611 SLG Faults and Sequence Reactance with 2 Ohms CLR Interfaced' 3MW DFIGs

Table 3.24: NODE611 SLG Faults and Sequence Reactance with 2 Ohms CLR Interfaced' 3MW DFIGs

DFIG Location	NODE650	NODE632	NODE671
SLG (A)	1135	1258	1458
Positive Sequence (Ω)	2.18453	2.00135	1.81518
Negative Sequence(Ω)	2.16406	1.9798	1.7926
Zero Sequence (Ω)	1.87339	1.64872	1.27516

3.4.2 Fuse-Fuse Coordination for SLG Faults with 2 Ohms CLR Interfaced' DFIG Connected at NODE650

A. Fuse-Fuse Time Margins for SLG Faults with 2 Ohms CLR Interfaced' 3MW DFIG Connected at NODE650

Table 3.25: Fuse-Fuse Time Margins for SLG Faults with 2 Ohms CLR Interfaced' 3MW DFIG Connected at NODE650

Fault Location	Upstream Fuse	Down-Stream Fuse	Fault Current (A)	Time Margin (s)
LINE671-684	F671	F671-684	1240	0.207
NODE684	F671-684	F684	1189	0.322
LINE684-611	F684	F684-611	1189	0.135
NODE611	F684-611	F611	1135	0.095

B. Fuse-Fuse TCC Curves for SLG Faults with 2 Ohms CLR Interfaced' 3MW DFIG Connected at NODE650

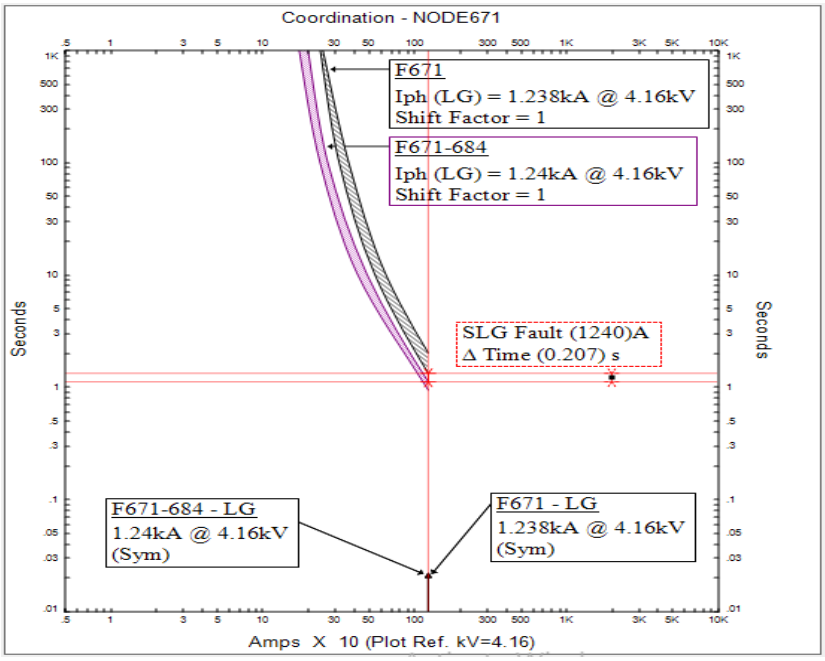

Figure 3.29: Fuses F671 and F671-684 TCC Curves for SLG Fault on LINE671-684 with 2 Ohms CLR Interfaced' 3MW DFIG Connected at NODE650

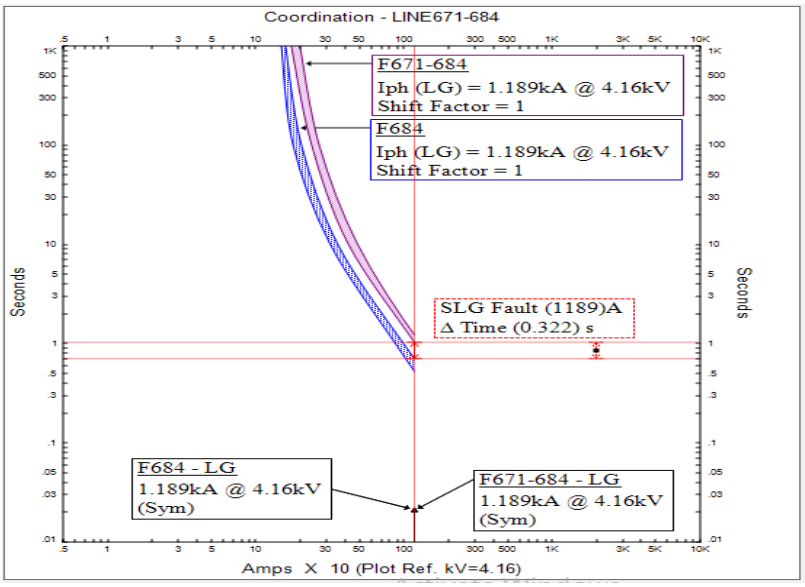

Figure 3.30: Fuses F671-684 and F684 TCC Curves for SLG Fault at NODE684 with 2 Ohms CLR Interfaced' 3MW DFIG Connected at NODE650

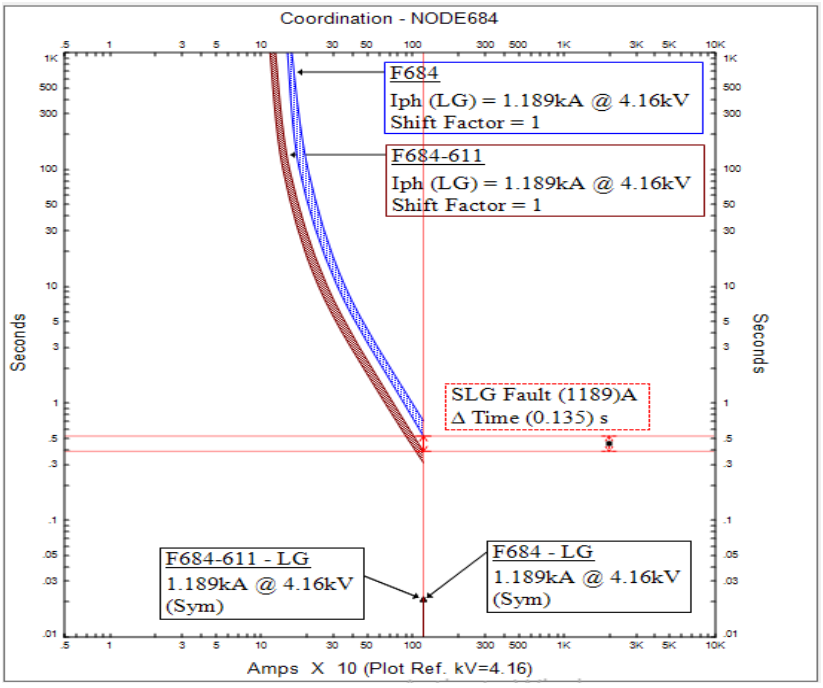

Figure 3.31: Fuses F684 and F684-611 TCC Curves for SLG Fault on LINE684-611 with 2 Ohms CLR Interfaced' 3MW DFIG Connected at NODE650

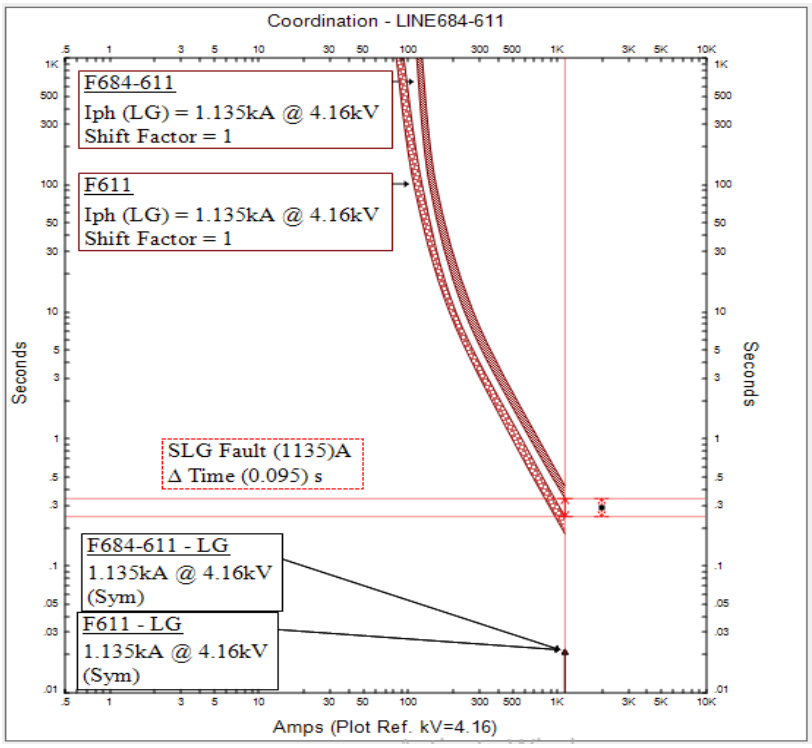

Figure 3.32: Fuses F684-611 and F611 TCC Curves for SLG Fault at NODE611 with 2 Ohms CLR Interfaced' 3MW DFIG Connected at NODE650

3.4.3. Fuse-Fuse Coordination for SLG Faults with 2 Ohms CLR Interfaced' DFIG Connected at NODE632

A. Fuse-Fuse Time Margins for SLG Faults with 2 Ohms CLR Interfaced' 3MW DFIG Connected at NODE632

Table 3.26: Fuse-Fuse Time Margins for SLG Faults with 2 Ohms CLR Interfaced' 3MW DFIG Connected at NODE632

Fault Location	Upstream Fuse	Down-Stream Fuse	Fault Current (A)	Time Margin (s)
LINE671-684	F671	F671-684	1388	0.151
NODE684	F671-684	F684	1324	0.249
LINE684-611	F684	F684-611	1324	0.101
NODE611	F684-611	F611	1258	0.079

B. Fuse-Fuse TCC Curves for SLG Faults with 2 Ohms CLR Interfaced' 3MW DFIG Connected at NODE632

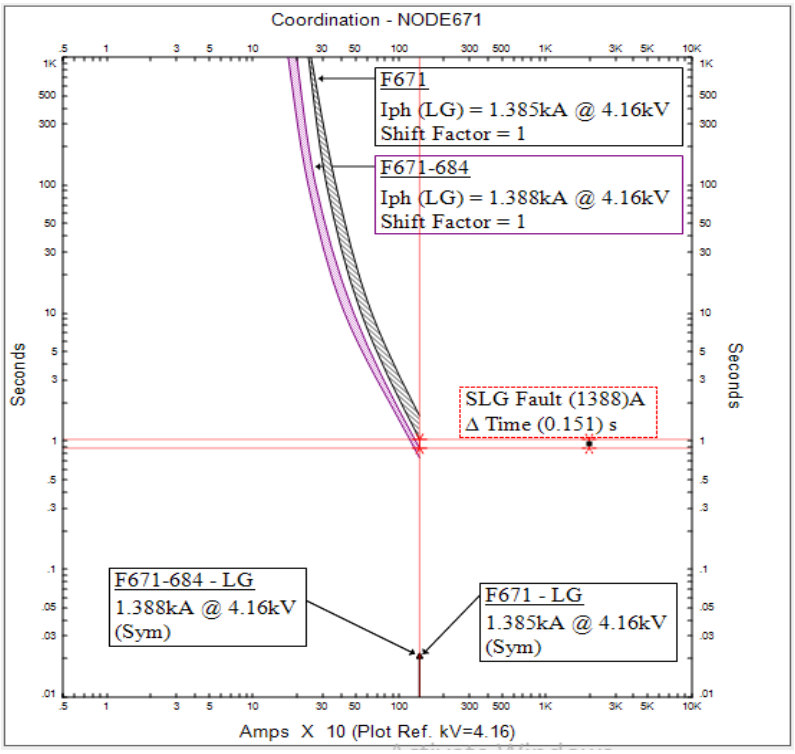

Figure 3.33: Fuses F671 and F671-684 TCC Curves for SLG Fault on LINE671-684 with 2 Ohms CLR Interfaced' 3MW DFIG Connected at NODE632

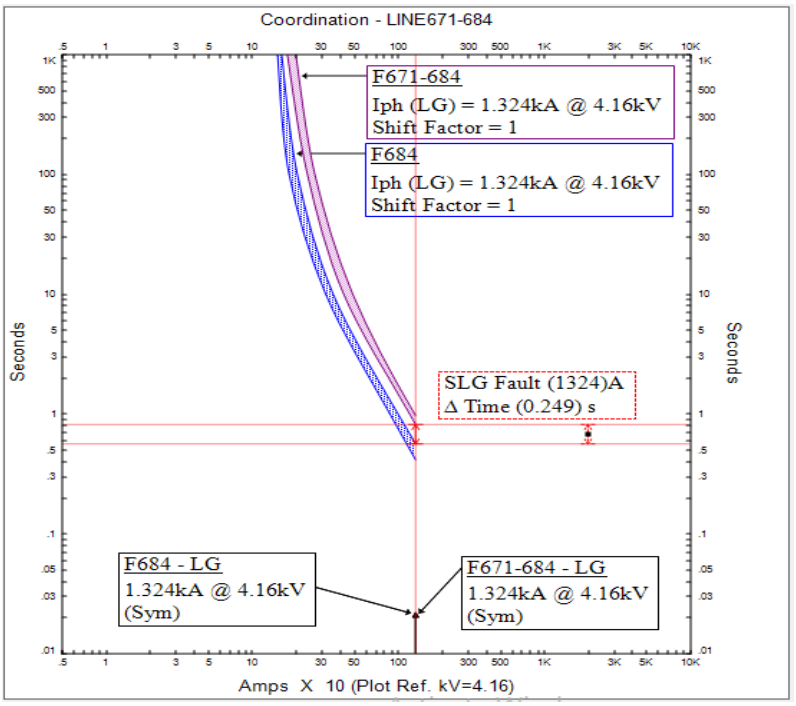

Figure 3.34: Fuses F671-684 and F684 TCC Curves for SLG Fault at NODE684 with 2 Ohms CLR Interfaced' 3MW DFIG Connected at NODE632.

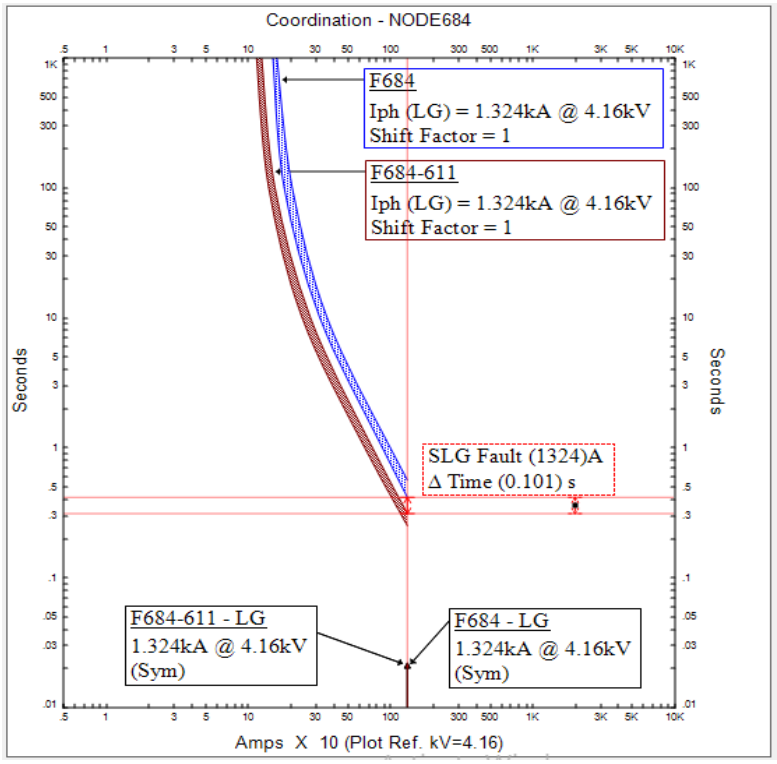

Figure 3.35: Fuses F684 and F684-611 TCC Curves for SLG Fault on LINE684-611 with 2 Ohms CLR Interfaced' 3MW DFIG Connected at NODE632.

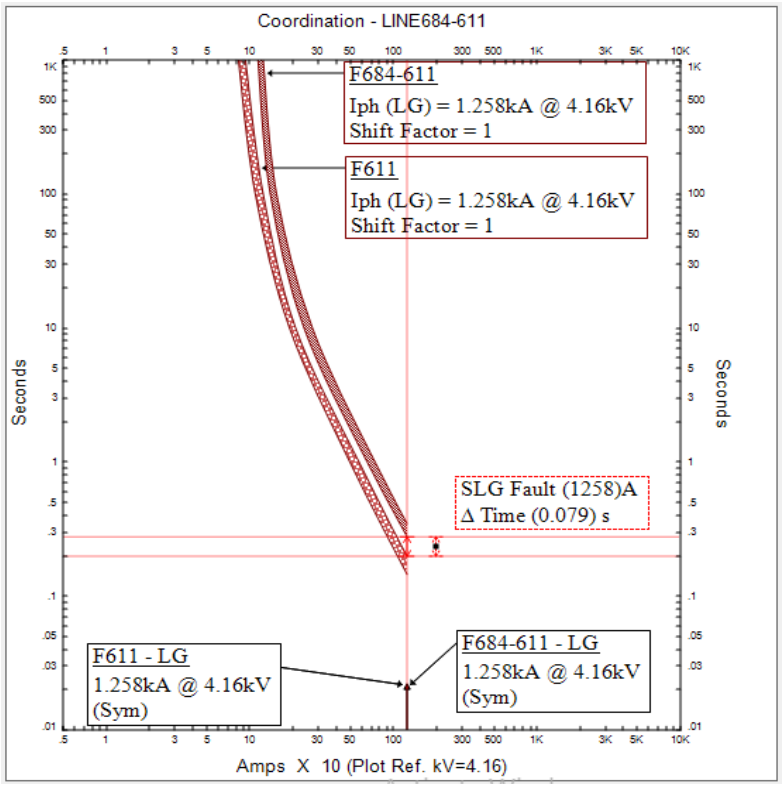

Figure 3.36: Fuses F684-611 and F611 TCC Curves for SLG Fault at NODE611 with 2 Ohms CLR Interfaced' 3MW DFIG Connected at NODE632

3.4.4. Fuse-Fuse Coordination for SLG Faults with 2 Ohms CLR Interfaced' DFIG Connected at NODE671

A. Fuse-Fuse Time Margins for SLG Faults with 2 Ohms CLR Interfaced' 3MW DFIG Connected at NODE671

Table 3.27: Fuse-Fuse Time Margins for SLG Faults with 2 Ohms CLR Interfaced' 3MW DFIG Connected at NODE671

Fault Location	Upstream Fuse	Down-Stream Fuse	Fault Current (A)	Time Margin (s)
LINE671-684	F671	F671-684	1631	3.35
NODE684	F671-684	F684	1546	0.173
LINE684-611	F684	F684-611	1546	0.067
NODE611	F684-611	F611	1458	0.059

B. Fuse-Fuse TCC Curves for SLG Faults with 2 Ohms CLR Interfaced' 3MW DFIG Connected at NODE671

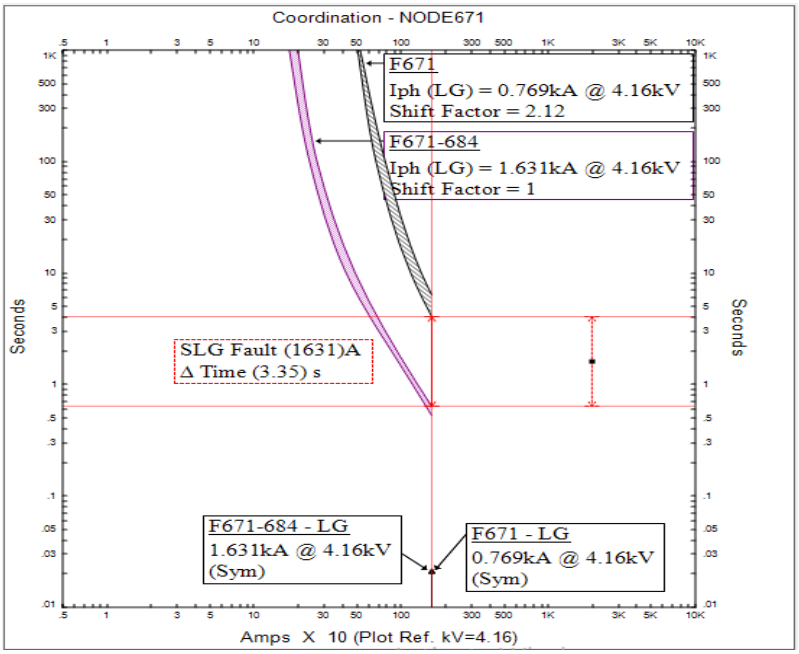

Figure 3.37: Fuses F671 and F671-684 TCC Curves for SLG Fault on LINE671-684 with 2 Ohms CLR Interfaced' 3MW DFIG Connected at NODE671

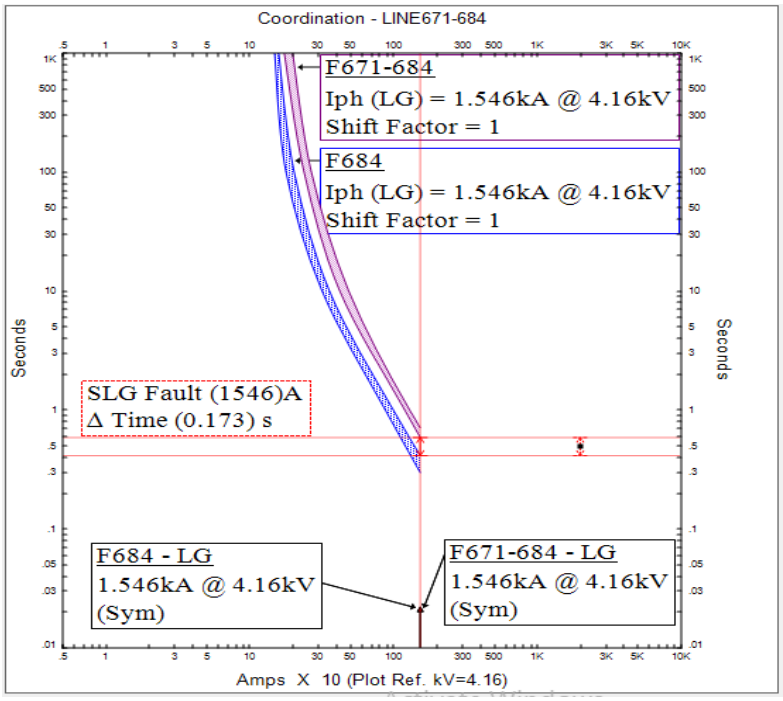

Figure 3.38: Fuses F671-684 and F684 TCC Curves for SLG Fault at NODE684 with 2 Ohms CLR Interfaced' 3MW DFIG Connected at NODE671

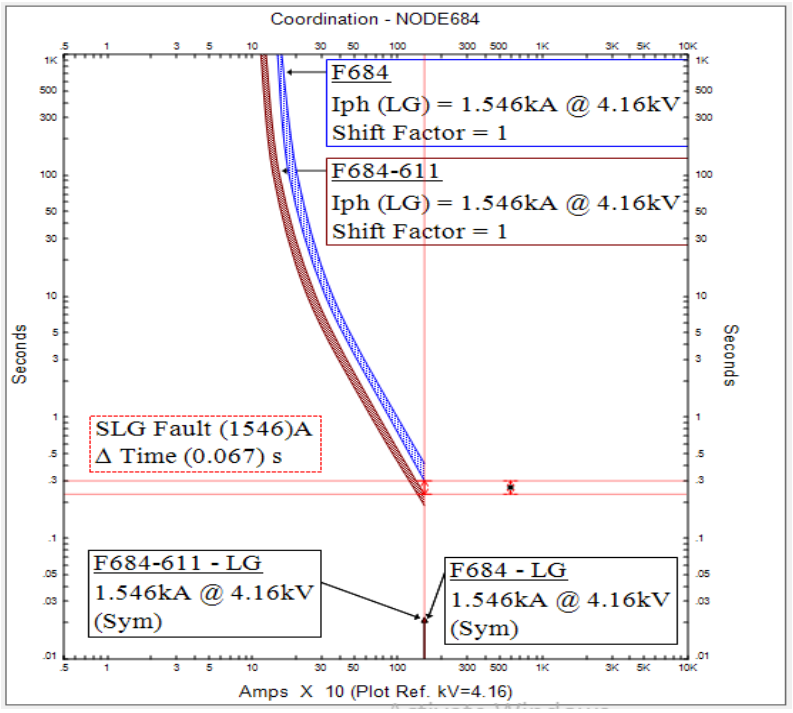

Figure 3.39: Fuses F684 and F684-611 TCC Curves for SLG Fault on LINE684-611 with 2 Ohms CLR Interfaced' 3MW DFIG Connected at NODE671

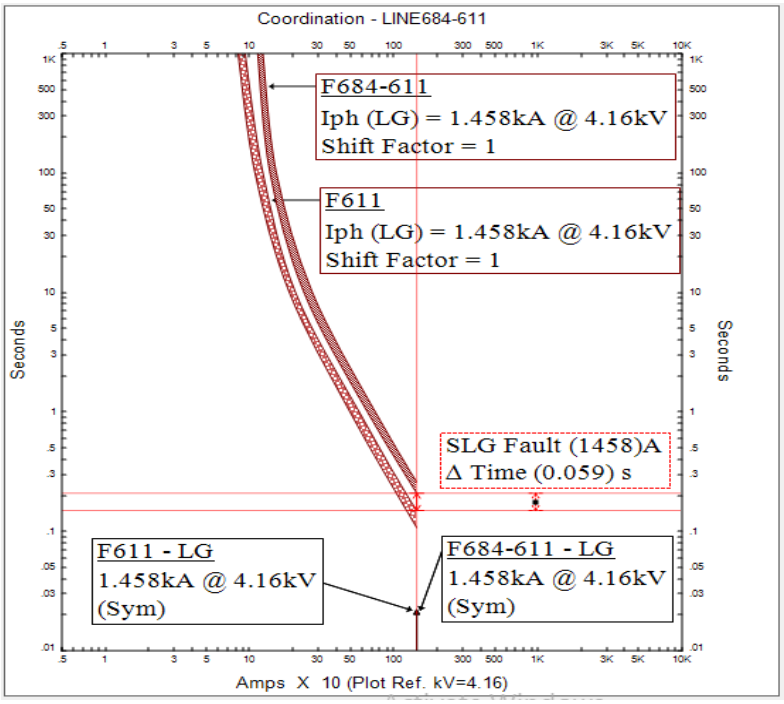

Figure 3.40: Fuses F684-611 and F611 TCC Curves for SLG Fault at NODE611 with 2 Ohms CLR Interfaced' 3MW DFIG Connected at NODE671

CHAPTER FOUR

RESULTS, ANALYSIS AND DISCUSSION

4.1 IEEE 13 Node Radial Test Feeder Conventional Fuse-Fuse Over-Current Protection Scheme

4.1.1 IEEE 13 Node Radial Test Feeder Conventional Fuse-Fuse Over-Current Protection Scheme ETAP Model

NEC240:101 and NEC450.3 stipulates that the current ratings for fuses used in developing a fuse-fuse over-current protection scheme for protecting electrical feeders are selected such that the fuses located at the farthest node on the feeder have the lowest current ratings. The subsequent fuses' current ratings increases gradually as the fuses are placed towards/nearer to the main grid substation/supply. The voltage ratings for the fuses must be equal to or greater than the feeder voltage profile and for a uniform coordination time margin between the coordinating fuses, one model/class of fuses is chosen for all the fuses used in developing the feeder fuse-fuse over-current protection scheme.

Three feeder components: two overhead line conductors denoted as LINE671-684 and LINE684-611, and a node denoted as NODE684 were chosen for the study because they were the farthest loaded feeder components from the main grid substation having overhead interconnections. The distance of the three feeder components from the main grid substation were: LINE671-684 4000 feet; NODE684 4300 feet; and LINE684-611 4300 feet. The three components were modelled to be protected by fuses from SLG short circuit faults occurring in the feeder at three fault locations namely: NODE684 4300 feet away from the main grid substation; LINE684-611 4300 feet away from the main grid substation; and NODE611 4600 feet away from the main grid substation. Each of the three components was protected by two fuses, an upstream fuse and a downstream fuse. LINE671-684 was protected by an upstream fuse F671-684 and a downstream fuse F684 from SLG faults occurring at NODE684; NODE684 was protected by an upstream fuse F684 and a downstream fuse F684-611 from SLG faults occurring on LINE684-611; and

LINE684-611 was protected by an upstream fuse F684-611 and a downstream fuse F611 from SLG faults occurring at NODE611. All the fuses chosen for the study were the fuses having the lowest current ratings for the fuse-fuse over-current protection scheme. Table 4.1 shows the upstream and the downstream fuses which would blow in a sequenced manner while clearing the SLG short circuit faults occurring at the three fault locations.

Table 4.1: LINE671-684, NODE684, and LINE684-611 Protective Fuses

Equipment	Fault Location	Upstream Fuse	Downstream Fuse
LINE671-684	NODE684	F671-684	F684
NODE684	LINE684-611	F684	F684-611
LINE684-611	NODE611	F684-611	F611

Table 4.2 shows a total of four fuses all of the same model, southern states and voltage rating 7.2 kV selected and placed at appropriate locations to protect the three feeder components from the SLG faults. The current ratings for the fuses met the NEC240:101 regulation which stipulates that the ratings for any fuse used to protect an overhead line conductor or a node should not have current ratings more than 300% of the ampacity of the overhead line conductor or the node it is protecting.

Table 4.2: Fuses: F671-684, F684, F684-611, and F611 Type and Ratings

Fuse ID	Rating (A)	Rating (kV)	Fuse Type	Ratings Speed
F671-684	150	7.2	Southern States	Slow
F684	125	7.2	Southern States	Slow
F684-611	100	7.2	Southern States	Slow
F611	75	7.2	Southern States	Slow

The four fuses were then placed and arranged such that their current ratings increases as the fuses are located nearer to the main grid substation. The composite TCC curve for the four fuses is shown in Figure 4.1 with fuse F611 with the lowest ratings of 75A being located at the bottom left hand corner of the composite TCC curve. Fuse F684-611 having the second lowest current ratings of 100 A was placed just above fuse F611 curve with the required time margin between them. Above fuse F684-611 curve is the curve for fuse F684 having the third lowest current rating of 125 A and the curve for fuse F671-684 with the fourth lowest current rating of 150 A following

just above the curve for F684 as shown in Figure 4.1. Figure 4.1 shows that as the fuses current ratings increased, their curves gradually moved from the bottom left hand corner towards the top right hand corner of the composite TCC curve.

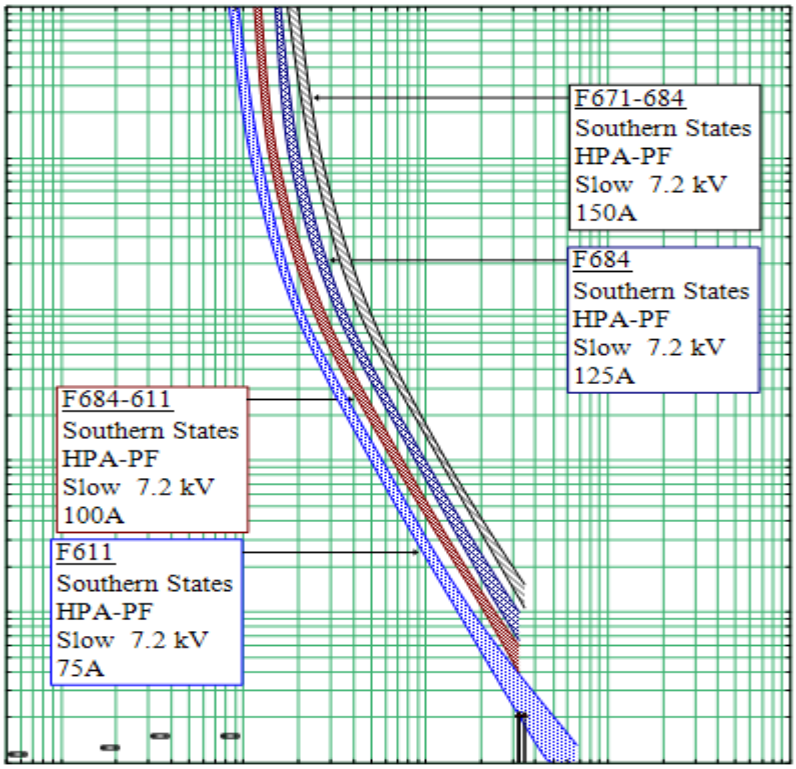

Figure 4.1: Fuses: F671-684, F684, F684-611, and F611 Composite TCC Curves

4.1.2 IEEE 13 Node Radial Test Feeder Equipment Protection

A. LINE 671-684 Protection Requirements

This is an overhead distribution line connected between NODE671 and NODE684 and it has an ampacity of 230 A. It is protected by two fuses, fuse F671-684 as the upstream fuse and fuse F684 as the downstream. The TCC curve for the overhead line conductor with its protective fuses is shown in Figure 4.2.The TCC curve shows the overhead line conductor's ampacity of 230 A at the upper decade at the 1000 seconds mark and the line conductors' short circuit damage curve located at the bottom three decades starting from 0.01 seconds to 10 seconds on the vertical axis scale. The TCC curve of Figure 4.2 shows the curves for fuses F671-684 and F684: both below and to the left of the line conductor's ampacity mark; both below and to

the left of the line conductors' intermediate thermal overload limit curve; both below and to the left of the line conductors' short circuit damage curve hence the overhead line is well protected by the two fuses. Fuse F671-684 continuous current rating of 150 A and fuse F684 continuous current rating of 125 A are both less than LINE671-684 300% ampacity rating of 690 A and so the two fuses' ratings meet the NEC 240.101 requirements for protecting the overhead distribution line.

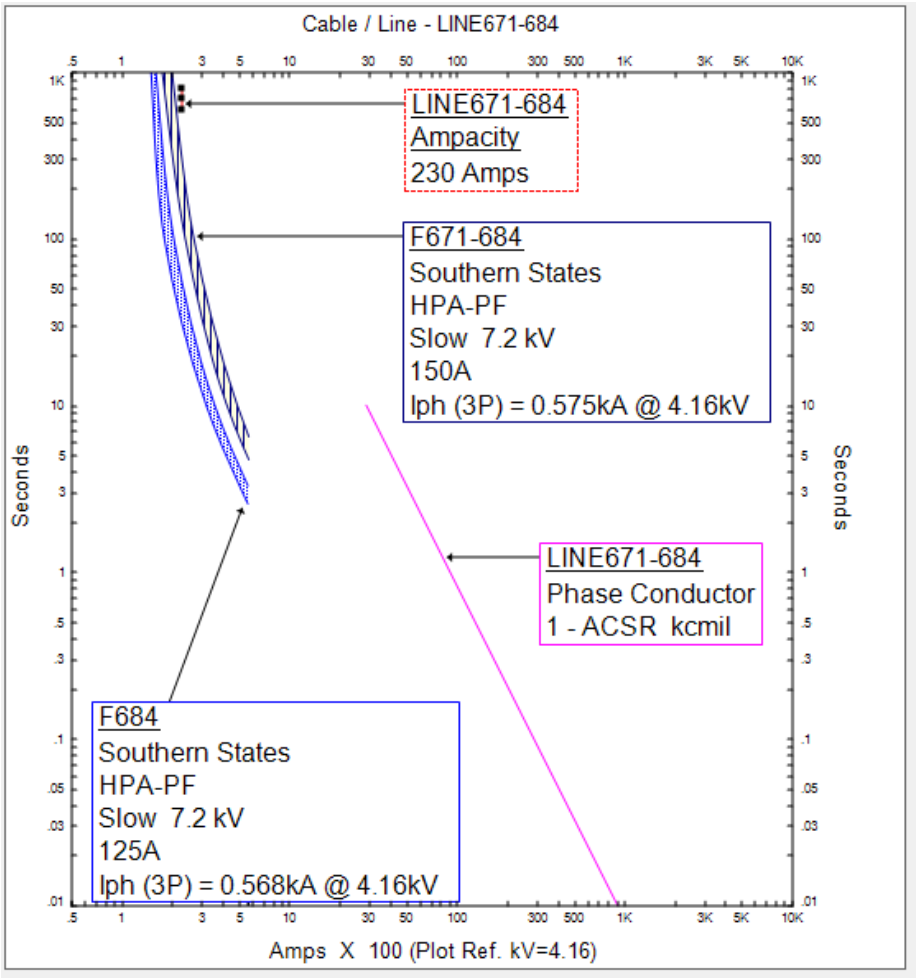

Figure 4.2: LINE671-684 Ampacity Mark, Short Circuit Damage Curve and Fuses F671-684 and F684 TCC Curves

B. NODE684 Protection Requirements

This is a node with an ampacity rating of 230 A and is protected by fuse F684 having a continuous current rating of 125 A. From the TCC curve of Figure 4.3 the curve for fuse F684 is located below and to the left of the node's ampacity mark at 1000 seconds mark at the upper decade of the TCC curve hence the node is well protected by the fuse. Fuse F684 continuous current of 125 A is less than NODE684 300% ampacity rating of 690 A and so fuse F684 current rating meet the NEC 240.101 requirements for protecting the node.

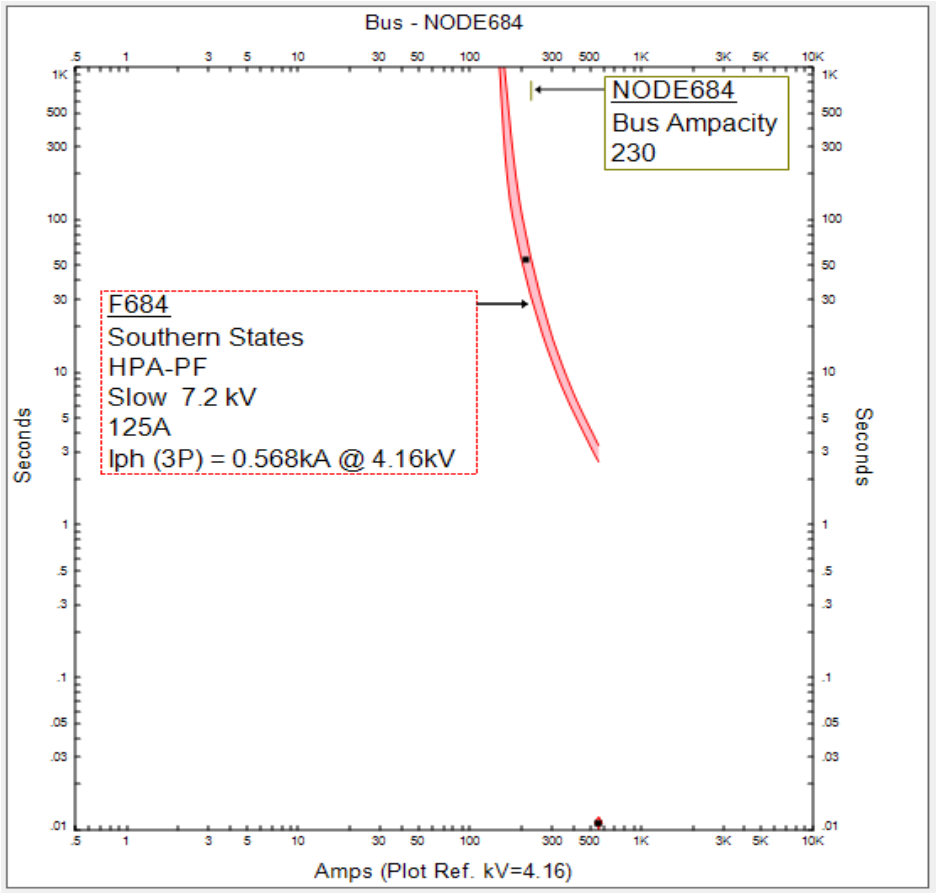

Figure 4.3: NODE684 Ampacity Mark and Fuse F684 TCC Curve

C. LINE684-611 Protection Requirements

This is an overhead distribution line connected between NODE684 and NODE611 and it has an ampacity of 230 A. It is protected by two fuses an upstream fuse F684-611 and a downstream fuse F611. The TCC curve for the overhead line with its

protective fuses is shown in Figure 4.4.The TCC curve shows the overhead line conductor's ampacity of 230 A at the upper decade at the 1000 seconds mark and the line conductor's short circuit damage curve located at the bottom three decades starting from 0.01 seconds to 10 seconds on the vertical axis scale. From the TCC curve of Figure 4.4, fuse F684-611 and fuse F611 TCC curves are: both below and to the left of the line conductor's ampacity mark; both below and to the left of the line conductors' intermediate thermal overload limit curve; and both below and to left of the line conductors' short circuit damage curve hence the overhead line is well protected by the fuses. The current ratings of 100 A for fuse F684-611 and 75 A for fuse F611 are less than LINE684-611 300% ampacity ratings of 690 A hence the fuses ratings meet the NEC 240:101 requirements for protecting the overhead line.

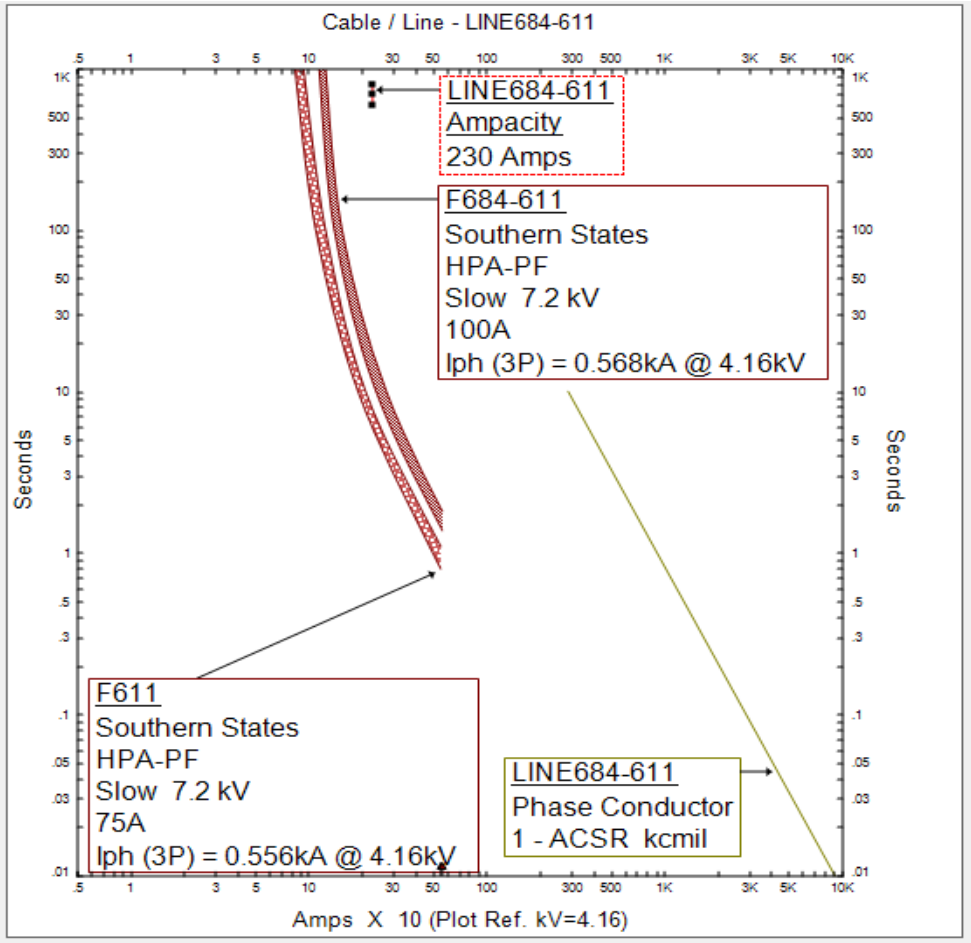

Figure 4.4: LINE684-611 Ampacity Mark, Short Circuit Damage Curve and Fuses F684-611 and F611 TCC Curves.

D. NODE611 Protection Requirements

This is a node with an ampacity rating of 230 A and is protected by fuse F611 having a continuous current rating of 75 A. From the TCC curve of Figure 4.5, the trip curve for fuse F611 is located below and to the left of the node's ampacity mark at 1000 seconds vertical axis mark at the upper decade of the TCC curve hence the node is well protected by the fuse. Fuse F611 continuous current rating of 75 A is less than NODE611 300% ampacity ratings of 690 A and so fuse F611 current rating meet the NEC 240.101 requirements for protecting the node.

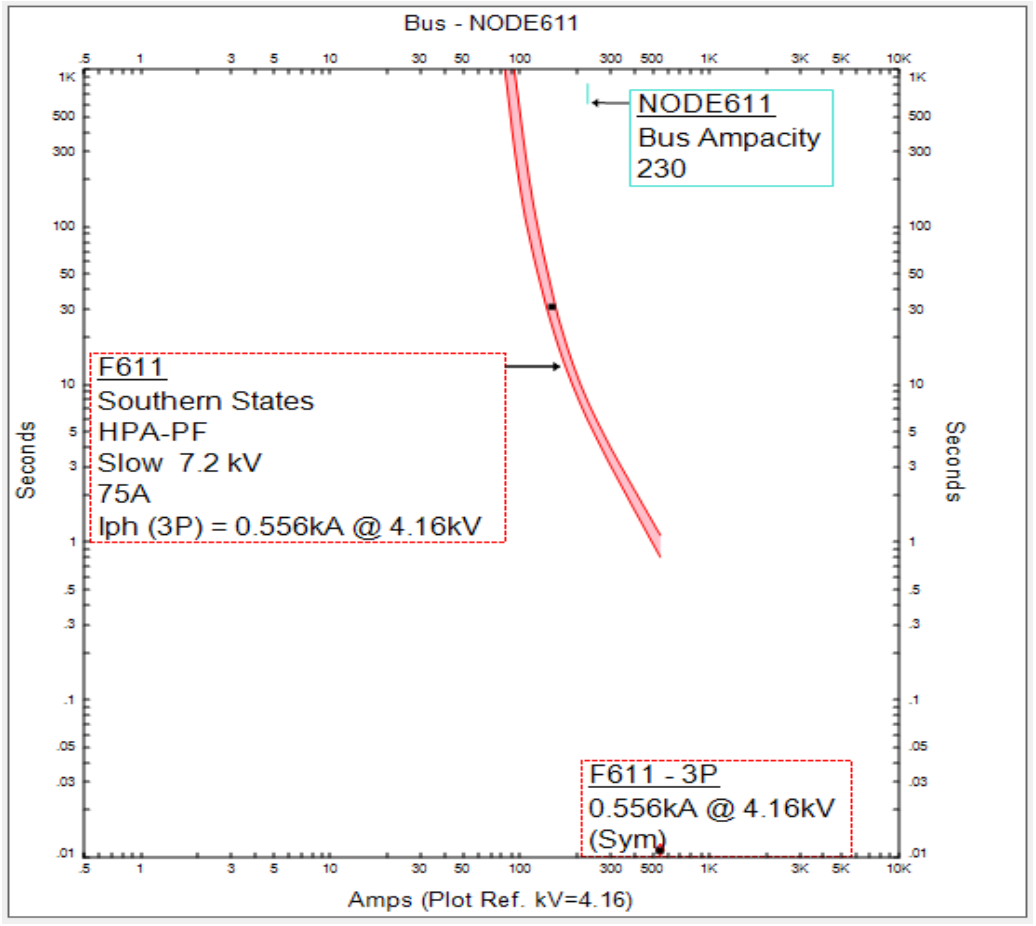

Figure 4.5: NODE611 Ampacity Mark and Fuse F611 TCC Curve

4.1.3 IEEE 13 Node Radial Test Feeder Fuse-Fuse Protection Coordination without WTGs

A. Fuses F671-684 and F684 Coordination for SLG Faults at NODE684 without WTGs

From Table 4.3, for an SLG fault of 697 A at NODE684, fuse F671-684 had a MMT of 3.103 seconds while fuse F684 had a TCT of 2.117 seconds and both fuses coordinated with a time coordination margin of 0.986 seconds while clearing the SLG fault of 697 A at NODE684.

Table 4.3: Fuses F671-684 and F684 Coordination for SLG Faults at NODE684 without WTGs

Fault Location	Fault Currents (A)	F671-684 MMT(s)	F684 TCT (s)	Time Margin (s)	Coordination Status
NODE684	697	3.103	2.117	0.986	Coordination

Figure 4.6 shows the TCC curve for fuses F671-684 and F684 coordination while clearing the SLG fault occurring at NODE684 without WTGs and it shows fuse F671-684 MMT curve and fuse F684 TCT curve both located above 2.117 seconds mark on the vertical axis scale above the foot of the TCC curve.

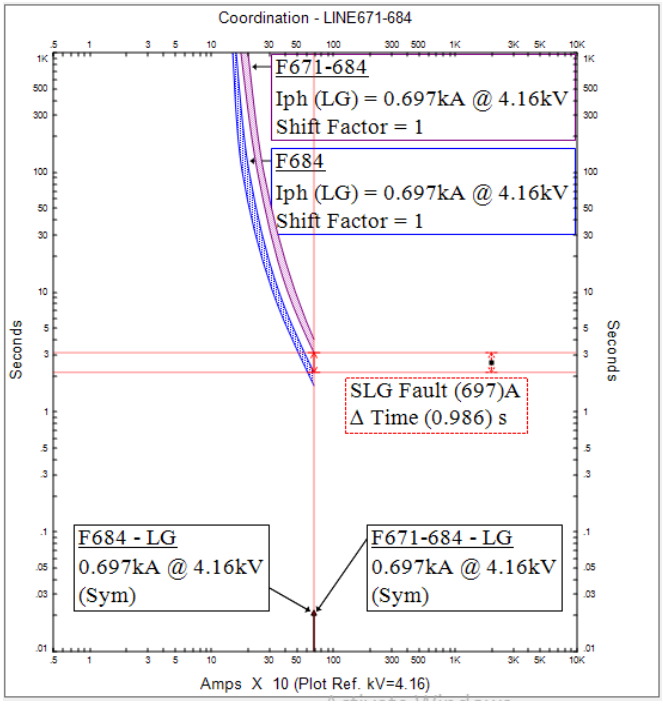

Figure 4.6: Fuses F671-684 and F684 TCC Curves for SLG Fault at NODE684 without WTGs

B. **Fuses F684 and F684-611 Coordination for SLG Faults on LINE684-611 without WTGs**

From Table 4.4, for an SLG fault of 697 A on LINE684-611, fuse F684 had a MMT of 1.649 seconds while fuse F684-611 had a TCT of 1.167 seconds both fuses coordinated with a time coordination margin of 0.482 seconds while clearing the SLG fault on LINE684-611.

Table 4.4: Fuses F684 and F684-611 Coordination for SLG Faults on LINE684-611 without WTGs

Fault Location	Fault Currents (A)	F684 MMT(s)	F684-611 TCT (s)	Time Margin (s)	Coordination Status
LINE684-611	697	1.649	1.167	0.482	Coordination

Figure 4.7 shows the TCC curve for fuses F684 and F684-611 coordination while clearing the SLG fault occurring on LINE684-611 without WTGs and it shows fuse F684 MMT curve and fuse F684-611 TCT curve both located above 1.167 seconds mark on the vertical axis scale above the foot of the TCC curve.

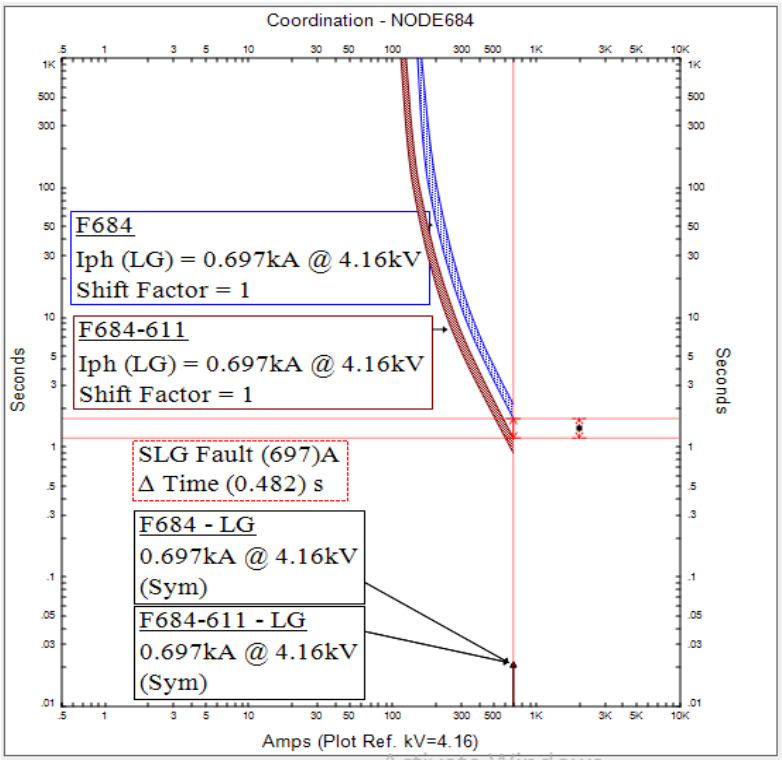

Figure 4.7: Fuses F684 and F684-611 TCC Curves for SLG Fault on LINE684-611 without WTGs

C. Fuses F684-611 and F611 Coordination for SLG Faults at NODE611 without WTGs

From Table 4.5, for an SLG fault of 679 A at NODE611, fuse F684-611 had a MMT of 0.944 seconds while fuse F611 had a TCT of 0.713 seconds both fuses coordinated with a time coordination margin of 0.231 seconds while clearing the SLG fault at NODE611.

Table 4.5: Fuses F684-611 and F611 Coordination for SLG Faults at NODE611 without WTGs

Fault Location	Fault Currents (A)	F684-611 MMT(s)	F611 TCT (s)	Time Margin (s)	Coordination Status
NODE611	679	0.944	0.713	0.231	Coordination

Figure 4.8 shows the TCC curve for fuses F684-611 and F611 coordinating while clearing the SLG fault occurring at NODE611 without WTGs and it shows fuse

F684-611 MMT curve and fuse F611 TCT curve located at 0.713 seconds mark on the vertical scale above the foot of the TCC curve.

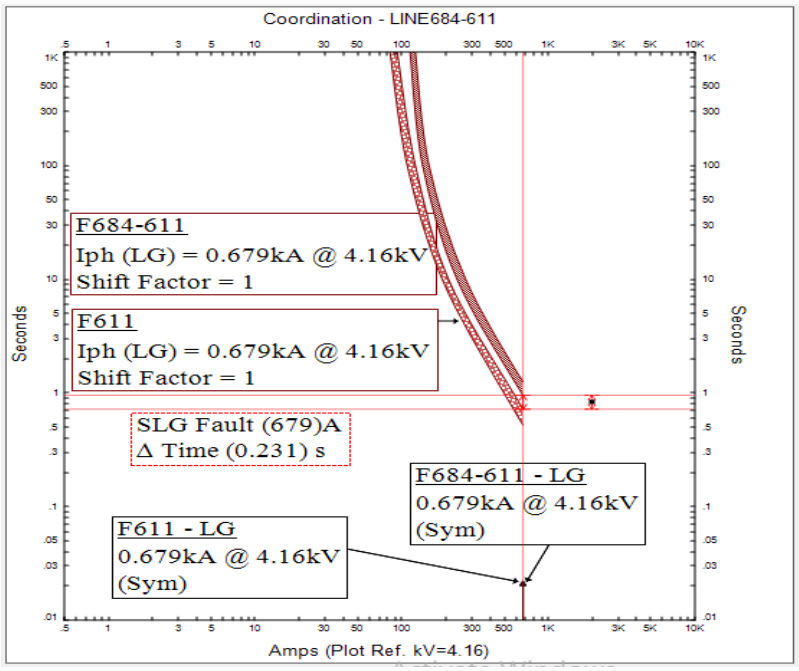

Figure 4.8: Fuses F684-611 and F611 TCC Curves for SLG Fault at NODE611 without WTGs

NEC240:101 stipulates that fuse-fuse coordination is achieved if, while clearing a fault, the time coordination margin between an upstream fuse and a downstream fuse is more than 0.025 seconds. While protecting LINE671-684 from an SLG fault of 697 A occurring at NODE684, fuse F671-684 and fuse F684 coordinated with a time margin of 0.986 seconds which is higher than the minimum required margin of 0.025 seconds hence the fuses coordinated. Consequently, fuses F684 and F684-611, and F684-611 and F611 coordinated with time margins of 0.482 seconds and 0.231 seconds respectively while clearing SLG faults of 697 A and 679 A occurring on LINE684-611 and NODE611 respectively. The fuse-fuse time coordination margins of 0.482 seconds and 0.231 seconds are higher than the minimum fuse-fuse miss-coordination margin of 0.025 seconds hence the fuses coordinated. All the fuses': current ratings; voltage ratings; and their TCC curves modelled to protect the test feeder components coordinated while clearing SLG faults occurring in the feeder.

4.2 Impacts of DFIGs and Type IV WTGs on IEEE 13 Node Radial Test Feeder Short Circuit Currents and Sequence Reactance

A detailed study was performed on the impacts 1MW and 3MW DFIGs and Type IV WTGs have on the feeder short circuit currents and sequence reactance. The DFIGs and the Type IV WTGs models were interchangeably connected at three different nodes on the feeder with the choice of the nodes being the distance the nodes were located from the main grid substation. This was to investigate the impacts the distance for placement of the WTGs from the main grid substation have on the variation on the magnitudes of the feeder short circuit currents and the feeder sequence reactance during a short circuit. The nodes were: NODE650 zero feet away from the main grid; NODE632 2000 feet from the main grid; and NODE671 4000 feet away from the main grid. All the chosen nodes for WTG placement were three phase nodes with three phase overhead lines interconnecting them with the rest of the test feeder nodes/loads.

4.2.1 Impacts of 1MW and 3MW DFIGs and Type IV WTGs on the Feeder Short Circuit Currents without CLRs

From Table 4.6, when the radial test feeder was short circuited without WTGs connected into it, the SLG fault currents at NODE684 was 697 A and at NODE611 was 679 A. When 1MW Type IV WTGs were interchangeably connected at NODE650, NODE632 and NODE671, the SLG fault currents at NODE611 increased gradually from 679 A to 728 A, 740 A and 754 A respectively as shown in Table 4.6. When the capacity of the 1MW Type IV WTGs were increased to 3MW, the SLG fault currents at NODE611 further increased: from 728 A to 952 A; from 740 A to 1001 A; and from 754 A to 1065 A for 3MW Type IV WTGs connected at NODE650, NODE632 and NODE671 respectively from Table 4.6.

Table 4.6: NODE684 and NODE611 SLG Fault Currents with 1MW and 3MW Type IV WTGs

SLG (A)	Without WTGs	Type IV WTGs					
		1MW			3MW		
		NODE 650	NODE 632	NODE 671	NODE 650	NODE 632	NODE 671
NODE684	697	751	764	780	992	1045	1114
NODE611	679	728	740	754	952	1001	1065

From Table 4.17, when the Type IV WTGs were replaced with DFIGs, the magnitudes of the SLG fault currents of 679 A at NODE611 further increased in magnitude to 1191 A, 1341 A and 1590 A for 1MW DFIGs connected at NODE650, NODE632 and NODE671.respectively. There was a further increase in the SLG fault currents at NODE611 from: 1191 A to 1626 A; 1341 A to 2074 A; and 1590 A to 3028 A when 3MW DFIGs were connected at NODE650, NODE632 and NODE671 respectively as shown in Table 4.7.

Table 4.7: NODE684 and NODE611 SLG Fault Currents with 1MW and 3MW DFIGs

SLG (A)	Without WTGs	DFIGs					
		1MW			3MW		
		NODE 650	NODE 632	NODE 671	NODE 650	NODE 632	NODE 671
NODE684	697	1251	1416	1696	1741	2263	3439
NODE611	679	1191	1341	1590	1626	2074	3028

Figure 4.9 shows a graphical representation on the variation on the magnitudes of the SLG fault currents at NODE684 and NODE611 with the change in the capacity and the location of the Type IV WTGs and the DFIGs placement. Figure 4.9 shows a gradual increase on the SLG fault currents at NODE684 and NODE611 for 1MW and 3MW Type IV WTGs as compared to a steep increase on the SLG fault currents at the same nodes for 1MW and 3MW DFIGs connected at NODE650, NODE632 and NODE671. From Figure 4.9, the pattern/rate of increase on the SLG fault currents at NODE611 was similar in how the fault currents increased at NODE684 with the only difference being that NODE684 had slightly higher magnitudes of the SLG fault currents as compared to the fault currents at NODE611.

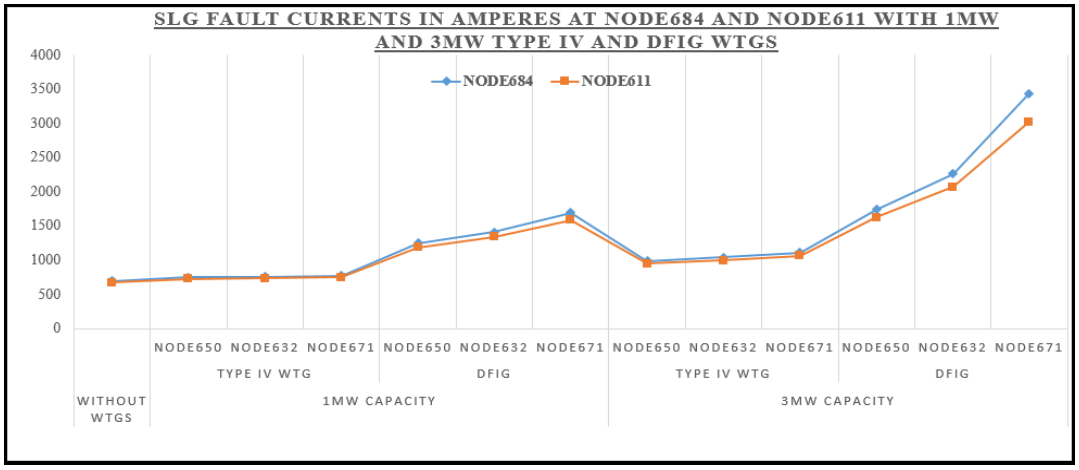

Figure 4.9: SLG Fault Currents in Amperes at NODE 684 and NODE611 with 1MW and 3MW Type IV WTGs and 3MW DFIGs

DFIG injected the highest SLG fault currents into the test feeder as compared to the contribution from the Type IV WTG. For both classes of the WTGs, an increase on their capacities from 1MW to 3MW further caused an increase in the SLG fault currents with 3MW DFIG having the highest increase on the test feeder SLG fault currents. The highest levels of the SLG fault currents for the WTGs was experienced when the WTGs were connected at NODE671 which was the farthest node from the main grid substation for WTG placement. The magnitudes of the SLG fault currents would again progressively reduce as the WTGs were connected at nodes closer to the main grid, NODE632 and NODE650 respectively. For both WTGs, the magnitudes of the SLG short circuit fault currents generally reduced in magnitudes as the faulted nodes are located farther away from the main grid substation NODE650. NODE611 had slightly lower magnitudes of the SLG fault currents as compared to the SLG fault currents at NODE684. It was concluded that the capacities, the location for placement, and the type of the WTG interfacing technology had great impacts on the magnitudes of the feeder SLG fault current magnitudes with 3MW DFIGs placed nearer to the faulted nodes injecting the highest amount of fault currents as compared to the magnitudes of the fault currents injected by the DFIGs and Type IV WTGs placed far from to the faulted nodes.

4.2.2 Impacts of 1MW and 3MW DFIGs and Type IV WTGs on the Feeder Sequence Reactance without CLRs

A. NODE684 and NODE611 Sequence Reactance with 1MW and 3MW DFIG and Type IV WTGs Connected at NODE671

From Table 4.8, without WTGs connected, the positive and the negative sequence reactance at NODE611 were of the same magnitude 4.26642 Ω while the zero sequence reactance was 1.89837 Ω. When a 1MW Type IV WTG was connected at NODE671, the sequence reactance would reduce in magnitude to: 3.30995 Ω for both the positive and negative sequence reactance; and 1.71326 Ω for zero sequence reactance from Table 4.8. When the capacity of the Type IV WTG was increased from 1 MW to 3MW the sequence reactance further reduced: from 3.30995 Ω to 1.51577 Ω for both the positive and the negative sequence reactance; and from 1.71326 Ω to 1.29413 Ω for zero sequence reactance.

Table 4.8: NODE684 and NODE611 Sequence Reactance with 1MW and 3MW Type IV WTG Connected at NODE671

Sequence Reactance (Ω)	Without WTGs		Type IV WTG			
			1MW		3MW	
	NODE 611	NODE 684	NODE 611	NODE 684	NODE 611	NODE 684
Positive	4.26642	4.18005	3.30995	3.22358	1.51577	1.4294
Negative	4.26642	4.18005	3.30995	3.22358	1.51577	1.4294
Zero	1.89837	1.8121	1.71326	1.62699	1.29413	1.20786

From Table 4.9, when the Type IV WTG was replaced with a DFIG, the positive sequence reactance at NODE611 further reduced in magnitudes: from 3.30995 Ω for 1MW Type IV WTG to 1.67661 Ω for a 1MW DFIG and from 1.51577 Ω for 3MW Type IV WTG to 0.8174 Ω for 3MW DFIG. Also the negative and zero sequence reactance reduced: from 3.30995 Ω for 1MW Type IV WTG to 1.61457 Ω for a 1MW DFIG and from 1.51577 Ω for 3MW Type IV WTG to 0.77282 Ω for 3MW DFIG for negative sequence reactance; and from 1.71326 Ω for 1MW Type IV WTG

to 1.19266 Ω for a 1MW DFIG and from 1.29413 Ω for 3MW Type IV WTG to 0.74238 Ω for 3MW DFIG for zero sequence reactance from Table 4.9.

Table 4.9: NODE684 and NODE611 Sequence Reactance with 1MW and 3MW DFIG Connected at NODE671

Sequence Reactance (Ω)	DFIG			
	1MW		3MW	
	NODE611	NODE684	NODE611	NODE684
Positive	1.67661	1.59024	0.8174	0.73103
Negative	1.61457	1.51325	0.77282	0.68645
Zero	1.19266	1.1064	0.74238	0.65611

Figure 4.10 shows a graphical representation on the variation on the magnitudes of the positive, negative and zero sequence reactance at NODE684 and NODE611 with the change in the capacity of the DFIG and the Type IV WTGs connected at NODE671. Both the positive and the negative sequence reactance were higher in magnitudes than the zero sequence reactance at NODE684 and NODE611.The pattern/rate of decrease on the positive, negative and zero sequence reactance at NODE611 was similar in how the sequence reactance reduced at NODE684 with all the three sequence reactances being slightly higher in magnitudes at NODE611 as compared to the sequence reactances at NODE684 from Table 4.8, Table 4.9 and Figure 4.10, respectively.

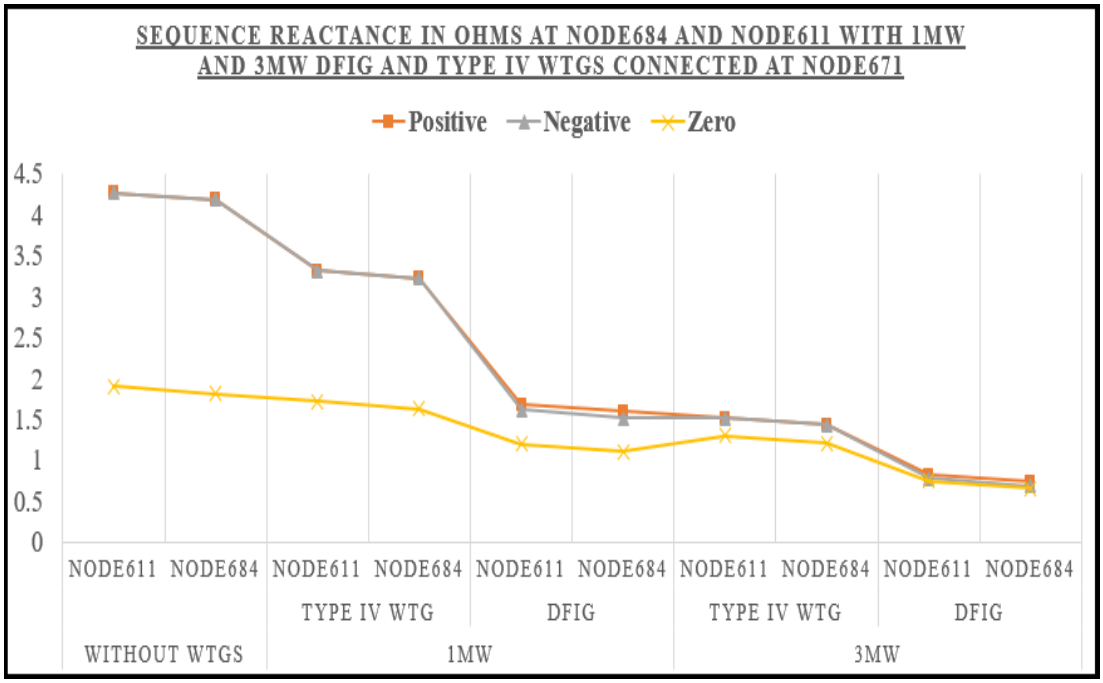

Figure 4.10: Positive, Negative and Zero Sequence Reactance in Ohms at NODE684 and NODE611 with 1MW and 3MW DFIGs and Type IV WTGs

NODE684 and NODE611 sequence reactance reduced once the WTGs were connected into the feeder and these magnitudes further reduced when the capacity of the WTGs were increased from 1MW to 3MW. Type IV WTGs caused a minimal reduction on the sequence reactance as compared to the reduction experienced for DFIGs. 3MW DFIG caused the highest reduction on the sequence reactance as compared to 3MW Type IV WTGs. The positive and the negative sequence reactance were both of equal magnitudes when Type IV WTGs were connected into the test feeder but the sequence reactance were not the same for DFIGs with the positive sequence reactance being higher than the negative sequence reactance. DFIG and Type IV WTG's increase in capacity caused a reduction on the feeder positive, negative and zero sequence reactances.

4.3 Impacts of DFIGs and Type IV WTGs on IEEE 13 Node Radial Test Feeder Fuse-Fuse Over-Current Protection Scheme

4.3.1 Impacts of 1MW and 3MW DFIGs and Type IV WTGs on Fuse-Fuse Coordination

Tables 4.10 and 4.11 shows that, as compared to 1MW DFIGs, 1MW Type IV WTGs and 3MW Type IV WTGs which had none of the fuses miss coordinating, 3MW DFIGs had a total of five pairs of fuses miss coordinating while clearing SLG faults occurring at NODE684, LINE684-611, and NODE611.

Table 4.10: Fuses F671-684, F684, F684-611, and F611 Coordination Time Margins in seconds for SLG Faults with 1MW and 3MW Type IV WTGs

Fault Location	Upstream Fuse	Down-Stream Fuse	Type IV WTG Placement					
			NODE650		NODE632		NODE671	
			1MW	3MW	1MW	3MW	1MW	3MW
NODE 684	F671-684	F684	0.844	0.476	0.815	0.429	0.781	0.373
LINE 684-611	F684	F684-611	0.412	0.212	0.397	0.186	0.379	0.159
NODE 611	F684-611	F611	0.202	0.128	0.196	0.118	0.189	0.106

Table 4.11 shows that: 3MW DFIG connected at NODE650 had none of the fuses miss coordinating; 3MW DFIG connected at NODE632 had two pairs of fuses miss coordinating, F684 and F684-611 at 0.022 seconds, and F684-611 and F611 at 0.0244 seconds for SLG faults occurring on LINE684-611 and at NODE611 respectively; and 3MW DFIG connected at NODE671 had three pairs of fuses miss coordinating F671-684 and F684 at 0.0193 seconds, F684 and F684-611 at 0.0038 seconds, and F684-611 and F611 at 0.0032 seconds for SLG faults occurring at NODE684, LINE684-611 and NODE611 respectively.

Table 4.11: Fuses F671-684, F684, F684-611 and F611 Coordination Time Margins in seconds for SLG Faults with 1MW and 3MW DFIGs

Fault Location	Upstream Fuse	Down-Stream Fuse	DFIG Placement					
			NODE650		NODE632		NODE671	
			1MW	3MW	1MW	3MW	1MW	3MW
NODE684	F671-684	F684	0.286	0.13	0.213	0.067	0.139	0.0193
LINE684-611	F684	F684-611	0.117	0.048	0.084	0.022	0.051	0.0038
NODE611	F684-611	F611	0.088	0.047	0.07	0.0244	0.049	0.0032

To investigate on the impacts the DFIGs have on: the upstream fuse minimum melting time (MMT) characteristics; the downstream fuse total clearing time (TCT) characteristics; the upstream fuse and the downstream fuse time coordination margins; and the location of the coordinating fuses' MMT and TCT curves along the vertical axis scale towards the 'foot' on the composite TCC curve, DFIGs were interchangeably connected at NODE650, NODE632, and NODE671.The bottom most section/part/decade of a TCC curve is referred to as the 'foot' of the curve and it is located between 0.1 seconds and 0.01 seconds vertical axis scale/marks on the TCC curve. It is at this 'foot' where fuses experience miss-coordination. The tracking of the closeness of the coordinating fuses' curves to the foot of a TCC curve was done by monitoring the location of the upstream fuse MMT curve and the downstream fuse TCT curve along the vertical axis scale of the TCC curve and this was presented through development of the coordinating fuses' TCC curves. The: fuse-fuse coordination time margins; the MMT characteristics; the TCT characteristics were monitored for fuses: F671-684 and F684; F684 and F684-611; and F684-611 and F611 once the DFIGs were connected into the feeder.

4.3.2 Impacts of 1MW and 3MW DFIG Connected at NODE671 on Fuses F684-611 and F611 Coordination

Table 4.12 shows that without WTGs, the SLG fault at NODE611 was 679 A and at this fault current, fuse F684-611 had a MMT of 0.944 seconds and fuse F611 had a TCT of 0.713 seconds both fuses coordinated with a time coordination margin of 0.231 seconds while clearing the SLG fault of 679 A.

When a 1MW DFIG was connected at NODE671, the SLG fault currents at NODE611 increased from 679 A to 1590 A. At the fault current of 1590 A, fuse F684-611 MMT of 0.944 seconds reduced to 0.174 seconds and fuse F611 TCT of 0.713 seconds reduced to 0.125 seconds with the two fuses now coordinating with a reduced time coordination margin of 0.049 seconds down from 0.231 seconds once the 1MW DFIG was connected. When the capacity of the DFIG was increased from 1MW to 3MW the SLG fault currents at NODE611 further increased from 1590 A to 3028 A as shown in Table 4.12. At the fault current of 3028 A, fuse F684-611 MMT of 0.174 seconds for 1MW DFIG further reduced to 0.0464 seconds while fuse F611 TCT of 0.125 seconds for 1MW DFIG further reduced to 0.0432 seconds with the two fuses now miss-coordinating with a much reduced/diminished time coordination margin of 0.0032 seconds down from a time coordination margin of 0.049 seconds for 1MW DFIG.

Table 4.12: Fuses F684-611 and F611 Coordination for SLG Fault at NODE611 with 1MW and 3MW DFIGs Connected at NODE671

DFIG Capacity	Fault Currents (A)	F684-611 MMT(s)	F611 TCT(s)	Time Margin(s)	Coordination Status
Without WTG	679	0.944	0.713	0.231	Coordination
1MW	1590	0.174	0.125	0.049	Coordination
3MW	3028	0.0464	0.0432	0.0032	Miss-Coordination

Figure 4.11 shows the curves for fuses F684-611 and F611 coordinating without WTGs on the left hand side and with 1MW DFIG on the right hand side while Figure 4.12 shows fuses F684-611 and F611 coordination for 1MW DFIG on the left hand side and for 3MW DFIG on the right hand side. Without WTGs, fuse F684-611 MMT and fuse F611 TCT curves are located above the foot at 0.713 seconds vertical axis mark show on the left hand side of Figure 4.11 and once a 1MW DFIG was connected at NODE671, the fuses curves shifted downwards from 0.713 seconds to 0.125 seconds vertical axis mark towards the foot of the TCC curve as shown graphically on the right hand side of Figure 4.11.

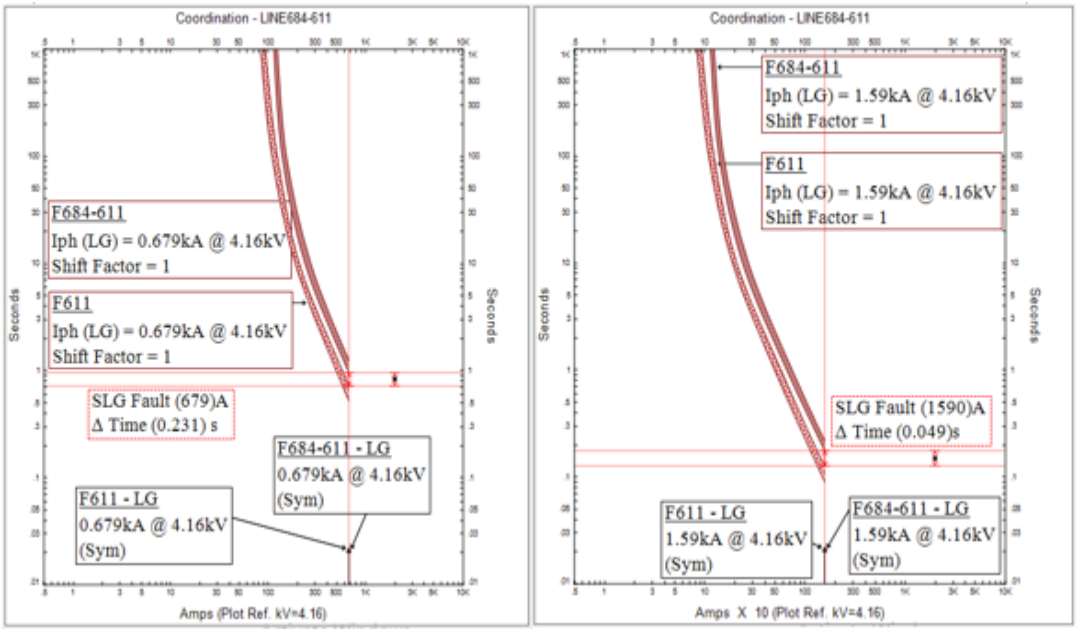

Figure 4.11: Fuses F684-611 and F611 TCC Curve for SLG Fault at NODE611 without WTGs and with 1MW DFIG Connected at NODE671

When the capacity of the DFIG was increased from 1MW to 3MW, fuse F684-611 MMT and fuse F611 TCT curves shifted further downwards along the vertical axis scale from 0.125 seconds above the foot for 1MW DFIG as shown graphically on the left hand side of Figure 4.12 to 0.0432 seconds at the foot of the TCC curve as shown graphically on the right hand side of Figure 4.12.

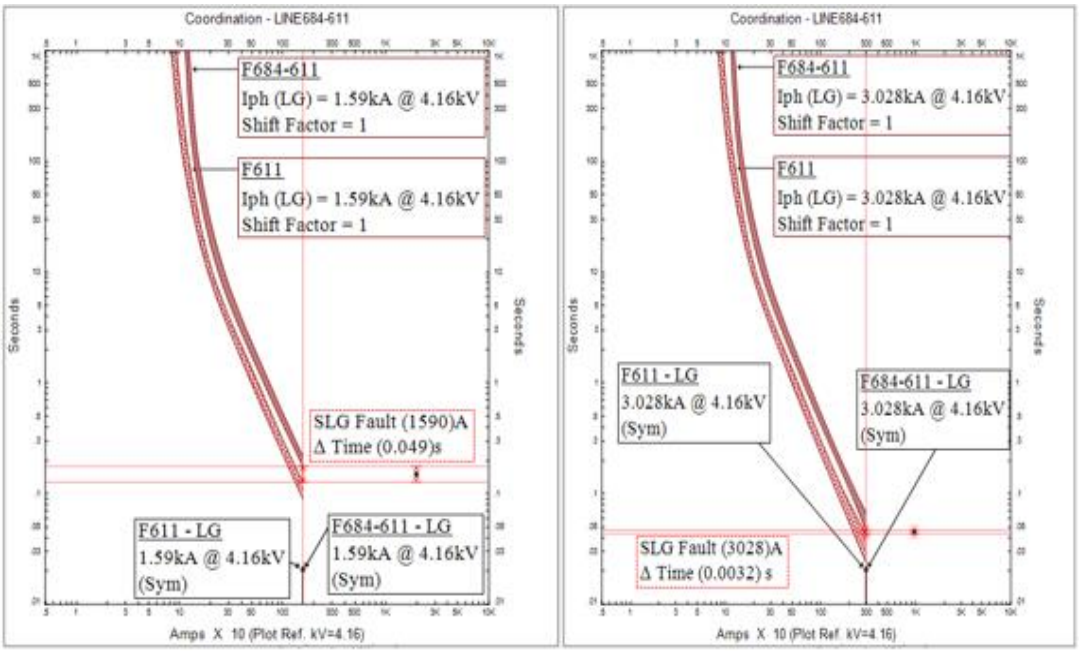

Figure 4.12: Fuses F684-611 and F611 TCC Curve for SLG Fault at NODE611 with 1MW and 3MW DFIGs Connected at NODE671

Capacity increase on the DFIGs connected at NODE671 from 1MW to 3MW caused: an increase in the SLG fault currents at NODE611; a reduction on the upstream fuse F684-611 MMT; a reduction on the downstream fuse F611 TCT; and a diminishing time coordination margin between the two fuses hence leading to the fuses miss coordinating. As the DFIG capacity increases, the MMT curve for fuse F684-611 and the TCT curve for fuse F611 moved downwards along the vertical axis scale to/towards the foot of the TCC curves of Figure 4.11 and Figure 4.12. A combined TCC curve of Figure 4.13 graphically demonstrates that, without WTGs and as the capacity of the DFIGs were increased from 1MW to 3MW, fuse F684-611 MMT and fuse F611 TCT curves respectively moved from the top left hand corner towards the bottom right hand corner to/towards the foot of the TCC curves.

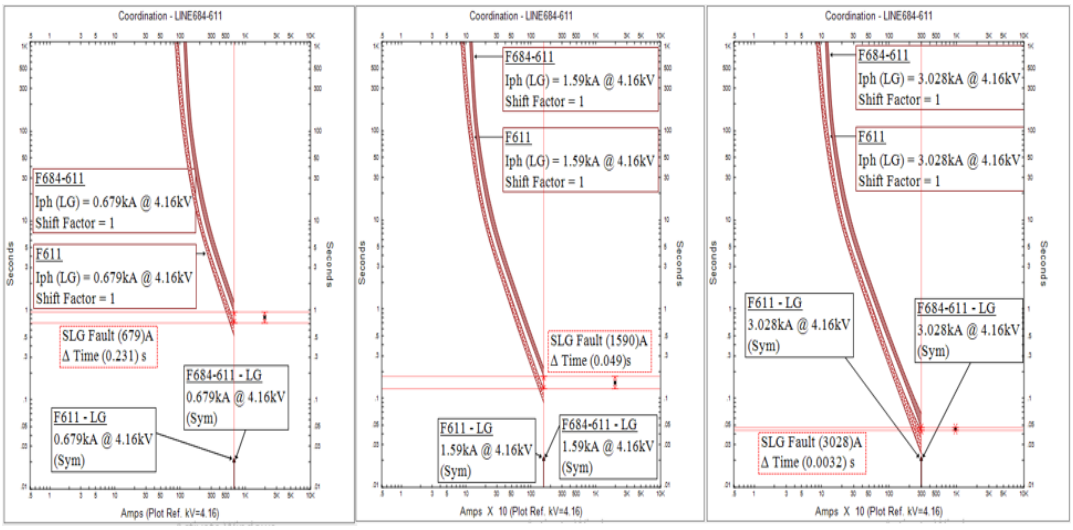

Figure 4.13: Fuses F684-611 and F611 TCC Curve for SLG Fault at NODE611 without WTG and with 1MW and 3MW DFIGs Connected at NODE671

4.3.3 Impacts of 3MW DFIG and 3MW Type IV WTG Connected at NODE671 on Fuses F684-611 and F611 Coordination

Table 4.13 shows that when a 3MW Type IV WTG was connected at NODE671, the SLG fault at NODE611 increased from 679 A to 1065 A and when a 3MW DFIG was connected at the same NODE671, the SLG fault at NODE611 further increased from 1065 A to 3028 A. At the fault current of 1065 A, fuses F684-611 and F611 coordinated with a time coordination margin of 0.106 seconds while at a fault current of 3028 A the fuses miss-coordinated at a much reduced time coordination margin of 0.0032 seconds as shown in Table 4.13. Fuse F684-611 MMT of 0.38 seconds at 1065 A reduced to 0.0464 seconds while fuse F611 TCT of 0.274 seconds reduced to 0.0432 seconds when the 3MW Type IV WTG was replaced with a 3MW DFIG from Table 4.13.

Table 4.13: Fuses F684-611 and F611 Coordination for SLG Faults at NODE611 with 3MW Type IV WTG and 3MW DFIG Connected at NODE671

WTG Interfacing Technology	Fault Currents (A)	F684-611 MMT(s)	F611 TCT(s)	Time Margin (s)	Coordination Status
Without WTGs	679	0.944	0.713	0.231	Coordination
3MW Type IVWTG	1065	0.38	0.274	0.106	Coordination
3MW DFIG	3028	0.0464	0.0432	0.0032	Miss-Coordination

Figure 4.14 shows the TCC curves for fuses F684-611 and F611 coordination while clearing the SLG fault occurring at NODE611 for 3MW Type IV WTG on the left hand side and for 3MW DFIG on the right hand side with both WTGs connected at NODE671.

For 3MW Type IV WTG, the MMT curve for fuse F684-611 and the TCT curve for fuse F611 were located above the foot at 0.274 seconds vertical axis scale as shown graphically on the left hand side of Figure 4.14, and when the 3MW Type IV WTG was replaced with a 3MW DFIG the fuses' curves shifted downwards along the vertical axis scale from 0.274 seconds to 0.0432 seconds to the foot of the TCC curve as shown graphically on the right hand side of the TCC curve of Figure 4.14.

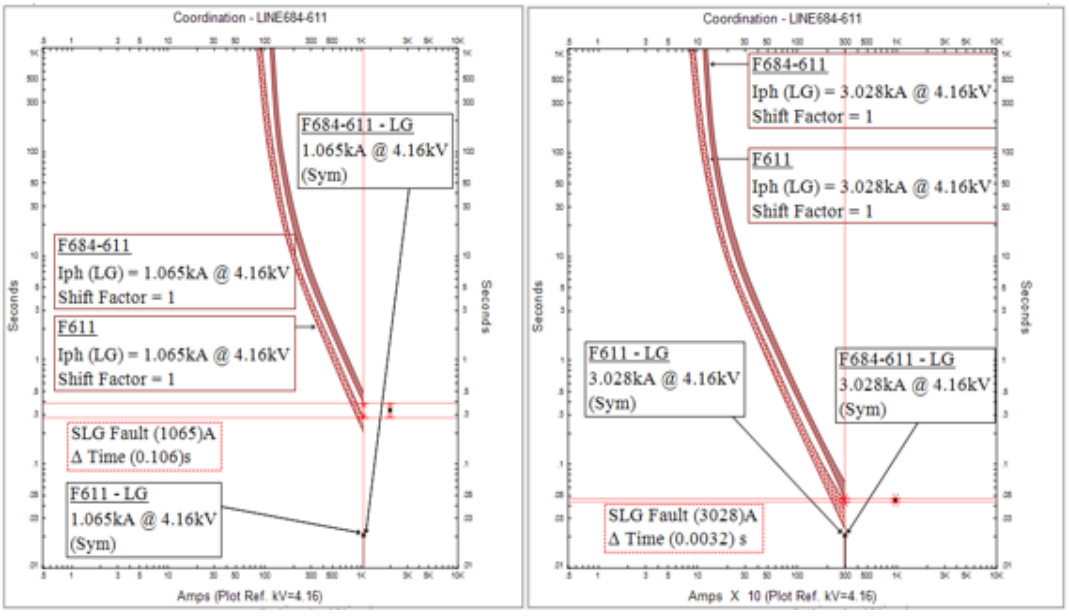

Figure 4.14: Fuses F684-611 and F611 TCC Curve for SLG Faults at NODE611 with 3MW Type IV WTG and 3MW DFIG Connected at NODE671

Even though the WTG models were of the same capacities and connected at the same NODE671, 3MW DFIG injected the highest short circuit currents into an SLG fault at NODE611 as compared to the contribution from the 3MW Type IV WTG. Due to the high short circuit currents contribution from the 3MW DFIG, there was a reduction on fuse F684-611 MMT; a reduction on fuse F611 TCT; and a diminishing time coordination margin between fuses F684-611 and F611 for 3MW DFIG as compared to the reductions due to a 3MW Type IV WTG. 3MW DFIG also caused the most shifting of the MMT curve of fuse F684-611 and the TCT curve of fuse F611 along the vertical axis scale to the foot of the TCC curve as compared to the shifting due to a 3MW Type IV WTG.

4.3.4 Impacts of 3MW DFIGs Connected at NODE650, NODE632 and NODE671 on Fuses F684-611 and F611 Coordination

A. Fuses F684-611 and F611 Coordination for SLG Faults at NODE611 without WTGs and with 3MW DFIG Connected at NODE650

From Table 4.14, without WTGs the SLG fault currents at NODE611 was 679 A with fuse F684-611 having a MMT of 0.944 seconds and fuse F611 having a TCT of 0.713 seconds. When a 3MW DFIG was connected at NODE650, the SLG fault currents at NODE611 increased from 679 A to 1626 A. At the SLG fault current of 1626 A, fuse F684-611 MMT reduced from 0.944 seconds to 0.167 seconds while fuse F611 TCT reduced from 0.713 seconds to 0.12 seconds. When the 3MW DFIG was connected at NODE650, the fuses time coordination margin reduced/diminished from 0.231 seconds without WTGs to 0.047 seconds.

Table 4.14: Fuses F684-611 and F611 Coordination for SLG Faults at NODE611 without WTGs and 3MW DFIG Connected at NODE650

DFIG Location	Fault Currents (A)	F684-611 MMT (s)	F611 TCT (s)	Time Margin (s)	Coordination Status
Without WTG	679	0.944	0.713	0.231	Coordination
NODE650	1626	0.167	0.12	0.047	Coordination

Figure 4.15 shows the TCC curves for fuses F684-611 and F611 without WTG connection on the left hand side and with 3MW DFIG connected at NODE650 on the right hand side. Without WTGs, the MMT curve for fuse F684-611 and the TCT curve for fuse F611 were located at 0.713 seconds on the vertical axis scale above the foot of the TCC curve as shown graphically on the left hand side of Figure 4.15. When the 3MW DFIG was connected at NODE650, the MMT curve for fuse F684-611 and the TCT curve for fuse F611 shifted downwards along the vertical axis scale from 0.713 seconds to 0.12 seconds closer to the foot as shown graphically on the right hand side of the TCC curve of Figure 4.15.

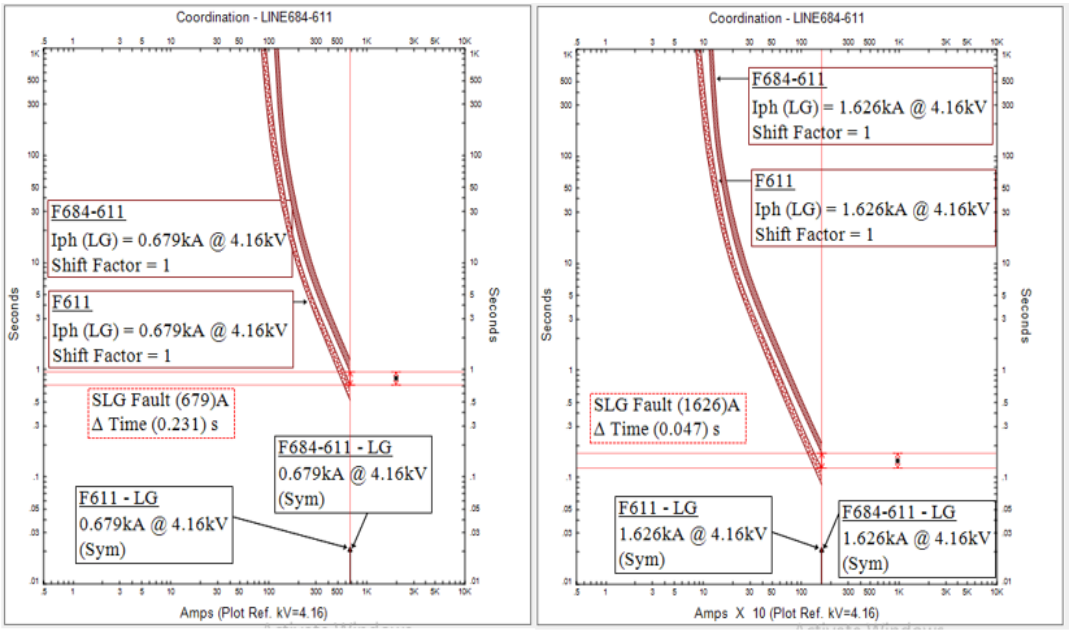

Figure 4.15: Fuses F684-611 and F611 TCC Curves for SLG Fault at NODE611 without WTGs and with 3MW DFIG Connected at NODE650

B. Fuses F684-611 and F611 Coordination for SLG Faults at NODE611 with 3MW DFIGs Connected at NODE650 and NODE632.

Table 4.15 shows that when the 3MW DFIG connected at NODE650 was moved to NODE632, the SLG fault currents at NODE611 increased from 1626 A to 2074 A. At an increased SLG fault current of 2074 A, fuse F684-611 MMT of 0.167 seconds and fuse F611 TCT of 0.12 seconds for 3MW DFIG connected at NODE650 reduced to a MMT of 0.103 seconds and a TCT of 0.0786 seconds when 3MW DFIG was

connected at NODE632. The fuses miss-coordinated with a reduced time miss-coordination margin of 0.0244 seconds down from a time coordination margin of 0.047 seconds when the 3MW DFIG was moved from NODE650 to NODE632.

Table 4.15: Fuses F684-611 and F611 Coordination for SLG Faults at NODE611 with 3MW DFIGs Connected at NODE650 and NODE632

DFIG Location	Fault Currents (A)	F684-611 MMT (s)	F611 TCT (s)	Time Margin (s)	Coordination Status
NODE650	1626	0.167	0.12	0.047	Coordination
NODE632	2074	0.103	0.0786	0.0244	Miss-Coordination

Figure 4.16 shows the TCC curves for fuses F684-611 and F611 with 3MW DFIG connected at NODE650 on the left hand side and with 3MW DFIG connected at NODE632 on the right hand side. The left hand side of Figure 4.16 graphically shows that, for 3MW DFIG connected at NODE650, the MMT curve for fuse F684-611 and the TCT curve for fuse F611 are located at 0.12 seconds on the vertical axis scale above the foot of the TCC curve and when the 3MW DFIG was moved to NODE632, the fuses' curves further shifted downwards on the vertical axis scale from 0.12 seconds to 0.0786 seconds to the foot of the TCC curve on the right hand side of Figure 4.16.

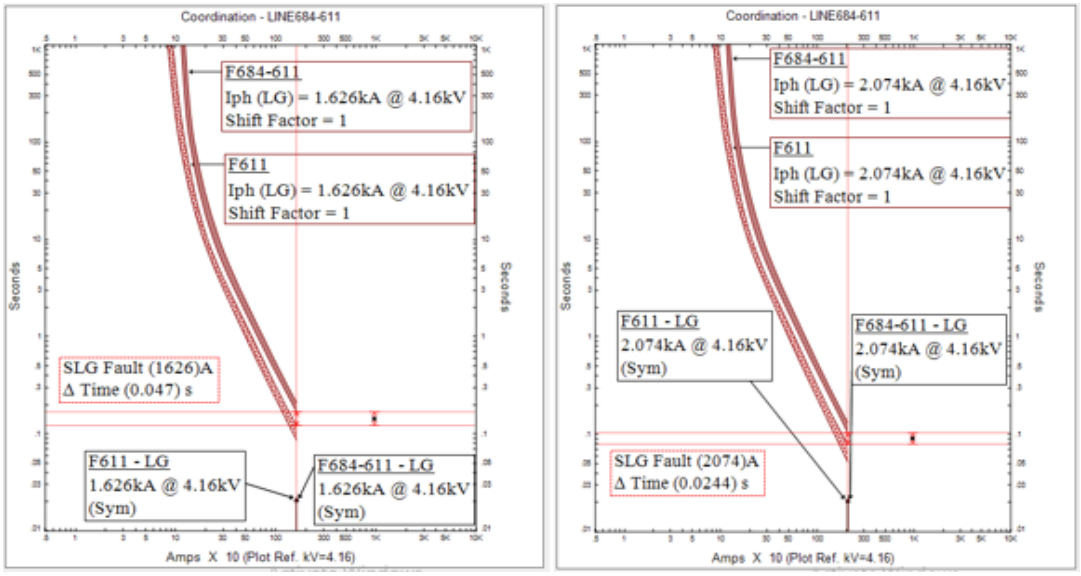

Figure 4.16: Fuses F684-611 and F611 TCC Curves for SLG Fault at NODE611 with 3MW DFIG Connected at NODE650 and NODE632

C Fuses F684-611 and F611 Coordination for SLG Faults at NODE611 with 3MW DFIGs Connected at NODE632 and NODE671

When the 3MW DFIG was further moved from NODE632 to NODE671, the SLG fault currents at NODE611 further increased from 2074 A to 3028 A as shown in Table 4.16. At the increased SLG fault current of 3028 A for 3MW DFIG connected at NODE671, fuse F684-611 MMT of 0.103 seconds and fuse F611 TCT of 0.0786 seconds for 3MW DFIG connected at NODE632 reduced to a MMT of 0.0464 seconds and a TCT of 0.0432 seconds respectively with the fuses now miss-coordinating with a much reduced time margin of 0.0032 seconds down from 0.0244 seconds for 3MW DFIG connected at NODE632.

Table 4.16: Fuses F684-611 and F611 Coordination for SLG Faults at NODE611 with 3MW DFIGs Connected at NODE632 and NODE671

DFIG Location	Fault Currents (A)	F684-611 MMT (s)	F611 TCT (s)	Time Margin (s)	Coordination Status
NODE632	2074	0.103	0.0786	0.0244	Miss-Coordination
NODE671	3028	0.0464	0.0432	0.0032	Miss-Coordination

Figure 4.17 shows the TCC curves for fuses F684-611 and F611 with 3MW DFIG connected at NODE632 on the left hand side and with 3MW DFIG connected at NODE671 on the right hand side. The left hand side of Figure 4.17 graphically shows that, for 3MW DFIG connected at NODE632, the MMT curve for fuse F684-611 and the TCT curve for fuse F611 are located at 0.0786 seconds on the vertical axis scale at the foot of the TCC curve and when the 3MW DFIG was moved to NODE671, the fuses' curves further shifted downwards on the vertical axis scale from 0.0786 seconds to 0.0432 seconds to the foot of the TCC curve on the right hand side of Figure 4.17.

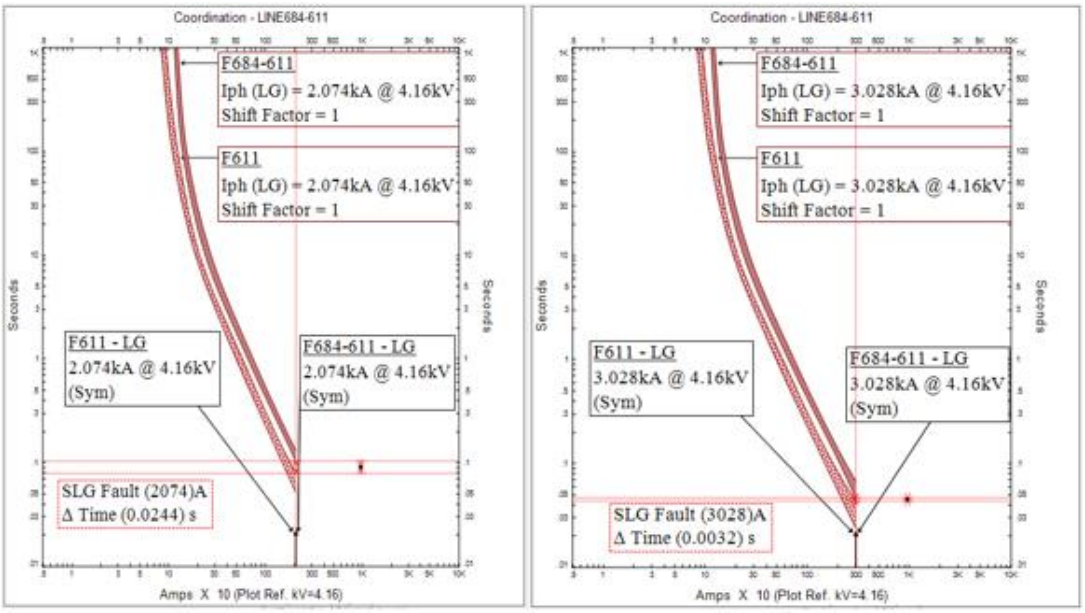

Figure 4.17: Fuses F684-611 and F611 TCC Curves for SLG Fault at NODE611 with 3MW DFIG Connected at NODE632 and NODE671

The time coordination margin for fuses F684-611 and F611 for an SLG fault at NODE611 was 0.231 seconds without WTGs. This time coordination margin reduced to: 0.047 seconds when a 3MW DFIG was connected at NODE650; 0.0244 seconds when a 3MW DFIG was connected at NODE632; and finally to 0.0032 seconds when a 3MW DFIG was connected at NODE671. The upstream fuse F684-611 MMT of 0.944 seconds without WTGs reduced to: 0.167 seconds when the 3MW DFIG was connected at NODE650; 0.103 seconds when the 3MW DFIG was connected at NODE632; and finally to 0.0464 seconds when the 3MW DFIG was connected at NODE671. Also the downstream fuse F611 TCT of 0.713 seconds without WTGs reduced to: 0.12 seconds when the 3MW DFIG was connected at NODE650; 0.0786 seconds when the 3MW DFIG was connected at NODE632; and finally to 0.0432 seconds when the 3MW DFIG was connected at NODE671.

Fuses F684-611 and F611 experienced diminishing time coordination margin as the DFIGs were connected closer to the faulted NODE611. NODE611 was: 4600 feet away from NODE650; 2600 feet away from NODE632; and 600 feet away from NODE671. NODE671 was the nearest node to the faulted NODE611 at 600 feet and when the 3MW DFIGs were connected at NODE671: fuse F684-611 had the least

MMT of 0.0464 seconds; fuse F611 had the least TCT of 0.0432 second; fuses F684-611 and F611 had the least time miss-coordination margin of 0.0032 seconds; and the fuses' MMT and TCT curves shifted the most downwards along the vertical scale towards the bottom right hand corner to the foot of the combined TCC curve of Figure 4.18.

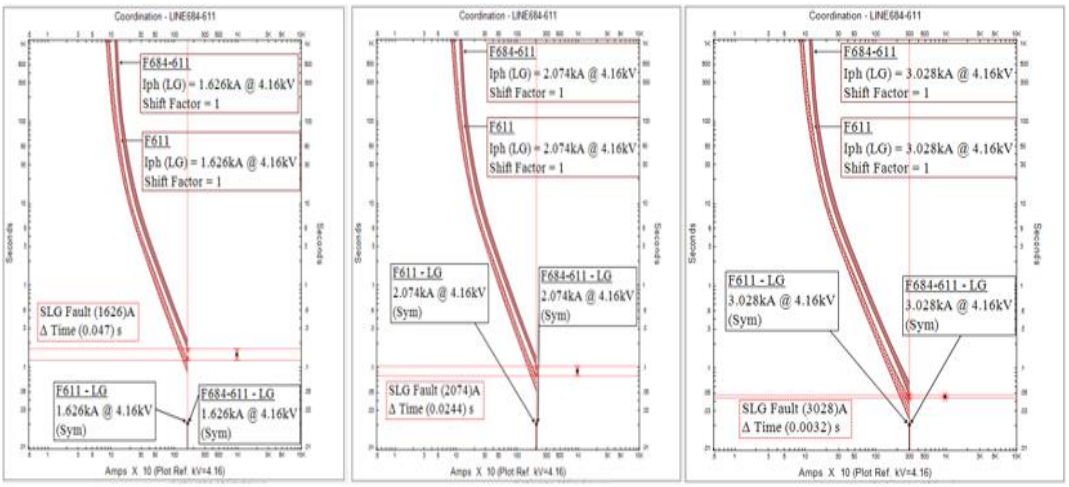

Figure 4.18: Fuses F684-611 and F611 TCC Curves for SLG Fault at NODE611 with 3MW DFIGs Connected at NODE650, NODE632 and NODE671

4.3.5 Impacts of 3MW DFIG Connected at NODE671 on Fuses: F671-684 and F684; F684 and F684-611; F684-611 and F611 Coordination.

A. Fuses: F671-684 and F684; F684 and F684-611 Coordination for SLG Faults at NODE684 and LINE684-611

Table 4.17 shows that for an SLG fault of 3439 A at NODE684, the upstream fuse F671-684 had a MMT of 0.11 seconds while the downstream fuse F684 had a TCT of 0.0907 seconds with the fuses having a time miss-coordination margin of 0.0193 seconds while clearing the SLG fault. When the SLG fault location was shifted from NODE684 to LINE684-611, fuse F684 which was the downstream fuse for a fault at NODE684 became the upstream fuse with fuse F684-611 being the downstream fuse for the SLG fault on LINE684-611. While clearing an SLG fault of 3439 A on LINE684-611, the upstream fuse F684 had a MMT of 0.0581 seconds while the downstream fuse F684-611 had a TCT of 0.0543 seconds both fuses having a

reduced time miss-coordination margin of 0.0038 seconds compared to 0.0193 seconds for the same magnitude of fault at NODE684.

Table 4.17: Fuses F671-684 and F684, F684 and F684-611 Coordination for SLG Faults at NODE684 and LINE684-611 with 3MW DFIG at NODE671

Fault Location	Fault Currents (A)	Upstream Fuse		Downstream Fuse		Time Margin (s)
		Fuse ID	MMT(s)	Fuse ID	TCT(s)	
NODE684	3439	F671-684	0.11	F684	0.0907	0.0193
LINE684-611	3439	F684	0.0581	F684-611	0.0543	0.0038

At a fault current of 3439 A at NODE684, fuse F671-684 MMT curve and fuse F684 TCT curve shown graphically on the left hand side of the TCC curve of Figure 4.19 are located at the foot at 0.0907 seconds vertical axis scale and once a fault of the same magnitude 3439 A occurred on LINE684-611, the coordinating fuses F684 MMT curve and F684-611 TCT curve moved further downwards in the foot from 0.0907 seconds to 0.0543 seconds vertical axis scale as shown graphically on the right hand side of the TCC curve of Figure 4.19. The fuses' coordinating curves for a fault on LINE684-611 are shifted downwards on the vertical axis scale as compared to the coordinating fuses' curves for the same magnitude of fault at NODE684.

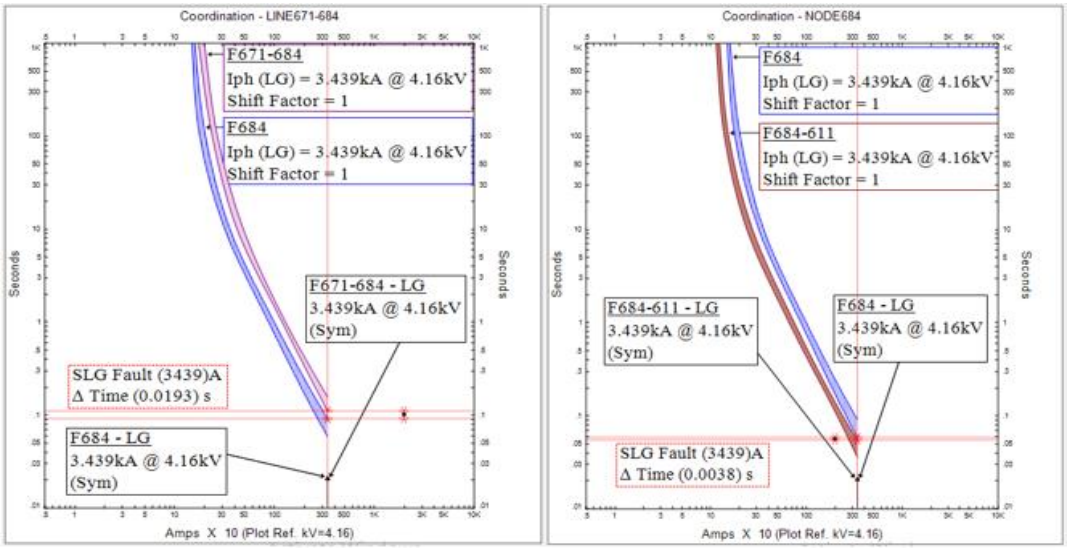

Figure 4.19: Fuses: F671-684 and F684; F684 and F684-611 TCC Curves for SLG Fault at NODE684 and LINE684-611 with 3MW DFIG Connected at NODE671

B. Fuses F684 and F684-611, F684-611 and F611 Coordination for SLG Faults on LINE684-611 and NODE611 with 3MW DFIG at NODE671.

From Table 4.18 when the SLG fault location was shifted from LINE684-611 to NODE611 the SLG fault current reduced from 3439 A to 3028 A and fuse F684-611 which was the downstream fuse for a fault on LINE684-611 is became the upstream fuse while fuse F611 is the downstream fuse for the fault at NODE611. While clearing the SLG fault of 3028 A at NODE611, the upstream fuse F684-611 had a MMT of 0.0464 seconds while the downstream fuse F611 had a TCT of 0.0432 seconds both fuses having a much reduced time miss-coordination margin of 0.0032 seconds down from a time coordination margin of 0.0038 seconds for an SLG fault of 3439 A on LINE684-611.

Table 4.18: Fuses F684 and F684-611, F684-611 and F611 Coordination for SLG Faults on LIE684-611, and NODE611 with 3MW DFIG at NODE671

Fault Location	Fault Currents (A)	Upstream Fuse		Downstream Fuse		Time Margin (s)
		Fuse ID	MMT(s)	Fuse ID	TCT(s)	
LINE684-611	3439	F684	0.0581	F684-611	0.0543	0.0038
NODE611	3028	F684-611	0.0464	F611	0.0432	0.0032

The left hand side of the TCC curve of Figure 4.20 shows that for an SLG fault of 3439 A on LINE684-611 fuse F684 MMT and F684-611 TCT curves were located at the foot of the TCC curve at 0.0543 seconds vertical axis scale and once a fault of 3028 A occurs at NODE611, the coordinating fuses F684-611 MMT and F611 TCT curves moved further downwards in the foot from 0.0543 seconds to 0.0432 seconds along the vertical axis scale as shown graphically on the right hand side of the TCC curve of Figure 4.20. The coordinating fuses' curves for an SLG fault at NODE611 are shifted much downwards on the vertical scale as compared to the coordinating fuses' curves for a fault on LINE684-611.

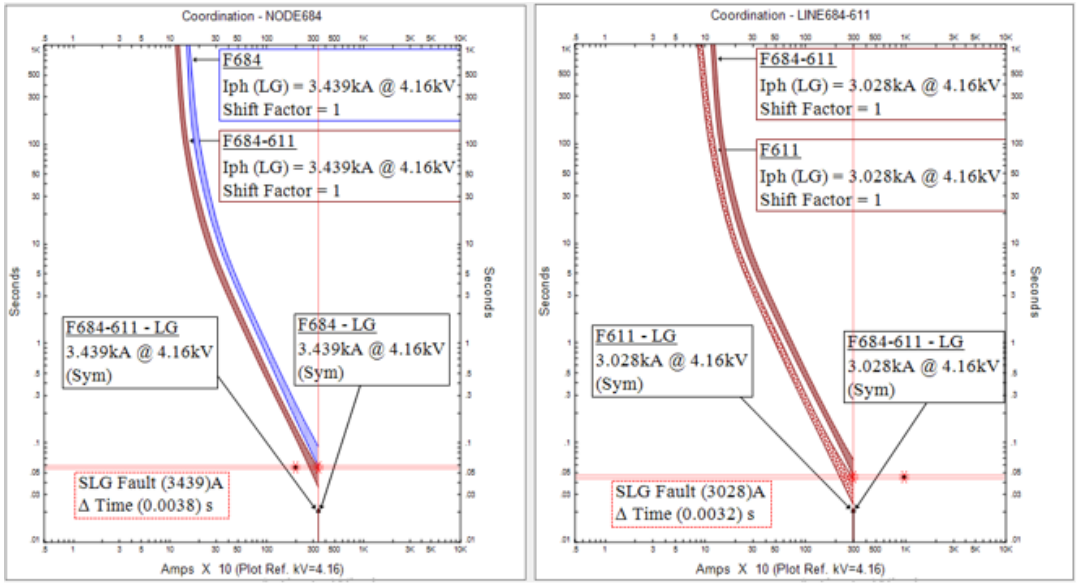

Figure 4.20: Fuses: F684 and F684-611; F684-611 and F611 TCC Curves for SLG Fault on LINE684-611 and NODE611 with 3MW DFIG Connected at NODE671

When a 3MW DFIG was connected at NODE671 there was an increase on the feeder SLG fault currents: from 697 A to 3439 A at NODE684; from 697 A to 3439 A on LINE684-611; and from 679 A to 3028 A at NODE611. These increase in the short circuit currents levels at the nodes caused a reduction/diminishing on the coordinating fuses: time coordination margins; MMT characteristics; and TCT characteristics.

Fuses: F671-684 and F684 miss-coordinated with a time margin of 0.0193 seconds while clearing an SLG fault of 3439 A occurring at NODE684; F684 and F684-611 miss-coordinated with a time margin of 0.0038 seconds while clearing an SLG fault of 3439 A occurring on LINE684-611; and F684-611 and F611 miss-coordinated with a time margin of 0.0032 seconds while clearing an SLG fault of 3028 A occurring at NODE611.

Even though the magnitudes of the SLG fault currents at NODE684 and LINE684-611 were of the same magnitude 3439 A, the coordinating fuses for the SLG fault on LINE684-611 miss-coordinated with a reduced time coordination margin of 0.0038

seconds as compared to the 0.0193 seconds miss-coordination margin for the same magnitude of fault occurring at NODE684.

The four fuses under the study had different current ratings of: 150 A for F671-684; 125 A for F684; 100 A for F684-611; and 75 A for F611. The fuses were also located at different distances from the main grid with: F611 at 4600 feet; F684-611 at 4300 feet; F684 at 4300 feet; and F671-684 at 4000 feet. It shows that fuses having higher current ratings and are located nearer to the main grid supply have a higher time coordination margin as compared to fuses having a lower current ratings and are located at the far end of the feeder. This is because fuses located at the far end of the feeder with the lowest current ratings had their MMT curves and TCT curves located more to the bottom left hand corner of the composite TCC curves at the foot as compared to the fuses having higher current ratings whose curves were located nearer to the maid grid supply.

4.4 Impacts of 2 Ohms CLR Interfaced' DFIGs on IEEE 13 NODE Radial Test Feeder Short Circuit Currents and Sequence Reactance

To minimize on the impacts the 3 MW DFIGs had on the increase on the test feeder SLG fault currents and the decrease/reduction on the test feeder positive, negative and zero sequence reactance, the 3MW DFIGs were coupled into the feeder with series 2 ohms CLRs. The summarised study on the impacts the 2 ohms CLRs have on the decrease on the SLG fault currents, and on the increase on the test feeder positive, negative and zero sequence reactance at NODE684, and NODE611 was done and the results analysed and presented using tables and graphs.

4.4.1 Impacts of 2 Ohms CLR Interfaced' 3MW DFIGs on the Feeder Short Circuit Currents.

Table 4.19 shows that when the radial test feeder was short circuited without WTGs the SLG short circuit fault currents at NODE611 and NODE684 were 679 A and 697 A respectively. Figure 4.21 shows that the SLG fault currents would increase from 679 A to 3028 A at NODE611 and from 697 A to 3439 A at when the radial test feeder was short circuited with 3MW DFIG connected at NODE671. When the 3MW

DFIG was coupled into the test feeder with a 2 Ohms CLR, the magnitudes of the fault currents at NODE611 and NODE684 reduced from 3028 A to 1458 A and from 3439 A to 1458 A respectively as shown in Table 4.19.

Table 4.19: NODE684 and NODE611 SLG Fault Currents with 2 Ohms CLR Interfaced' 3MW DFIG Connected at NODE671

SLG Fault (A)	3MW DFIG Placement at NODE671		
	Without WTG	Without CLR	With 2Ohm CLR
NODE684	697	3439	1546
NODE611	679	3028	1458

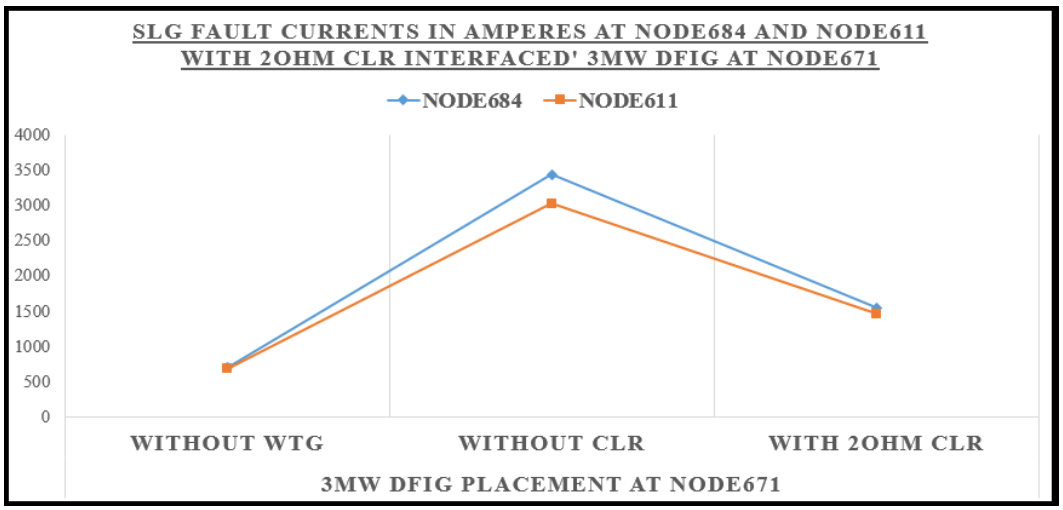

Figure 4.21: NODE684 and NODE611 SLG Fault Currents with 3MW DFIGs without CLR and with 2 Ohm CLR.

2 Ohms CLR reduced the SLG fault currents on the test feeder to levels which the conventional over-current protection scheme could handle. The SLG fault currents at NODE611 and NODDE684 gradually reduced when 2 ohms CLRs were used to interface 3MW DFIGs into the test feeder.

4.4.2 Impacts of 2 Ohms CLR Interfaced' 3MW DFIGs on the Feeder Sequence Reactance.

Table 4.20 shows that when the radial test feeder was short circuited without WTGs, the positive, negative and zero sequence reactance at NODE611 were 4.26642 Ω, 4.26642 Ω and 1.89837 Ω respectively. These values reduced in magnitude to:

0.81739 Ω for positive sequence; 0.77282 Ω for negative sequence; and 0.74238 Ω for zero sequence when the radial test feeder was short circuited with 3MW DFIG connected at NODE671. When the 3MW DFIG was coupled into the test feeder with 2 Ohms CLRs, the magnitudes of the sequence reactance at NODE611 increased: from 0.81739 Ω to 1.81518 Ω for positive sequence; from 0.77282 Ω to 1.7926 Ω for negative sequence; and from 0.74238 Ω to 1.27516 Ω for zero sequence. The same pattern of the sequence reactance variation at NODE611 was experienced for the sequence reactance at NODE684 with the only difference being the magnitudes of the sequence reactance at NODE611 were higher compared to the sequence reactance at NODE684.

Table 4.20: NODE684 and NODE611 Sequence Reactance with 2 Ohms CLR Interfaced' 3MW DFIG Connected at NODE671

Sequence Reactance (Ω)	3MW DFIG Placement at NODE671					
	Without WTG		Without CLR		With 2Ohm CLR	
	NODE 611	NODE 684	NODE 611	NODE 684	NODE 611	NODE 684
Positive	4.26642	4.18005	0.81739	0.73103	1.81518	1.72881
Negative	4.26642	4.18005	0.77282	0.68645	1.7926	1.70622
Zero	1.89837	1.8121	0.74238	0.65611	1.27516	1.18889

Figure 4.22 shows that once the 3MW DFIGs were connected into the feeder, there was a drastic reduction on the sequence reactance at NODE611 and NODE684 during a short circuit event but when the 3MW DFIGs were coupled into the feeder with 2 ohms CLRs, there was a gradual increase on the feeder positive, negative and zero sequence reactance at the faulted nodes. The zero sequence reactance had the lowest magnitudes for the three sequence reactance at both nodes with NODE611 having the three sequence reactance slightly higher than NODE684.

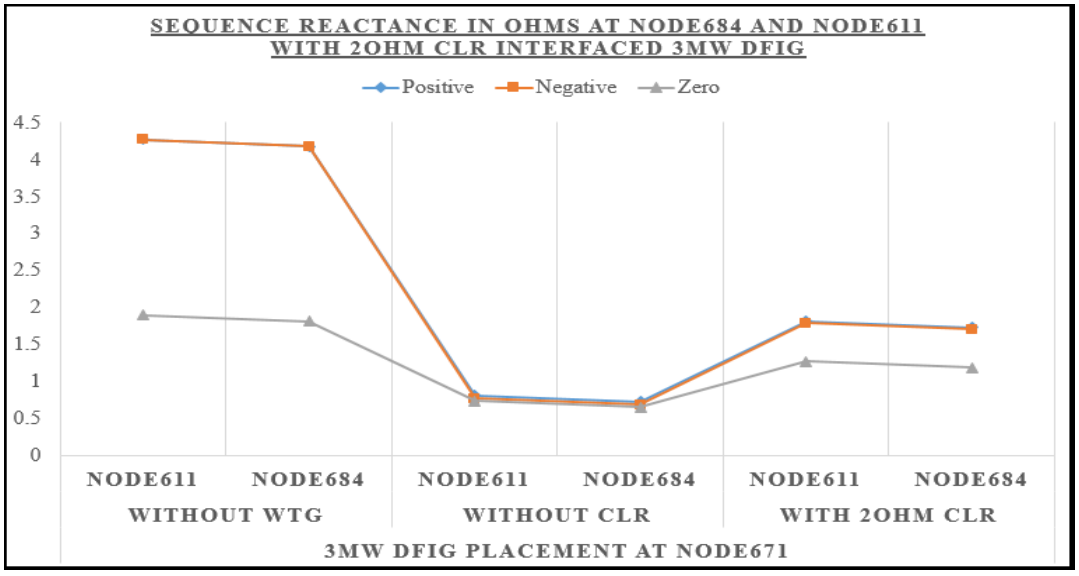

Figure 4.22: NODE684 and NODE611 Sequence Reactance in Ohms with 2 Ohms CLR Interfaced' 3MW DFIG Connected at NODE671

To mitigate on the drastic reduction on the positive, negative and zero sequence reactance during a fault, the DFIGs which were the highest contributors to the short circuit faults were coupled into the feeder using series CLRs. The analysis above shows that the connection of 2 ohm series CLRs at the DFIGs point of coupling to the feeder increased the positive, negative and zero sequence reactance at NODE684 and NODE611 to levels almost equal to when the short circuit was performed without WTGs connected.

4.5 Impacts of 2 Ohms CLR Interfaced' DFIGs on IEEE 13 Node Radial Test Feeder Fuse-Fuse Over-Current Protection Scheme.

4.5.1 Impacts of 2 Ohms CLR Interfaced' 3MW DFIGs on Fuses F671-684 and F684 Coordination.

Table 4.21 shows that when a 3MW DFIG was connected into the feeder without CLRs at NODE671, fuse F671-684 MMT of 0.11 seconds and fuse F684 TCT of 0.0907 seconds miss-coordinated with a time margin of 0.0193 seconds while clearing an SLG fault of 3439 A occurring at NODE684. When the 3MW DFIG was coupled into the feeder with a 2 ohm CLR, the SLG fault current of 3439 A at

NODE684 reduced to 1546 A. At the reduced fault current of 1546 A, fuse F671-684 MMT increased from 0.11 seconds to 0.582 seconds and fuse F684 TCT increased from 0.0907 seconds to 0.409 seconds with the two fuses coordinating with a time margin of 0.173 seconds an increase from the 0.0193 seconds miss-coordination margin when the SLG fault current was 3439 A.

Table 4.21: Fuses F671-684 and F684 Coordination for SLG Faults at NODE684 with 2 Ohms CLR Interfaced' 3MW DFIGs

CLR Placement	Fault Currents (A)	F671-684 MMT (s)	F684 TCT (s)	Time Margin (s)	Coordination Status
Without CLR	3439	0.11	0.0907	0.0193	Miss-Coordination
With 2 Ohm CLR	1546	0.582	0.409	0.173	Coordination

Figure 4.23 shows the TCC curves for fuses F671-684 and F684 for 3MW DFIG connected into the feeder without CLRs on the left hand side and with 2 ohms CLR on the right hand side. When the 3MW DFIG was connected into the feeder without CLRs, the MMT curve for fuse F671-684 and the TCT curve for fuse F684 were located at 0.0907 seconds on the vertical axis scale at the foot of the TCC curve as shown graphically on the left hand side of Figure 4.23. When the 3MW DFIG was connected into the feeder with a 2 ohm CLR, the MMT and the TCT curves for fuse F671-684 and fuse F684 respectively shifted upwards along the vertical axis scale from 0.0907 seconds to 0.409 seconds above the foot as shown graphically on the right hand side of the TCC curve Figure 4.23.

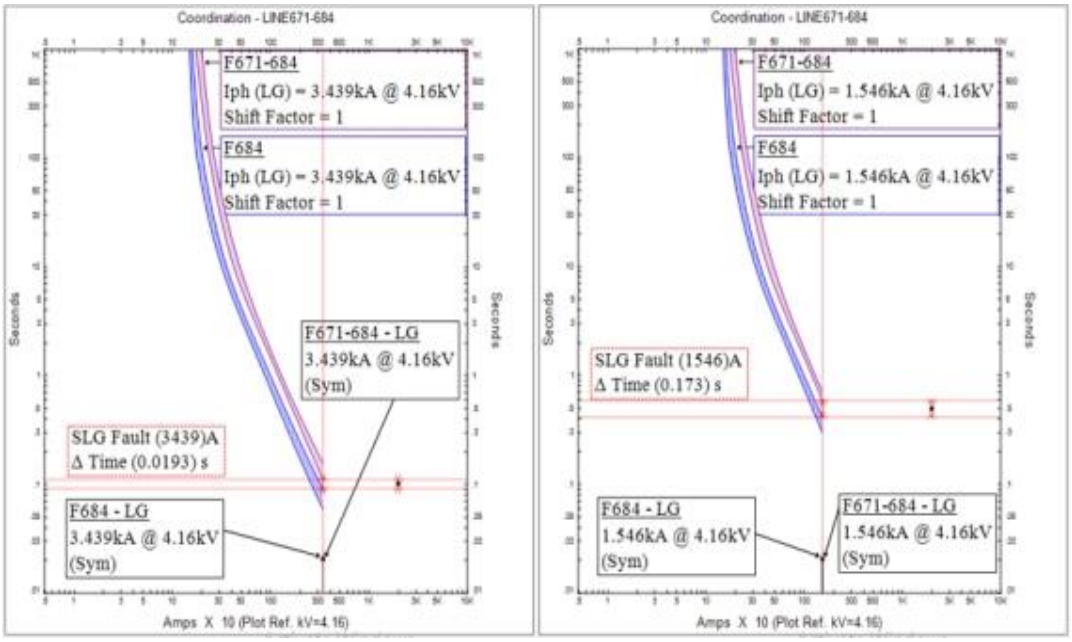

Figure 4.23: Fuses F671-684 and F684 TCC Curves for SLG Fault at NODE684 with 3MW DFIG Connected at NODE671 without CLR and with 2 Ohm CLR

4.5.2 Impacts of 2 Ohms CLR Interfaced' 3MW DFIGs on Fuses F684 and F684-611 Coordination

Table 4.22 shows that when a 3MW DFIG was connected into the feeder without CLRs at NODE671, fuse F684 MMT of 0.0581 seconds and fuse F684-611 TCT of 0.0543 seconds miss-coordinated with a time margin of 0.0038 seconds while clearing an SLG fault of 3439 A occurring on LINE684-611. When the 3MW DFIG was coupled into the feeder with a 2 ohm CLR, the SLG fault current of 3439 A at LINE684-611 reduced to 1546 A. At the reduced fault current of 1546 A, fuse F684 MMT increased from 0.0581 seconds to 0.295 seconds and fuse F684-611 TCT increased from 0.0543 seconds to 0.228 seconds with the two fuses coordinating with a time margin of 0.067 seconds an increase from the 0.0038 seconds miss-coordination margin when the SLG fault current was 3439 A.

Table 4.22: Fuses F684 and F684-611 Coordination for SLG Fault occurring on LINE684-611 with 2 Ohm CLR Interfaced' 3MW DFIGs

CLR Placement	Fault Currents (A)	F684 MMT (s)	F684-611 TCT (s)	Time Margin (s)	Coordination Status
Without CLR	3439	0.0581	0.0543	0.0038	Miss-Coordination
With 2 Ohm CLR	1546	0.295	0.228	0.067	Coordination

Figure 4.24 shows the TCC curves for fuses F684 and F684-611 for 3MW DFIG connected into the feeder without CLRs on the left hand side and with 2 ohms CLR on the right hand side. When the 3MW DFIG was connected into the feeder without CLRs, the MMT curve for fuse F684 and the TCT curve for fuse F684-611 were located at 0.0543 seconds on the vertical axis scale at the foot of the TCC curve as shown graphically on the left hand side of Figure 4.24. When the 3MW DFIG was connected into the feeder with a 2 ohm CLR, the MMT and the TCT curves for fuse F684 and fuse F684-611 respectively shifted upwards along the vertical axis scale from 0.0543 seconds to 0.208 seconds above the foot as shown graphically on the right hand side of the TCC curve of Figure 4.24.

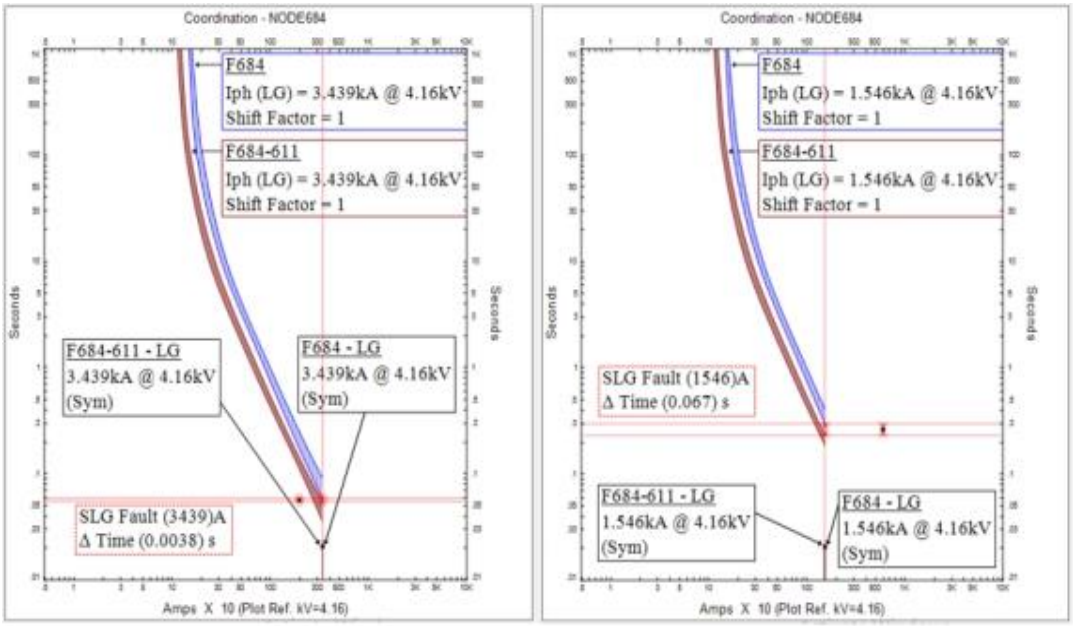

Figure 4.24: Fuses F684 and F684-611 TCC Curves for SLG Fault on LINE684-611 with 3MW DFIG Connected at NODE671 without CLR and with 2 Ohm CLR

4.5.3 Impacts of 2 Ohms CLR Interfaced' 3MW DFIG on Fuses F684-611 and F611 Coordination

Table 4.23 shows that when a 3MW DFIG was connected into the feeder without CLRs at NODE671, fuse F684-611 MMT of 0.0464 seconds and fuse F611 TCT of 0.0432 seconds miss-coordinated with a time margin of 0.0032 seconds while clearing an SLG fault of 3028 A occurring at NODE611. When the 3MW DFIG was coupled into the feeder with a 2 ohm CLR, the SLG fault current of 3028 A at NODE611 reduced to 1458 A. At the reduced fault current of 1458 A, fuse F684-611 MMT increased from 0.0464 seconds to 0.206 seconds and fuse F611 TCT increased from 0.0432 seconds to 0.147 seconds with the two fuses coordinating with a time margin of 0.059 seconds an increase from the 0.0032 seconds miss-coordination margin when the SLG fault current was 3028 A.

Table 4.23: Fuses F684-611 and F611 Coordination for SLG Fault at NODE611 with 2 Ohms CLR Interfaced' 3MW DFIGs

CLR Placement	Fault Currents (A)	F684-611 MMT (s)	F611 TCT (s)	Time Margin (s)	Coordination Status
Without CLR	3028	0.0464	0.0432	0.0032	Miss-Coordination
With 2 Ohm CLR	1458	0.206	0.147	0.059	Coordination

Figure 4.25 shows the TCC curves for fuses F684-611 and F611 for 3MW DFIG connected into the feeder without CLRs on the left hand side and with 2 ohms CLR on the right hand side. When the 3MW DFIG was connected into the feeder without CLRs, the MMT curve for fuse F684-611 and the TCT curve for fuse F611 were located at 0.0432 seconds on the vertical axis scale at the foot of the TCC curve as shown graphically on the left hand side of Figure 4.25. When the 3MW DFIG was connected into the feeder with a 2 ohm CLR, the MMT and the TCT curves for fuse F684-611 and fuse F611 respectively shifted upwards along the vertical axis scale from 0.0432 seconds to 0.147 seconds above the foot as shown graphically on the right hand side of the TCC curve of Figure 4.25.

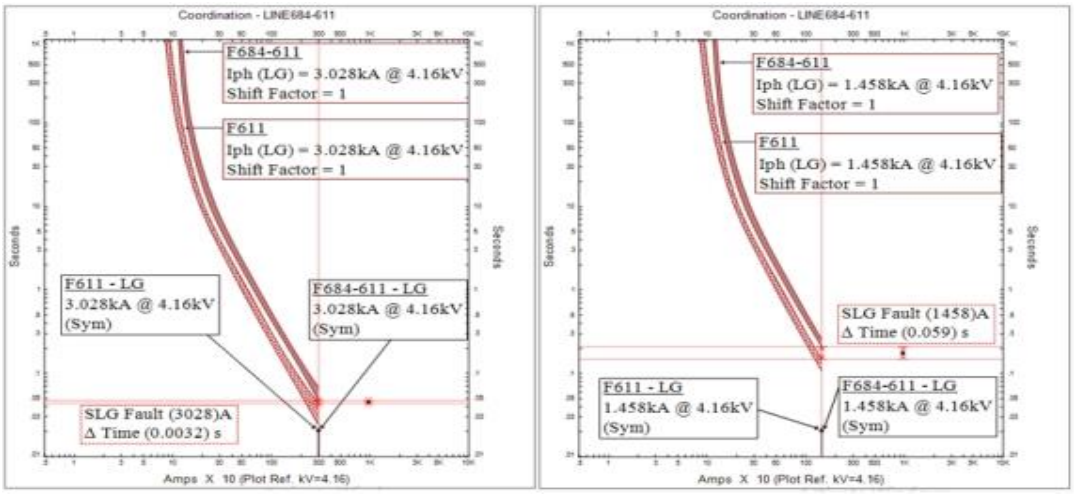

Figure 4.25: Fuses F684-611 and F611 TCC Curves for SLG Fault at NODE611 with 3MW DFIG Connected at NODE671 without CLR and with 2 Ohm CLR

Once the 3MW DFIGs were coupled into the feeder using 2 ohm CLRs: the SLG short circuit fault currents at the faulted nodes reduced in magnitude; the upstream fuses MMT increased; the downstream fuses TCT increased; and the time coordination margins between the coordinating fuses increased. The coordinating fuses MMT and TCT curves which were initially located at the foot of the TCC curves shifted upwards above the foot.

4.6 Summary

WTG connection onto a radial test feeder caused an increase in the feeder SLG fault current levels. The factors that affected the increase in the SLG fault current levels were: the WTG interfacing technology; the capacity of the WTGs; the location for placement of the WTGs; and the location of faults with reference to the distance from the main grid. The increase in the SLG fault current levels caused a decrease in the upstream fuses MMT; a decrease on the downstream fuse TCT; a reduction on the time coordination margins between the coordinating fuses; and the most shifting of the MMT and TCT curves of the coordinating along the vertical axis scale towards the foot of the TCC curves.

DFIG interfacing technology caused the highest increase in the feeder SLG fault currents at NODE611 and NODE684 as compared to Type IV WTGs. Capacity

increase for the two WTG models from 1MW to 3MW caused a further increase in the feeder SLG fault current levels.

DFIGs also caused the most diminishing time coordination margins between the coordinating fuses as compared to Type IV WTGs. For the three feeder components chosen for the study, DFIGs had the most fuse-fuse miss coordination as compared to Type IV WTGs. 3MW DFIG had a total of 5 pairs of fuses miss coordinating while 3MW Type IV WTGs had node of the fuses miss coordinating.

DFIGs caused: the lowest MMT for the upstream fuses; the lowest TCT for the downstream fuses; and the most shifting of the MMT and TCT curves along the vertical axis scale towards the foot of the TCC curves for the coordinating fuses.

DFIG placement at NODE671 had: the highest increase in the SLG fault current levels at NODE611 and NODE684; the lowest MMT for the upstream fuses; the lowest TCT for the downstream fuses; and the least time coordination margins between the coordinating fuses as compared to DFIGs placed at NODE650 and NODE632. This was because NODE671 was the nearest node from the faulted nodes, 300 feet from NODE684 and 600 feet from NODE611. DFIG placement at NODE632 had NODE684 at 2300 feet and NODE611 at 2600 feet; while DFIG placement at NODE650 had NODE684 at 4300 feet and NODE611 at 4600 feet. Also DFIG placement at NODE671 had the least: positive, negative and zero sequence reactance at NODE684 and NODE684 as compared to DFIGs connected at NODE632 and NODE650 with the variation on the sequence reactance impacting a lot on the SLG fault current levels.

The location of fault from the main grid NODE650 also impacted a lot on the magnitudes of the SLG fault currents. NODE611 with a distance of 4600 feet from the main grid had the least magnitudes of the SLG fault currents as compared to the currents at NODE684 which was 4300 feet from the main grid. The SLG fault currents at NODE611 were relatively lower in magnitudes as compared to the fault currents at NODE684. This is because nodes located far from the main grid substation had higher sequence reactance as compared to nodes nearer to the main grid.

During a short circuit, Type IV WTG creates a short circuit path from where it is located on the feeder to where we have the main grid substation at NODE650. This is evident in the case that for Type IV WTGs, there are no TCC curves between fuse F671 and fuse F671-684 for both 1MW and 3MW Type IV WTGs connected at NODE671. Type IV WTG placement at NODE671 created a short circuit path from NODE671 to the main grid NODE650. For Type IV WTGs connected at NODE632 and NODE650, TCC curves between fuse F671 and fuse F671-684 were available because the short circuit paths shifted upwards towards the main grid to NODE632 and NODE650 respectively.

CHAPTER FIVE

CONCLUSION AND RECOMMENDATIONS

5.1 Conclusion

Integrating WTGs into power system networks poses challenges of maintaining coordination among OCPDs like fuses. Series current liming reactors have emerged as a solution to facilitate a seamless integration of the WTGs onto the network without compromising on the systems' over-current protection schemes.

The intermittent nature of the WTG power generation causes high short circuit currents in the power systems networks. The high short circuit fault currents can lead to equipment damage, system downtime and costly repairs hence by limiting the fault currents, CLRs protect the power system equipment and components from damage thus extending their lifespan and reducing regular and costly maintenance cost.

Fuses are essential OCPDs in power systems designed to isolate faults and protect the power system equipment from short circuit faults however, in networks with renewable energy sources like the WTGs, fuse-fuse coordination experience diminishing time coordination margins due to the increased short circuit current levels. By limiting the short circuit current levels, CLR restores fuse-fuse coordination during a fault event through selective fault isolation before the faults propagate throughout the network hence minimizing the impact of faults on the overall power system operation improving on the overall reliability and stability of the network. This is especially important in critical applications where downtime can have significant consequences such as in industrial plants or healthcare facilities.

Compared to alternative solutions such as upgrading infrastructure or implementing complex protection schemes, CLRs offer a cost-effective way to restore fuse-fuse coordination. The CLRs can be easily installed in existing power systems networks without the need for extensive modifications making them a practical and efficient solution for improving the networks' over-current protection schemes. Series CLRs are flexible in sizing and placement hence can easily accommodate intermittent

changes in the distribution networks once the DGs are connected to easily adapt to the evolving power systems distribution network requirements. CLRs have modular designs without switching devices and that can be used to facilitate an easier adaptation of the renewable energy technologies onto conventional distribution networks' over-current protection schemes.

5.2 Recommendations

With the prominence that the fault current limiting devices have gained in fault current limitation, advanced fault current detection techniques utilizing artificial intelligence are need to enhance the speed and accuracy of fault detection and fault clearance hence researches on development of more advanced relays should be enhanced. Intelligent relays which can perform fault current limitations and can re-coordinate a power system network's over-current protect scheme have to be developed to mitigate on the issues of OCPDs miss-coordination from the ever increasing short circuit current levels contribution from the DGs. The intelligent and smart relays also would aid in the rapid development of the smart grids which is the trend in distribution network developments.

Equations and computer algorithms needs to be developed for sizing the current limiting reactors. The algorithms would also aid in the placement of the current limiting reactors at appropriate locations on the networks for optimum OCPDs coordination in the smart grids.

The intermittent nature of WTGs poses a great challenge to power system reactive power management and control. The issues emanate from the varied operating conditions of the WTGs impacting on the consistency of their power output. Since the WTGs are developed from induction generators, their reactive power capabilities are limited hence advanced control strategies needs to be developed for controlling the WTGs to mitigate and enhance their reactive power management especially for large wind turbine generator power plants since reactive power management affects the networks sequence reactance.

REFERENCES

Abdel-Salam, M., Abdallah, A., Kamel, R., & Hashem, M. (2017). Improvement of protection coordination for a distribution system connected to a microgrid using unidirectional fault current limiter. *Ain Shams Engineering Journal*, *8*(3), 405-414.

Aderibigbe, M. A., Adoghe, A. U., Agbetuyi, F., & Airoboman, A. E. (2022, April). Impact of Distributed Generations on Power Systems Stability: A Review. In 2022 IEEE Nigeria 4th International Conference on Disruptive Technologies for Sustainable Development (NIGERCON) (pp. 1-5). IEEE.

Aishwarya, Devi R, (2014). Active and Reactive Power Regulation of a Grid Connected Wind Energy Conversion System with Doubly Fed Induction Generator. *International Journal of Advanced Research in Electrical, Electronics and Instrumentation Engineering*, *3*(2)

Akpeh, V. A., Madueme, T. C., Ezechukwu, O. A., Ogboh, V. C., & Echedom, V. C. (2015). A methodology for implementing fault current limiting reactors (CLRs) on feeders with minimal constant power losses. *Global Journal of Engineering, Design & Technology*, *4*(5), 1-7.

Akpeh, V. A., Madueme, T. C., Ezechukwu, O. A., Ogboh, V. C., & Echedom, V. C. (2015). A methodology for implementing fault current limiting reactors (CLRs) on feeders with minimal constant power losses. *Global Journal of Engineering, Design & Technology*, *4*(5), 1-7.

Alam, M. S., Abido, M. A. Y., & El-Amin, I. (2018). Fault current limiters in power systems: A comprehensive review. *Energies*, *11*(5), 1025.

AL-Kababjie, M. F, & M AL-Taee, S. (2009). Adapting Distance Relay Using Artificial Neural Networks. *Al-Rafidain Engineering Journal (AREJ)*, *17*(3), 72-82.

Amon, Filho, J., Fernandez, P. C., Rose, E. H., D'Ayinz, A., & Castanheira, A. (2009). Brazilian successful experience in the usage of current limiting reactors for short-circuit limitation. In *Proceedings XI Symposium of Specialists in Electric Operational and Expansion Planning*.

Antonova, G., Nardi, M., Scott, A., & Pesin, M. (2012, April). Distributed generation and its impact on power grids and microgrids protection. In *2012 65th annual conference for protective relay engineers* (pp. 152-161). IEEE.

Basso, T. (2014). *IEEE 1547 and 2030 standards for distributed energy resources interconnection and interoperability with the electricity grid* (No. NREL/TP-5D00-63157). National Renewable Energy Lab.(NREL), Golden, CO (United States).

Bhasker, K., Balavignesh, S., & Kumar, V. S., (2014). Advanced Control Strategy for DFIG Based Wind Turbines for Power System Fault Ride Through.

Bui, D. M., Le, P. D., Nguyen, T. P., & Nguyen, H. (2021). An adaptive and scalable protection coordination system of overcurrent relays in distributed-generator-integrated distribution networks. *Applied Sciences*, *11*(18), 8454.

Bussman Cooper, (nd). Selective Coordination https://www.eaton.com/content /dam/eaton/products/electrical-circuit-protection/fuses/solution-center/ bus-ele- tech-lib-fuses-selective-coordination.

Codes and Standards Application Data—Transformers, Secondary Conductors, and Overcurrent Protection Application of Overcurrent Protection Rules to Transformers and Primary and Secondary Conductor" .Bulletin No. 0110DB0201 September 2002 Lexington, KY, USA

Contreras, A. F., Ramos, G. A., & Ríos, M. A. (2012). Methodology and design of an adaptive overcurrent protection for distribution systems with DG. *International Journal of Engineering & Technology*, *12*(4), 128-136.

Douglin, R. H. (2012). *An investigation of the utilization of smart meter data to adapt overcurrent protection for radial distribution systems with a high penetration of distributed generation* (Doctoral dissertation, Texas A & M University).

Dupuis, M., Mahoney, N., Padmanabhan, A., & Bhuvaneshwaran, K. (2017, April). Negative-sequence overcurrent considerations for induction motor loads. In *2017 70th Annual Conference for Protective Relay Engineers (CPRE)* (pp. 1-8). IEEE.

El-Ela, A. A. A., El-Sehiemy, R. A., Shaheen, A. M., & Ellien, A. R. (2022). Review on active distribution networks with fault current limiters and renewable energy resources. *Energies*, *15*(20), 7648.

El-Ela, A. A. A., El-Sehiemy, R. A., Shaheen, A. M., & Ellien, A. R. (2022). Review on active distribution networks with fault current limiters and renewable energy resources. *Energies*, *15*(20), 7648.

ELG4126 Wind Turbine Generators for Wind Power Plants "https://www.site.uottawa.ca/~rhabash/ELG4126WindGenerators."

Elmarkabi, I. M. (2004). *Control and protection of distribution networks with distributed generators*. North Carolina State University.

Funmilayo, H. (2010). *A New Approach to Mitigate the Impact of Distributed Generation on the Overcurrent Protection Scheme of Radial Distribution Feeders* (Doctoral dissertation, Texas A & M University).

Golrang, R. (2014). *Control of doubly fed induction generator based wind energy conversion system* (Doctoral dissertation).

Gonen, T. (2009). *Electrical power transmission system engineering: analysis and design*. CRC press.

Hewiston, L. G., Brown, M., & Balakrishnan, R. (2004). Practical Power Systems Protection, IDC Tehcnologis.

Jadhar, S., & Harchandani, R. (2015). 'Grid Interfacing Technologies for Distributed Generation and Power Quality Issues-A Review. *International Journal of Innovative and Emerging Research in Engineering*, *2*(3), 233-237.

Javadian, S. A. M., & Massaeli, M. (2011). Impact of distributed generation on distribution systems reliability considering recloser-fuse miscoordination-a practical case study. *Indian Journal of Science and Technology*, 1279-1284.

Kamel, A., Alaam, M. A., Azmy, A. M., & Abdelaziz, A. Y. (2013). Protection coordination for distribution systems in presence of distributed generators. *Electric power Components and systems*, *41*(15), 1555-1566.

Kersting, W. H. (2001, January). Radial distribution test feeders. In *2001 IEEE Power Engineering Society Winter Meeting. Conference Proceedings (Cat. No. 01CH37194)* (Vol. 2, pp. 908-912). IEEE.

Lopes, J. P., Hatziargyriou, N., Mutale, J., Djapic, P., & Jenkins, N. (2007). Integrating distributed generation into electric power systems: A review of drivers, challenges and opportunities. *Electric power systems research*, *77*(9), 1189-1203.

Majeed, W. S., Nasser, A. I., & Al-Bahrani, L. T. (2023). A Comprehensive Review for Application of Fault Current Limiters in Power Systems. *Al-Iraqia Journal for Scientific Engineering Research*, *2*(2), 45-57.

Majeed, W. S., Nasser, A. I., & Al-Bahrani, L. T. (2023). A Comprehensive Review for Application of Fault Current Limiters in Power Systems. *Al-Iraqia Journal for Scientific Engineering Research*, *2*(2), 45-57.

Muljadi, E., & Gevorgian, V. (2011, July). Short-circuit modeling of a wind power plant. In *2011 IEEE Power and Energy Society General Meeting* (pp. 1-9). IEEE.

Muljadi, E., Samaan, N., Gevorgian, V., Li, J., & Pasupulati, S. (2010, July). Short circuit current contribution for different wind turbine generator types. In *IEEE PES general meeting* (pp. 1-8). IEEE.

Paliwal, P., Patidar, N. P., & Nema, R. K. (2012). A comprehensive survey of optimization techniques used for Distributed Generator siting and sizing. *2012 Proceedings of IEEE Southeastcon*, 1-7.

Rajapakse, A., Majumder, R., Energy, S. G. R., & Nelson, R. (2020). Modification of Commercial Fault Calculation Programs for Wind Turbine Generators. *IEEE Power Energy Society (June 2020)*, 81.

Ravindranath, B., & Chander, M. (1977). *Power system protection and switchgear*. New Age International.

Rini, Ann Jerin, Prabaharan N, Palanisamy K, & Umashankar, S., (2017). Frequency Control of a Stand-Alone Hybrid Wind and Solar Based Distributed Generation System through an Optimized Energy Storage. Retrieved from https://www.researchgate.net/publication/318035009.

Samadi, A., & Chabanloo, R. M. (2020). Adaptive coordination of overcurrent relays in active distribution networks based on independent change of relays' setting groups. *International Journal of Electrical Power & Energy Systems*, *120*, 106026.

Schweitzer, E. O., & Zocholl, S. E. (2004, April). Introduction to symmetrical components. In *proceedings of the 58th Annual Georgia Tech Protective Relaying Conference, Atlanta, GA.*

Shobole, A., Baysal, M., Wadi, M., & Tur, M. R. (2020). An adaptive protection technique for smart distribution network. *Elektronika ir Elektrotechnika*.

Smith, T. P. (2006). The ABC's of Over-current Coordination-Analyzer. *Published for electrical engineers by E POWER ENGINEERING*.

Soria, O. A., Enríquez, A. C., & Guajardo, L. T. (2014). Overcurrent relay with unconventional curves and its application in industrial power systems. *Electric power systems research*, *110*, 113-121.

Square, D. (2006). Guide to Power System Selective Coordination 600V and below. *Schneider Electric*.

Tambun, R. C. S., Banjar-Nahor, K. M., Hariyanto, N., Rahman, F. S., & Rahmani, R. (2021, October). Adaptive protection coordination scheme for distribution system under penetration of distributed generation. In *2021 3rd International Conference on High Voltage Engineering and Power Systems (ICHVEPS)* (pp. 355-360). IEEE.

Tian, P., Li, Z., & Hao, Z. (2019). A Doubly-Fed Induction Generator Adaptive Control Strategy and Coordination Technology Compatible with Feeder Automation. *Energies*, *12*(23), 4463.

Valenzuela, A., Simani, S., & Inga, E. (2021). Automatic overcurrent protection coordination after distribution network reconfiguration based on peer-to-peer communication. *Energies*, *14*(11), 3253.

Varetsky, Y., & Gajdzica, M. (2023). Study of short circuit and inrush current impact on the current-limiting reactor operation in an industrial grid. *Energies*, *16*(2), 811.

Yadav, S., Choudhary, G. K., & Mandal, R. K. (2014). Review on fault current limiters. *Int. J. Eng*, *3*(4).Kare, V. (2018, Jume). Review on Reactors for Limiting the Fault Current. *Journal of Emerging Technologies and Innovative Research (JETIR)*, *5*(6)

Yin, J. (2021). Research on short-circuit current calculation method of doubly-fed wind turbines considering rotor dynamic process. *Frontiers in Energy Research*, *9*, 686146.

Yin, J. (2021b). Improved Short-Circuit Current Calculation of Doubly Fed Wind Turbines with Uninterrupted Excitation. *Frontiers in Energy Research*, *9*, 686138.

Yousaf, M, & Tahir, Mahmoud, (2017). Protection Coordination for a Distribution System In The Presence Of Distributed Generation. *Turkish Journal of Electrical Engineering and Computer Sciences*

Zayandehroodi, H., Mohamed, A., Shareef, H., & Mohammadjafari, M. (2011). A Comprehensive review of protection coordination methods in power distribution systems in the presence of DG. *Prz. Elektrotechniczny*, *87*(8), 142-148.

APPENDICES

Appendix I: IEEE 13 Node Radial Test Feeder ETAP Model Three Phase and SLG Short Circuit Fault Currents

Faulted NODE ID	Three Phase Fault Currents in Amperes	SLG Fault Currents in Amperes
NODE611	556	679
NODE632	609	810
NODE633	597	779
NODE634	4367	5429
NODE645	597	777
NODE646	589	757
NODE650	647	935
NODE652	558	671
NODE671	575	715
NODE675	572	707
NODE680	560	675
NODE684	568	697
NODE692	575	715

Appendix II: IEEE 13 Node Radial Test Feeder ETAP Model Positive, Negative and Zero Sequence Reactance

Faulted NODE ID	Positive/Negative Sequence Reactance in Ohms	Zero Sequence Reactance in Ohms
NODE611	4.26642	1.89837
NODE632	3.90891	0.97988
NODE633	3.98072	1.17125
NODE634	0.06219	0.0248
NODE645	3.98114	1.18825
NODE646	4.02868	1.31746
NODE650	3.68607	0.2768
NODE652	4.23085	1.93707
NODE671	4.13252	1.68289
NODE675	4.15143	1.73127
NODE680	4.24553	2.03491
NODE684	4.18005	1.8121
NODE692	4.13252	1.68289

Appendix III: IEEE 13 Node Radial Test Feeder ETAP Model Equipment Protection Landmarks and TCC Curves

A. CABLE684-652 PROTECTION LANDMARKS AND TCC CURVES

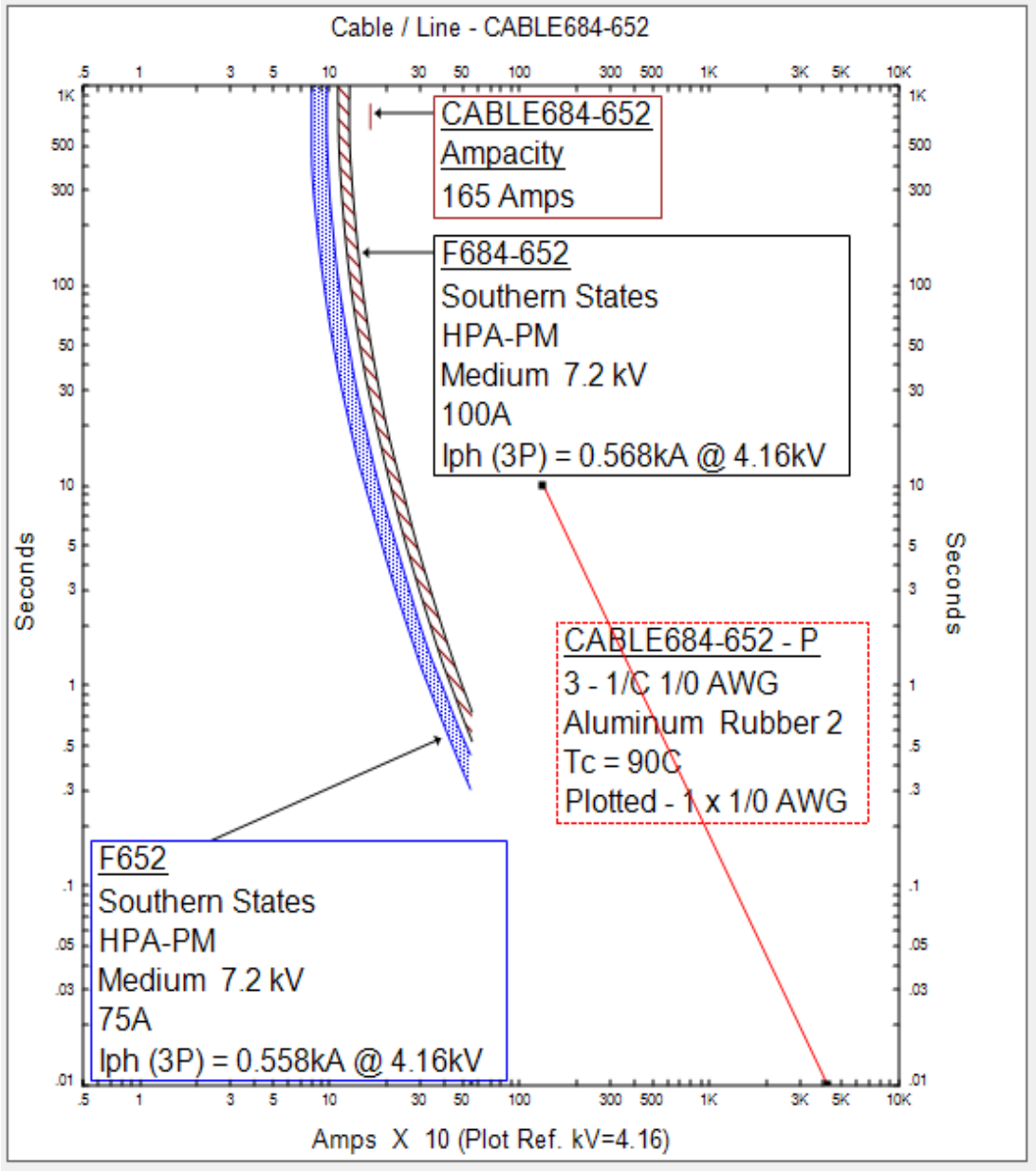

B. CABLE692-675 PROTECTION LANDMARKS AND TCC CURVES

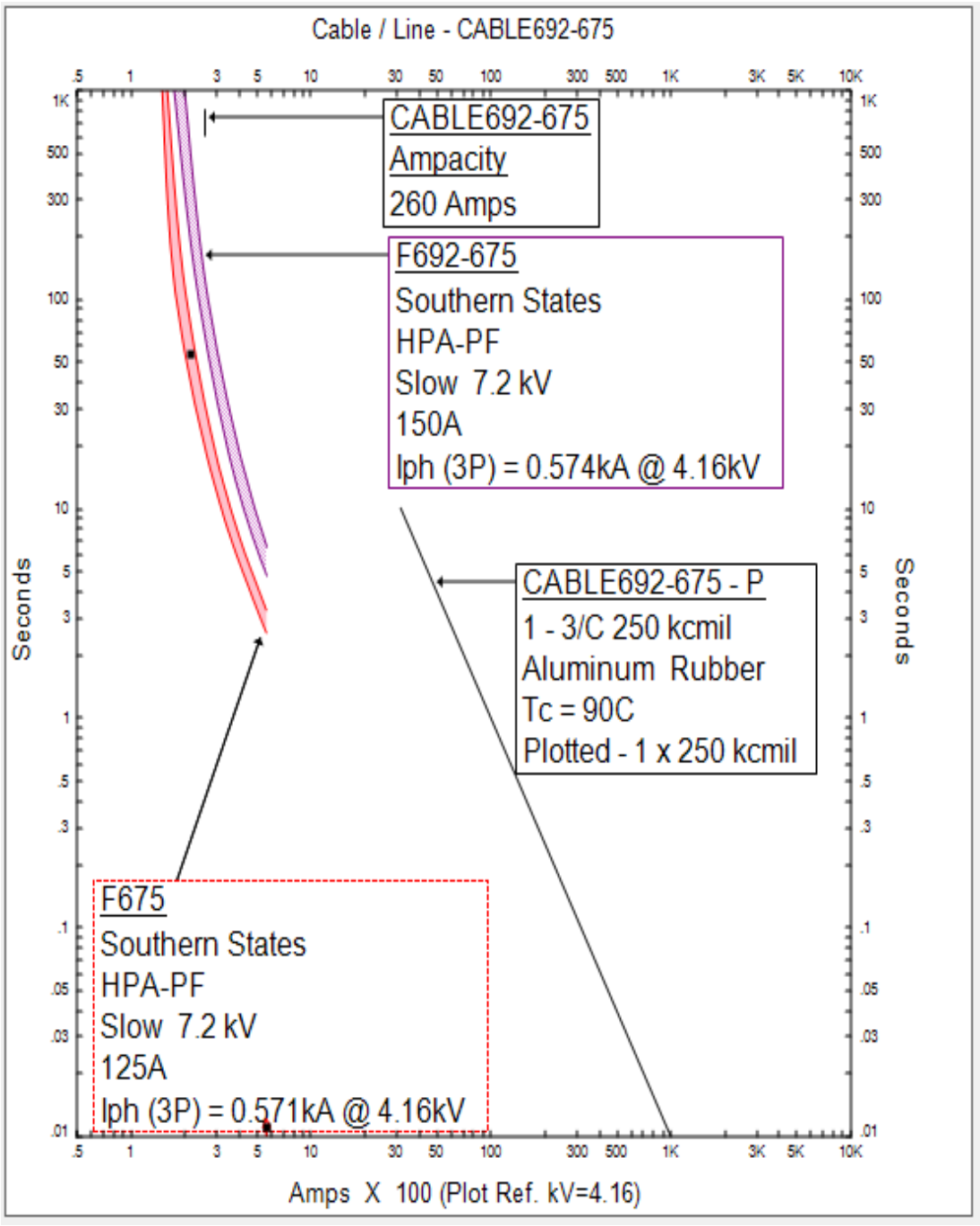

C. LINE632-633 PROTECTION LANDMARKS AND TCC CURVES

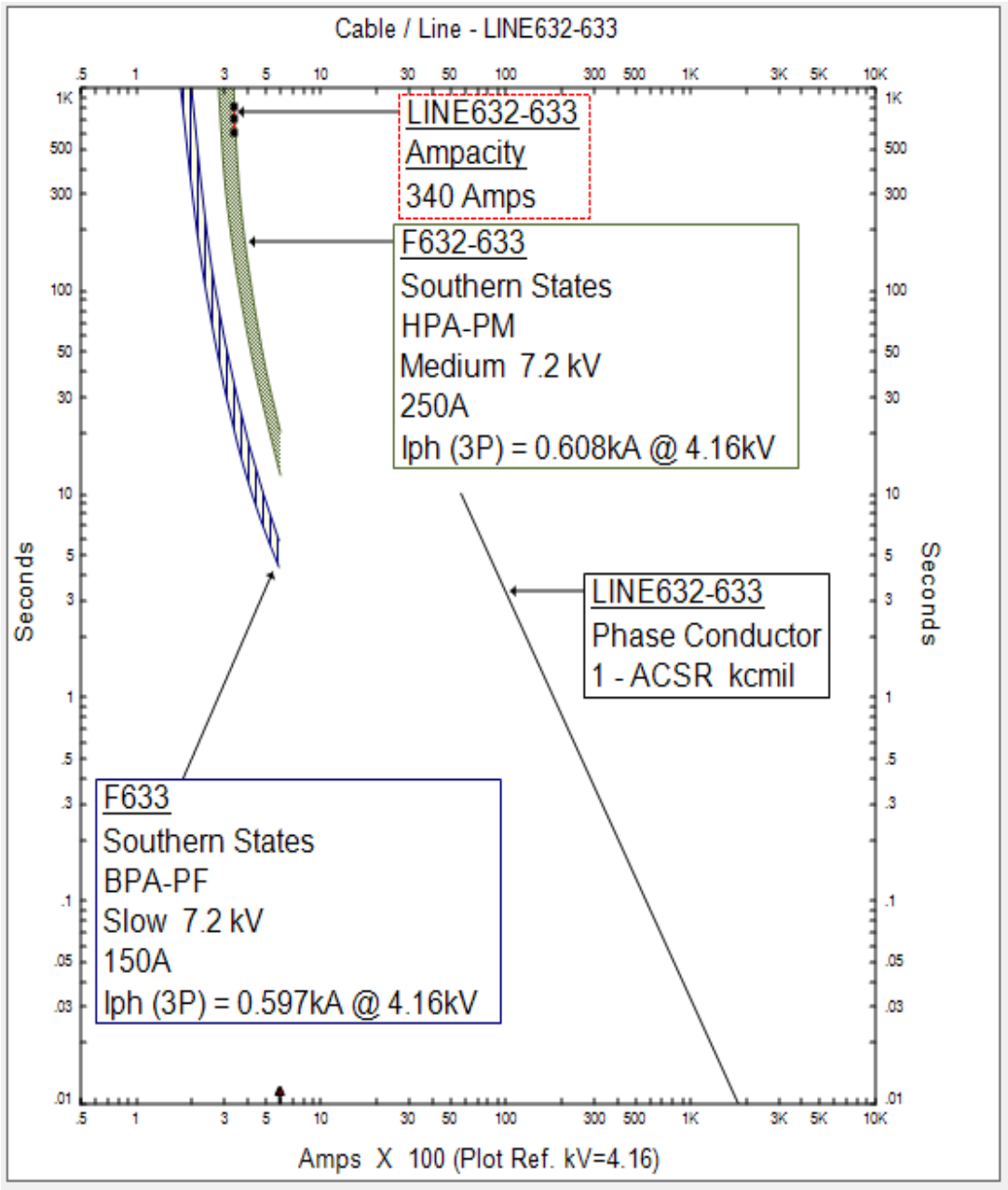

D. LINE632-645 PROTECTION LANDMARKS AND TCC CURVES

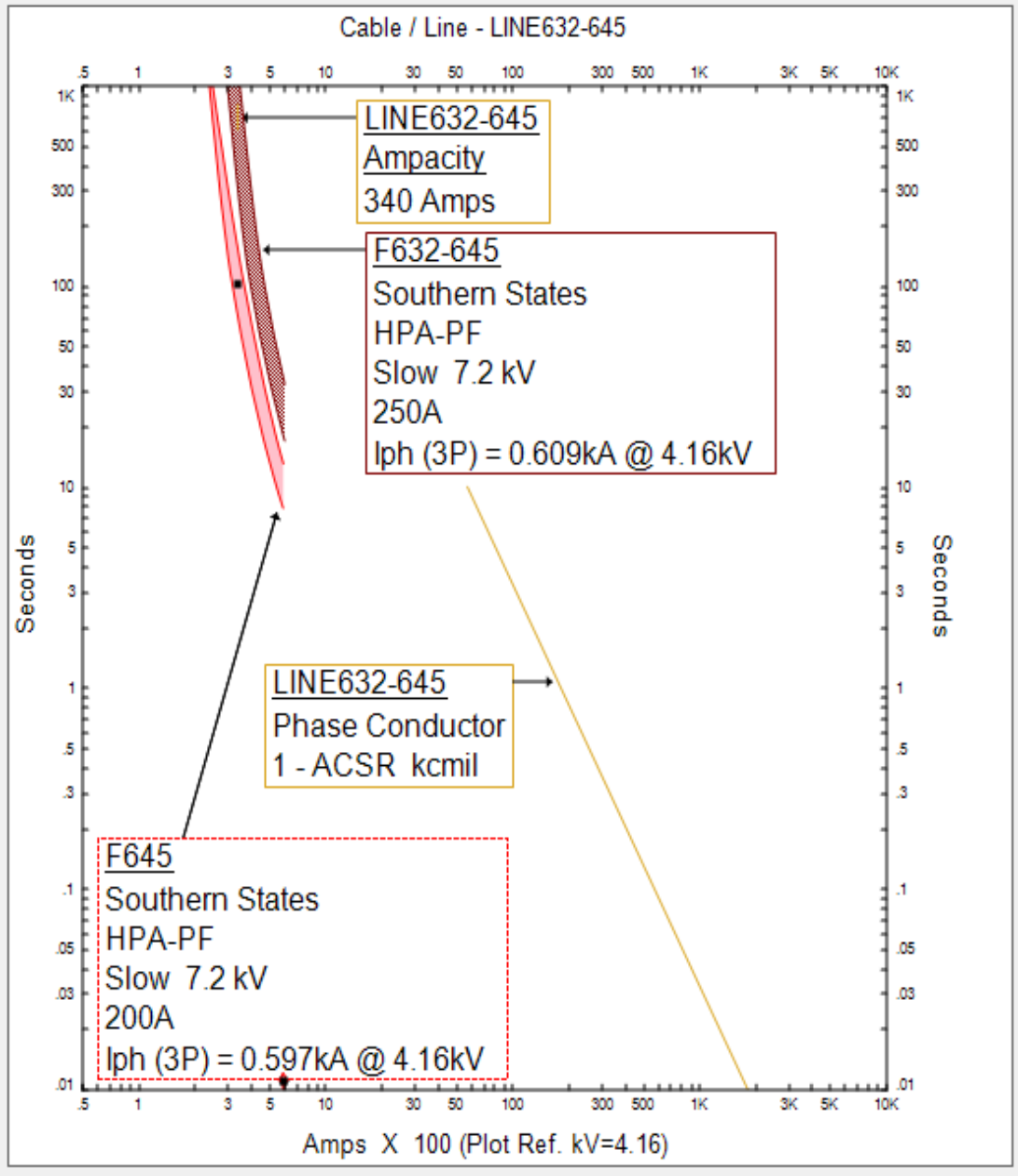

E. LINE632-671 PROTECTION LANDMARKS AND TCC CURVES

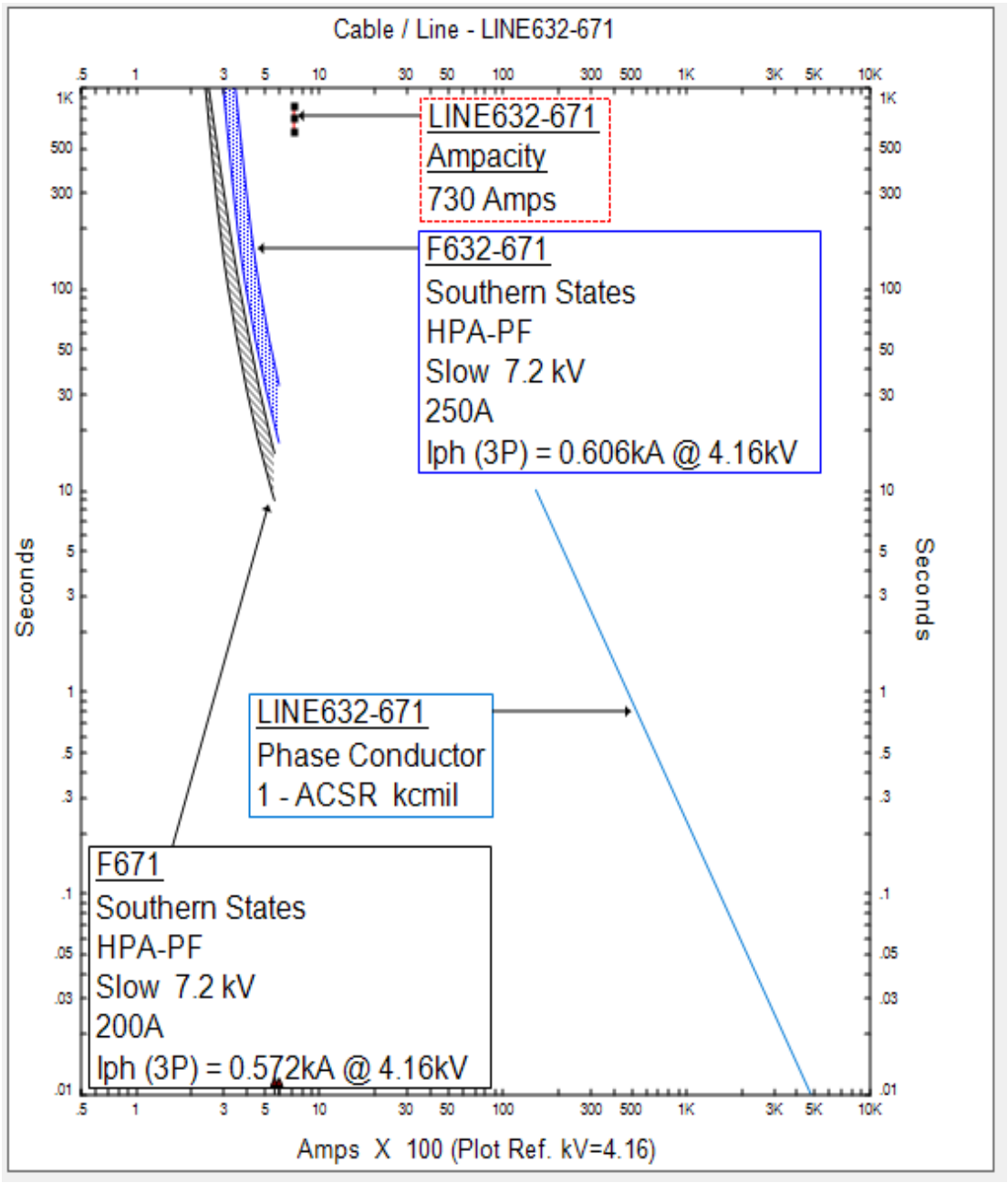

F. LINE671-680 PROTECTION LANDMARKS AND TCC CURVES

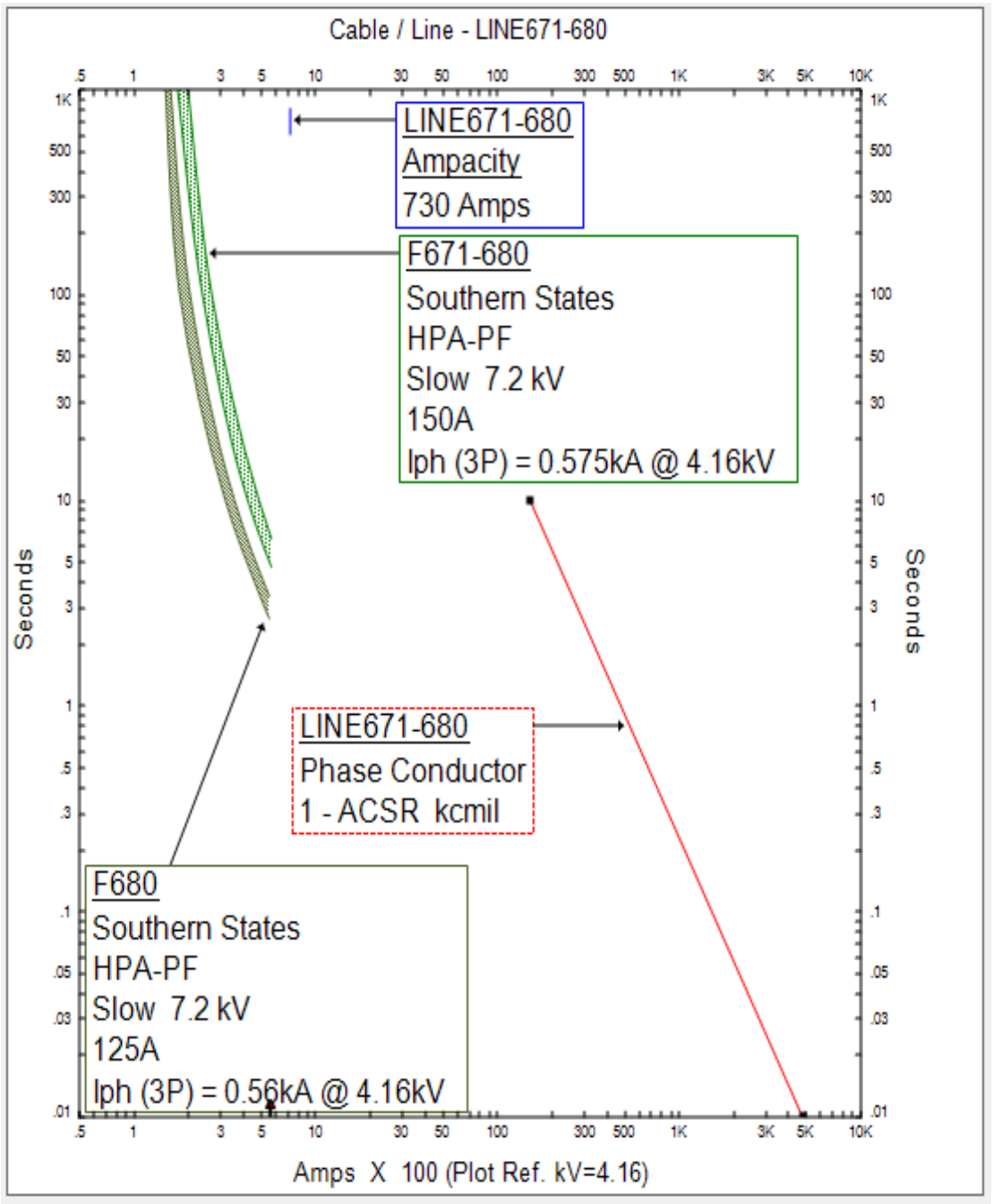

G. LINE671-684 PROTECTION LANDMARKS AND TCC CURVES

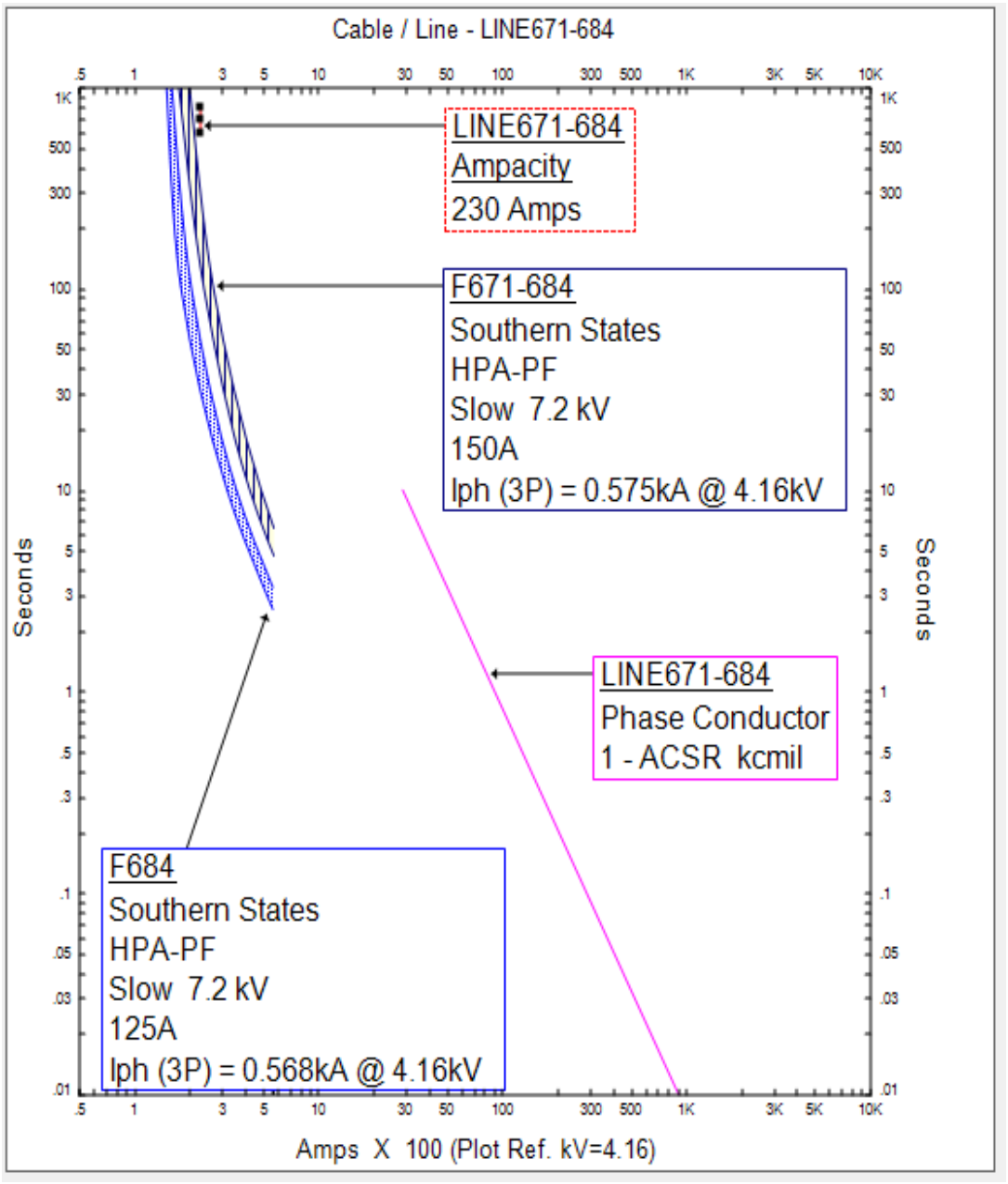

H. LINE684-611 PROTECTION LANDMARKS AND TCC CURVES

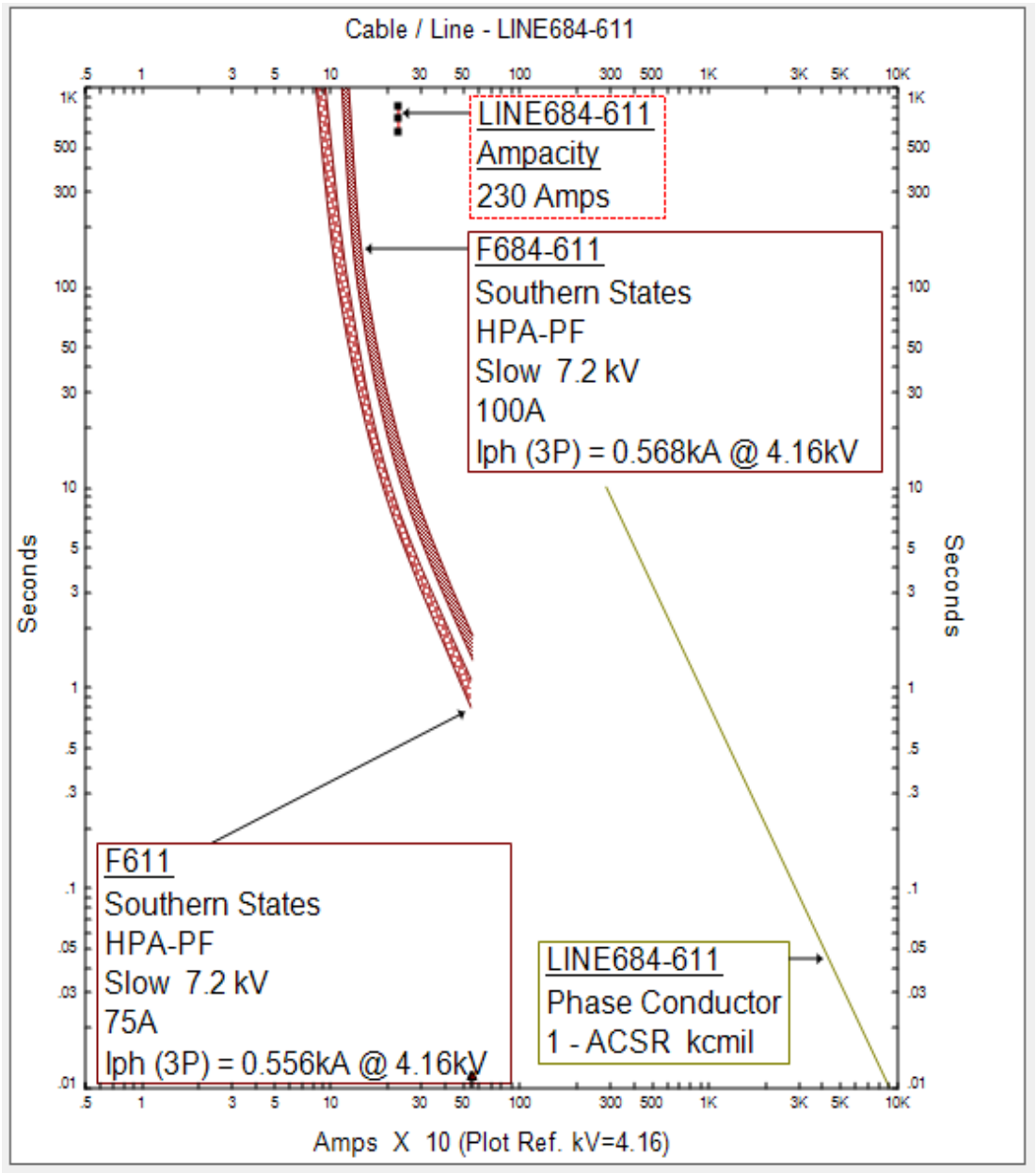

I. LINE645-646 PROTECTION LANDMARKS AND TCC CURVES

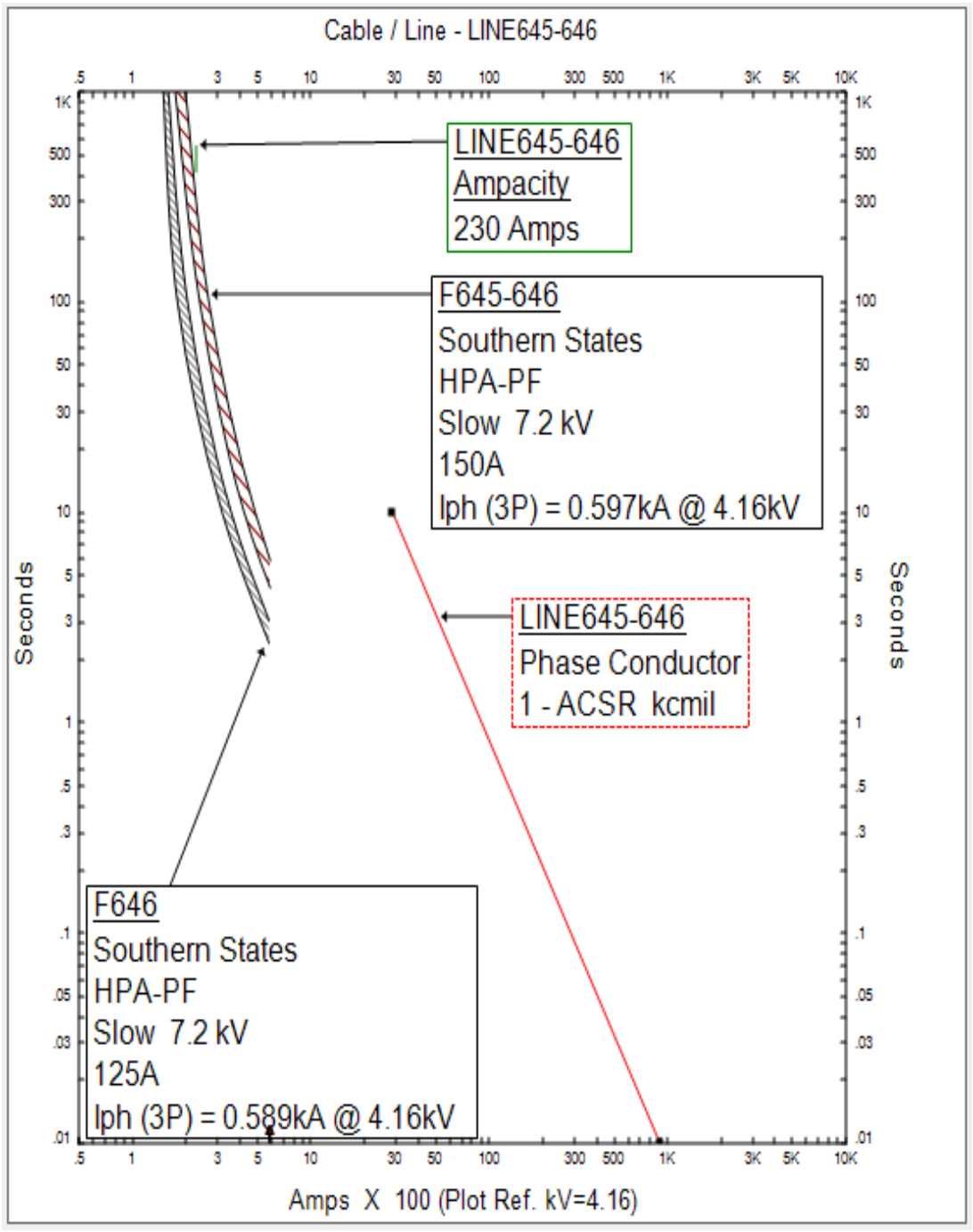

J. LINE650-632 PROTECTION LANDMARKS AND TCC CURVES

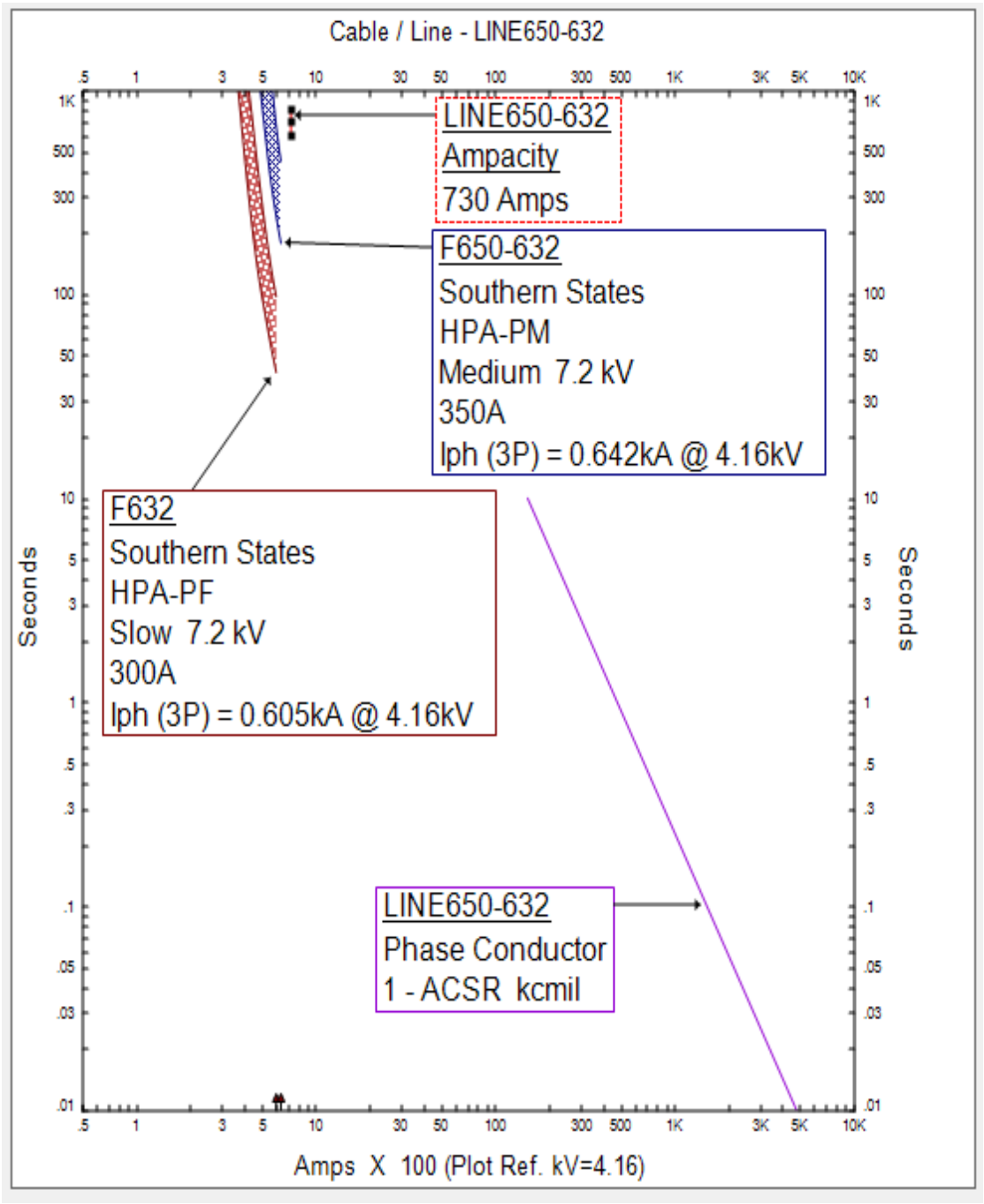

K. IN-LINE TRANSFORMER FULL LOAD AMPERE MARK, MAGNETIZING INRUSH POINTS AND DAMAGE CURVES

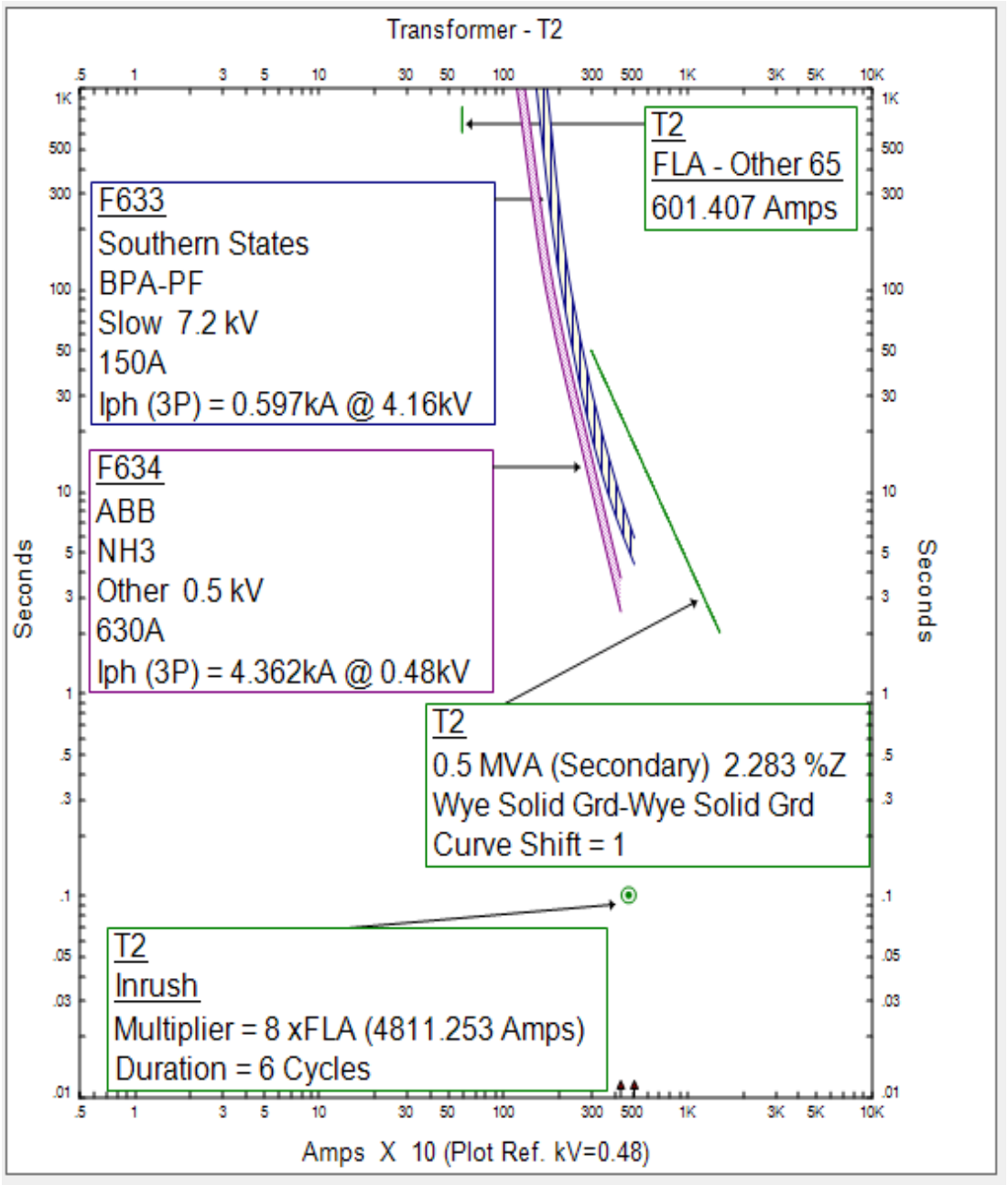

Appendix IV: IEEE 13 Node Radial Test Feeder ETAP Model Nodes Protection Landmarks and TCC Curves

A. NODE611 PROTECTION LANDMARKS AND TCC CURVES

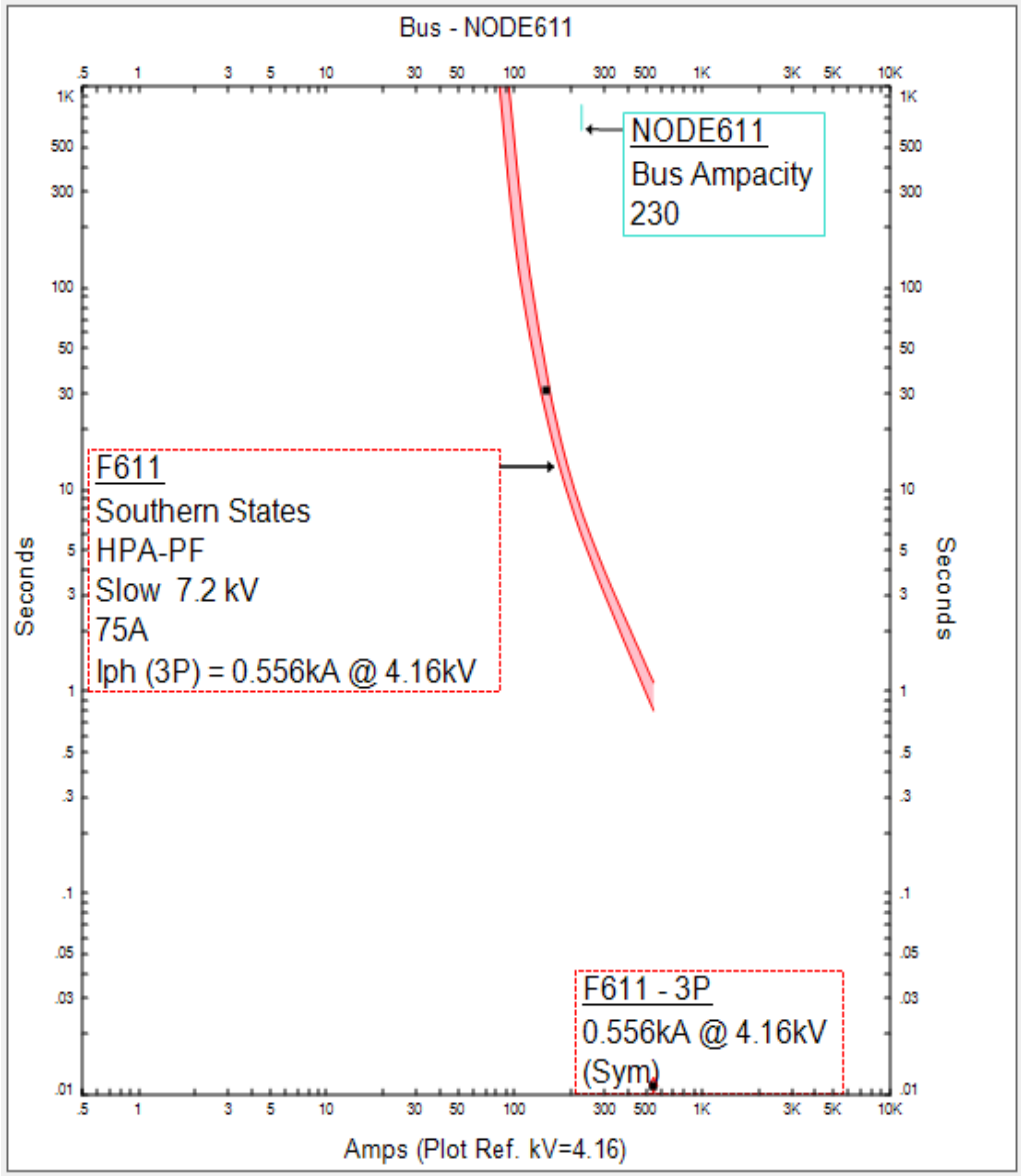

B. NODE632 PROTECTION LANDMARKS AND TCC CURVES

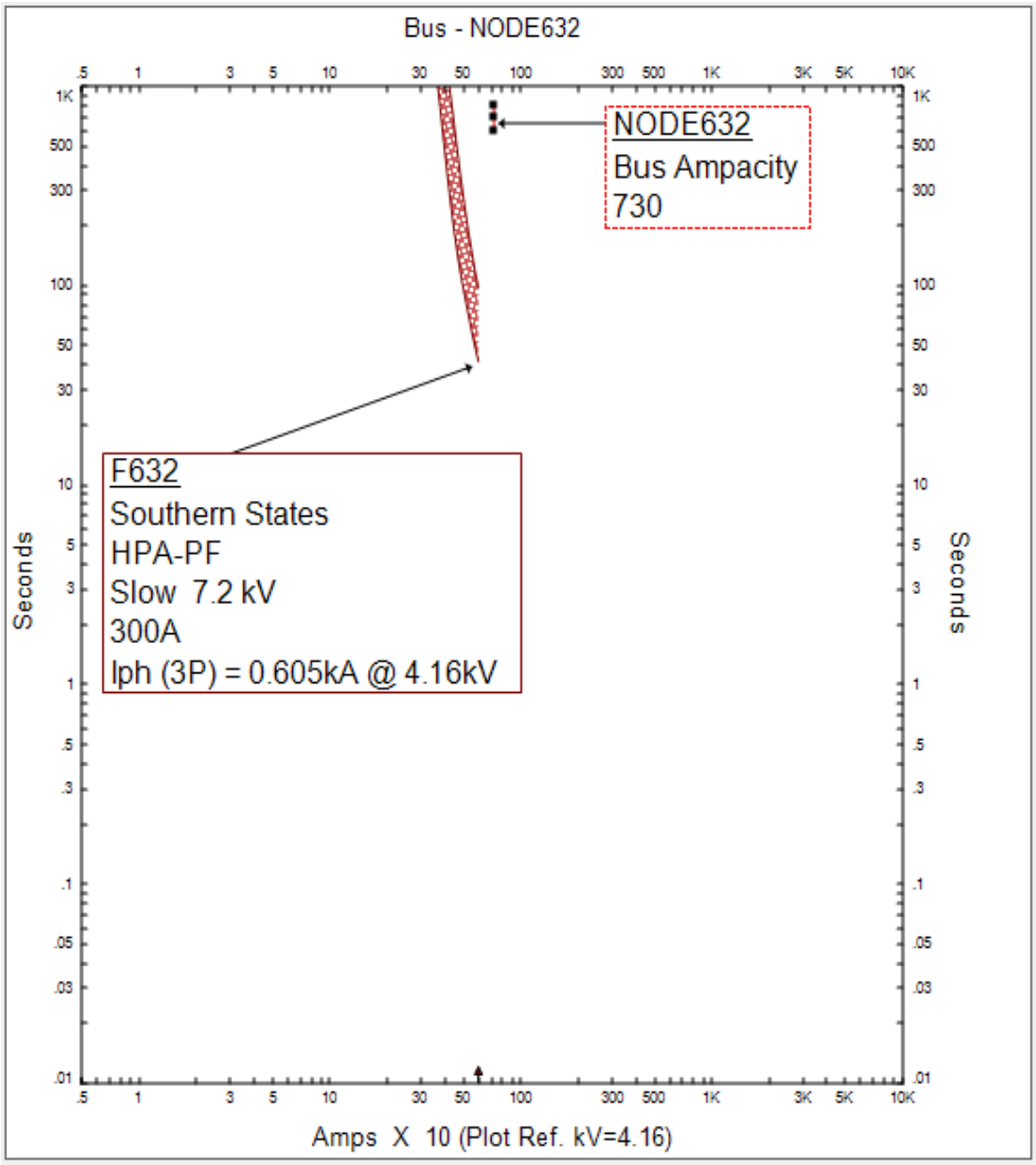

C. NODE645 PROTECTION LANDMARKS AND TCC CURVES

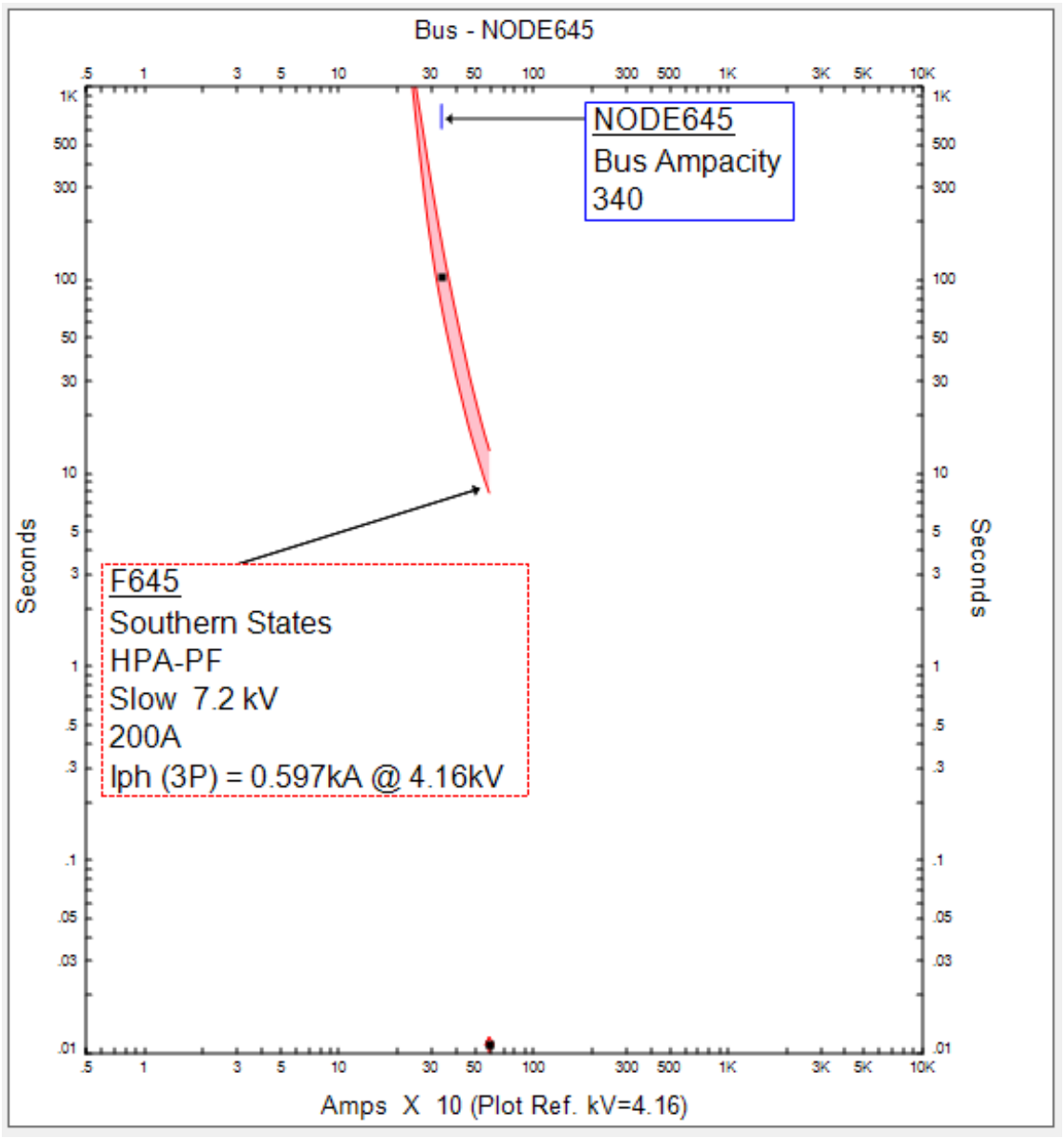

D. NODE650 PROTECTION LANDMARKS AND TCC CURVES

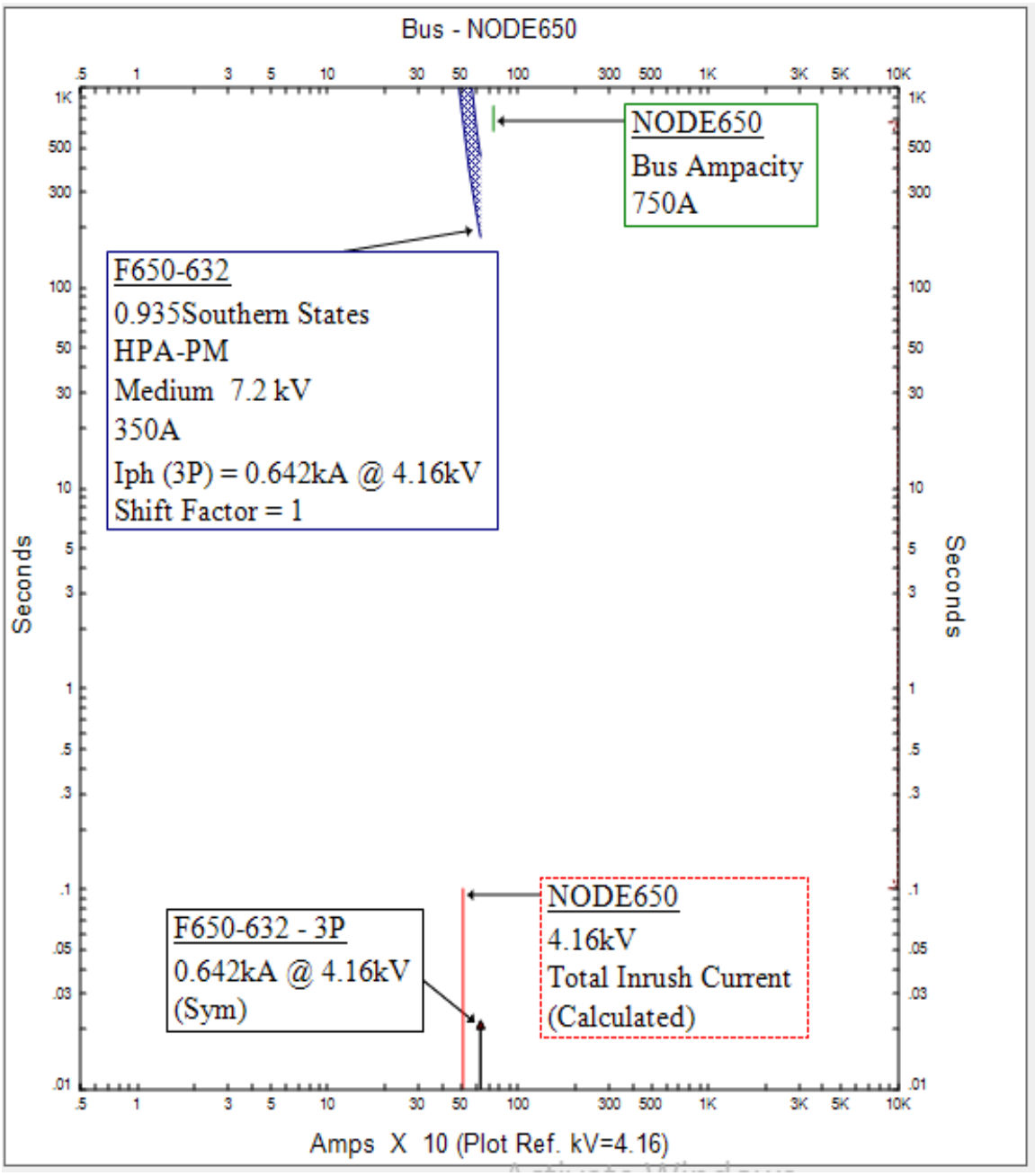

E. NODE671 PROTECTION LANDMARKS AND TCC CURVES

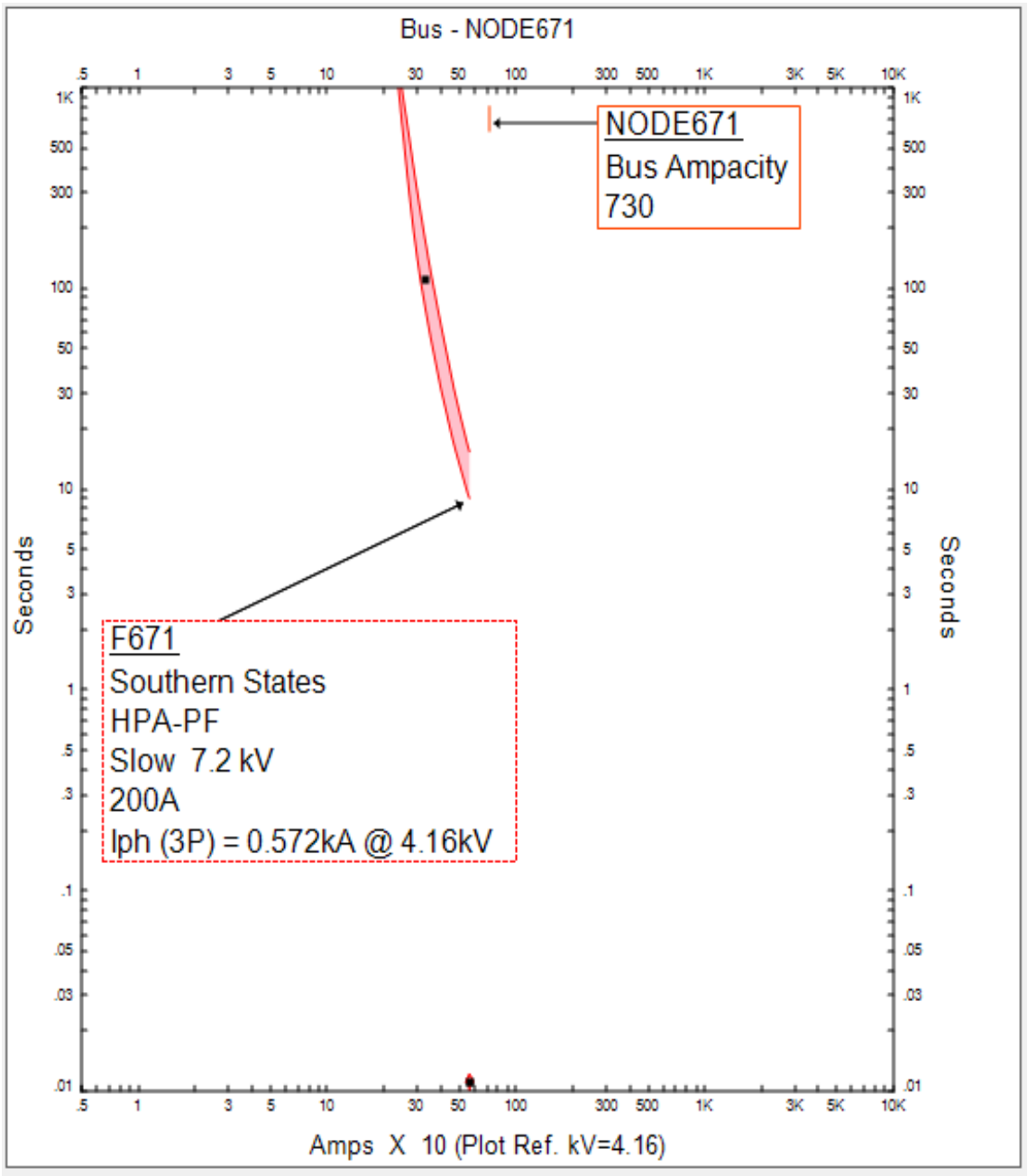

F. NODE675 PROTECTION LANDMARKS AND TCC CURVES

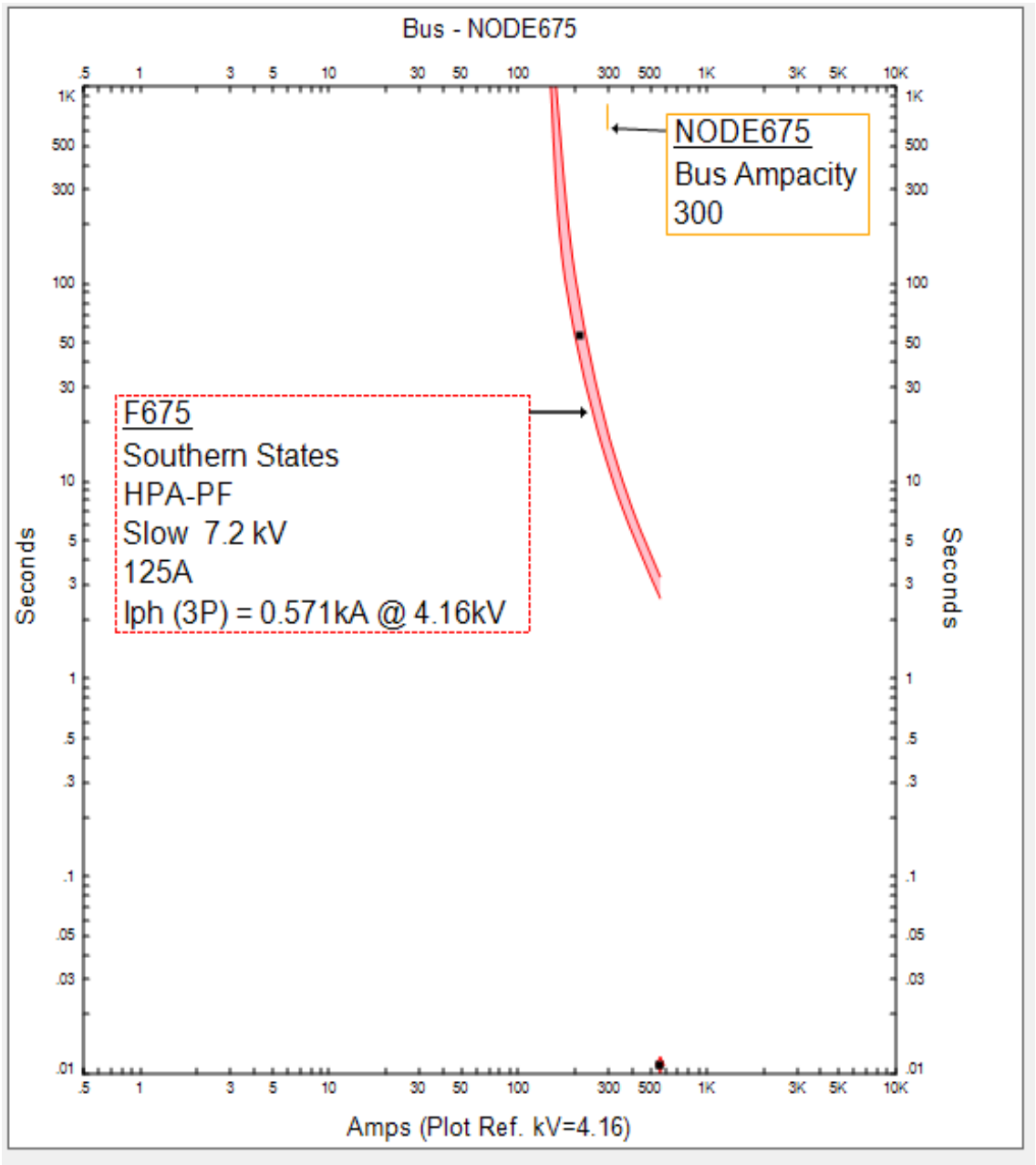

G. NODE684 PROTECTION LANDMARKS AND TCC CURVES

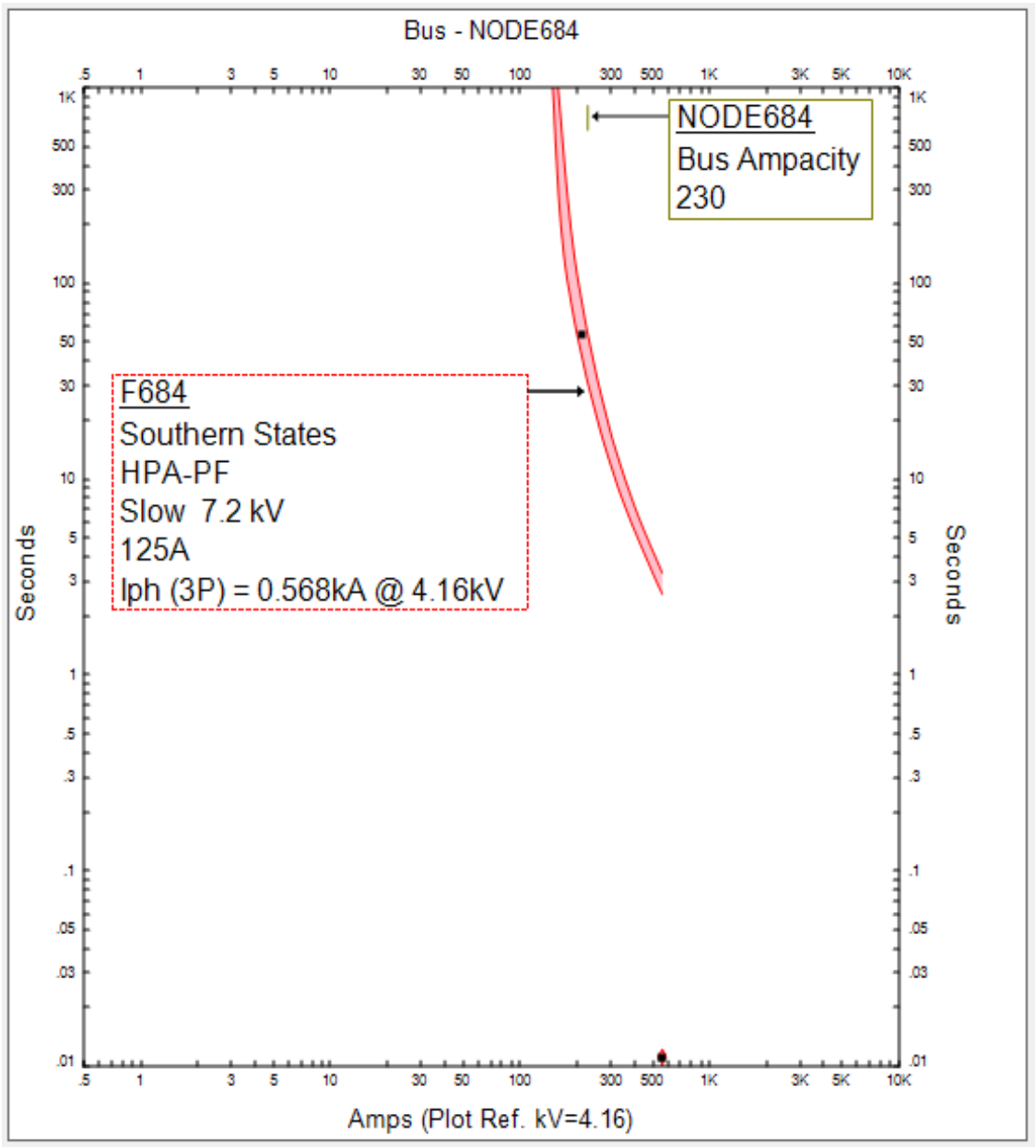

Appendix V: IEEE 13 Node Radial Test Feeder ETAP Model Primary Protection Zones Fuse-Fuse Coordination TCC Curves

A. FUSES F684-652 AND F652 TCC CURVES FOR SLG FAULTS AT NODE652

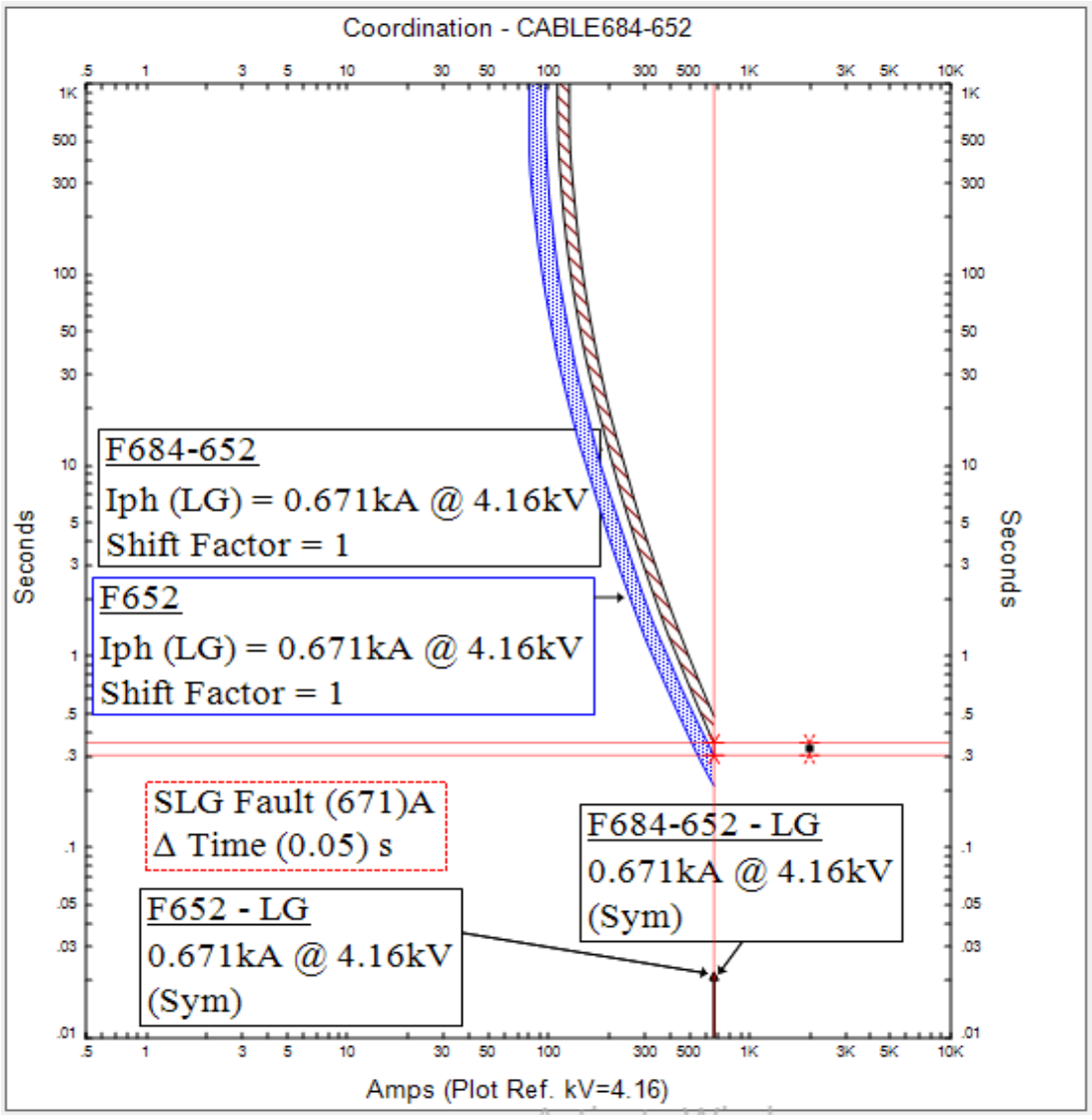

B. FUSES F692-675 AND F675 TCC CURVES FOR SLG FAULT AT NODE675

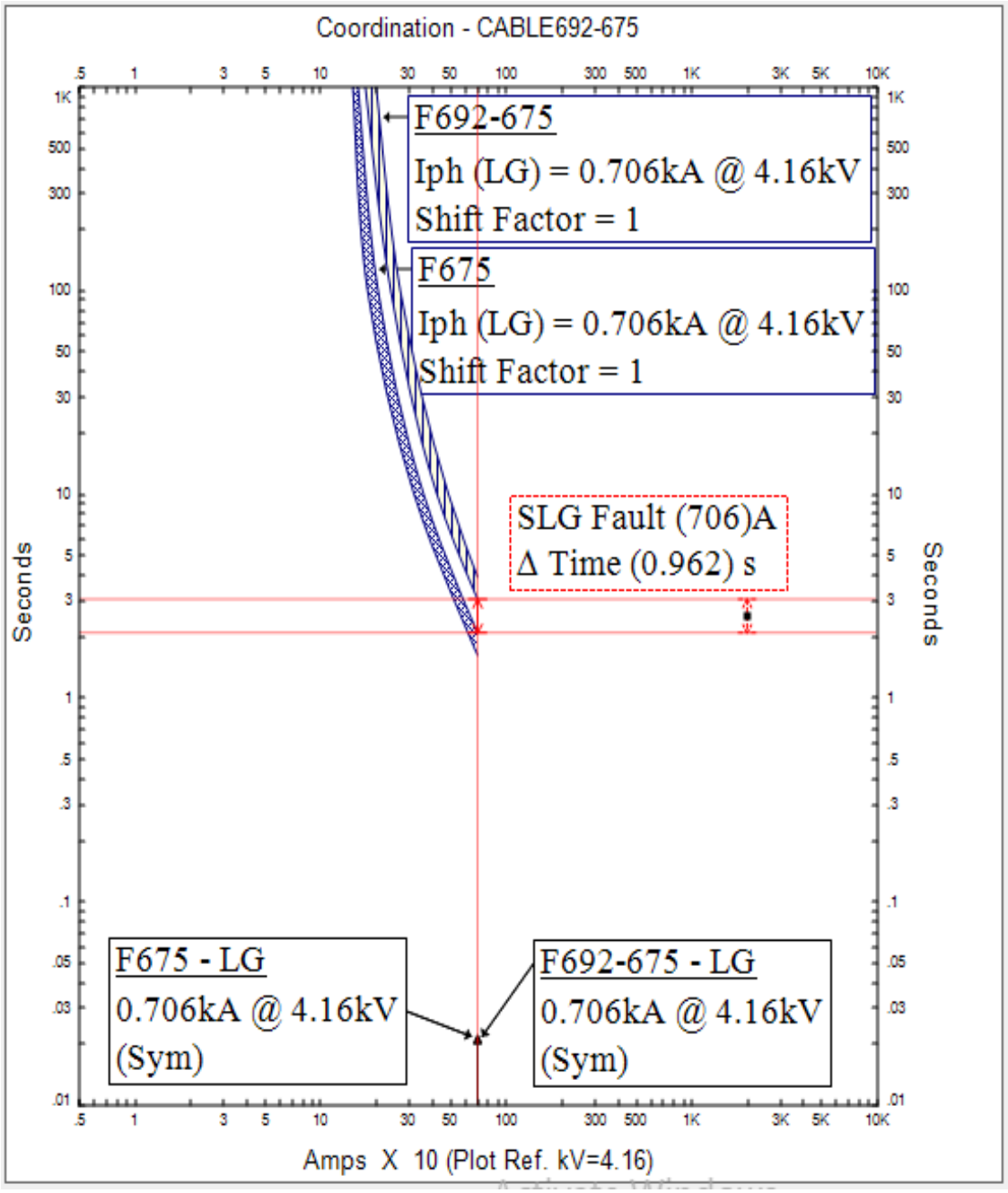

C. FUSES F632-633 AND F633 TCC CURVES FOR SLG FAULT AT NODE633

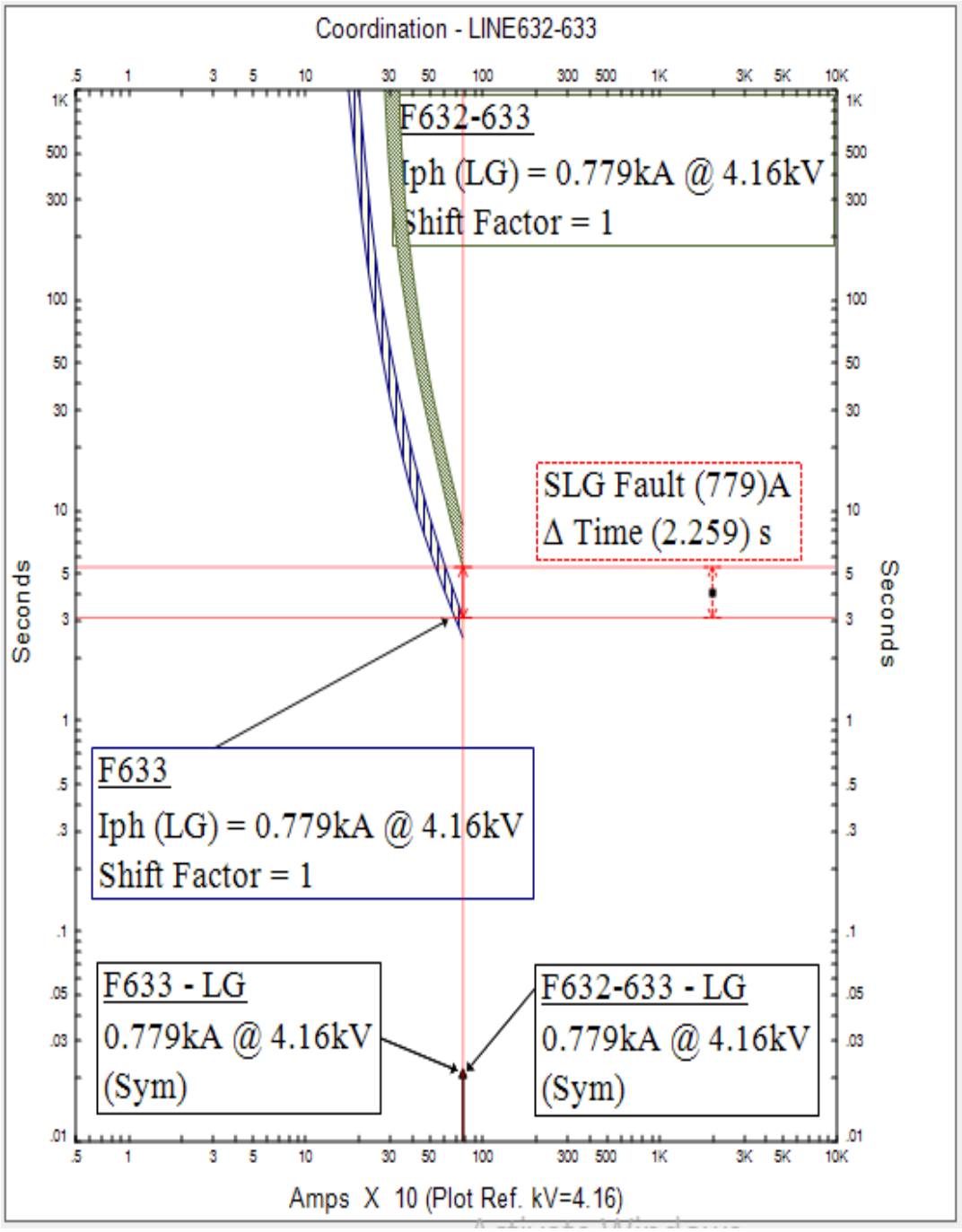

D. FUSES F632-645 AND F645 TCC CURVES FOR SLG FAULT AT NODE645

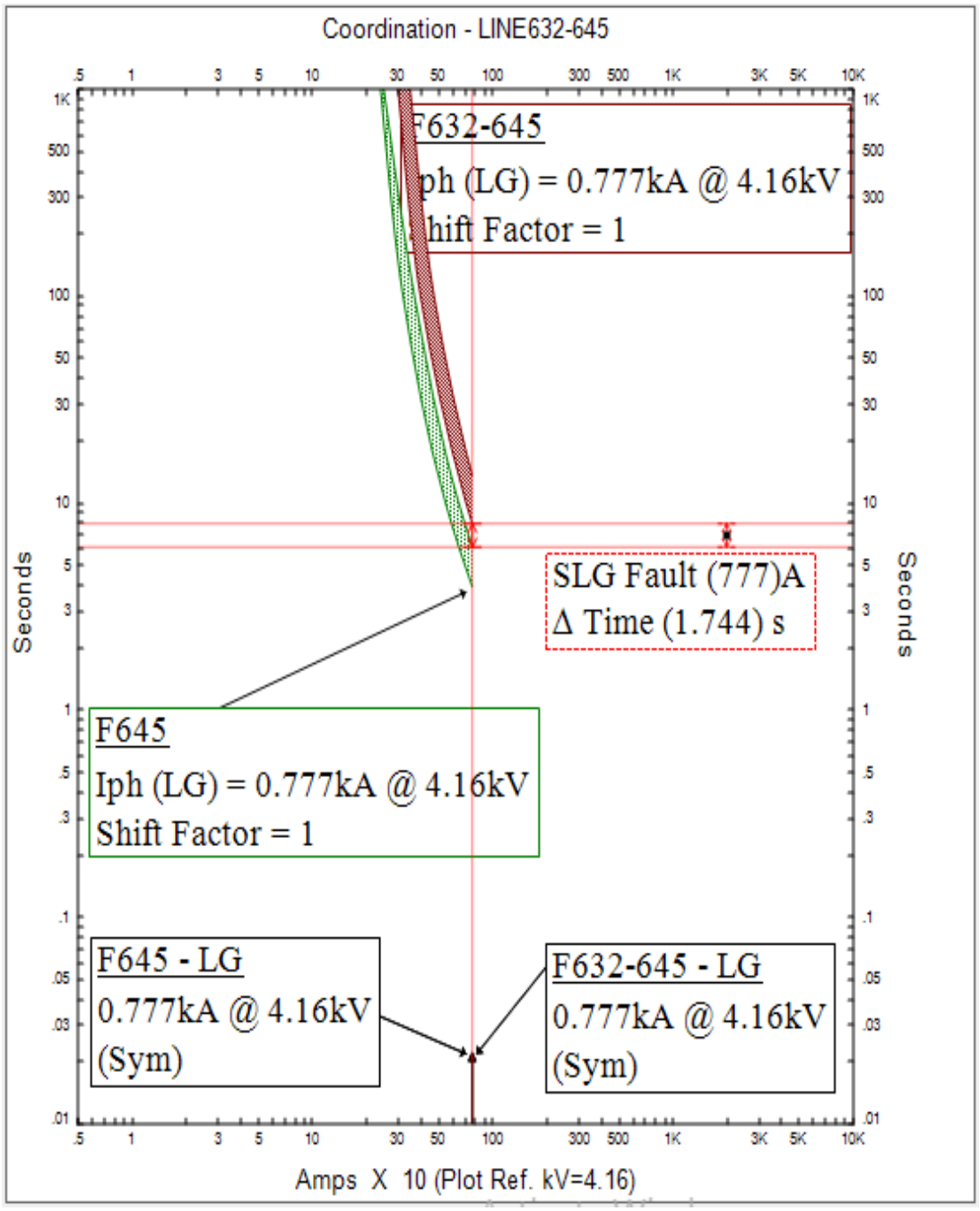

E. FUSES F632-671 AND F671 TCC CURVES FOR SLG FAULT AT NODE671

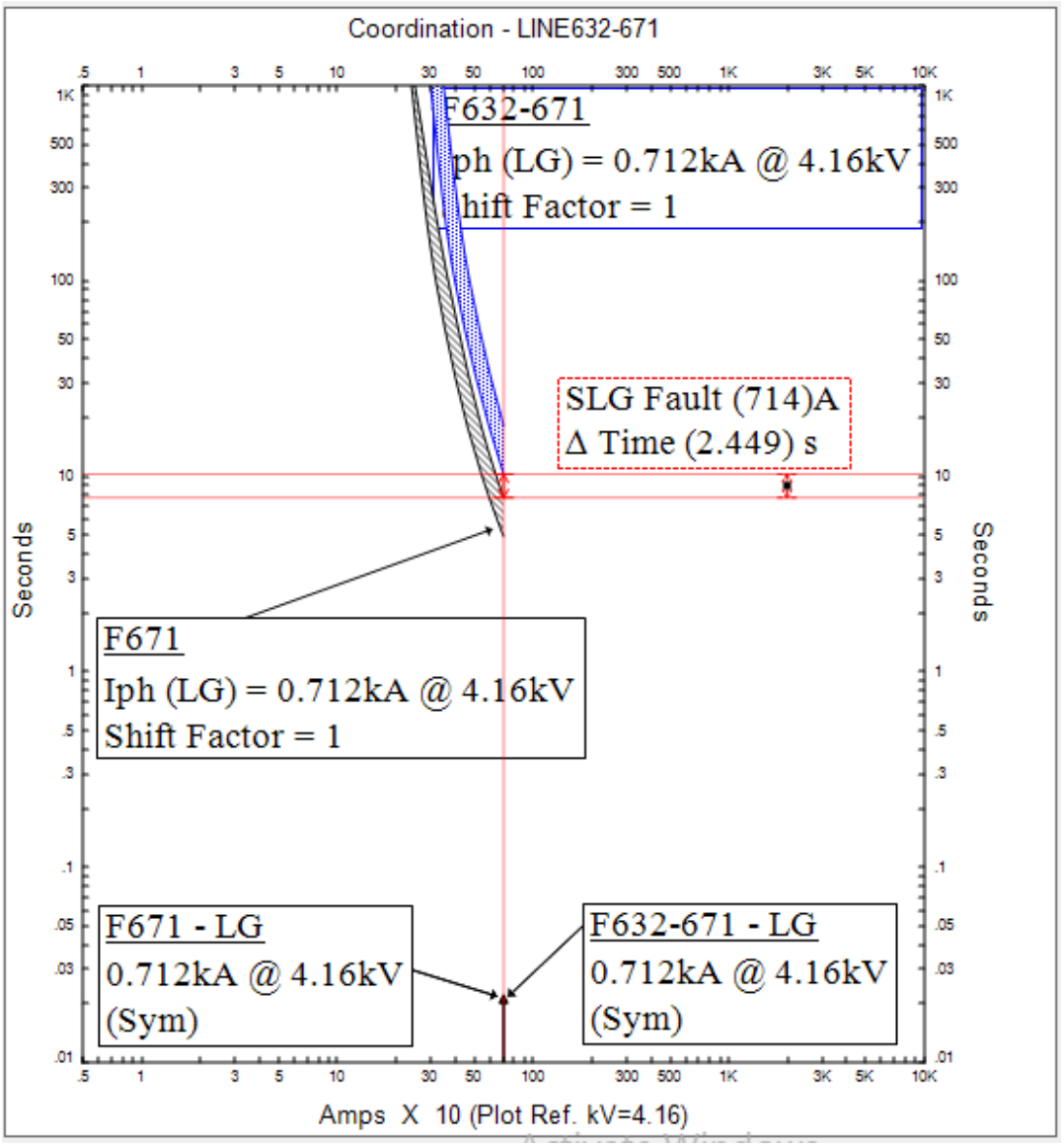

FUSES F645-646 AND F646 TCC CURVES FOR SLG FAULT AT NODE646

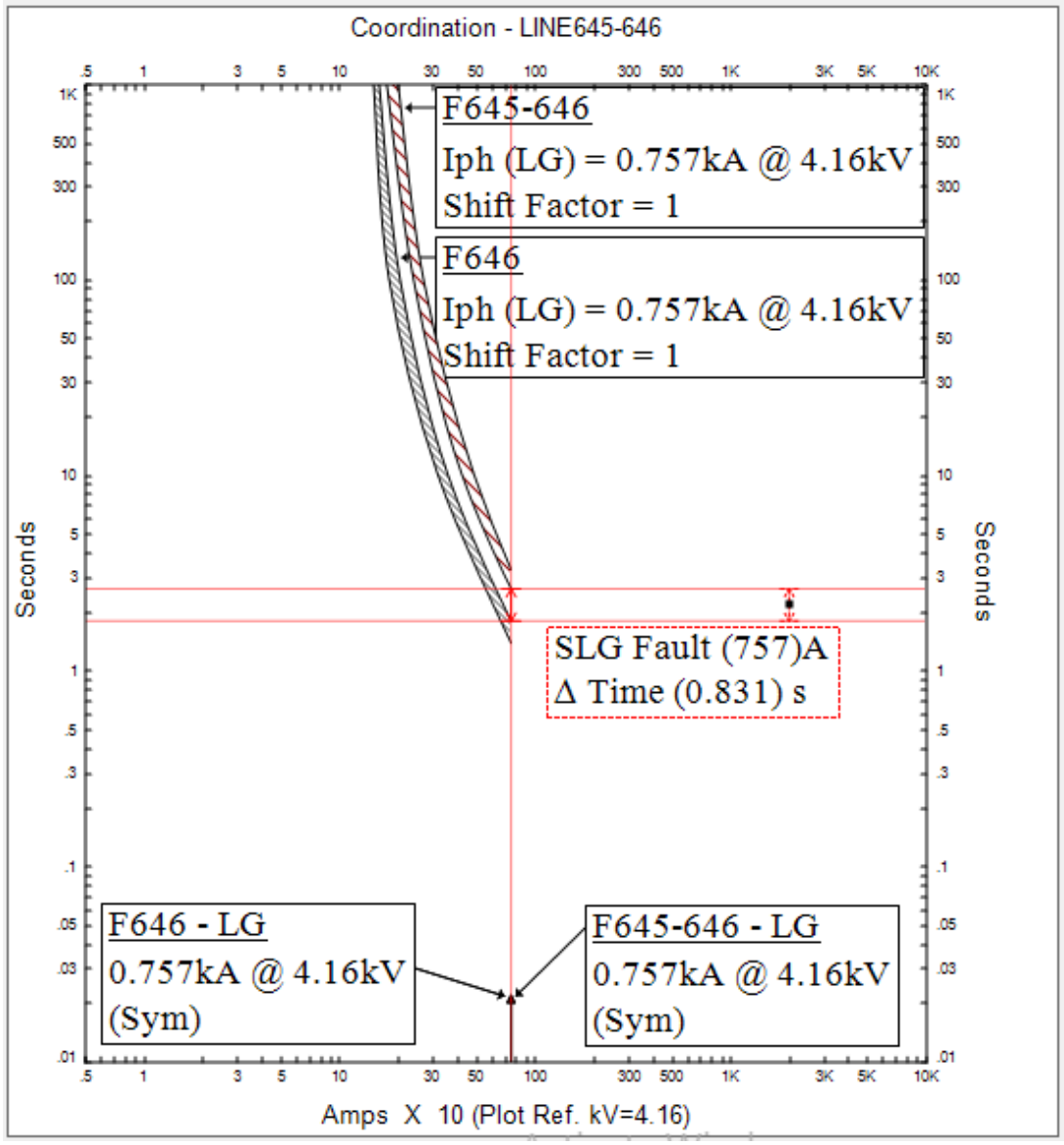

F. FUSES F650-632 AND F632 TCC CURVES FOR SLG FAULT AT NODE632

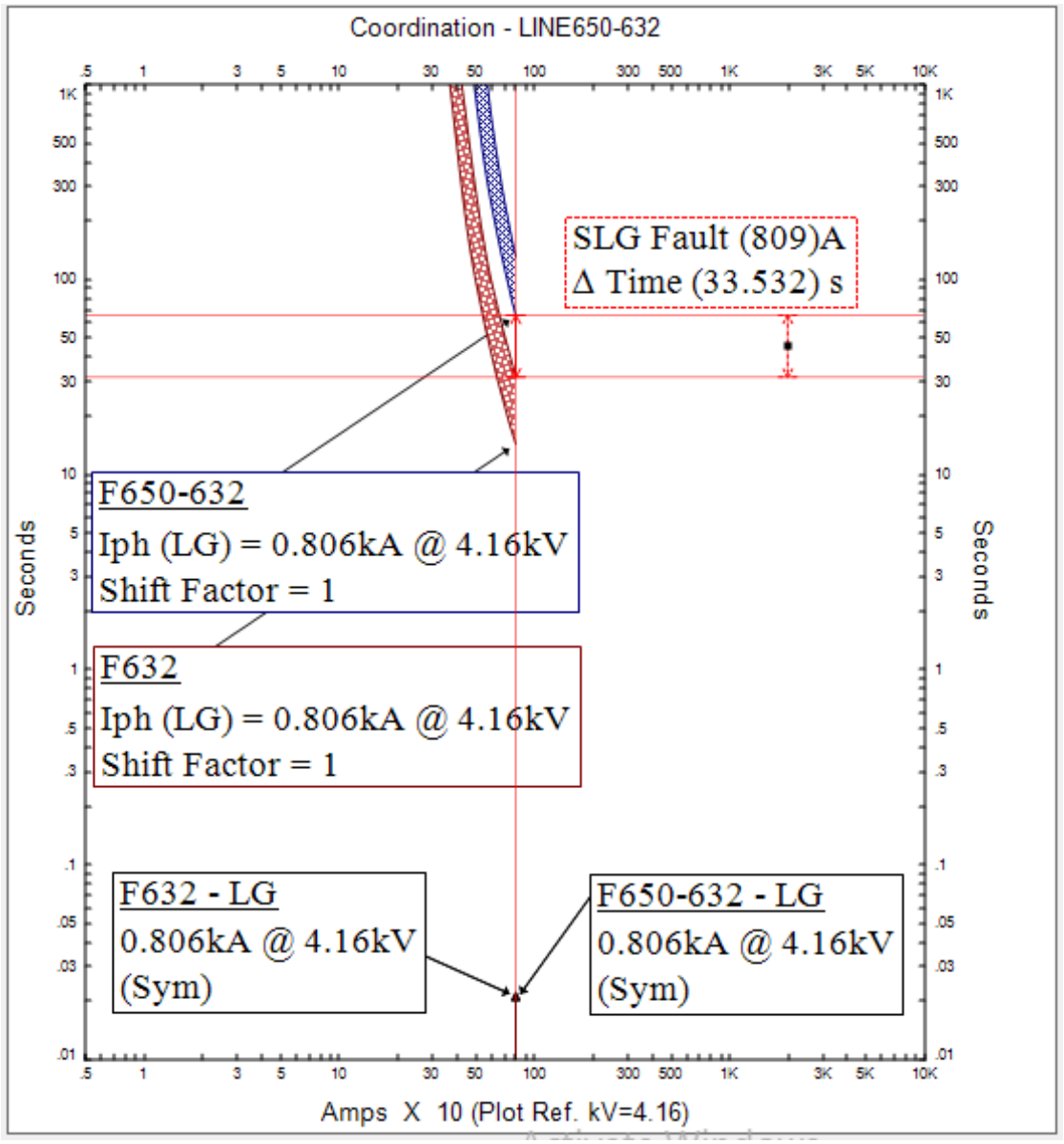

G. FUSES F671-680 AND F680 TCC CURVES FOR SLG FAULT AT NODE680

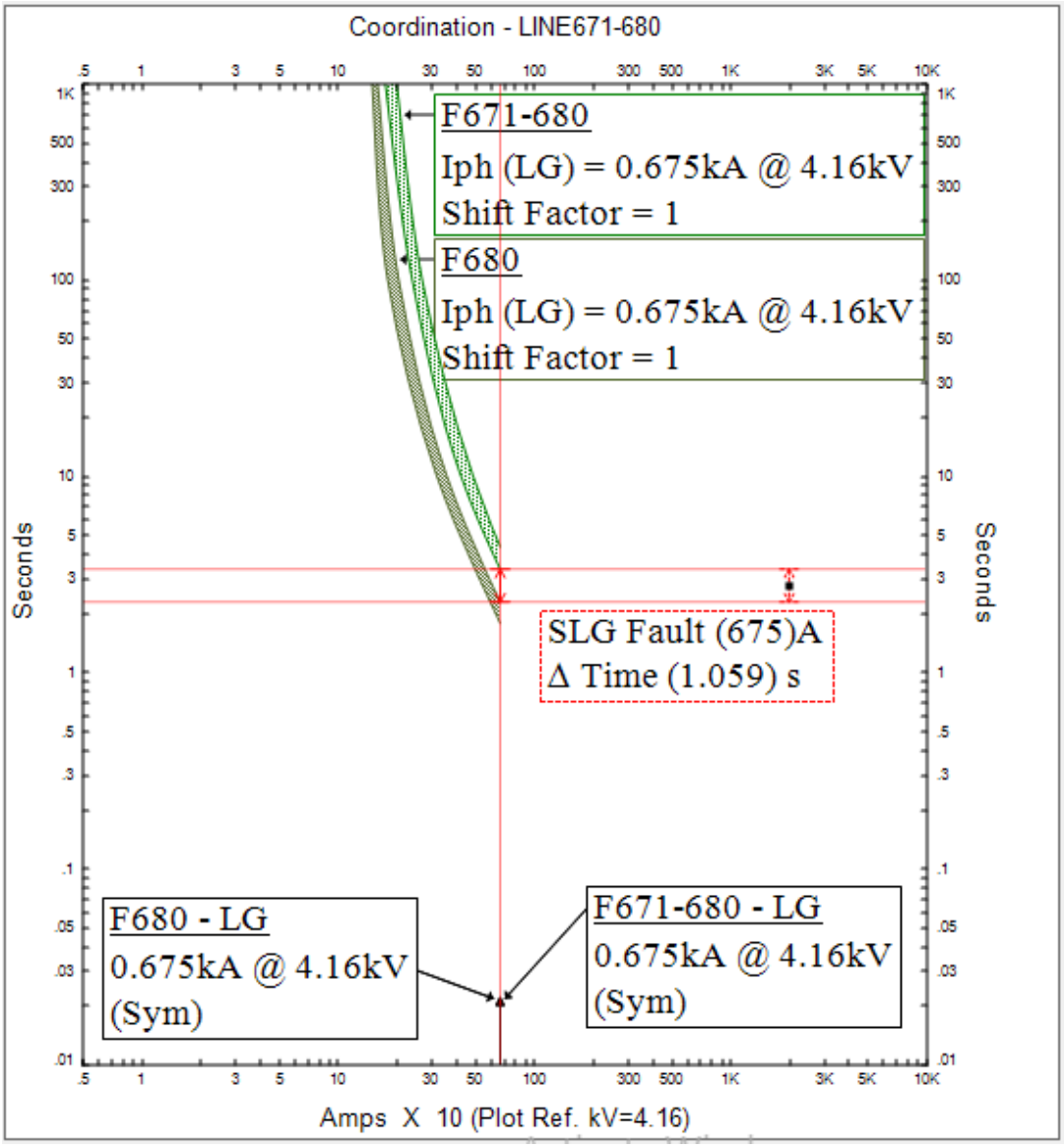

H. FUSES F671-684 AND F684 TCC CURVES FOR SLG FAULT AT NODE684

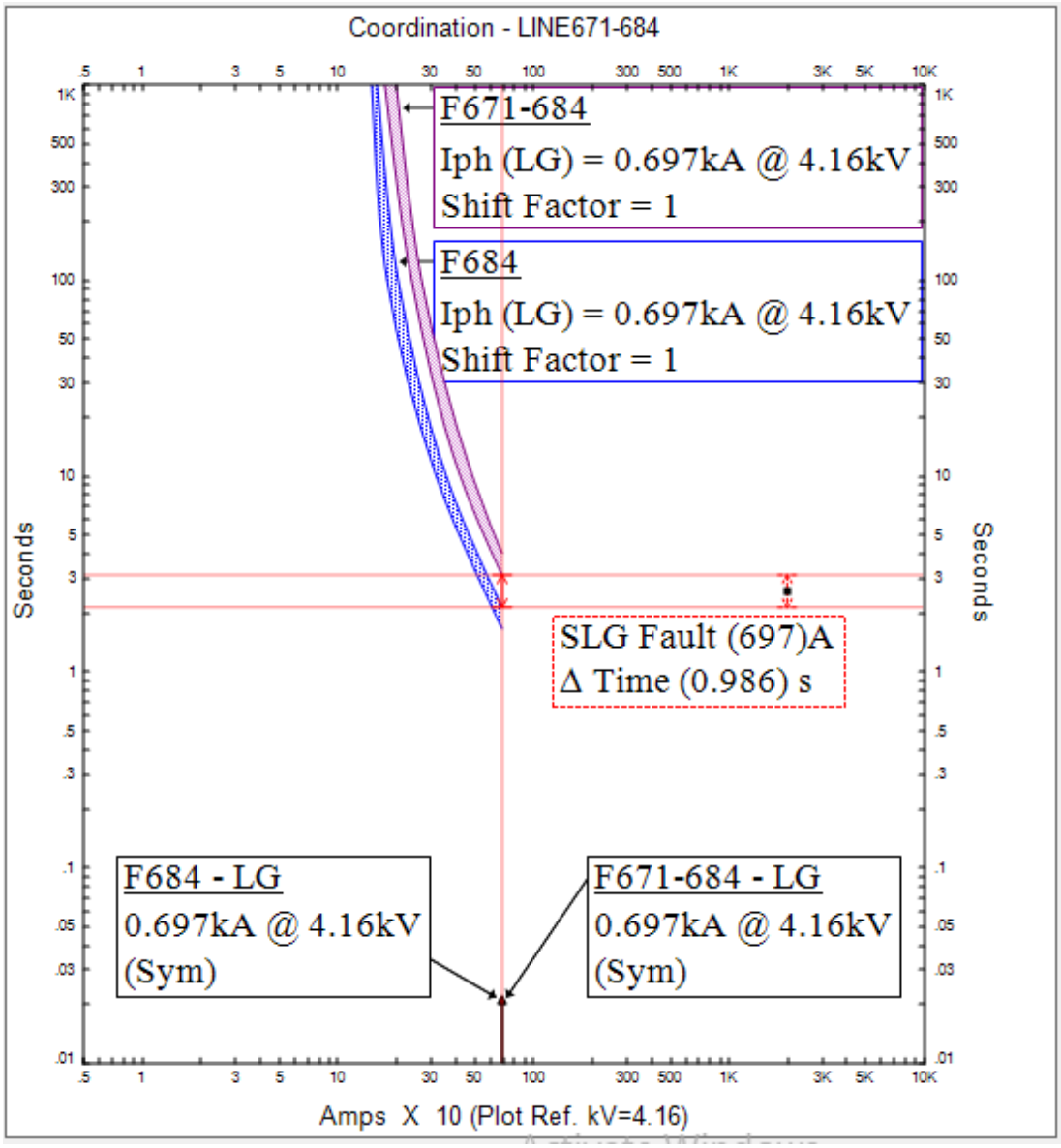

I. FUSES F684-611 AND F611 TCC CURVES FOR SLG FAULT AT NODE611

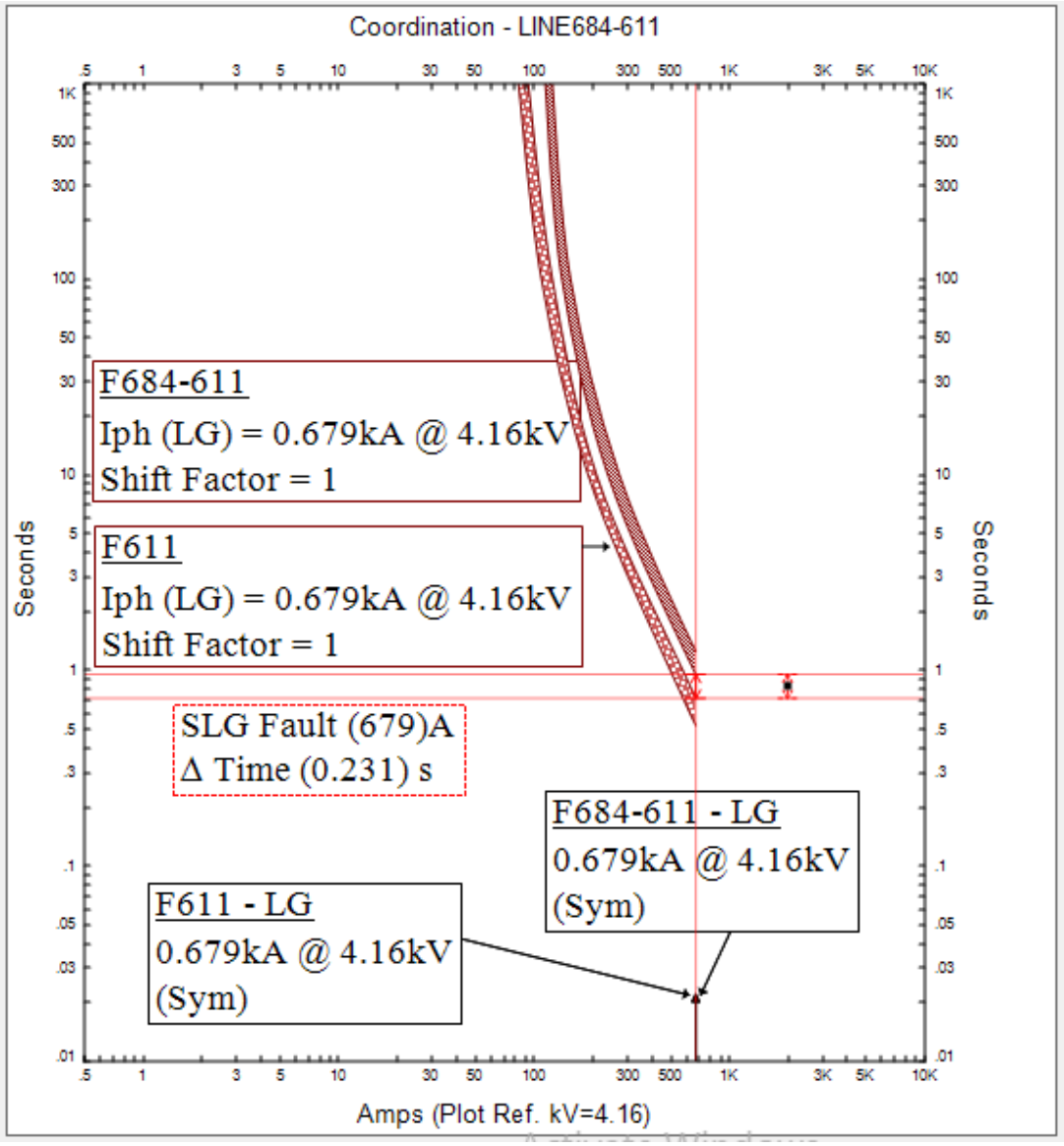

K. FUSES F633 AND F634 TCC CURVES FOR SLG FAULT AT NODE634

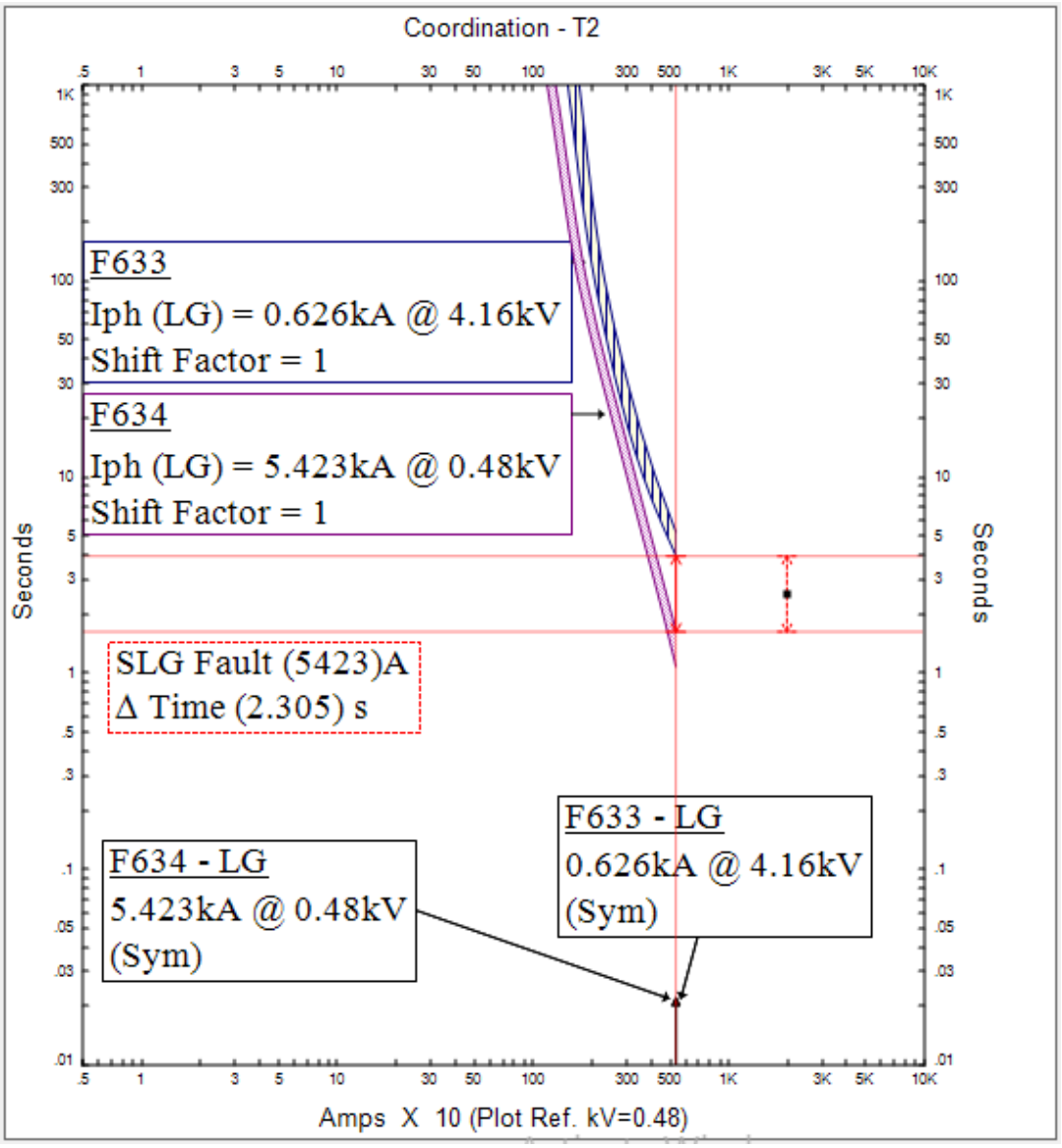

Appendix VI: IEEE 13 Node Radial Test Feeder ETAP Model Back-Up Protection Zones Fuse-Fuse Coordination TCC Curves

A. FUSES F632 AND F632-633 TCC CURVES FOR SLG FAULT ON LINE632-633

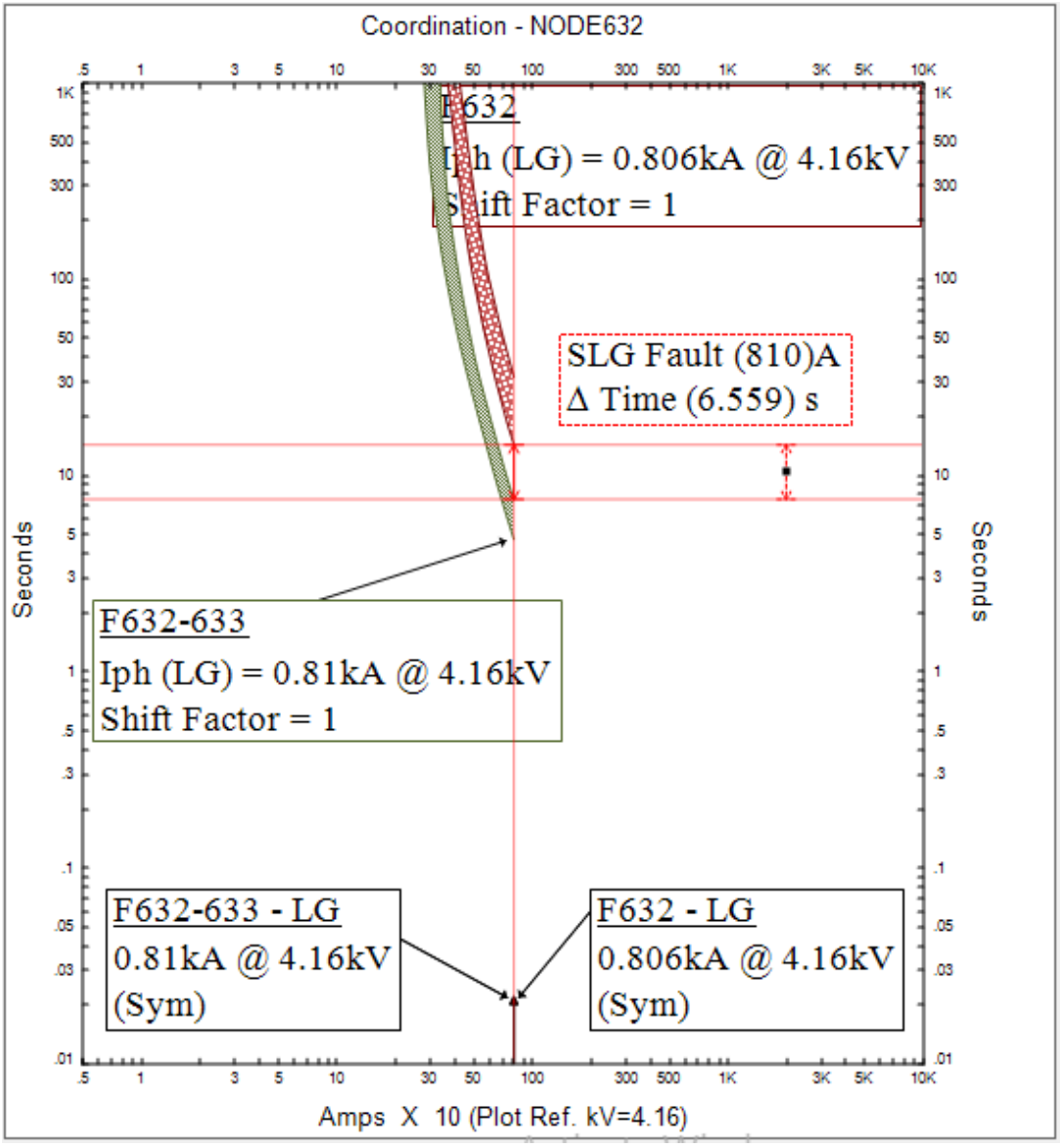

B. FUSES F632 AND F632-645 TCC CURVES FOR SLG FAULT ON LINE632-645

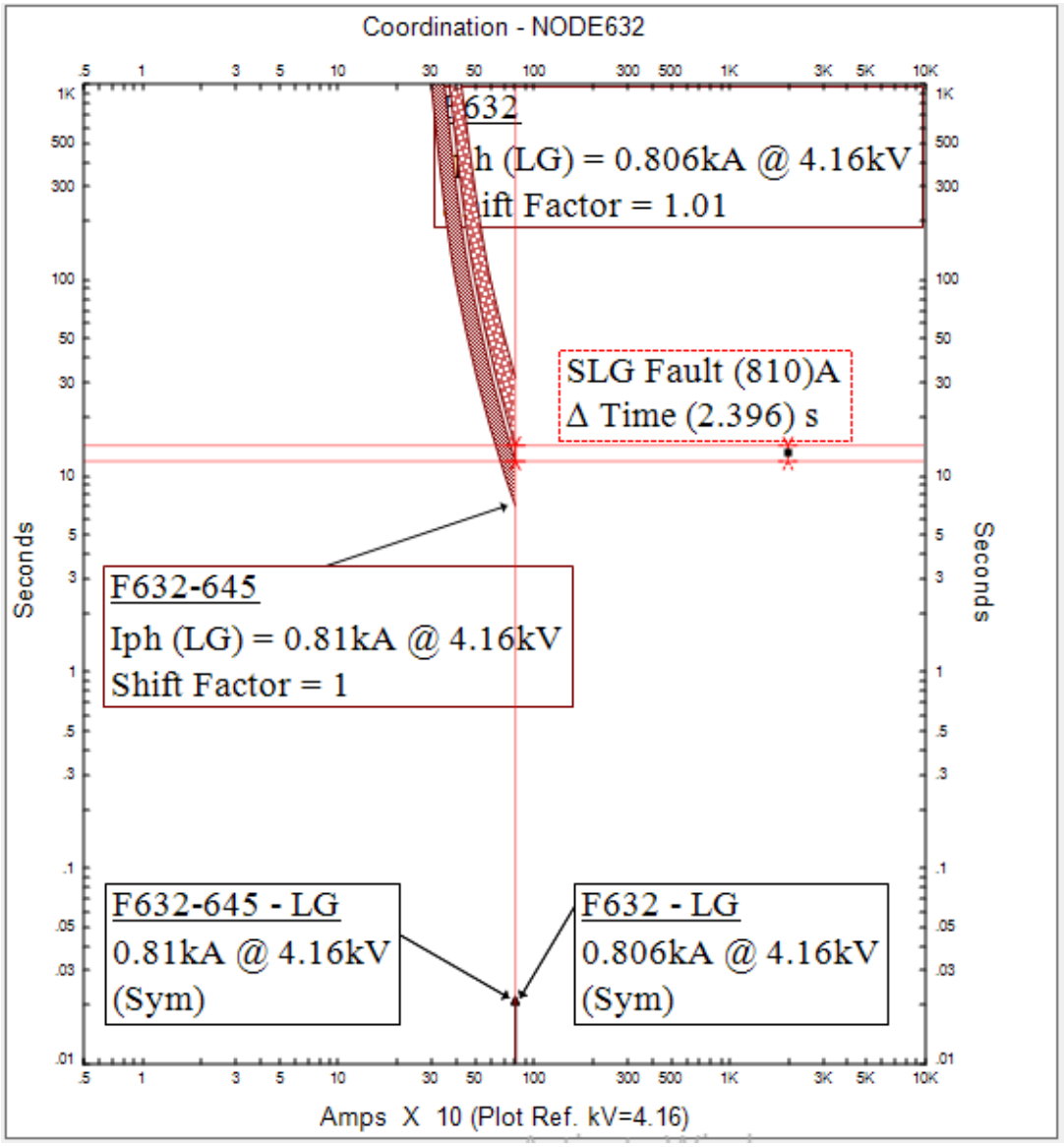

C. FUSES F632 AND F632-671 TCC CURVES FOR SLG FAULT ON LINE632-671

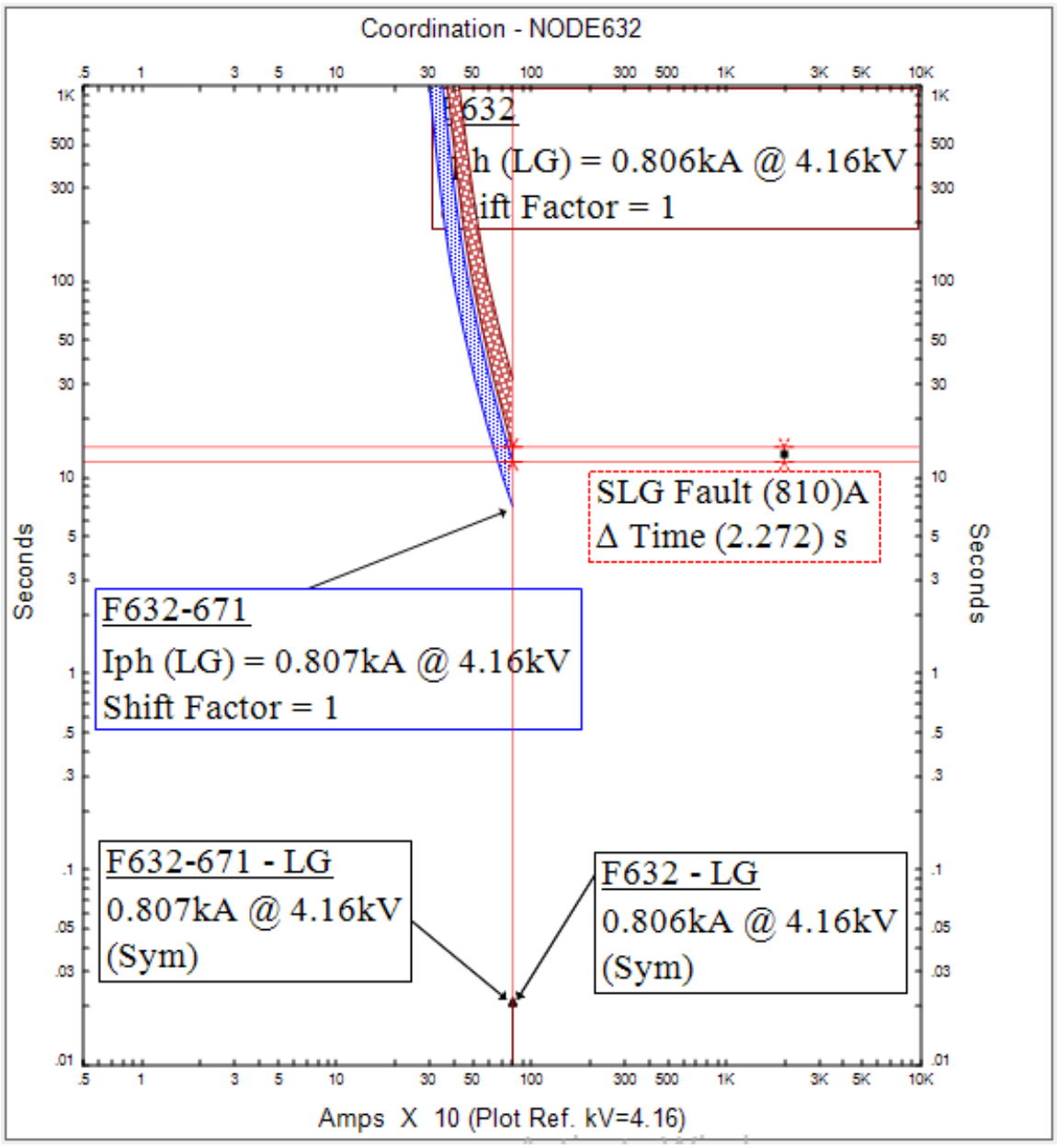

D. FUSES F645 AND F645-646 TCC CURVES FOR SLG FAULT ON LINE645-646

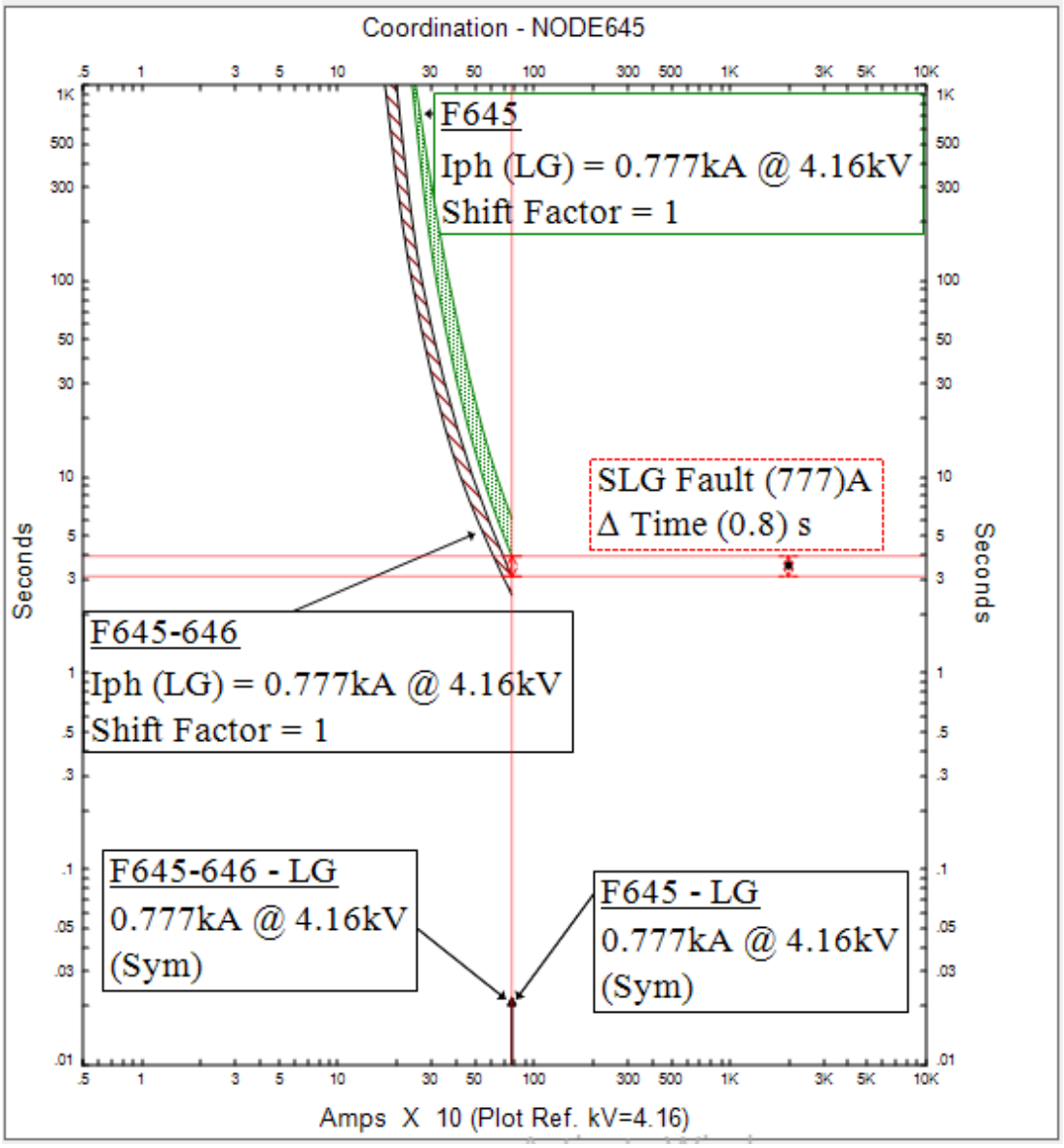

E. FUSES F671 AND F671-680 TCC CURVES FOR SLG FAULT ON LINE671-680

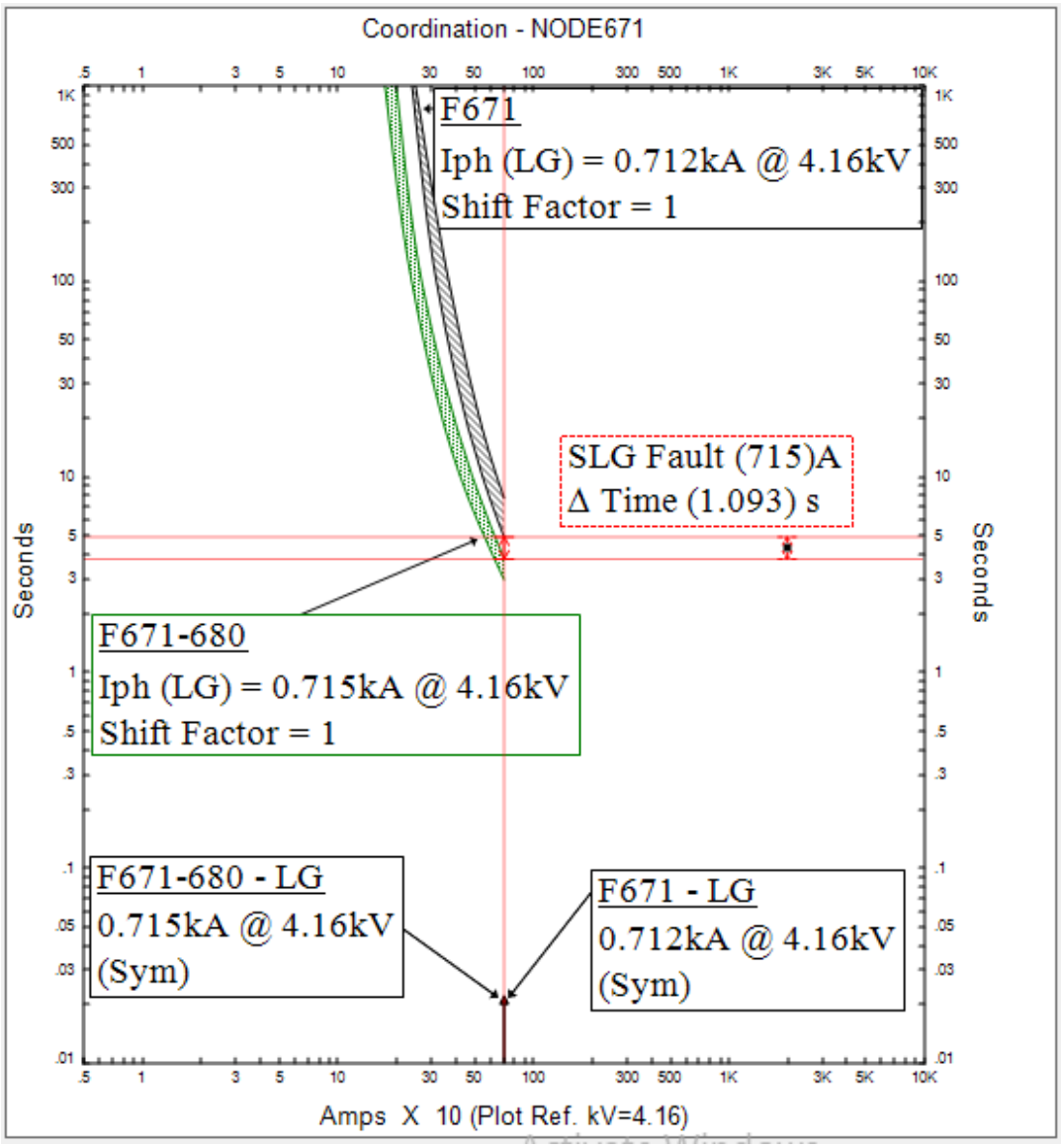

F. FUSES F671 AND F671-684 TCC CURVES FOR SLG FAULT ON LINE671-684

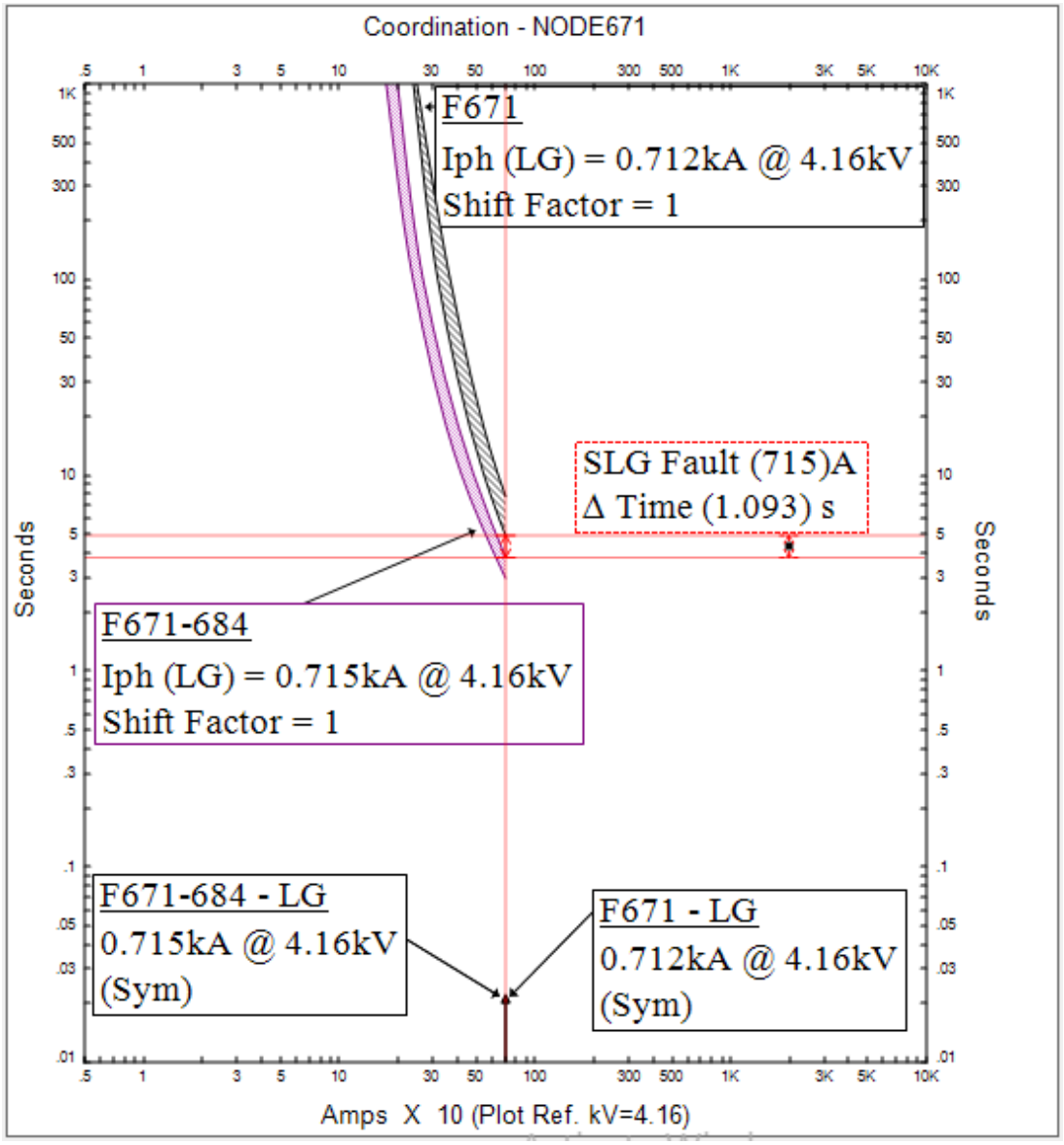

G. FUSES F671 AND F692-675 TCC CURVES FOR SLG FAULT ON CABLE692-675

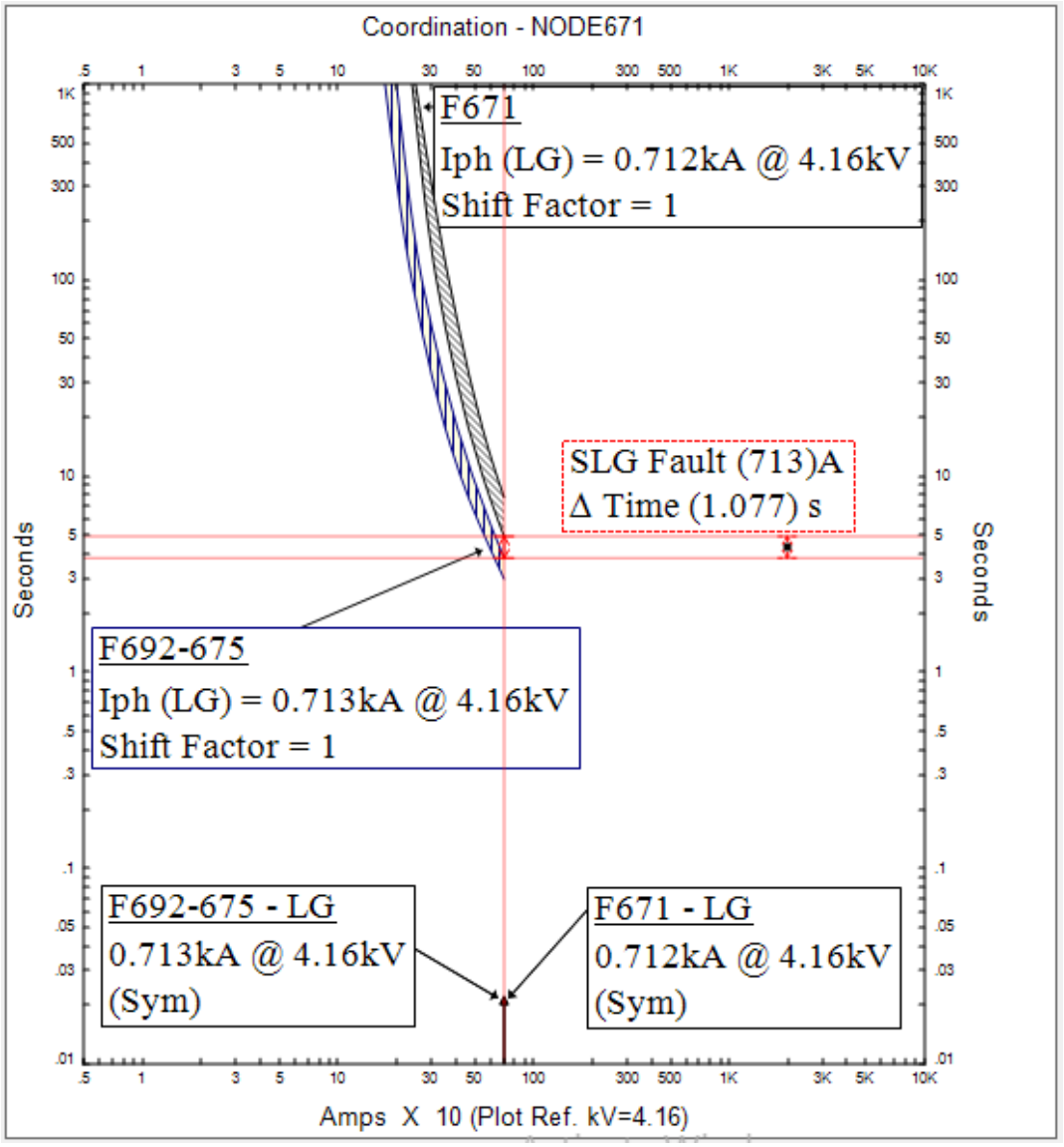

H. FUSES F684 AND F684-611 TCC CURVES FOR SLG FAULT ON LINE684-611

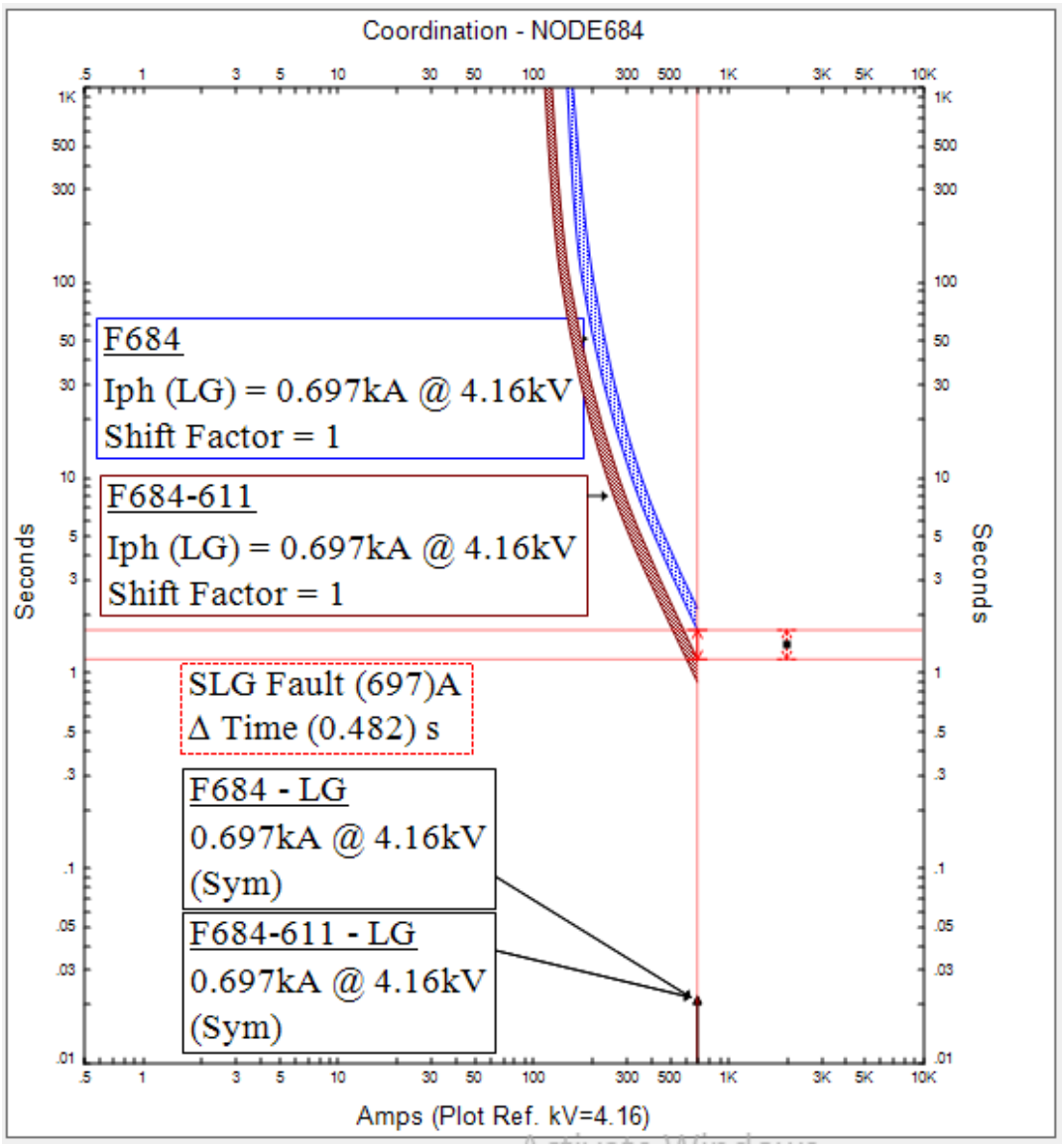

I. FUSES F684 AND F684-652 TCC CURVES FOR SLG FAULT ON CABLE684-652